Hydrogeological characterisation of regional faults and dolerite dykes in the Precambrian Basement and Karoo Supergroup (Tete Province, Mozambique)

Submitted as partial requirement for the degree

M.Sc Hydrogeology

Submitted to:

Department of Geology

School of Physical Sciences

Faculty of Natural and Agricultural Sciences

University of Pretoria

Submitted by:

Raymond Clifford Minnaar

27007295

February 2019

DECLARATION:

I, Raymond Clifford Minnaar, declare that the dissertation, which I hereby submit for the degree MSc at the University of Pretoria, is my own work and has not previously been submitted by me for a degree at this or any other tertiary institution.

Full names:	Raymond Clifford Minnaar
Student number:	27007295
Date submitted:	11 February 2019
Degree:	M.Sc. Hydrogeology
Topic of work:	Hydrogeological characterisation of regional faults and dolerite dykes in the Precambrian Basement and Karoo Supergroup (Tete Province, Mozambique)
Supervisor:	Dr. M.A. Dippenaar
Co-supervisor:	Prof. J.L. Van Rooy
Signature:	

ACKNOWLEDGEMENTS:

I would like to acknowledge the following individuals for their contribution and support to this dissertation:

- Dr Matthys A Dippenaar from the University of Pretoria for mentorship and valuable input.
- Mr Cornelius Roets for his support and valuable input during the fieldwork phase of the project.

ABSTRACT:

Faults and dolerite dykes within Basement- and Karoo-aquifers in northern Mozambique may increase groundwater occurrence but may also be barriers to groundwater flow. Should observation boreholes drilled into regional and local faults as well as dykes show a response to aquifer testing, it would be deduced that these hydrogeological discontinuities are not barriers to groundwater flow. The approach adopted for this study included a sequential process involving data acquisition through a hydrogeological fieldwork programme consisting of geophysical surveys, borehole drilling, aquifer testing, and groundwater level monitoring. The Zambezi Border and geological contact faults were characterised by high variability in hydraulic properties. Aquifer testing resulted in drawdown in observation boreholes as well as a reduction in piezometric surface in the installed vibrating wire piezometers located in different aquifer units, indicating the Zambezi Border- and geological contact-faults were not barriers to groundwater flow. Not all the northwest-southeast trending dykes acted as barriers to groundwater flow, as there were discreet intervals with relatively high permeability present.

Table of Contents

Table of Figures

Table of Tables

List of abbreviations

2D	Two-dimensional
3D	Three-dimensional
CDT	Constant discharge test
EOH	End-of-hole
ERT	Electrical resistivity tomography
ID	Inside diameter
K	Hydraulic conductivity (metre/day)
MAG	Magnetic (ground magnetic geophysical survey method)
MAP	Mean annual precipitation
OD	Outside diameter
REV	Representative elementary volume
RMS	Root mean square
SDT	Step drawdown test
T	Transmissivity (metre^2/day)
TLB	Tractor loader backhoe
uPVC	Unplasticised polyvinyl chloride
VWP	Vibrating wire piezometer
ZB	Zambezi Border

Units of measurements

Ω.m	Ohm metre
km	Kilometre
L/s	Litres / second
m	Metre
m/d	Metre / day
m^2/d	Metre^2 / day
mamsl	Metres above mean sea level
mbgl	Metres below ground level
mm	millimetre
nT	Nano-Tesla

1 INTRODUCTION

1.1 Rationale

Fractured rock aquifers are generally considered as a combination of porous rock matrix and secondary fractures with groundwater flow being structurally controlled (Dippenaar et al., 2009). The characteristics of fractured rock aquifers are highly dependent on several factors such as the composition of the rock mass, neotectonics, weathering, climatic conditions (historic and prevailing), geomorphology, and intrusion of younger lithologies (Dippenaar and Van Rooy, 2014). Generally, groundwater occurrence is increased due to the presence of secondary hydrogeological features. Zones of increased groundwater occurrence are typical targets for water supply but constitutes a major operational challenge and potential hazard in underground and open-pit mining. Furthermore, Cook (1982) also states that the pressure of groundwater in geologic discontinuities affects slope stability. Overestimation of groundwater inflows into mine workings may have severe financial implications by negatively affecting mine planning or ultimately mine feasibility. To ensure safe operational mine conditions it is vital to understand the hydraulic behaviour of secondary hydrogeological features that may be intersected during mine operations.

Faults and dolerite dykes within Basement and Karoo aquifers in northern Mozambique may increase groundwater occurrence but may also be barriers to groundwater flow. Groundwater occurrence may be enhanced along faults and dyke contact zones within the Basement and Karoo Supergroup aquifers (Dippenaar et al. 2009; Bredenkamp et al. 2017). Dolerite dykes of the Karoo Supergroup are geological discontinuities and are typically associated with increased permeability and groundwater occurrence. However, Karoo Supergroup dykes may also act as semi- to impermeable barriers to the movement of groundwater (Woodford and Chevallier, 2002).

Should observation boreholes drilled into these faults and dykes show a response to aquifer testing, it would be deduced that these features are not hydrogeological barriers to groundwater flow.

1.2 Aim and objectives

The main aim of the study was to qualitatively determine the hydrogeological characteristics of key geological structures within the study site. The following objectives were set for this study:

- Determine if the regional Zambezi Boundary Fault is a hydrogeological barrier to groundwater flow or not.
- Determine if geological contact faults between the Basement- and Karoo-formations are hydrogeological boundaries or not.
- Establish if northwest/southeast trending dolerite dyke intrusions are hydrogeological barriers or not.

1.3 Scope and outline of the dissertation

The approach adopted for this study included a sequential process consisting of three general phases. The first phase consisted of a data acquisition phase, which involved a desktop review off all available groundwater related data of the study area and a fieldwork programme. The second phase involved a data analysis phase in order to determine the hydrogeologic parameters and contribute to the conceptual understanding of the targeted geological structures. The final data appraisal phase involved the hydrogeological characterisation of the targeted geological structures within the study site.

2 LITERATURE

The theoretical state of knowledge of the hydrogeological regimes of the geological structures listed in Section 1.2 is given. A detailed description of the qualitative methodologies in order to characterise the occurrence of groundwater associated with the geological structures within the study area is given in Section 4.

The three main stratigraphic units within the study area consist mainly of Precambrian Basement, Karoo Supergroup formations (Carboniferous-Cretaceous), and Post-Karoo Supergroup formations (Cretaceous to Quaternary). These hard rock aquifer units may be associated with moderate to high permeabilities due to the presence of fracturing. Primary alluvial aquifers are beyond the scope of this study.

Fractures and discontinuities are important geological structures in terms of groundwater occurrence within fractured rock aquifers. These discontinuities enable the storage and movement of water through them. The main flow paths in fractured hard rock are along joints, fractures, shear zones, faults and other discontinuities. However, discontinuities such as faults and dykes may also act as barriers to water flow (Bear, 1993).

2.1 Basement aquifers

Crystalline Basement formations form up to 40% of the land area of sub-Saharan Africa. Basement formations are typically described as poor or minor aquifers as they have low storativity, water quality and water supply potential (Adams, 2009). However, increased groundwater occurrence is possible where favourable lithology, structural features and weathering coincide. Crystalline Basement aquifers typically form a two-layer system comprising weathered/ regolith zone that is underlain by fractured bedrock. The weathered/ regolith zone (depending on the overall thickness) and the fractured Basement rock matrix form a composite aquifer unit. Basement aquifers are characterised by a complex network of fractures resulting from weathering, lithostatic decompression, and neotectonics (Bakundukize et al., 2016; Macdonald and Edmunds, 2014). Weathering depth is extremely variable and depends on numerous factors and may reach 80 m, even in semi-arid to arid regions. Fractures, dykes and zones of weathering are typical zones of increased groundwater occurrence and transmissivity (Adams, 2009).

Fresh Basement formations within Southern Africa are characterised by low primary porosity, permeability and storage capacity. Groundwater occurrence is therefore associated

with secondary hydrogeological features such as faulting, fracturing and/or the influence of dykes. Fracturing and fissuring typically occur within zones of lithological contact zones, such as dyke, fault and shear zones. Kirchner (2009) notes that in Basement aquifers in Southern Africa, the groundwater storage is usually from other reservoirs with higher porosity (such as the weathered zone or overlying formations with higher porosity) that can supply Basement secondary hydrogeological features. Bakundukize et al. (2016) in their study of Precambrian Basement aquifers in Barundi stated that the weathered aquifer unit serves as the main storage unit, whereas the fractured Basement lithology serves as the main transmissive unit. Dippenaar et al. (2009) investigated Basement aquifers in South Africa and noted that the transmissivity of these secondary hydrogeological features is dependent on the fracture aperture, frequency and interconnectivity. Groundwater movement through Basement aquifers are mainly associated with secondary features and not the rock matrix. Deyassa et al. (2014) attributed high pumping test discharge rates from wells and hydraulic conductivity values from Precambrian Basement aquifers in northern Ethiopia to the relatively high conductivity of fractures which characterises fractured Basement aquifers in the region. Low hydraulic parameters found in western Ethiopia were attributed to a thin weathered/ regolith layer, which significantly reduces the storage capacity and recharge to the underlying fractured Basement aquifer unit.

According to Dippenaar et al. (2009) and Sami (2009) the neotechtonics influences groundwater occurrence within geologically complex terrain. The geodynamics and tectonic history of an area needs to be understood in order to infer the hydraulic characteristics of secondary features.

Dykes in the Tete area strike at preferential directions and are controlled by regional geological activity and is described in more detail in Section 2.3.4. Holland and Witthüser (2011) further states that depending on the strike of the dyke relative to the groundwater flow direction, the dyke may act as a barrier or conduit to groundwater flow.

Aquifers developed in Basement formations typically consist of (1) composite and weathered bedrock aquifers, and (2) deeper fractured bedrock aquifers. The composite/ weathered aquifer comprises regolith of variable thickness that overlies fractured bedrock and the deeper fractured crystalline bedrock aquifer is characterised by an intact and unweathered matrix with an intricate fractured network (Holland and Witthüser, 2011).

Holland and Witthüser (2011) state that the results from seven studies conducted in Basement aquifers within southern Africa indicated a highly variable thickness of the

weathering zone, ranging between 8 and 50 m. Furthermore, borehole yields in Basement aquifers vary considerable depending on the lithology, presence of geological discontinuities/structures and weathering zones. Research conducted in Zimbabwe found transmissivities of Basement aquifers ranged between 0.5 and 100 m^2/d. Further analyses of a database of boreholes in Basement aquifers consisting of 2 322 transmissivity values and 3 019 sustainable yields, resulted in median transmissivity values and recommended borehole yields of 11 m^2/d and 0.5 L/s per day, respectively. In Basement aquifers increased groundwater occurrence depends on the permeability of geological structures and the transmissivity of the bedrock. Ganyaglo et al. (2017) investigated fractured rock aquifers in Ghana and found that the transmissivity ranged between 0.3 to 35.7 m^2/d.

Extensive analysis of boreholes in Namibia and the Lowveld region of South Africa revealed that main water strikes in Basement aquifers are predominantly located 10 to 40 m below the water table (Kirchner, 2009). Holland and Witthüser (2011) found that the mean water strike depth of Basement formations was between 28.1 and 35.6 mbgl. At the water table increased weathering and mineral precipitation occurs due to circulating groundwater (Kirchner, 2009; Holland and Witthüser, 2011).

Porosity values of Basement formations are typically low, and varies between 0.17 and 0.29% (Kirchner, 2009; Holland and Witthüser, 2011). Lovell (2009) states that Basement formations mainly have secondary porosity due to weathering and fracturing. Kirchner (2009) determined after long term pumping tests (>18 months) that Basement formations in Namibia typically have a storativity value of approximately 0.005. The main groundwater storage medium is usually the weathered overburden (Braune and Mutheiwana, 2009).

2.2 Karoo Supergroup aquifers

Karoo aquifers in the Main Karoo Basin have been classified by Botha et al. (1998) and Botha and Cloot (2004) as multi-layered and multi-porous, where bedding-parallel fractures form the main conduits of groundwater flow. Campbell et al. (2016) also noted that groundwater occurrence and movement in Karoo aquifers are controlled by its multi-layer stratigraphy, historical stress conditions and the presence of dolerite intrusions. However, the fracture apertures and areal extent are limited and not able to store large quantities of groundwater, making primary porosity the main groundwater storage unit in Karoo aquifers. Botha and Cloot (2004) also indicated that vertical and sub-vertical fractures in Karoo aquifers occur

frequently and serve as preferential flow paths and not as the main storage unit. The main storage unit of groundwater in Karoo aquifers are the rock matrix itself. Botha and Cloot (2004) and Woodford and Chevallier (2002) state that two type of flow are present within the Karoo aquifers, namely bedding-parallel fracture flow and matrix flow. The occurrence and characteristics of the bedding-parallel fractures largely contribute to the unique and complex behaviour of Karoo Supergroup aquifers. Groundwater flow in Karoo aquifers occur from the rock matrix to fractures. However, the global behaviour of Karoo aquifers is additionally influenced by the presence of dolerite dykes and other geological structures. Thus, the hydrogeological properties of Karoo aquifers are determined by its very complex geometry.

The Karoo Supergroup, consisting predominantly of sedimentary formations (sandstone, mudstone, shale and siltstone), is generally characterised by low permeability and low groundwater yields (Woodford and Chevallier, 2002). Due to the relatively high density of shales and the poorly sorted nature of sandstones of the Moatize and Matinde Formations, they are usually associated with low-yielding groundwater yields of less than 1 L/s (Bredenkamp et al., 2017). The porosity and density of Karoo Supergroup shales vary between 2-10% and 2400-2600 kg/m^3 (Woodford and Chevallier, 2002). Groundwater occurrence is increased in Karoo sedimentary units due to the presence of fracturing, especially near dolerite dykes, sills or rings (Chevallier et al., 2001).

The Karoo aquifer water strikes are mainly associated with minor fracturing, most likely bedding plane fracturing on the contact with major coal seams. Bredenkamp et al. (2017) found that Karoo Supergroup aquifers within the study area mainly had transmissivity values varying between 0.05 and 1.5 m^2/d and storativity between approximately 0.001 and 0.00001. Bredenkamp et al. (2017) also noted that groundwater occurrence may be enhanced along faults and dyke contact zones within the Karoo Supergroup formations. Larsen et al. (2002) investigated Karoo aquifers in western Zimbabwe and indicated widely varying transmissivity values that ranged between approximately 0.09 and 400 m^2/d.

2.3 Secondary hydrogeological features and groundwater occurrence

2.3.1 General

The rate of flow through a porous medium is described by Darcy's law as being proportional to the loss of head, and inversely proportional to the length of the flow path (Kruseman and

de Ridder, 1994). More detail about Darcy's law and the concept of continuum; microscopic and macroscopic flow; representative elementary volume (REV); limits of Darcy's law; and fractured flow are given in publications such as:

- Bear (1993)
- Dippenaar and Van Rooy (2016)
- Dippenaar et al. (2014)
- Freeze and Cherry (1979)
- Kruseman and de Ridder (1994)
- Singhal and Gupta (2010)
- Woodford and Chevallier (2002)

The key characteristic of fractured rock aquifers, such as Basement and Karoo aquifers, are the large variability of hydraulic properties (Dippenaar et al., 2009; Botha et al., 1998). The variability of hydraulic properties is often highly anisotropic (Cook, 2003) and anisotropy is a key characteristic of fractured rock aquifers (Kruseman and de Ridder, 1994). Numerous conceptual models are used to characterise porous media aquifer systems but are not always adequate to describe fractured rock aquifers (Bear, 1993; Cook, 2003).

The main flow paths in fractured rock aquifers are along joints, fractures, dykes, fault zones and other discontinuities. Fractures and other discontinuities are able to store and move fluid through them (Singhal and Gupta, 2010). Due to the limited aperture and areal extent of fractures in Karoo aquifers, these discontinuities are unable to store vast amounts of groundwater. Two very important points were made by Woodford and Chevallier (2002) from detailed geological studies of Karoo aquifers, namely:

- Flow in Karoo formations obeys Darcy's Law as it resembles flow through a porous medium.
- The Karoo formations act as the main storage unit of groundwater but are not able to release the stored water over small areas compared to secondary structures.

Matrix flow will be the main flow type in stressed Karoo aquifers, unless a fracture system has extremely large aperture and areal extent (Woodford and Chevallier, 2002). Botha et al. (1998) states that a drop in piezometric pressure will result in groundwater leaking from the matrix to the fracture system. In Basement aquifers, Holland and Witthüser (2011) state that the permeability of a fracture system is dependent on the aperture, frequency and interconnectivity of single fractures. Furthermore, Dippenaar et al. (2009) also states that all

groundwater movement as well as storage predominantly takes place in secondary hydrogeological structures (such as fractures) and/or from the weathered zone, since the Basement rock matrix has very low primary porosity. The dominant flow types in fractured Basement and Karoo aquifers are briefly discussed below.

2.3.2 Fracture flow

The hydraulic conductivity of a fracture or discontinuity typically varies to a large extent to that of the intact rock matrix, as the intact rock matrix has a much greater resistance to groundwater flow predominantly due to small interstitial pore spaces (Campbell et al., 2016; Dippenaar et al., 2009).

Groundwater flow in a fractured medium is controlled by various parameters, including properties of discrete fractures and the fracture system, the Reynolds number, and the friction factor. Basement and Karoo aquifer fractures might not have the degree of connectivity to satisfy percolations models. Discrepancies exist in these models and other theories applied to fracture flow as the fractures do not generally have constant apertures and are not smooth and parallel (Dippenaar et al., 2009). Horizontal fracture models such as the Gringarten-Ramey model cannot completely quantify flow in Karoo aquifers, as these models cannot account for the fluid flow from the matrix towards the fracture (Woodford and Chevallier, 2002). In Karoo aquifers Botha et al. (1998) found that the flux of groundwater through water-bearing fractures depends on the fracture aperture, as well as the flux from the rock matrix. The discharge rate determined from a simple parallel plate fracture model depends highly on the aperture of the fracture as well as the piezometric pressure within the fracture (Bear (1993)).

Holland and Witthüser (2011) found from their study that no correlation existed between increased groundwater occurrence and the proximity to a lineament. However, the orientation of the lineament in relation to the neo-tectonic stress regime influenced borehole yields. Lineaments striking NE and ENE to E in the Limpopo Plateau and Letaba Lowveld (South Africa) respectively, had above average transmissivity and borehole yields.

2.3.3 Matrix flow

Although the hydraulic conductivity of the rock matrix might be very low (ca. 10^{-6} – 10^{-8} m/s), there will still be a flux of groundwater from the matrix to a water-bearing fracture as defined by Darcy's law, as long as there is a piezometric pressure difference from the matrix towards the fracture. Over large areal extents groundwater flow can be significant, despite

the flux being small. The matrix of Karoo formations is able to supply large quantities of groundwater to a fracture with large areal extent and sufficient aperture (Botha et al., 1998).

Holland and Witthüser (2011) state that nearly all of the groundwater storage in Basement aquifers is within secondary hydrogeological structures since the Basement formation matrix has extremely low primary porosity.

2.3.4 Dykes

Dolerite dykes of the Karoo Supergroup are geological discontinuities and are typically associated with thin and linear zones of relatively higher permeability which act as conduits for groundwater flow. However, Karoo Supergroup dykes may also act as semi-permeable to impermeable barriers to the movement of groundwater (Woodford and Chevallier, 2002). Van Wyk and Witthüeser (2011) noted that dolerite dykes are amongst the most important geological structures that have a strong bearing on groundwater flow occurrence and flow direction within Karoo aquifers in South Africa and are generally semi-permeable/impermeable.

In the Tete area, dolerite dykes are mostly elongated continuous to sub-continuous and trend NE-SW and NW-SE. Data gathered by SRK from a hydrogeological study in Tete indicated that dolerite dykes in the region dip at steep angles of approximately 75-80 degrees to the southeast and are not vertical as classical assumed (SRK, 2014).

Botha et al. (1998) concluded from their study that linear dolerite dykes contribute significantly towards increased groundwater occurrence in Karoo aquifers in South Africa. They ascribed this to two properties of the dolerite dykes, in that they are relatively easily identifiable by magnetic geophysical methods, and that during the emplacement period the dolerite dykes only baked the nearby surrounding formations, resulting in the formation of fractures. However, it was noted in their study that linear dolerite dykes do not significantly influence the physical behaviour of the Karoo aquifer, other than possibly forming internal boundaries within the aquifer.

Bredenkamp et al. (2017) indicate that groundwater occurrence is typically advanced along dyke contact zones within the Basement and Karoo aquifers in northern Mozambique. Sami (2009) stresses the importance of considering the geological nature of structures such as dykes and Holland and Witthüser (2011) found that dykes trending E-W and NE-SW typically have increased groundwater occurrence in the Limpopo Basement aquifers of South Africa.

Therefore, dyke orientation plays a role in transmissivity and yields of boreholes. Increased groundwater occurrence is found adjacent to intrusive dykes in Basement aquifers where fracturing and deep weathering prevails (Dippenaar and Van Rooy, 2014).

Woodford and Chevallier (2002) state that dolerite dykes have been and are still presently preferred targets for groundwater within the Main Karoo Basin due to the following key reasons:

- There is an apparent higher probability of groundwater occurrence in or next to a dyke.
- Dykes are relatively easy to detect with remotely-sensed imagery or relatively simple and cheap geophysical techniques and are typically visible to the naked eye in the field.
- Dykes on a local scale have relatively simple and regular 3D geometry, which makes it easy to conceptualise.

Woodford and Chevallier (2002) state that 80% of successful boreholes drilled into Karoo Supergroup sedimentary rocks in South Africa were directly or indirectly related to dolerite intrusions. High permeability of the dyke contact zone was found by Van Wyk (1963) to be a result of shrinkage joints developed during cooling of the intrusion. Due to the thermal effects from the emplacement of the dolerite dykes, the surrounding host Karoo Supergroup rocks have been fractured, which significantly increases yield of boreholes adjacent to the dykes (Van Wyk and Witthüser, 2011). More than 25% of boreholes surveyed by Woodford and Chevallier (2001) in the Victoria West area (South Africa) were drilled into or alongside dolerite dykes. Enslin (1951) found that induration and crushing of the Karoo Supergroup sedimentary rock due to dolerite dyke emplacement increases permeability and changed the contact zone into an aquifer. The contact zone aquifer is located between the dyke and the saturated and low permeability Karoo Supergroup country rock.

Woodford and Chevallier (2002) discusses the geometry, structure and mechanism of emplacement in greater detail as well as several aspects that affect the occurrence of groundwater in or near Karoo Supergroup dolerite dykes. These aspects include:

- Contact metamorphism and distance from dyke contact
- Width of dyke
- Dip of dyke
- Transgressive fracturing

- Jointing parallel to the dyke contact
- Effect of dyke attitude and drainage

In Karoo aquifers, fine grained formations such as siltstone, mudrock and shale weather to a dark brown cohesive soil. Along secondary hydrogeological structures such as faults, these rock types weather to clay at depth due to preferential leaching in the vadose zone. The presence of clay typically reduces the permeability of secondary features and sedimentary formations (Woodford and Chevallier, 2002). Botha et al. (1998) note that the weathering of Karoo dolerite dykes depends on the degree of fracturing, width of the dyke, and grain size. Dykes typically wider than eight metres exhibit a chill-margin zone that is normally between 0.5-1.5 metres wide and containing well-developed thermal-shrinkage fractures. Furthermore, thin dykes with widths less than three metres tend to be more resistant to weathering than dykes with larger widths. Groundwater occurrence is not typically enhanced within the first 50 metres below ground surface between Karoo sediments and dolerite dykes.

Botha et al. (1998) noted that high-yielding boreholes were usually located in close proximity to highly weathered fine- to medium-grained dolerite dykes. Even though dolerite dykes are commonly associated with increased groundwater occurrence, they may not always result in increased groundwater occurrence, as dykes are often impermeable and may compartmentalise the aquifer and possibly reduce the extent of groundwater structures.

Bredenkamp et al. (2017) state that increased groundwater occurrence typical occur along faults and fractured dyke contact zones within the Karoo aquifers and/ or Basement formations. Most high yielding boreholes in their study were located in structures associated with NE-SW trending structures. Furthermore, the study indicated that in the Tete area, NW-SE trending dolerite dykes and structures are possible barriers to groundwater flow. The Bredenkamp et al. (2017) study indicated that approximately 15% of recorded groundwater interceptions in the Tete study area were associated with dolerite dykes, and that borehole yields were extremely variable, ranging between dry and up to 9 L/s.

2.4 Weathering

In Basement formations Holland and Witthüser (2011) found that deeper weathering will enhance groundwater occurrence in water-bearing fractures. However, in semi-arid climates

the weathering zone is relatively thin and unable to store and transmit significant quantities of water. Bakundukize et al. (2016) from their review of Precambrian Basement aquifers in Burundi noted that prolonged in-situ weathering of Basement rock results in a weathered layer that is clay-rich, which has a high porosity and low hydraulic conductivity and serves as the main water storage unit. Deyassa et al. (2014) investigated Precambrian Basement aquifers in Ethiopia and found that the thickness of the weathering layer/ regolith varied significantly. The variation in the thickness of the weathered/ regolith layer was also coupled with textural variation with depth. Furthermore, Deyassa et al. (2014) found that geomorphology was a main factor that controlled the occurrence of aquifers in Basement rocks in Ethiopia.

3 STUDY AREA

3.1 Locality

The study area is located near the towns of Moatize and Tete within the Tete Province of northwest Mozambique, near the Malawi border (Figure 3-1).

The non-perennial Moatize River transects the study site and flows into the Ruvubue River. The Ruvubue River is located towards the north of the study site and flows towards the west into the Zambezi River, located downstream of the Cahora Bassa Lake. The topography is mostly undulating with local gradients towards streams and the Moatize River, with the Basement lithology forming the high lying ridges and hills.

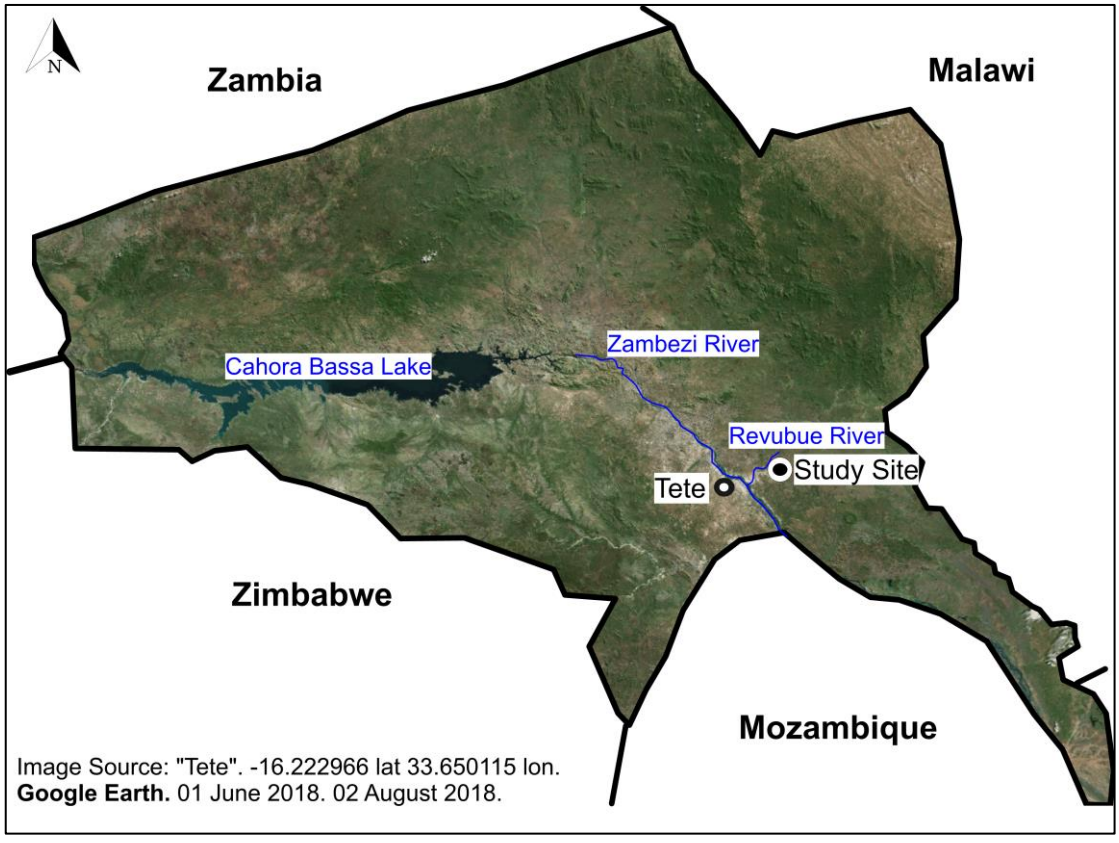

Figure 3-1: Locality of the Tete province (northwest Mozambique) and neighbouring countries indicating the position of the study area.

3.2 Physiography and climate

The Mean Annual Precipitation (MAP) is approximately 642 mm per annum at Tete, occurring over an average of 72 days from October to March, with the highest rainfall in January and February. Mean monthly temperatures range from a minimum of 15°C in July to

a maximum of 34°C in November. Highest temperatures are usually recorded in late October or early November. Relative humidity varies between 29% and 77%, being lowest towards the end of the dry season in September and October and increasing with the onset of the rains in November to reach a maximum in February (SRK, 2014).

The annual average potential evaporation is approximately 2270 mm/annum, which is at its highest during the hot dry season when the relative humidity is low. The lowest evaporation depth occurs in June. The region has a negative moisture index, with evaporation exceeding average rainfall.

3.3 Geology

3.3.1 Regional geology

The Zambezi Basin is structurally dominated by the Zambezi rift, trending predominantly E-W to NW-SE, and is graben-controlled. The three main stratigraphic units within the study area are the Precambrian Basement, Karoo Supergroup formations (Carboniferous-Cretaceous), and Post-Karoo Supergroup formations (Cretaceous to Quaternary) (Hatton and Fardell, 2012) and the study site and simplified regional geology of the Tete Province are illustrated in Figure 3-2.

Basement rock is defined as Precambrian aged igneous or metamorphic rock formations (Dippenaar and Van Rooy, 2014). According to Bicca et al. (2017), the assemblages of the Basement formations in Tete partially preserve evidence of two orogenic events. The first event relates to the Rodinia Supercontinent geotectonics (1.35-1.0 Ga), and is associated with the intrusion of the Basement gabbro-anorthosite Suite, which was controlled by NW-SE trending ductile shear zones. The second orogenic event relates to the Pangea breakup event and the N-S orientated East African Orogeny (650-620 Ma) as well as the E-W orientated Kuunga Orogeny (600-500 Ma), which formed the Zambezi Belt. The Basement formations comprises mainly of gneiss, anorthosite, gabbro, schist, pyroxenite and meta-sediments (Hatton and Fardell, 2012).

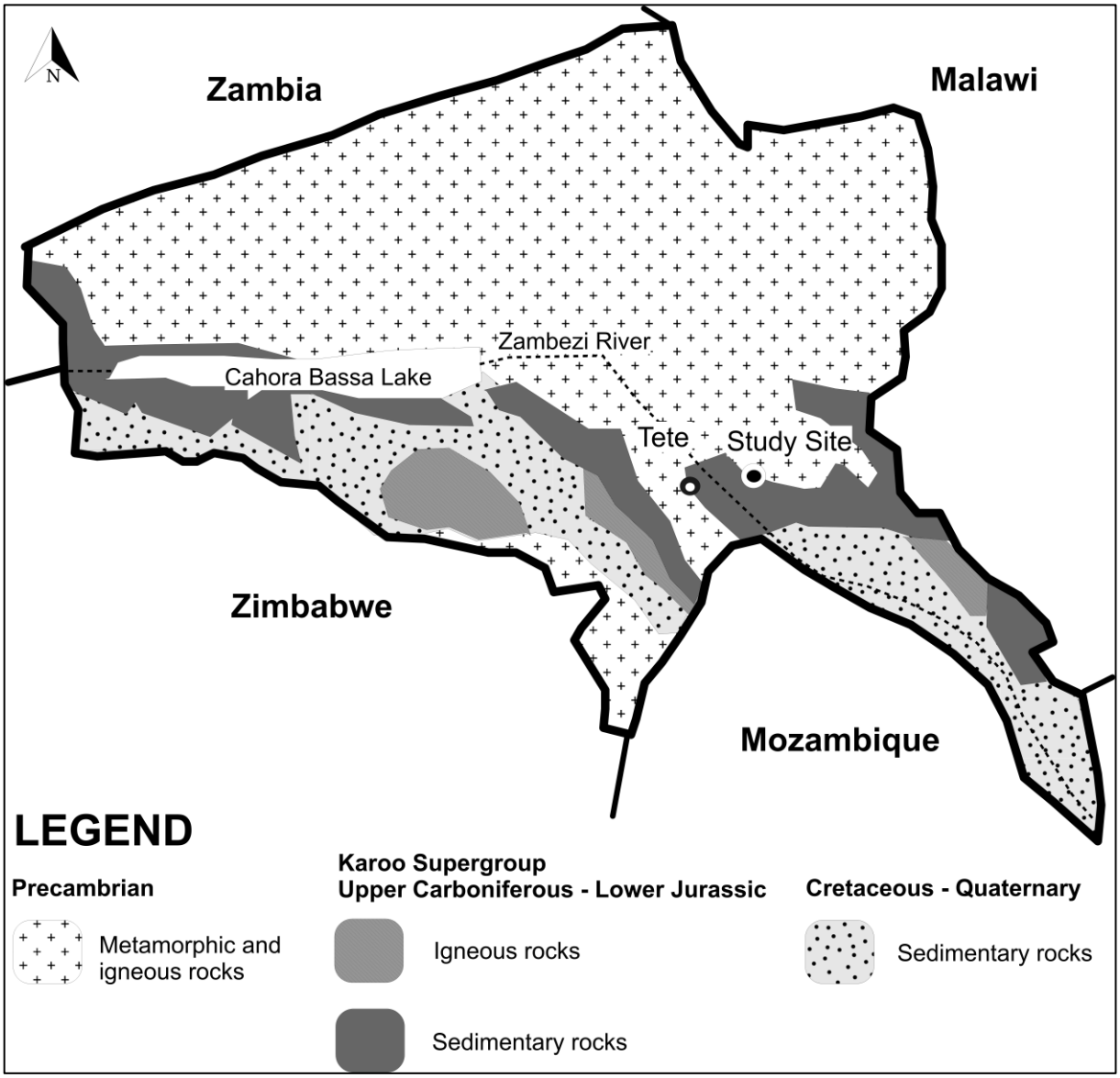

Figure 3-2: Simplified geology map of the Tete province (northwest Mozambique) and Zambezi basin indicating the position of the study area (adapted from Fernandes et al., 2015).

Rift basins within the Zambezi Basin were developed by fault related reactivation of Pan African high strain zones of the Zambezi belt. The transtentional stress produced by the movement along strike-slip faults, associated with the NW-SE Zambezi pre-transform fault system, lead to the formation of graben to half graben-type basins (Fernandes et al., 2015). Karoo Supergroup rocks filled these rift basins located on tectonically active Basement formations, including the emplacement of dolerite dykes and sills of lower Jurassic age (Vasconcelos et al., 2014). Bicca et al. (2017) note that evidence for a tectonically active Basement is well recorded by various geological discontinuities within early Permian Karoo

Supergroup formations. Anticlines and synclines, striking NW-SE, occur inside the graben, and longitudinal-, concentric-, drag-, and transverse-faults also occur within the basin (Vasconcelos et al., 2014).

3.3.2 Local geology

On a local scale, the Zambezi Basin is divided into three sub-basins (Hatton and Fardell, 2012), and the study site is located within the easternmost Moatize-Minjova sub-basin. The Moatize-Minjova sub-basin trends NW-SE, and the Karoo Supergroup rocks unconformably overlie the Basement formations and is in fault-bounded contact to the NW and SE of the basin (Fernandes et al., 2015; Vasconcelos et al., 2014). The Moatize-Minjova sub-basin is characterised by a series of northwest to west trending, listric, sub-basin parallel extensional faults and northeast to east-northeast basin/sub-basin transfer faults (Fernandes et al., 2015; Vasconcelos et al., 2014). Bicca et al. (2017) undertook a structural analysis of the Karoo Supergroup in northwestern Mozambique based on 1 568 traced regional lineaments coupled to field-based ground truthing. The structural analysis produced from the traced lineaments allowed the definition of six structural populations that may have a close relation with pre-, syn- and post-depositional basinal cycles. The analysis of fractures and faults led to definition of two important structural patterns, an E-W and N-NW to S-SE grouping. The kinematic indicators observed in the Karoo formations mainly characterised these faults as transcurrent, dextral and normal. Most faults and fractures were found to be vertical to sub-vertical (dipping mostly greater than 80 degrees) indicating that kinematics must be preferably extensional or directional. Right-handed faults predominate, along with filled fractures with the same orientation, postulating a transtensional stress.

The Karoo Supergroup in the Moatize-Minjova Sub-basin consists of carboniferous tillite and fluvio-glacial deposits and Permo-Triassic clastic rocks, as well as Upper Karoo units consisting of Lower Jurassic volcano-sedimentary formations (Catuneanu et al., 2005; Fernandes et al., 2015). However, the Upper Karoo units are not well represented within the Moatize-Minjova Sub-basin, except for some dolerite dykes and sills of the Rukore Suite, emplaced during the final stages of the Karoo Supergroup (Fernandes et al., 2015). The Vúzi Formation (tillitic), which is Upper Carboniferous in age, represents the lowermost formation of the Karoo Supergroup within the Tete Province and correlates with the Dwyka Formation of South Africa's Main Karoo Basin. Locally, as in the rest of the Tete Province basins, there are only a few outcrops of the Vúzi Formation, as this formation only occurs in paleo-depressions of the Pre-Karoo landscape. The Lower Permain Moatize Formation

conformably overlies the Vúzi Formation and is equivalent to the South African Main Karoo Basin's Vryheid Formation of the Ecca Group. Where the Vúzi Formation is not present, the Moatize Formation unconformably overlies the Basement formations. The Matinde Formation, middle/upper Permian aged, overlies the Moatize Formation and is equivalent to the Volksrust Formation of the South African Ecca Group. The local scale site stratigraphy is illustrated in Figure 3-3. Woodford and Chevallier (2002), Catuneanu, et al. (2005), and Johnson et al. (2006) describe the lithostratigraphy and depositional history of the Karoo Supergroup in more detail.

The fault separating the Karoo Supergroup and Basement formations in the NE margin of the Moatize-Minjova sub-basin is known as the Zambezi Border (ZB) fault, Border Fault (Vasconcelos et al., 2014) or Zambezi Boundary Fault (Bredenkamp et al., 2017). The ZB fault is approximately 30 kilometres long, strikes NW-SE, and dips approximately 45 degrees SW (Vasconcelos et al., 2014). A schematic block diagram illustrating the Karoo sediments deposited in a half graben, dolerite intrusions, and the ZB fault is given in Figure 3-4.

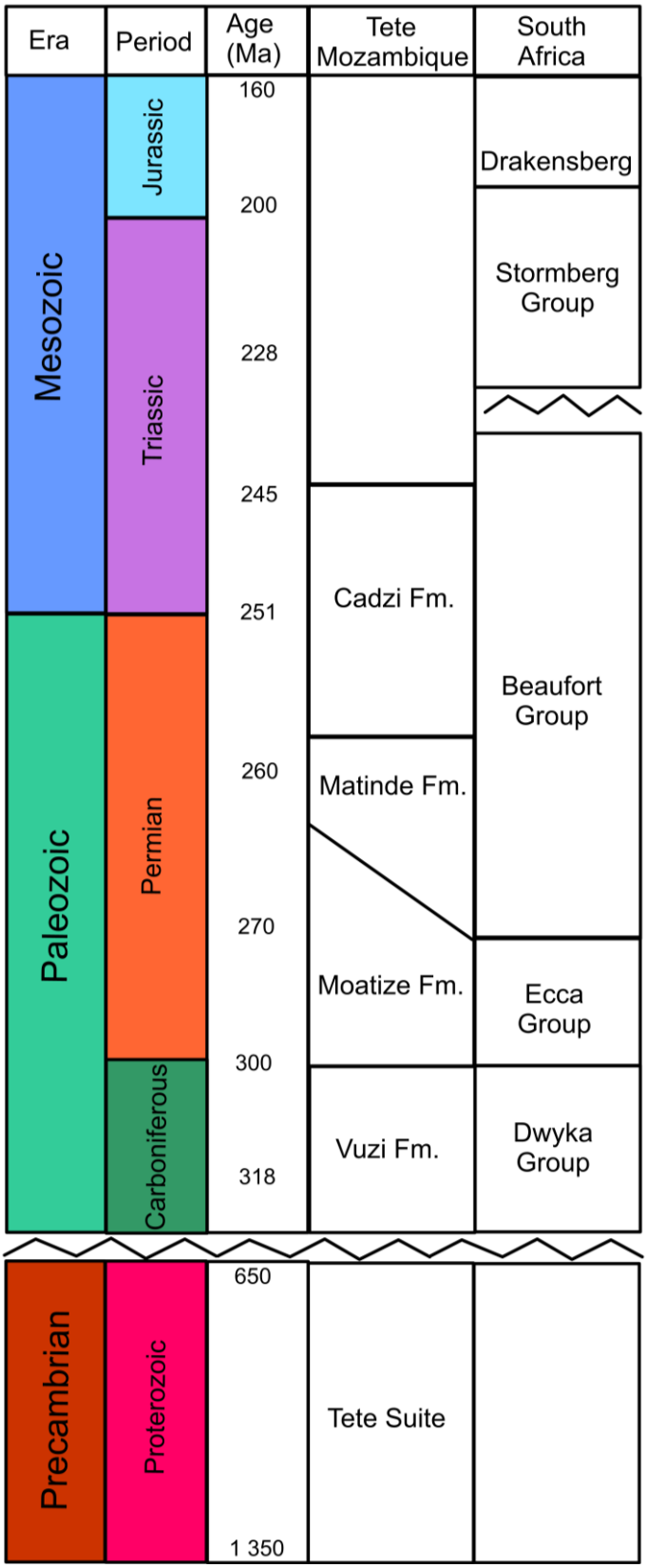

Figure 3-3: Site stratigraphy of Basement and Karoo Supergroup, showing the Mozambique and equivalent South African Karoo Supergroup formations.

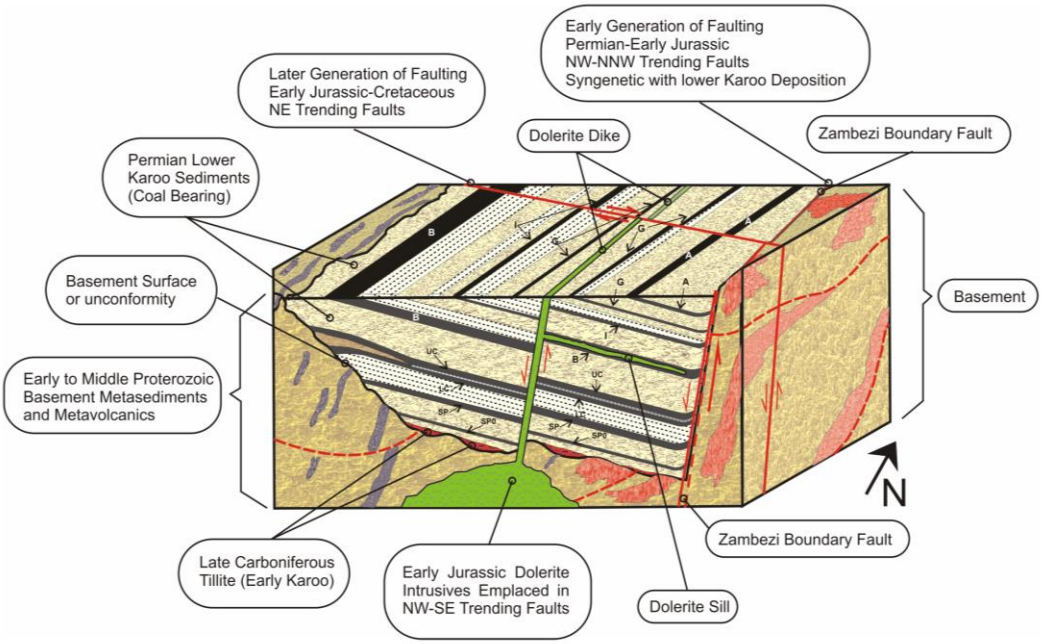

Figure 3-4: Schematic block diagram of Karoo sediments deposited in a half graben structure, Basement formations, and the ZB fault (Bredenkamp et al., 2017).

Dolerite dykes and sills intruded the Karoo Supergroup and Basement formations during the early to middle Jurassic Period (Hatton and Fardell, 2012; Bredenkamp et al., 2017). Field structure orientations from brittle faults and fractures in Permian formations consist of post-Karoo reactivation patterns, relating to an NNE-SSW extension. This extension was most likely due to the breakup of Pangea and the initial stages of the Great East African Rift System (Bicca et al., 2017). The Karoo dolerite includes a wide range of petrological facies and consists of an interconnected network of dykes and sills. Woodford and Chevallier (2002) provides detail on the geometry, structure and mechanism of emplacement of Karoo dolerite dykes and sills.

4 METHODOLOGY

4.1 Introduction

A detailed description of the qualitative methodologies in order to characterise the occurrence of groundwater associated with the geological structures within the study area is given below. The fieldwork was conducted between July 2016 and February 2017 and included surface geophysical surveying, borehole drilling, aquifer testing, and monitoring equipment installation.

4.2 Geophysical survey

4.2.1 Geophysical survey and drilling site selection

Geophysical surveying methods were used in conjunction with information gathered after an initial site reconnaissance visit, available local geological data, topographical maps, and satellite imagery to conceptualise the subsurface geological characteristics and to aid in siting the well drilling locations. This systematic use of available site observations, local geology data, site maps, and geophysics surveying for identifying areas of increased groundwater potential, is described by MacDonald et al. (2005) as the geological triangulation method. Rock outcrops are often covered by soil, alluvial deposits or weathering products, making it difficult to identify specific geological structures in the field. Geophysical exploration becomes one of the methods of increasing importance to locate such structures (Kirchner, 2009; Sami, 2009).

Geophysical surveys respond to the differences in physical properties of geological formations and features, and not to the geological feature as such. The first step in determining which geophysical methods to use is to determine which physical properties would vary spatially as a result of the geological situation. The geophysical survey targeted the following main geological features:

- The Zambezi Border fault
- Dolerite dyke intrusions
- Geological faulted contact between the Karoo Supergroup and Basement formations
- Mapped local fault in the Karoo Supergroup formations.

The electrical resistivity tomography (ERT) survey method was considered for investigating the Zambezi Border Fault, the geological faulted contact between the Karoo Supergroup-

and Basement-formations, and faulting in the Karoo Supergroup formations. The ground magnetic survey method, to investigate the presence of dolerite dykes and sills, was considered to be potentially the most practical and appropriate method to use.

4.2.2 ERT survey

ERT has been extensively applied in various geological, environmental, and engineering studies to obtain 2D and 3D high-resolution images of the subsurface resistivity in complex geology at relatively shallow depths (Balakrishna et al., 2014; Chambers et al., 2010; Chandra et al., 2010; Collella et al., 2004; Pellerin, 2001; Rizzo et al., 2004). ERT involves injecting a direct or quasi-direct current into the ground through two current electrodes and measuring the resulting potentials between a separate electrode pair along the traverse, allowing the apparent resistivity measurements of the subsurface material to be obtained by using Ohm's Law (Colella et al. 2004; Suski et al., 2010; Telford et al., 1990; Zhou et al., 2000). Different electrode configurations are used to introduce electric current and to measure the generated potentials, such as the Wenner, Schlumberger (gradient), pole-dipole, and double-dipole arrays, which are extensively described together with other electrode configurations in Telford et al. (1990) and Dahlin and Zhou (2011).

True electrical resistivity with depth is calculated from the measured apparent resistivity by means of various inversion processes. The inversion process is based on the smoothness constrained least squares inversion with the use of a quasi-Newton optimisation method. The method iteratively adjusts the calculated resistivity so that a relatively small difference exists between the calculated and measured resistivity values. The Root Mean Square (RMS) error is usually used as a measure of the difference between the calculated and measured resistivity values (McClymonet et al., 2011; Mojica et al., 2017; Rizzo et al., 2004; Suski et al., 2010; Telford et al., 1990). The variation in calculated true resistivity, both laterally and vertically, across the length of the profile can be represented as a 2D high-resolution image.

The main advantages of the ERT methodology are that it a globally accepted and cost-effective non-invasive geophysical method, and its efficacy in determining the geoelectrical changes within the subsurface is well demonstrated (Balakrishna et al., 2014; Caputo et al., 2003; Chambers et al., 2009; Chandra et al., 2016; Colella et al., 2004; Mojica et al., 2017; Rao et al., 2012; Rizzo et al., 2004; Zhou et al., 2000). ERT has several advantages over other geophysical methods due to its relative simplicity, efficiency, and robustness of the equipment and field data collection procedure (Balakrishna et al., 2014; Chambers et al., 2009; Kumar et al., 2016; Mojica et al., 2017), which makes it especially well suited in

remote and poorly developed regions where logistical conditions are challenging (Suski et al., 2010).

Recently ERT has been used more extensively in the identification and characterisation of geologic faults in complex geological and different tectonic environments, as described by:

- Bufford et al. (2012)
- Caputo et al. (2003)
- Colella et al. (2004)
- Mojica et al. (2017)
- Rizzo et al. (2004)
- Suski et al. (2010)
- Tejero et al. (2017)
- Zielke-Olivier and Vermeulen (2017)

Caputo et al. (2003) confirmed the reliability of using ERT to map faults in Middle Pleistocene, Holocene, Triassic, late Quaternary, Palaeozoic, and late Villafranchian aged formations. Colella et al. (2004) concluded that ERT is an optimal method to contribute to the determination of the shape of Quarternary sedimentary basins and to identify fault traces at depth in Quarternary, Holocene, and Pleistocene aged formations. Zielke-Olivier and Vermeulen (2017) successfully confirmed the presence of faults within a graben system in a Permian aged Karoo Supergroup basin. ERT was used by Bufford et al. (2012) to contribute to the investigation of the geometry and nature of faults within the Okavango Rift Zone, which consist primarily of Precambrian crystalline Basement, Upper Karoo dolerite, and Quarternary sediments. A study conducted by Rizzo et al. (2004) indicated that ERT was successfully used to determine the shape of the bedrock and the recognition of surface faults within a Pleistocene-Holocene basin and Quaternary fault network. Suski et al. (2010) used ERT to confirm the presence of a fault within Jurassic, Permian, Cretaceous, and Quaternary formations. An investigation conducted by Mojica et al. (2017) showed the successful determination of fault geometry within Tertiary basalt and Oligocene Tertiary sediments. Tejero used ERT to identify the unconformable fault between Basement meta-sediments and igneous rocks and the Cretaceous sedimentary rocks, in order to address the structure of the Guadiana Basin in Spain.

Resistivity of rock types is affected primarily by lithology and age, which affects the porosity of the rock medium and salinity of contained water. Porosity and the salinity of the contained water also affect the resistivity of a particular rock type. However, water is by far

the main controlling factor that influences resistivity of a rock type, as only a small change in the percentage water affects the resistivity immensely. The resistivity of various rock types is listed in Telford et al. (1990), and generally igneous rocks types typically have the highest resistivity, sediments the lowest, and metamorphic rocks an intermediate value. The resistivity of gabbro ranges typically between 10^3 and 10^6 Ω.m (Telford et al., 1990), and a study conducted by Chirindja et al. (2017) indicated Basement gabbro in Mozambique with resistivity ranging between 10^2–10^3 Ω.m. The resistivity of the sedimentary Karoo Supergroup lithology is expected to range between 20-10^3 Ω.m (Telford et al., 1990; Zielke-Olivier and Vermeulen, 2017). However, significant overlapping of resistivity values between formations is possible (Telford et al., 1990).

Due to the difference in lithology, age, porosity, water salinity, and potential water saturation between the gabbro-anorthosite Basement and the sedimentary Karoo Supergroup formations, contrast in resistivity between the two different geological formations was expected. The anticipated boundary between the two contrasting electrical resistivity zones was expected to potentially delineate the location of the ZB Fault.

The apparent resistivity measured is a volume-averaged value and is affected by all geological layers or formations through which the injected current flows, as it is extremely difficult to determine the in-situ resistivity values of soil and geologic formations (Zhou et al., 2000). The 2D or 3D high-resolution resistivity images are inherently based on indirect (non-invasive) information that could contain distortions due to resistivity variations in areas adjacent to the transect line (Chambers et al., 2011). Sharp boundaries and discontinuities will be displayed as a smoothed image and will appear as transitional on any processed image due to the smoothness constrained inversion process, which makes precise identification of the locations and geometries of interfaces, boundaries and/or discontinuities difficult to determine (Chambers et al., 2008; Zhou et al., 2000). The processed and modelled 2D images created after the data inversion process are non-unique, as different geological models may produce similar profiles of calculated resistivity (Chambers et al., 2008; Suski et al., 2010).

4.2.3 Ground magnetic survey

The ground magnetic survey method, which measures variations in the Earth's magnetic field, has been extensively used in geophysical exploration, especially in geological fault and groundwater related studies at shallow depths (Woodford and Chevallier, 2002; Holland and Witthüser, 2011; Ajayakumar et al., 2017; Laletsang et al., 2007; Gibson et al., 2004).

A buried magnetic feature produces a magnetic field, and the magnitude and direction of the magnetic field can vary vastly laterally across the Earth's surface. The magnetic minerals in rock cause magnetic anomalies, and the magnetisation of rocks generally depends on the present geomagnetic field and the magnetic mineral content of the rock (Telford et al., 1990). The Earth's magnetic field is close to uniform over a local scale. The total magnetic field at any given point on the Earth's surface is the vector addition of both the buried magnetic feature and the Earth's local magnetic field.

Magnetometers used in ground magnetic surveys measure the strength of the magnetic field on surface and not directly the strength of magnetisation of geological features. The proton precession magnetometer usually abbreviated to proton magnetometer measures the total strength of the magnetic field but does not measure its direction. The proton magnetometer therefore measures a total field anomaly or sometimes referenced to as a total intensity anomaly (Mussett and Aftab Khan, 2000). The principles and elementary theory are thoroughly described in Telford et al. (1990) and Mussett and Aftab Khan (2000).

The sensor of a proton precession magnetometer is only required to be roughly orientated and the readings of the magnetometer do not drift with time, in contrast with other magnetometer types. Proton precession magnetometers require a few seconds to make a reading and the instrument is best kept stationary during this process (Mussett and Aftab Khan, 2000). Ground magnetic surveys are relatively inexpensive, the instrumentation is easy to operate and interpretation of data from geological features are relatively easy to perform using either standard anomaly curves or with computer software (Woodford and Chevallier, 2002; Mussett and Aftab Khan, 2000). The use of magnetometers in the Karoo Basin to trace the position and orientation of dolerite intrusions formed part of some pioneering geophysical groundwater exploration in South Africa. Magnetic surveys are the most efficient way to trace dolerite intrusions and have been successfully used in South Africa for more than 50 years (Woodford and Chevallier, 2002).

Ferrous objects such as motor vehicles, railway lines, fences, power lines, etc. can cause unwanted effects on the survey measurements, and give rise to sharp localised anomalies. Interpreting such localised anomalies should be done keeping in mind the effect of ferrous objects on the survey measurements. The magnetic anomaly of a buried magnetic feature is relatively complex and similar to ERT data interpretation magnetic survey methods lack uniqueness of interpretation (Telford et al., 1990). The magnetic survey methods depend on

both the direction of magnetisation of the magnetic minerals contained in the rock and on the Earth' magnetic field.

4.3 Drilling

A variety of drilling methods exists and has been developed over time for the development of groundwater supply and hydrogeological investigations in many geologic conditions. The selection of the drilling method used in various hydrogeological applications depends on the ultimate purpose of the well, the hydrogeological environment, the depth and diameter envisioned, and economic factors. In unconsolidated deposits and hard-rock formations drilling is the only feasible approach when compared to dug, bored, jetted and driven wells (Freeze and Cherry, 1979).

The results from the geophysical surveying are not directly related to lithological variation and interpreted data must be calibrated and verified with ground truth data collected through invasive investigation methods such as drilling. The use of geophysical surveying cannot replace the need for invasive investigations, such as drilling, but may potentially reduce invasive investigation costs and reduce the number of invasive sample points required (Chambers et al., 2011; Balakrishna et al., 2014).

The two drilling techniques that were used during the drilling programme are briefly discussed below.

4.3.1 Rotary-percussion air drilling

Monitoring wells, when designed and constructed appropriately, provide representative hydraulic head and quality information of the aquifer (Weight, 2008). Rotary-percussion air drilling is the most economical and fastest drilling method for drilling boreholes into self-supporting hardrock and semi-consolidated formations. The rotary and pneumatic percussion action of the down-the-hole hammer and drill-bit effectively shatters and fractures the geological formation. The drilling fluid of the conventional rotary method is forced down the inside of the drill stem and out through openings in the drill-bit. The drill cuttings are carried to surface by the drilling fluid flowing back to surface between the annulus between the outside of the drill pipe and the hole wall. The reverse circulation rotary method basically involves reversing the drilling fluid direction. The penetration rates for rotary-percussion air drilling are directly related to the compressive strength of the geological formation. Water will be blown to surface as soon as a water-bearing zone is encountered and allows a progressive indication of any changes in the quality and quantity

of groundwater as drilling progresses. The cumulative measurement of the water blown to surface is referred to as the blow yield. The blow yield is only a qualitative indication of the water yield from the borehole and various factors can positively or negatively affect the measured blow yield (Woodford and Chevallier, 2002; Freeze and Cherry, 1979).

The design of a monitoring well should consider the surface housing and the casing. The most appropriate well design includes both solid and slotted casings. The slotted casing serves to stabilise the formation and restricting the inflow of fine aquifer material into the well. In fractured hardrock formations, the slotted screen provides the maximum amount of open area and is commonly inserted from the static groundwater level to a depth just below the last unstable fracture zone or to the main water-bearing fracture (Woodford and Chevallier, 2002). Development of the well by backwashing, through continual air injection by the drill rig, draws the fines out of the aquifer through the well screen and up to surface. The removal of fines from the formation increases the efficiency of the well, as fines create turbulence near the well (Weight, 2008). An artificial gravel pack is typically emplaced between the well screen and borehole annulus to improve the inflow properties from the formation (Woodford and Chevallier, 2002).

4.3.2 Inclined hydraulic-rotary core drilling

Hydraulic-rotary coring, also known as diamond drilling, provides relatively undisturbed rock samples that reveals the geological sequence beneath the drilling location. The basic techniques involved in rotary-percussion air drilling are similar to that of hydraulic-core rotary drilling. A drilling fluid is injected and circulated to carry drill cuttings to surface. However, the coring drill-bit is designed to cut the perimeter of the penetrated rock material, which results in intact material to remain and enter the core barrel (Shuter and Teasdale, 1989). The physical examination of rock core can typically identify fractures and faulting, as well as determining if these structures are open and able to allow groundwater flow through them. Most hydrogeological investigations commonly install only vertical boreholes. However, installing boreholes in the inclined orientation maximises the number of non-horizontal and vertical fractures, faults and/or dykes intersected (Cushman and Tartakovsky, 2017).

4.4 Aquifer properties and characterisation

4.4.1 Packer tests

Packer tests are used to determine the hydraulic conductivity of an individual horizon, by isolating it with an inflatable packer (Singhal and Gupta, 2010). Conventional constant discharge test (CDT) water level response represents an average over the aquifer thickness, whereas packer tests are able to provide information on separate layers, structures, or the vertical distribution of hydraulic parameters (Botha et al., 1998).

During a packer test the rate of flow and/ or pressure in the isolated test section is measured (Yihdego, 2017). In fractured rock aquifers, three types of packer tests can be used and include:

- Standard Lugeon (injection test) – average hydraulic conductivity over test section
- Modified Lugeon – directional hydraulic conductivity in relation to fracture network
- Cross-hole – three dimensional properties from an array of test holes.

A detailed description of the abovementioned tests is given in Botha et al. (1998), Jones et al. (2017), Singhal and Gupta (2010), and Yihdego (2017), and is briefly discussed below.

The standard Lugeon (injection) packer test methodology was used to determine the hydraulic conductivity of discreet intervals or contact zones, identified from the drilling results. The standard Lugeon test method is relatively low cost and is carried out in drilled holes (vertical or inclined) with static groundwater levels below the ground surface. A standard Lugeon tests involves injecting water at specific pressures and measuring the resulting pressure within the isolated section. The pressure is periodically increased and eventually decreased in gradual steps. The response of the isolated aquifer section to the increasing and decreasing injection pressures provides information on the rock, fracture and/ or geological structure behaviour (Jones et al., 2017).

The modified Lugeon test is used when the geometry of fracture network is well known and the orientation of the drilled holes are perpendicular to a considered fracture set (Singhal and Gupta, 2010). Since no information was available on the existence and orientation of possible fracture networks at the study site, the modified Lugeon test method was not considered. Cross-borehole packer tests are able to provide information on the full spatial distribution of hydraulic parameters (Botha et al., 1998), relative permeabilities and interconnectedness between various fracture sets (Singhal and Gupta, 2010). However, Botha et al. (1998) found in their study in Karoo aquifers that the geometry of the aquifer

must be known prior to cross-borehole testing, and that in highly heterogeneous aquifers the cross-borehole packer testing is not very useful.

Data from the injection packer testing is used to calculate the test interval hydraulic conductivity by use of the Thiem (1906) equation. The Thiem equation and assumptions are given in detail in Kruseman and de Ridder (1994). More information on calculating hydraulic conductivity with the use of the Thiem (1906) equation is given in Royle (2002).

4.4.2 Pumping tests

The basic principal of any pumping test is measuring the groundwater level drawdown and discharge rate of the pumped well and potentially any observation piezometers/boreholes and using this data in an appropriate well-flow equation to calculate the hydraulic properties of an aquifer (Kruseman and de Ridder, 1994).

A pumping test usually consists of a step drawdown test (SDT), a constant discharge test (CDT) and a recovery test. The SDT is used to determine the rate of the CDT, which is calculated from the borehole hydraulic efficiency. The SDT involved measuring drawdown while the discharge rate is incrementally increased in in steps. The CDT was conducted at the pumping rate determined from the multiple-rate discharge test analyses. The CDT data is able to provide the aquifer's hydraulic parameters and the conceptual model. The recovery test is also used to calculate the aquifer's hydraulic parameters and also gives an indication on the extents of the aquifer, or the extents and connectivity between fractures (SABS, 1998).

All pumping test analyses were based on the Cooper-Jacob (1946) approximation of the Theiss transient-state flow equation and is explained in more details in Kruseman and de Ridder (1994).

4.4.3 Pumping tests data analyses

In general, well hydraulic equations assume a homogeneous and isotropic medium. However, most aquifer hydraulic properties vary significantly in both the horizontal and vertical directions and are neither homogeneous nor isotropic. Fractured rock aquifers are inherently anisotropic (Kruseman and de Ridder, 1994).

Kruseman and de Ridder (1994) notes that the majority of solutions (such as the Theiss and Cooper-Jacob solutions) used for evaluating pumping tests are based on the following assumptions and conditions:

- Confined aquifer conditions
- The aquifer has infinite areal extent
- The aquifer medium is assumed to be homogeneous, isotropic, and has a uniform thickness
- Piezometric surface is horizontal prior to aquifer testing
- Aquifer testing is conducted at a constant discharge rate
- The borehole penetrates the entire thickness of the aquifer
- Flow to the well is horizontal.

Leaky or fractured double porosity aquifer models provided the most suitable solution for pumping test data in Basement formations (Holland and Witthüser, 2011). Kruseman and de Ridder (1994) state that most fractured rock aquifers can be described as double porosity aquifers, with fluid flow being through the fractures, radial, and in a transient state. However, Woodford and Chevallier (2002) highlights that matrix flow from the aquifer to the fracture should also be considered, for Karoo aquifers at least, and that more complex solutions will be required, such as the transient matrix-to-fracture flow solution developed by Boulton and Streltsova (1977).

The Cooper-Jacob approximation of the Theis transient-state flow solution is based on the assumptions and conditions listed above and is conceptually the incorrect solution to use for many fractured aquifers pumping test data (Woodford and Chevallier, 2002). However, Woodford and Chevallier (2002) state that the Cooper-Jacob solution still provides acceptable estimation of aquifer properties, as transmissivity values calculated by using the Cooper-Jacob compared to other models, such as Boulton-Streltsova (1977), resulted in very similar results.

4.5 Vibrating wire piezometers

A groundwater monitoring network enables the creation of piezometric surface maps, providing information into the nature of boundaries and direction of groundwater flow. In fractured rock formations, the observation boreholes or piezometers should be placed in relation to identified hydrogeological structures in order to assess whether or not these structures act as barriers or conduits to flow (Singhal and Gupta, 2010).

Monitoring of groundwater levels is usually done by installing piezometers and/or observation boreholes. Groundwater level changes in observation boreholes within fractured rock aquifers should be interpreted with care, as the water level or pressure head

change within the matrix and fracture may differ (Singhal and Gupta, 2010). Morton et al. (2008) also states that open borehole water levels should be interpreted apart from pressure heads measured in point piezometers.

Morton et al. (2008) recommend that a monitoring network, especially in mining hydrogeological projects, should include the measurement of pressure heads within important geological formations and/or hydrogeological structures.

The type of piezometer used depends largely on the location, the complexity of the geological formations and hydrogeological structures. Traditionally used open standpipe piezometers, described in Mikkelsen and Green (2003), require a significant volume of water and a narrow pipe diameter in order to obtain a relatively instant measurement. These piezometers are installed with large amounts of sand around the piezometer intake to ensure rapid movement of water around the piezometer to equalise pressure head changes. However, for diaphragm-based piezometers such as vibrating wire piezometers (VWPs), only small amounts of water flow are required compared to traditional open standpipe piezometers. VWPs are usually fully grouted with an appropriate cement-bentonite mixture, which eliminates the use of the sand layer around each individual piezometer. The fully grouted method involves fully backfilling a drilled borehole (drilled vertically, horizontally, or at an inclined angle) with a cement-bentonite grout mixture with the VWPs installed at predetermined depths. Detailed descriptions regarding the preparation and installation procedures for the fully grouted method are given in Contreras et al. (2008), Marefat et al. (2017), Mikkelsen and Green (2003), Simeoni et al. (2011), and Wan and Standing (2014).

5 DATA ACQUISITION

5.1 Geophysical survey

5.1.1 ERT survey

Apparent electrical resistivity measurements were obtained through the use of a multi-electrode ABEM LUND Terrameter SAS4000 resistivity imaging system. The ERT survey consisted of:

- Two 300 m traverses (T-5 and T-6)
- Five 400 m traverses (T-2, T-4, T-7, T8, and T9)
- One 900 m traverse (T-3)
- One 1000 m traverse (T-1).

Limited geological outcrop of Basement and Karoo formations at the area of traverse T-2 was used to orientate the ERT survey perpendicular across the possible position of the ZB Fault in a southwest-northeast direction. Due to topographical variation and no geological outcrop, profiles T-7, T-8, and T-9 were positioned in a semi-grid formation across the inferred ZB fault position. Geological outcrop of Basement and Karoo formations was used to orientate traverses T-5 and T-6 perpendicular across the faulted contact. Traverse T-1 was positioned perpendicular along two NW-SE trending dykes that were visible on surface, as these dykes weathered positively compared to the Karoo sedimentary formations. Traverse T-4 was positioned perpendicular across an inferred mapped fault within the Karoo sedimentary formation. Traverse T-3 was positioned along a dolerite sill, which was visible from the side of a road cutting. The location of the ERT traverses as well as start and end points are illustrated in Figure 5-1.

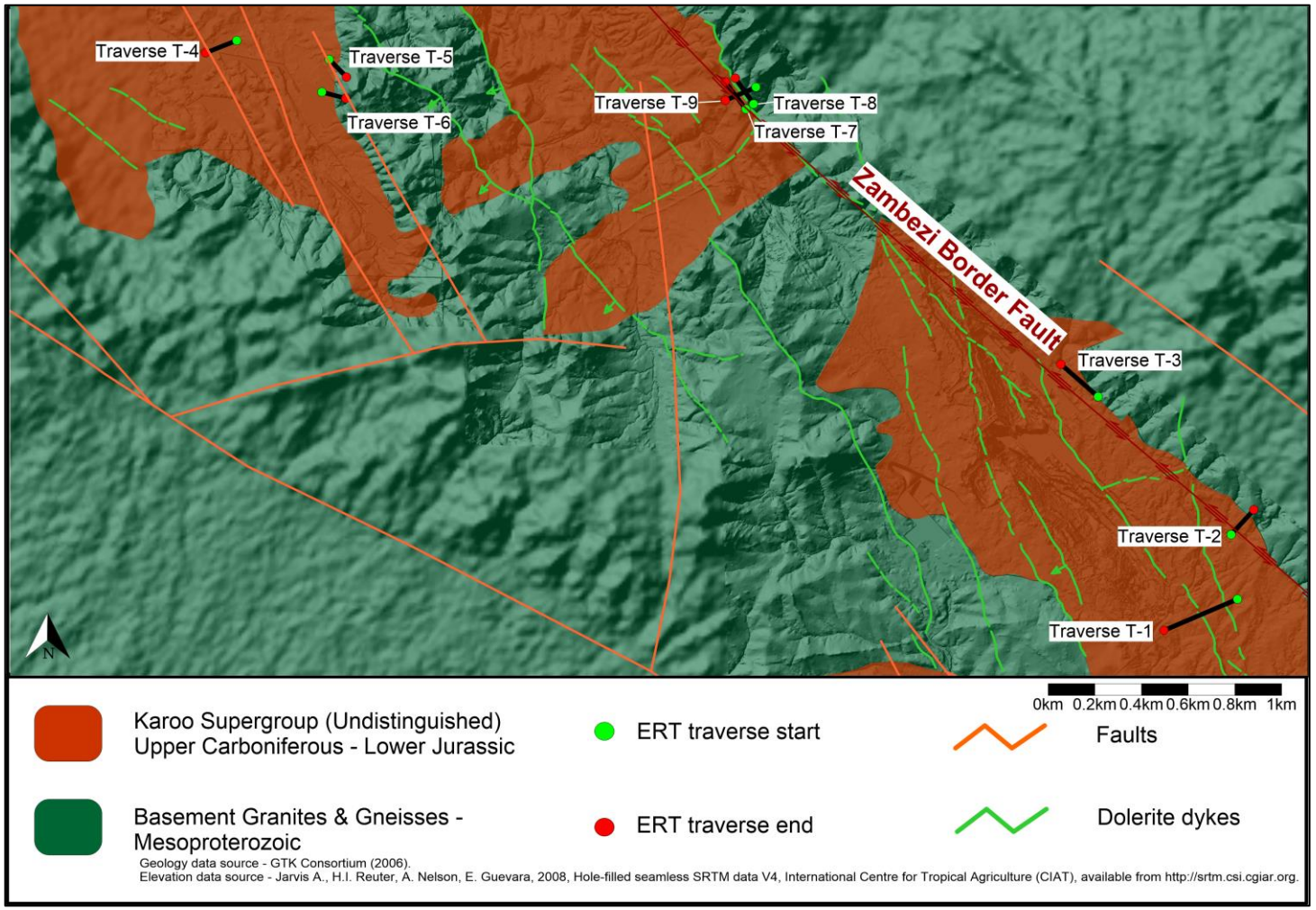

Figure 5-1: Topography and general geology of the Moatize-Minjova sub-basin and study area, illustrating the electrical resistivity tomography (ERT) traverse locations and the inferred Zambezi Border fault.

The Wenner array geometry, with 5 m electrode spacing, was used for all nine ERT profiles, since it generally produces a high signal-to-noise ratio and has low noise contamination compared to other array geometries, even though it may not always produce high resolution images at depth (Dahlin and Zhou, 2004; McClymont et al., 2011). Apparent resistivity data points measured with error values larger than 2.5 % were not used.

Apparent electrical resistivity is inverted with the use of the least-squares smoothness constrained inversion process. The 2D pseudo-sections were created with the use of the robust (L1 norm) scheme, which is less sensitive to noisy data and is the preferred method when sharp boundaries in the geology are expected. The inversion of the apparent resistivity data and the 2D pseudo sections were processed with the use of the RES2DINV software developed by Geomoto, and the software and methods are extensively described in Loke and Dahlin (2002) and Loke and Barker (1996). Convergence was achieved during the inversion process after 5 to 7 iterations with an average root mean square (RMS) error of 6.8%. The 2D electrical resistivity pseudo-sections were used to approximate the location of the ZB fault and geological contact fault zones.

5.1.2 Ground magnetic survey

The magnetic survey was conducted with the use of a GEOTRON G5 Proton Magnetometer. The magnetic (MAG) survey was orientated and conducted across the resistivity survey traverses in order to overlap the two datasets (Figure 5-1). The ground magnetic (MAG) survey was conducted after each ERT traverse and the magnetometer was configured with a sensor height of approximately 1.5 m a station spacing of 5 m. Readings at each station were stacked five times and an average value was recorded.

5.2 Drilling

Drilling targets were identified at inferred geophysical anomalies from the ERT and MAG surveys. A percussion rotary drill rig was commissioned to drill the vertical test boreholes and a core drill rig was commissioned to undertake inclined core drilling. The design and construction of the inclined core- and monitoring-boreholes are discussed below. The locations of the vertical rotary percussion and inclined core boreholes as well as the boreholes aquifer tested are illustrated in Figure 5-2.

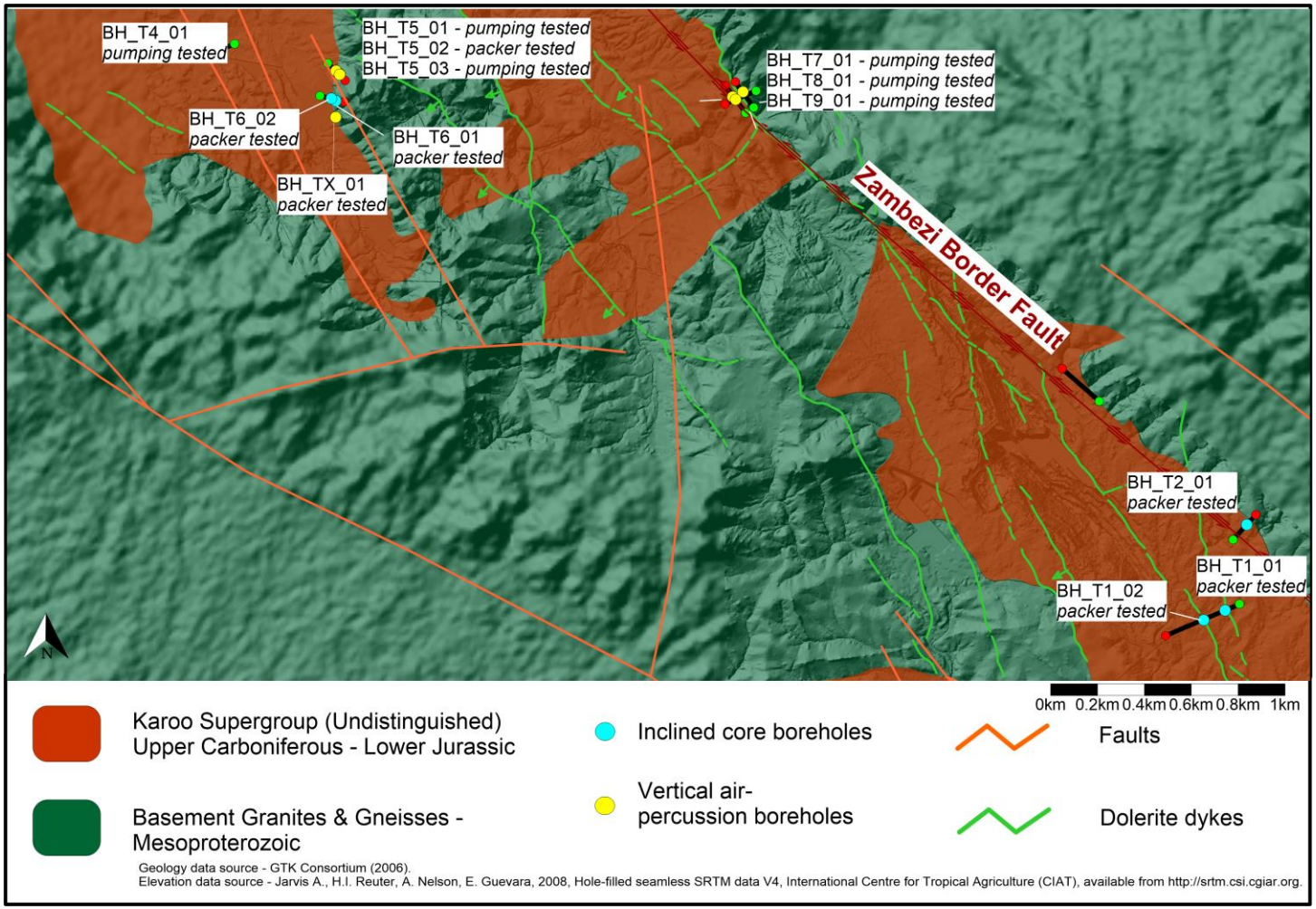

Figure 5-2: Topography and general geology of the Moatize-Minjova sub-basin and study area, illustrating the vertical percussion and inclined rotary core borehole locations and aquifer tested boreholes.

5.2.1 Rotary percussion air drilling

Eight monitoring boreholes were drilled across the project site using conventional 6.5-inch rotary-percussion air drilling. Boreholes underwent full casing construction and entailed using a 5-inch diameter uPVC casing. A distribution of 60% horizontal slotted screen (0.45mm slots) and 40% solid casing was allowed for during construction. Centralisers were installed every 20 metres on the entire casing column length to ensure a uniform annulus thickness. An end cap was placed at the base of the casings to seal the bottom opening. Clean, uniform quartzite gravel, with a grain size varying between 3 and 5 millimetres, was used for gravel packing and a 0.5 m thick bentonite sanitary seal was installed on top of the gravel packing, after which the annular space between the top of the bentonite seal and up to 1.5 m from surface, was backfilled with drill cuttings and a second bentonite seal was installed. A 300-mm long (165 mm OD, with 4mm wall thickness) steel casing was installed to protect the uPVC casing above surface. The steel casing was securely cemented into the ground. A cement block with 0.8 m diameter and 0.3 m depth was constructed around each of the monitoring borehole standpipes. A lockable steel cap was fitted on top of the standpipe.

5.2.2 Inclined hydraulic-rotary core drilling

A total of five inclined core boreholes were installed at an angle of 70 degrees to the horizontal. The inclined core holes were drilled using standard HQ size coring (3.8-inch or 95 mm). The inclined core boreholes were constructed using only 6-inch steel surface casing to the base of the unconsolidated overburden and highly weathered zone. Upon completing the installation of the steel surface casings, an approximately 300 mm long steel standpipe was installed to protect the surface casing. A cement block with 0.8 m diameter and 0.3 m depth was constructed around each of the monitoring borehole standpipes. A lockable steel cap was fitted on top of the standpipe.

5.3 Aquifer testing

5.3.1 Packer tests

On completion of the drilling phase, five inclined core and two monitoring boreholes were selected for injection-type (Lugeon) packer testing. Single and double inflatable packers ranging in size from 56 mm for the incline core boreholes to 85 mm for the monitoring boreholes were utilised for testing. The testing was conducted by lowering the single and/or double test packers to various predetermined depths in the boreholes, depending on the

lithological logs. The single and/or double test packers were inflated by means of a hand pump and the test section sealed off. Water was injected under pressure by using a water pump and respective valves. The water was injected at specific pressure steps and the resulting pressure was monitored and recorded when the flow reached a quasi-steady state condition. Each packer test step was conducted for 15 minutes.

5.3.2 Pumping tests

A total of three SDT and six CDT and recovery tests were conducted. Two submersible pumps were commissioned to conduct the aquifer testing; A 2.2-kiloWatt (kW) pump for low yielding boreholes (0.1 to 2.0 L/s) and a 5-kW pump for higher yielding boreholes (>2.0 L/s). Electronic water level loggers were installed in tested and monitoring boreholes and set to record readings at 30 second intervals. The aquifer tests entailed the following:

5.3.2.1 Step drawdown tests

A step drawdown test (SDT) during which the borehole was pumped at a constant discharge rate for up to 60-minutes for each step, thereafter the steps were repeated at progressively higher discharge rates. During the SDT the drawdown over time was recorded for the borehole being tested. After the test has stopped, the residual drawdown was measured until approximately 90% recovery of the water level was reached. The data was analysed to determine the constant discharge rate required for the constant discharge tests for each borehole.

5.3.2.2 Constant discharge tests

Constant discharge tests (CDT) were performed for a specific time depending on the individual borehole yields and the boreholes were pumped at a constant rate based on the SDT results, and the drawdown over time in the pumping borehole was recorded. Discharge measurements were taken at regular time intervals to ensure that the constant discharge rate was maintained throughout the test period. Boreholes within close proximity of the abstraction borehole were equipped with electronic water level loggers. The transmissivity and storativity (where observation boreholes were present) were estimated from the constant discharge test results.

5.3.2.3 Recovery tests

Recovery testing provided an indication of the ability of the boreholes and groundwater system to recover from the stress of continual groundwater abstraction. This ability can

again be analysed to provide information in regard to the hydraulic properties of the groundwater system. The recovery period follows directly after pumping cessation of the CDT. The residual drawdown over time (water level recovery) was measured until approximately 90% recovery (of the initial water level) was reached in each pump tested borehole.

The aquifer test data were processed with the use of AQTESOLV PRO Version 4.5 software developed by Glenn M. Duffield, Hydrosolve Inc.

5.4 Vibrating wire piezometers

After completion of the drilling and packer testing, selected formations and/or discontinuities were identified for the installation of multi-level vibrating wire piezometers (VWP). Direct read-out cables were spliced and connected accordingly for each VWP. The VWP were lowered to the required depths and connected to a central Geokon datalogger unit located at the borehole surface nested within the borehole headworks.

A grouting mixture of 70% cement and 30% bentonite was prepared to grout VWP sensors in-situ. The grouting mixture was inserted using a gravity-based method. Before installation the VWPs were individually calibrated and a protective slotted uPVC cover was installed around each piezometer.

6 DATA ANALYSIS

6.1 Geophysical survey and proposed drilling targets

The ERT and MAG survey results and the proposed drilling targets are discussed below for each geophysical profile.

6.1.1 Profile T-1

The results from ERT profile T-1 generally indicated low to intermediately high resistivity throughout the profile length. The resistivity up to an average depth of 20 metres from surface ranged between approximately 12.2 and 387.5 Ω.m. At depth the resistivity on average ranged between 3.89 and 590 Ω.m. At stations 160 m and 870 m very low to low resistivity ranging between 0.5 and 1.86 Ω.m was observed.

Two dolerite dykes were visible on surface at stations 220 m and 490 m. At station 490 m a magnetic reading change of up to 688 nT was calculated. No significant change in magnetic readings were noticed at the dolerite dyke at station 220 m.

Two drilling targets, BH_T1_01 and BH_T1_02, were identified for inclined rotary core drilling at stations 250 m and 470 m respectively. These two borehole drilling targets were positioned in order to drill through the two dolerite dykes.

6.1.2 Profile T-2

The resistivity results from ERT profile T-2 can broadly be divided into three sections. The southwest section of the profile, starting at station 0 m, is characterised by a low-to-intermediate high resistivity zone from surface to an average depth of 15 mbgl, with resistivity ranging between approximately 36 and 180 Ω.m. At depth the southwest section is characterised by intermediate-to-high resistivity zone, ranging between 45 to 350 Ω.m. The second section is characterised by very low resistivity, located at the central portion, ranging between 10 – 35 Ω.m. The upper central portion of profile T-2 is characterised by a thin resistivity zone, not exceeding more than 2 to 3 m in depth. The resistivity of this thin upper portion ranges between 90 – 225 Ω.m. The third section located at the northeast portion of the profile, consists of an intermediate-to-high upper resistivity zone, ranging between 55 – 225 Ω.m from surface to an average depth of 20 m. At depth the zone is characterised by very high resistivity that exceeds 350 Ω.m.

The southwest section of the traverse had relatively uniform magnetic readings ranging between 30 893 and 31 000 nT. The northeast section of the traverse had erratic magnetic readings that ranged between 30847 and 30995 nT.

A change in soil colour and texture was noticed between station 210 m and 230 m. One inclined drilling position, BH_T2_01, was proposed at station 225m in order to target the low resistivity zone at the central part of the traverse that potentially represents the ZB fault.

6.1.3 Profile T-3

The shallow portion of the traverse, up to an average depth of approximately 20 m below surface, is characterised by low to intermediate high resistivity. The resistivity of the shallow zone ranged between 2.44 and 134.5 Ω.m. The southeast section at depth, between stations 0 m and 420 m, is characterised by intermediate high resistivity, ranging between 16 and 186 Ω.m. The northwest section of the profile, at depth, is characterised by high to very high resistivity values ranging between 300 and 642 Ω.m.

The magnetic survey broadly indicated three magnetic anomalies at stations 150m, 500m, and 760m, with a total change in magnetic readings of 19 nT, 160 nT, and 391 nT respectively.

No drilling target was proposed for profile T-3 as access to the site was inaccessible for a drilling rig during the fieldwork phase.

6.1.4 Profile T-4

Profile T-4 is characterised by very low to low resistivity along the entire traverse length. The shallow portion of the profile up to a depth of approximately 15 mbgl had very low resistivity ranging between 4.3 and 24.8 Ω.m. At depth the profile is characterised by low resistivity ranging between 60 and 101.2 Ω.m.

The magnetic readings along the traverse length did not change significantly and ranged between 31 363 nT and 31 429 nT.

No significant electrical resistivity or magnetic anomalies were identified. One proposed drilling position, BH_T4_01, was proposed at station 155m in order to potentially characterise the Karoo formation within the study site.

6.1.5 Profile T-5

The northwest section of the traverse between stations 0 m and 160 m is characterised by very low resistivity up to a depth of approximately 15 mbgl that ranges between 10 and 101 Ω.m. At depth the northwest section has very low to low resistivity ranging between 17.5 and 143 Ω.m. The southeast section of the traverse between stations 170 m and 300 m had intermediate high resistivity to a depth of approximately 7 – 15 mbgl ranging between 101 and 480 Ω.m. At depth the southeast section has very high resistivity ranging from 480 and in excess of 2 000 Ω.m. Between stations 160 m and 170 m a contact area at depth between the low and high resistivity zones were observed, with predominantly low resistivity ranging between 59 and 143 Ω.m.

The magnetic survey readings did not change significantly across the traverse length, except at station 170 m where a change of 277 nT was calculated.

Three boreholes were proposed to be drilled along profile T-5. Proposed borehole BH_T5_01, positioned at station 165 m, aims to target the contact zone between the high and low resistivity areas at depth, and the single ground magnetic survey anomaly. BH_T5_02 positioned at station 140 m aimed to target the Karoo formation and BH_T5_03 at station 200 m targeted the Basement formation.

6.1.6 Profile T-6

The resistivity can broadly be classified into two zones, a very low to low resistivity zone at the western section and an intermediate high to very high resistivity zone at the eastern section. The western section between stations 0 m and 165 m, up to a depth of approximately 20 mbgl, had very low to low resistivity ranging between 7 and 42.2 Ω.m. At depth the western section had low resistivity ranging between 59 and 242 Ω.m. The eastern section, between stations 165 m and 300 m, up to a depth of approximately 20 mbgl had intermediate high resistivity values between 143 and 342 Ω.m. At depth the eastern section is characterised by very high resistivity ranging from 581 and in excess of 2 000 Ω.m. A contact zone between the high and low resistivity zones at depth were noticed at station 165 m.

The magnetic readings across the traverse length did not change significantly, apart from a 557 nT change at station 220 m.

Two inclined borehole drilling positions, namely BH_T6_01 and BH_T6_02, were proposed at stations 190 m and 155 m respectively. Both drilling positions aim to target the contact zone between the high and low resistivity zones at depth.

6.1.7 Profile T-7

The resistivity results from Profile T-7 can be broadly divided into four sections. The southern section of the profile and the first approximate 160 m of the traverse, is characterised by an upper intermediate to high resistivity zone, ranging between 120 – 245 Ω.m, to an average depth of 5 – 10 m. The remaining parts of the southern section has low-to-intermediate high resistivity ranging between 40 – 370 Ω.m. The central portion of the profile is characterised by low resistivity, ranging between 0.5 – 5 Ω.m. The upper part of the central portion consists of a 10 m thick low-to-intermediate high resistivity zone, ranging between 40 – 120 Ω.m. The northern section of the profile consists of an intermediately high resistivity zone at depth, ranging between 14 – 120 Ω.m. The upper shallow zone of the northern portion of the profile has intermediate-to-high resistivity, ranging between 40 – 245 Ω.m, located at a depth of between 10 – 15 m. At the deeper part of the central portion, it appears that there potentially may be a transition to a very high resistivity zone that exceeds 370 Ω.m.

The magnetic readings did not change significantly along the traverse length, apart from an anomaly at station 50 m where a 195 nT change was observed.

The proposed drilling position at station 230 m (BH_T7_01) targeted the very low resistivity zone at shallow depths within the central portion of profile T-7.

6.1.8 Profile T-8

The results from ERT profile T-8 generally indicated high to very high resistivity throughout the profile length. At approximately 200 m and 300 m along the profile length very high resistivity zones exists, with resistivity exceeding 3 000 Ω.m. The entire profile is characterised by a shallow intermediate-to-high resistivity zone at an average depth of 10 m. The southern section of the profile consists of a generally high resistivity zone, ranging between 375 – 1 050 Ω.m. At approximately 220 m, at the central section of the profile, an intermediate high resistivity zone is observed and is located between the two very high resistivity zones.

The southeast section of traverse T-8 did not have recorded magnetic readings that significantly change. The northwest section between stations 260 m and 400 m had magnetic readings that varied between 31 480 nT and 30 963 nT.

Calcite outcrop was noticed at the northwest section of the traverse between 260 m and 340 m.

Proposed drilling position BH_T8_01, positioned at station 230 m, targeted the low resistivity zone between the two surrounding high resistivity zones.

6.1.9 Profile T-9

ERT profile T-9 can generally be classified into three sections. The eastern section up until 160 m along the profile length is characterised by a high to very high resistivity zone, with resistivity generally exceeding 370 Ω.m. The shallow upper portion of the eastern section up to a depth of 15 mbgl consists generally of a high resistivity zone, ranging between 245 – 720 Ω.m. The central section of the profile consists of a zone where the resistivity appears to gradually decrease along the profile length towards the western section. The resistivity of the central section ranges between 80 – 370 Ω.m. The western section is generally characterised by low-to-intermediate high resistivity, ranging between 1.5 – 40 Ω.m. The shallow upper zone of the western section is characterised by an intermediate high resistivity zone of approximately 120 Ω.m.

The magnetic survey readings did not change significantly along the traverse length. An anomaly was identified between stations 160 m and 180 m and had a total change in magnetic readings of 442 nT.

A dolerite dyke outcrop was noticed at station 180 m.

BH_T9_01, the proposed drilling position for profile T-9, targeted the contact zone between the low-to-intermediate high and the very high resistivity zones.

The 2D ERT pseudo-sections and magnetic survey results for Profiles T-1 to T-9 together with proposed drilling positions and orientations are given in Appendix A (Figure A-0-1 to Figure A-0-9).

6.2 Drilling

6.2.1 Rotary percussion air drilling

Boreholes BH_T4_01, BH_T5_01, BH_T5_02, BH_T5_03, BH_T7_01, BH_T8_01, BH_T9_01 and BH_TX_01 were drilled with an air percussion drilling rig. During the initial site reconnaissance, the proposed position of BH_TX_01 was set aside as a potential drilling location in order to target the geological contact fault between the Basement- and Karoo-formations. The site was previously cleared of vegetation and soil and the transition from Basement- to Karoo-formation was clearly visible on surface. No geophysical survey was conducted at this site and the drilling position was visually marked on surface.

6.2.1.1 BH_T4_01

No significant electrical resistivity or magnetic anomalies were identified during the geophysical survey. The goal of borehole BH_T4_01 was to intersect Karoo formation lithology. Borehole BH_T4_01 was drilled with the air percussion method to a depth of 106 mbgl and only Karoo formation was encountered. Completely weathered residual siltstone was encountered up to a depth of 3 mbgl. Highly weathered soft siltstone was encountered to a depth of 32 mbgl and slightly weathered coal was encountered from 32 – 41 mbgl. Slightly weathered siltstone was logged between 41 – 47 mbgl and slightly weathered sandstone between 47 – 61 mbgl. Slightly weathered siltstone was logged between 61 – 106 mbgl. Two water strikes were encountered at 12 mbgl and 75 mbgl and only seepage was measured as the final borehole blow yield.

6.2.1.2 BH_T5_01

Proposed borehole BH_T5_01 targeted the contact zone between the high and low resistivity areas at depth and the single magnetic survey anomaly which potentially represents the geological contact fault. Borehole BH_T5_01 was drilled using the air percussion drilling method to a depth of 60 mbgl and Basement and Karoo Supergroup formations were encountered. Highly weathered residual siltstone was present up to 8 mbgl and medium to slightly weathered Karoo Supergroup siltstone was encountered from 8 – 21 mbgl. Slightly weathered gabbro-anorthosite Basement formation was encountered from 21 – 60 mbgl. The contact zone between the Basement and Karoo formations represents the position of the unconformable geological contact fault. A single water strike was encountered at 48 mbgl and the final borehole blow yield was measured at 1.4 L/s.

6.2.1.3 BH_T5_02

BH_T5_02 targeted the Karoo formation lithology adjacent to the inferred geological contact fault. Borehole BH_T5_02 was drilled using the air percussion drilling method to a depth of 80 mbgl and Basement and Karoo Supergroup formations, as well as the geological contact fault were encountered. The upper 10 m consisted of completely weathered residual siltstone soil. Slightly weathered siltstone was encountered from 10 – 19 mbgl. Slightly weathered siltstone and coal occurred between 19 – 48 mbgl, and slightly weathered siltstone occurred from 48 – 49 mbgl. Slightly weathered Basement occurred at the last drilling section between 49 – 80 mbgl, and the geological contact fault between the Basement and Karoo formations is represented at 49 mbgl. One water strike was struck at a depth of 58 mbgl and the final borehole blow yield was measured at 0.25 L/s.

6.2.1.4 BH_T5_03

BH_T5_03 targeted the Basement formation lithology adjacent to the inferred geological contact fault. Borehole BH_T5_03 was drilled with the air percussion method to a depth of 60 mbgl and only Basement formation was encountered. Completely weathered residual gabbro-anorthosite soil was encountered to a depth of 18 mbgl and slightly weathered gabbro-anorthosite encountered from 18 – 60 mbgl. No water strike was encountered and only seepage was measured as the final borehole blow yield.

6.2.1.5 BH_T7_01

Borehole BH_T7_01 targeted the low resistivity zone and the possible high resistivity zone at depth at the central section of ERT profile T-7 and the geology encountered during air percussion drilling to a total depth of 50 mbgl. Highly weathered gabbro-anorthosite colluvium up to 8 mbgl was encountered and medium to slightly weathered Karoo Supergroup siltstone between 8 – 26 mbgl. Slightly weathered Basement gabbro-anorthosite was present from 26 – 50 mbgl, and the contact between the Basement and sedimentary formations, which represents the ZB fault, is characterised by black highly weathered material at 26 mbgl. Two water strikes were encountered at 26 mbgl and 46 mbgl, and the final borehole blow yield was measured at 0.31 L/s.

6.2.1.6 BH_T8_01

The low resistivity zone at the central section of ERT profile T-8 located between the two very high resistivity zones was the target area for drilling. Borehole BH_T8_01 was drilled

with the air percussion method to a depth of 60 mbgl and only Basement formation was encountered. Highly weathered gabbro-anorthosite was encountered to a depth of 14 mbgl and slightly weathered gabbro-anorthosite encountered from 14 – 60 mbgl. A single water strike was encountered at 47 mbgl and only seepage was measured as the final borehole blow yield.

6.2.1.7 BH_T9_01

The central transitional section between the eastern high resistivity and the western low resistivity sections of ERT profile T-4 was the target area for drilling. Borehole BH_T9_01 was drilled using the air percussion drilling method to a depth of 50 mbgl and Basement- and Karoo Supergroup-formations were encountered. Highly weathered gabbro-anorthosite colluvium was present up to 14 mbgl and medium to slightly weathered Karoo Supergroup siltstone was encountered from 14 – 23 mbgl. The ZB fault and contact zone at 23 mbgl was characterised by black and highly weathered material and slightly weathered gabbro-anorthosite Basement formation was encountered from 23 – 50 mbgl. A single water strike was encountered at 47 mbgl and the final borehole blow yield was measured at 12 L/s.

6.2.1.8 BH_TX_01

Proposed borehole BH_TX_01 targeted the geological contact fault between the Basement and Karoo formations. The transition from Basement to Karoo formation was visible on ground surface, as the site has previously been cleared of vegetation and the top soil horizon. No geophysical survey was conducted and the drilling position for BH_TX_01 was visually determined. Borehole BH_TX_01 was drilled using the air percussion drilling method to a depth of 100 mbgl and Basement-and Karoo-formations were encountered. Highly weathered siltstone was present up to 9 mbgl and medium weathered Karoo Supergroup siltstone was encountered from 9 – 26 mbgl. Slightly weathered gabbro-anorthosite Basement formation was encountered from 26 – 100 mbgl. The contact zone between the Basement- and Karoo-formations represents the position of the unconformable geological contact fault at 26 mbgl. A single water strike was encountered at 46 mbgl and the final borehole blow yield was measured at 0.1 L/s.

6.2.2 Inclined hydraulic-rotary core drilling

Boreholes BH_T1_01, BH_T1_02, BH_T2_01, BH_T6_01 and BH_T6_02 were drilled with a rotary core drilling rig and positioned at an angle of 70 degrees to the horizontal.

6.2.2.1 BH_T1_01

Borehole BH_T1_01 targeted the dolerite dyke that was visible on surface. The geophysics survey did not show clear anomalies within close proximity to the dyke location on surface. Borehole BH_T1_01 was drilled to a total drilling length of 53.06 m (approximately 45.95 mbgl) with the use of inclined core drilling and at an angle of 70 degrees to the horizontal in an approximately easterly direction. Approximately 11 m of residual soil and completely weathered Karoo Supergroup sandstone were encountered, and medium weathered Karoo formation sandstone was present between 11 – 29 m. Black and slightly weathered siltstone and coal were present between 29 m and 38 m. A slightly weathered Karoo Supergroup dolerite intrusion was encountered between 38 – 43.5 m. Black and slightly weathered siltstone and coal were also present below the dolerite dyke between 43.5 m and 49 m. Grey and slightly weathered siltstone was encountered between 49 m and 53.06 m. The strike of the dolerite dyke is approximately NW-SE.

6.2.2.2 BH_T1_02

Borehole BH_T1_02 targeted the second dolerite dyke that was visible on surface along geophysics traverse T1. The ERT survey did not show a clear anomaly within close proximity to the dyke location on surface. However, the magnetic survey showed a significant magnetic anomaly in close proximity to the dyke on surface. Borehole BH_T1_02 was drilled to a total drilling length of 125.08 m (approximately 108.32 mbgl) with the use of inclined core drilling and at an angle of 70 degrees to the horizontal in an approximately westerly direction along the geophysics traverse. Approximately 9 m of residual soil and completely weathered Karoo Supergroup sandstone were encountered, and medium-to-slightly weathered Karoo formation sandstone were present between 9 – 91 m. Slightly weathered Karoo Supergroup dolerite intrusion was encountered between 91 – 116 m. Black and slightly weathered siltstone was also present below the dolerite dyke between 116 m and end-of-hole (EOH) at 125.08 m. The dolerite dyke strikes parallel to the dyke identified at BH_T1_01 in a NW-SE direction.

6.2.2.3 BH_T2_01

The drilling position of borehole BH_T2_01 targeted the contact zone between the very high resistivity of the northeast section and the very low resistivity of central section of the ERT profile T-2. Borehole BH_T2_01 was drilled to a total drilling length of 71.12 m (approximately 60 mbgl) with the use of inclined core drilling and at an angle of 70 degrees to the horizontal in an approximately northeast direction. Approximately 14 m of residual soil and completely weathered Karoo Supergroup siltstone were encountered, medium to slightly weathered coal and highly fractured intercalated siltstone and sandstone of the Karoo Supergroup were present between 14 – 33 m. Slightly weathered Karoo Supergroup dolerite intrusion was encountered between 33 – 47 m, and Basement gabbro-anorthosite between 47 – 71 m. The contact between the Karoo Supergroup formations and the Basement gabbro-anorthosite was characterised by a black, highly weathered and fractured zone at 47 mbgl, with soft clay infill material. The ZB fault was at the contact area at 47 m. During drilling, water loss was experienced at approximately 19 m.

6.2.2.4 BH_T6_01

Borehole BH_T6_01 targeted the contact zone between the high and low resistivity zones at depth. Borehole BH_T6_01 was drilled to a total drilling length of 137.05 m (approximately 118.69 mbgl) with the use of inclined core drilling and at an angle of 70 degrees to the horizontal in an approximately north westerly direction. Highly weathered gabbro-anorthosite was encountered to a depth of 14 mbgl and slightly weathered gabbro-anorthosite encountered from 14 – 60 mbgl. Unweathered gabbro-anorthosite was encountered from 60 – 138.05 m. BH_T6_01 was not successful in drilling through the inferred geological fault contact and into the Karoo formations. During drilling, water loss was experienced at 31 m.

6.2.2.5 BH_T6_02

The drilling position for borehole BH_T6_02 was set as a secondary drilling target, as BH_T6_01 failed to drill into the inferred geological contact between the Basement- and Karoo-formations. A tractor loader backhoe (TLB) was used to dig a single test pit 35 m to the northwest of BH_T6_01. The results from the shallow excavated test pit confirmed the presence of Karoo formation lithology. Borehole BH_T6_01 was drilled to a total drilling length of 40.12 m (approximately 34.75 mbgl) with the use of inclined core drilling and at an angle of 70 degrees to the horizontal in an approximately south easterly direction.

Approximately 2 m of colluvium was encountered, originating from the surrounding Basement formation hillside. Highly weathered shale of the Karoo Supergroup was present between 2 – 18 m. Highly weathered and fractured mudstone was encountered from 18 – 21 m. A highly weathered and fractured Karoo Supergroup dolerite intrusion with a soft intact clay infilling was encountered between 21 – 26 m. Moderately weathered mudstone was encountered from 26 – 28 m. Moderately weathered Basement gabbro-anorthosite was encountered between 28 – 40.12 m. The contact between the Karoo Supergroup formations and the Basement gabbro-anorthosite is characterised by a black, highly weathered and fractured zone at 21 mbgl and 26 mbgl, with soft clay infill material. The geological fault contact was located at 28 m.

6.2.3 Summary of geophysical survey and drilling results

The Basement formations intersected during drilling were associated with very high resistivity zones that ranged between 350 – 3 000 Ω.m. The resistivity values for the Basement formations generally agree with literature values stated by Telford et al. (1990) for gabbro formations ranging between 10^3 – 10^6 Ω.m. Furthermore, a study conducted by Chirindja et al. (2017) found Precambrian Basement formation resistivity, in northeast Mozambique, ranging between 220 – 5 000 Ω.m. The Basement formations encountered during drilling indicated the presence of predominantly completely-to-slightly weathered gabbro-anorthosite. Majority of the Basement gabbro-anorthosite samples examined during geological logging generally indicated slightly weathered and very hard rock formations, accounting for the relatively high resistivity observed from the ERT survey results.

The Karoo Supergroup formations were characterised by low to intermediately high resistivity zones ranging between 40 – 370 Ω.m, which fall within the stated range for clastic sedimentary formations stated by Telford et al. (1990) and observations made by Zielke-Olivier and Vermeulen (2017). Resistivity values given by Telford et al. (1990) for fine grained clastic rocks range between 20 - 10^3 Ω.m. Resistivity values of the Karoo Supergroup formations in central South Africa, in a study conducted by Zielke-Olivier and Vermeulen (2017) ranged between 10 – 10^2 Ω.m. Drilling results indicated Karoo formations consisting of predominantly completely-to-slightly weathered siltstone, coal, and sandstone.

The geophysics survey did not show clear anomalies within close proximity to the identified dyke location on surface at BH_T1_01 and the ERT survey did not show a clear anomaly within close proximity to the dyke location on surface at BH_T1_02. Telford et al. (1990)

highlights the point that a buried magnetic object may not always be detected by magnetic survey methods, as these methods depend on both the direction of magnetisation of the magnetic minerals contained in the rock and on the Earth' magnetic field. However, the magnetic survey showed a significant magnetic anomaly in close proximity to the dyke on surface at BH_T1_02.

The geological contact- and ZB-faults were targeted by geophysical survey results where a contact zone between the very high and very low resistivity areas at depth were noticed. Drilling results from BH_T2_01, BH_T5_01, BH_T5_02, BH_T6_02, BH_T7_01, and BH_T9_01 indicated that the contact zone between the high and low ERT values represents the Basement- and Karoo-formations unconformable geological contact fault as well as the ZB fault located in the northeast section of the study site. Drilling results indicated that the contact fault is generally characterised by black, highly weathered and soft Karoo- and Basement-formation material.

Low yielding water strikes were generally encountered within boreholes at approximately 12, 26, 46 - 48, 58, and 75 mbgl and ranged between a rate of less than 0.1 L/s to 1.4 L/s. A single water strike was encountered at 47 mbgl in BH_T9_01 with a final measured borehole blow yield of 12 L/s. Boreholes that were drilled into only Basement formation lithology had very low blow yields of less than 0.1 L/s.

The geological borehole logs for the boreholes drilled with the use of vertical rotary percussion drilling are given in Appendix B and illustrated in Figure B-0-1 to Figure B-0-8. The geological borehole logs for the boreholes drilled with the use of inclined hydraulic-rotary core drilling are given in Appendix B and illustrated in Figure B-0-9 to Figure B-0-13. A summary of the drilling results and chosen aquifer testing method are given in Table 6-1.

Table 6-1: Drilling results summary indicating borehole method, encountered geology and chosen aquifer testing method.

Borehole ID & drilling method		Depth drilled [m]	Borehole Inclination	Water strike depth [mbgl]	Blow yield [L/s]	Geology	Aquifer test method
Inclined Core Boreholes	BH_T1_01	53.06	70°			Karoo/ Dyke	Packer testing
	BH_T1_02	125.08				Karoo/ Dyke	Packer testing
	BH_T2_01	71.12				Karoo/ Basement	Packer testing
	BH_T6_01	137.05				Basement	Packer testing
	BH_T6_02	40.12				Karoo/ Basement	Packer testing
Percussion Boreholes	BH_T4_01	106	90°	12, 75	Seepage	Karoo	Pumping testing
	BH_T5_01	60		48	1.4	Karoo/ Basement	Pumping testing
	BH_T5_02	80		58	0.25	Karoo/ Basement	Packer testing
	BH_T5_03	60		-	-	Basement	Pumping testing
	BH_T7_01	50		26, 46	0.3	Karoo/ Basement	Pumping testing
	BH_T8_01	60		47	Seepage	Basement	Pumping testing
	BH_T9_01	50		47	12	Karoo/ Basement	Pumping testing
	BH_TX_01	100		46	0.1	Karoo/ Basement	Packer testing

6.3 Aquifer testing

6.3.1 Packer tests

Packer testing was undertaken in order to determine hydraulic properties of various lithological units intersected during drilling. A total of 48 tests were carried out in 7 boreholes (BH_T1_01, BH_T1_02, BH_T2_01, BH_T5_02, BH_T6_01, BH_T6_02, and BH_TX_01) using both single and straddle packer configuration. Injection packer testing was undertaken whereby water was injected at several pressure steps. The variation of injection pressures gives a qualitative understanding of the conditions at the test section. Pressure and fluid rates were measured on surface during testing at regular intervals. True interval pressures at the packer depth were also measured at regular intervals by a downhole

pressure transducer. Due to the instability of the weathered zone and risk to possible collapse, no packer testing was conducted within the weathered zone. Packer tests were only conducted in fresh rock below the weathered zone and/or static groundwater level. Potentially permeable zones were identified through the geological logs and on-site core inspections.

Calculated hydraulic conductivity values are given below for each borehole tested section. Complete packer test results are given in Appendix A.

6.3.1.1 BH_T1_01

A total of six packer tests were conducted in BH_T1_01, consisting of one single packer test and five double packer tests. Relatively high permeability (2 x 10^{-2} m/d) was measured at the bottom interval from 44 to 53.06 mbgl within the Karoo Supergroup formation. Very low permeability (< 1 x 10^{-10} m/d) was measured in the remaining test section between 14 and 44 mbgl within the Karoo Supergroup sedimentary and dolerite lithology. Static groundwater level was measured at 9.86 mbgl before the start of the testing.

6.3.1.2 BH_T1_02

A total of 13 tests were conducted, consisting of one single packer test and 12 double packer tests between 14 and 113 mbgl. The borehole was blocked at 117 mbgl, preventing the lowering of the packers and the testing of the of the last section of the drilled borehole. Permeability was moderate from 103 to 113 mbgl (1.8 x 10^{-2} m/d) within the dolerite dyke and from 50 mbgl to 60 mbgl within the Karoo Supergroup, and generally extremely low throughout the rest of the borehole (< 1 x 10^{-10} m/d). Static groundwater level was measured at 7.84 mbgl. The packers experienced a slippage problem during the test of section 83 – 93 mbgl, whereby the packers were unable to remain in a fixed location. The main cause for this was potentially due to the softness of the Karoo formation sandstone within this section. The packers were lifted three metres and the test was restarted between 80 – 90 mbgl.

6.3.1.3 BH_T2_01

A total of six single packer tests were conducted in BH_T2_01 between 15 and 71.12 mbgl. Generally, very low permeability was encountered in the Karoo Supergroup, Zambezi Fault contact and Basement Complex from 20 to 71.12 mbgl (5 x 10^{-5} m/d). Very high permeability

was encountered in the Karoo Supergroup lithology from 15 to 20 mbgl (6.4 x 10^{-1} m/d). The static groundwater level was measured at 10.86 mbgl before packer testing.

6.3.1.4 BH_T5_02

A total of 6 test were conducted, 3 single packer tests between 50 and 80 mbgl within the Basement formations, and 3 double packer tests between 20 and 50 mbgl located within the Karoo formations and the geological contact fault zone. High permeability was encountered between 50 and 60 mbgl and from 20 to 30 mbgl, located in the Karoo formations. There was no permeability (< 1.0 x 10^{-10} m/d) from 60 to 80 mbgl in the Basement Complex, and moderately high permeability in the Karoo Supergroup and geological contact fault from 30 to 50 mbgl.

6.3.1.5 BH_T6_01

A total of 7 single packer tests were conducted in borehole BH_T6_01 that only intersected Basement formation. The only significant permeability was encountered between 30 and 50 mbgl (1.5 x 10^{-1} m/d). The single packer configuration was changed to a double packer configuration in order to determine the interval where higher permeability occurred between 7 to 40 mbgl. However, the borehole was blocked / collapsed at 31 mbgl. It is therefore likely that the permeability could have been between 30 to 40 mbgl, as water loss occurred during drilling at 31 mbgl and significant fracturing were observed during drill core inspection.

6.3.1.6 BH_T6_02

A total of 5 tests were conducted (1 single- and 4 double- packer configuration tests) in borehole BH_T6_02. High permeability (6.6 x 10^{-2} m/d) was measured from 32.3 to 40.12 mbgl within the Basement and Karoo formation contact zone. Very low permeability (< 1.0 x 10^{-10} m/d) was measured between 12.3 and 32.3mbgl within the Karoo Supergroup lithology and geological contact fault zone.

6.3.1.7 BH_TX_01

A total of 6 single packer tests were conducted in borehole BH_TX_01 between 30 to 100 mbgl. Permeability was generally low, with moderately high permeability (3.6 x 10^{-3} – 5.1 x 10^{-3} m/d) between 60 and 70 mbgl within the Basement formation, and moderately high to high permeability (7.4 x 10^{-2} m/d) from 30 to 40 mbgl within the Karoo formations and geological contact fault.

6.3.2 Pumping tests

A total of three SDT and six CDT and recovery tests were conducted. The test results are summarised for each borehole below and the aquifer parameters were estimated using the Cooper-Jacob (1946) solution for the calculation of aquifer transmissivity as discussed in section 4.4.2. Late-time data was used to determine the hydraulic characteristics from the pump test data.

6.3.2.1 BH_T7_01

Borehole BH_T7_01 had a blow yield approximately 0.31 L/s, indicating a potentially very low yielding borehole. Therefore, the multi rate testing for borehole BH_T7_01 consisted of three 60-minute steps at pumping rates of 0.2 L/s, 0.3 L/s, and 0.4 L/s. The pump was lowered to a depth of 49 mbgl, and static groundwater level was measured at 13.67 mbgl, resulting in an available drawdown of 35.33 metres. The CDT pumping rate was set at 0.2 L/s, as the drawdown for the first multi-rate tests was measured at 4.6 metres. The drawdown for the second and third multi-rate tests measured were relatively large, at 7.64 and 13.54 metres.

The CDT was conducted for a duration of 1350 minutes (22.5 hours), and the recovery test took approximately 560 minutes (9 hours) to recover to 96% of the groundwater level before the start of pumping testing. Boreholes BH_T8_01 and BH_T9_01 were equipped with electronic water level loggers and served as observation boreholes. Observation borehole BH_T8_01 (Basement formation) and BH_T9_01 (Basement/Karoo formations and ZB fault) are approximately 125 metres and 36 metres away, respectively, from testing borehole BH_T7_01.

The CDT was ended after 1350 minutes as the groundwater level reached the pump inlet depth. The pumping rate was limited by the minimum possible rate available from the submersible pump. The transmissivity of borehole BH_T7_01 was interpreted to be very low and calculated in the order of approximately 1 x 10^{-1} m^2/day, according to the Cooper-Jacob (1946) solution. No significant drawdown was measured in observation boreholes BH_T8_01. A maximum drawdown of 0.64 m was measured in observation borehole BH_T9_01.

6.3.2.2 BH_T8_01

Borehole BH_T8_01 had no measurable blow yield during the drilling phase, indicating a potentially very low yielding borehole. Therefore, no multi-rate testing for borehole BH_T8_01 was conducted and the CDT rate was initially set at a minimum pumping rate of 0.2 L/s. The pump was lowered to a depth of 59 mbgl, and static groundwater level was measured at 17.13 mbgl, resulting in an available drawdown of 41.87 metres.

The CDT test was conducted for a duration of 155 minutes (2.5 hours), and the recovery test took approximately 720 minutes (12 hours) to recover to the groundwater level before the start of pumping testing. Boreholes BH_T7_01 and BH_T9_01 were equipped with electronic water level loggers and served as observation boreholes. Observation borehole BH_T7_01 (Basement/Karoo formations and ZB fault) and BH_T9_01 (Basement/Karoo formations and ZB fault) are approximately 140 metres and 125 metres away, respectively, from testing borehole BH_T8_01.

The CDT was ended after 155 minutes as the groundwater level reached the pump inlet depth. Ideally, the pumping testing of BH_T8_01 should have exceeded at least eight hours. However, the pumping rate was limited by the minimum possible rate available from the submersible pump. The transmissivity of borehole BH_T8_01 was interpreted to be very low and calculated in the order of approximately 4.6 x 10^{-2} m^2/day, according to the Cooper-Jacob (1946) solution. Drawdown measured in observation boreholes BH_T7_01 and BH_T9_01 was less than 0.1 metres.

6.3.2.3 BH_T9_01

Measured blow yield of 12 L/s for borehole BH_T9_01 indicated a potentially high yielding borehole. Therefore, the multi rate testing for borehole BH_T9_01 consisted of three 60-minute steps at pumping rates of 2 L/s, 4 L/s, and 7 L/s. The pump was lowered to a depth of 46 mbgl, and static groundwater level was measured at 11.74 mbgl, resulting in an available drawdown of 34.26 metres. The final step of the multi-rate test resulted in a drawdown of 1.3 metres.

The pumping rate for the CDT was set at a maximum available pump rate of 8.0 L/s. The CDT was conducted for a duration of 960 minutes (16 hours), and the recovery test took approximately 190 minutes (3 hours) to recover to the groundwater level before the start of pumping testing. Boreholes BH_T8_01 and BH_T7_01 were equipped with electronic water level loggers and served as observation boreholes. Observation borehole BH_T8_01

(Basement formation) and BH_T7_01 (Basement/Karoo formations and ZB fault) are approximately 140 metres and 36 metres away, respectively, from testing borehole BH_T9_01.

At the end of the CDT, a total drawdown of 5.15 metres was measured and transmissivity of BH_T9_01 was calculated in the order of 80 m^2/day, according to the Cooper-Jacob (1946) solution. Pumping testing yield was limited by the maximum available yield of the available submersible pump. A maximum drawdown of 0.1586 metres was measured in observation borehole BH_T8_01. Borehole BH_T7_01 had a maximum drawdown of approximately 2.32 metres.

6.3.2.4 BH_T4_01

Borehole BH_T4_01 had no measurable blow yield during the drilling phase, indicating a potentially very low yielding borehole. Therefore, no multi-rate testing for borehole BH_T4_01 was conducted and the CDT rate was initially set at a minimum pumping rate of 0.2 L/s. The pump was lowered to a depth of 70 mbgl, and static groundwater level was measured at 2.20 mbgl, resulting in an available drawdown of 67.80 metres.

The CDT was conducted for a duration of 1681 minutes (28 hours), and the recovery test took approximately 245 minutes (±4 hours) to recover to the groundwater level before the start of pumping testing.

The CDT was ended after 1 681 minutes as the groundwater level reached the pump inlet depth. The transmissivity of borehole BH_T4_01 was interpreted to be very low and calculated in the order of approximately 8.3 x 10^{-1} m^2/day, according to the Cooper-Jacob (1946) solution.

6.3.2.5 BH_T5_01

Measured blow yield of 1.4 L/s for borehole BH_T5_01 indicated a potentially low to moderately high yielding borehole. Therefore, the multi rate testing for borehole BH_T5_01 consisted of four 60-minute steps at pumping rates of 1.2 L/s, 2.4 L/s, 3.0 L/s, and 4.5 L/s. The pump was lowered to a depth of 59 mbgl, and static groundwater level was measured at 12.13 mbgl, resulting in an available drawdown of 46.87 metres. The multi-rate test resulted in drawdowns of 2.4, 3.03, 4.01, and 31.23 metres, respectively for each multi-rate step.

The pumping rate for the CDT was set at 4.0 L/s. The CDT was conducted for a duration of 2 880 minutes (48 hours), and the recovery test took approximately 996 minutes (16.5

hours) to recover to 90% of the groundwater level before the start of pumping testing. Borehole BH_T5_03 was equipped with electronic water level loggers and served as an observation borehole. Observation borehole BH_T5_03 (Basement formation) is approximately 40 metres away from testing borehole BH_T5_01.

At the end of the CDT, a total drawdown of 23 metres was measured and transmissivity of BH_T5_01 was calculated in the order of 3 m^2/day, according to the Cooper-Jacob (1946) solution. A maximum drawdown of 1.96 metres was measured in observation borehole BH_T5_03.

6.3.2.6 BH_T5_03

Borehole BH_T5_03 had no measurable blow yield during the drilling phase, indicating a potentially very low yielding borehole. Therefore, no multi-rate testing for borehole BH_T5_03 was conducted and the CDT rate was initially set at a minimum pumping rate of 0.2 L/s. The pump was lowered to a depth of 59 mbgl, and static groundwater level was measured at 15.51 mbgl, resulting in an available drawdown of 43.49 metres.

The CDT was conducted for a duration of 60 minutes (1 hour), and the recovery test took in excess of 48 hours to completely recover to the groundwater level before the start of pumping testing. Borehole BH_T5_01 was equipped with electronic water level loggers and served as an observation borehole. Observation borehole BH_T5_01 (Basement/Karoo formations and geological fault contact) is approximately 40 metres away from testing borehole BH_T5_03.

The CDT was ended after 60 minutes as the groundwater level reached the pump inlet depth. Ideally, the pumping testing of BH_T5_03 should have exceeded at least eight hours. However, the pumping rate was limited by the minimum possible rate available from the submersible pump. The transmissivity of borehole BH_T5_03 was interpreted to be very low and calculated in the order of approximately 2.9 x 10^{-2} m^2/day, according to the Cooper-Jacob (1946) solution. Drawdown measured in observation boreholes BH_T5_01 was less than 0.1 metres.

6.3.3 Summary of aquifer testing results

6.3.3.1 Packer tests

The permeability of the Karoo formations was generally very low to moderately-high, ranging from less than 1.0 x 10^{-10} m/d to 6.4 x 10^{-1} m/d. Relatively high permeability (2.2 x 10^{-2} m/d) was measured from 44 to 53.06 mbgl in borehole BH_T1_01. Very high permeability was encountered from 15 to 20 mbgl (6.4 x 10^{-1} m/d) in the borehole that intercepted the ZB fault, borehole BH_T2_01. Permeability was also high between 20 to 30 mbgl and 50 to 60 mbgl in borehole BH_T5_02. Moderately-high permeability was encountered between 30 and 40 mbgl within borehole BH_T6_02.

Permeability of the dolerite dyke intercepted in borehole BH_T1_01 and BH_T6_02 was very low. However, permeability was moderately-high from 103 to 113 mbgl (1.8 x 10^{-2} m/d) within the dolerite dyke intercepted in borehole BH_T1_02. The top and bottom contact zones with the dolerite dyke in borehole BH_T1_02 and the top contact zone of the dolerite dyke in borehole BH_T1_01 had very low permeability.

The packer testing results indicated that the ZB fault generally had low to moderately high permeability. Generally, the permeability ranged from low to moderately-high within the geological fault contact zones.

Very low permeability was measured during packer testing in the Basement formations (< 1.0 x 10^{-10} m/d). The only significant permeability in the Basement formations were encountered between 30 and 50 mbgl (1.5 x 10^{-1} m/d) in borehole BH_T6_01, between 32.3 and 40.12 mbgl in borehole BH_T6_02, and between 60 and 70 mbgl within BH_TX_01.

The packer results indicating the test sections and results relative to the geological logs are given in Appendix C and illustrated in Figure C-0-1 to Figure C-0-7. The packer test results are summarised and given in Table 6-2.

Table 6-2: Packer testing results summary indicating test sections and calculated hydraulic conductivity.

Site ID		Test depth [mbgl]		Test section length [m]	Hydraulic Conductivity [m/day]
		From	To		
Incline core boreholes	BH_T1_01	14	20	6	0.00E+00
		20	26	6	0.00E+00
		26	32	6	0.00E+00
		32	38	6	0.00E+00
		38	44	6	0.00E+00
		44	53.06	9.06	2.23E-02
	BH_T1_02	14	20	6	0.00E+00
		20	26	6	0.00E+00
		26	32	6	0.00E+00
		32	38	6	0.00E+00
		38	44	6	0.00E+00
		50	60	10	5.38E-03
		60	70	10	0.00E+00
		70	80	10	0.00E+00
		80	90	10	0.00E+00
		83	93	10	0.00E+00
		93	103	10	0.00E+00
		103	113	10	1.79E-02
		44	125.08	81.08	2.49E-03
	BH_T2_01	15	20	5	6.39E-01
		20	71.12	51.12	5.11E-05
		30	71.12	41.12	5.19E-05
		35	71.12	36.12	5.84E-05
		45	71.12	26.12	1.04E-04
		48	71.12	23.12	0.00E+00
	BH_T6_01	30	50	20	1.51E-01
		50	137.05	87.05	9.84E-05
		70	137.05	67.05	1.21E-04
		90	137.05	47.05	8.58E-04
		98	137.05	39.05	1.28E-05
		108	137.05	29.05	3.06E-05
		118	137.05	19.05	6.31E-05
	BH_T6_02	17.3	22.3	5	2.08E-04
		22.3	27.3	5	0.00E+00
		27.3	32.3	5	3.36E-04
		32.3	40.12	7.82	6.58E-02
Percussion boreholes	BH_T5_02	20	30	10	1.42E-02
		30	40	10	5.11E-03
		40	50	10	3.57E-03
		50	60	10	7.41E-02
		60	80	20	0.00E+00
		70	80	10	0.00E+00
	BH_TX_01	30	100	70	5.18E-03
		40	100	60	1.80E-03
		50	100	50	1.80E-03
		60	100	40	2.37E-03
		70	100	30	1.86E-04
		90	100	10	3.10E-04

6.3.3.2 Pumping tests

The one borehole tested that intersected only Karoo formations, borehole BH_T4_01, had no measurable blow yield during the drilling phase and the transmissivity was interpreted to be very low and calculated in the order of approximately 8.3 x 10^{-1} m^2/day.

Boreholes BH_T5_03 and BH_T8_01 intersected Basement formations and the transmissivity was interpreted to be very low and calculated in the order of approximately 2.9 x 10^{-2} m^2/day – 4.6 x10^{-2} m^2/day. Drawdown measured in the observation boreholes that intersected Basement- and Karoo- formations, as well as geological fault contact and the ZB fault, was less than 0.1 metres.

Borehole BH_T5_01 intersected the geological fault contact between the Basement- and Karoo- formations and transmissivity was calculated in the order of 3 m^2/day. Drawdown of 1.96 metres was measured in the observation borehole BH_T5_03 that intersected Basement formation.

Boreholes BH_T7_01 and BH_T9_01 intersected Basement- and Karoo- formations as well as the regional ZB fault and the calculated transmissivity ranged between 1.1 x 10^{-1} m^2/day and 80 m^2/day. During the CDT of borehole BH_T7_01, no significant drawdown was measured in observation boreholes BH_T8_01 that intersected Basement formations. A maximum drawdown of 0.64 metres was measured in observation borehole BH_T9_01. At the end of the CDT of borehole BH_T9_01, a maximum drawdown of 0.16 metres was measured in observation borehole BH_T8_01 and borehole BH_T7_01 had a maximum drawdown of approximately 2.32 metres.

The processed pumping test and observation data are given in Appendix D and illustrated in Figure D-0-1 to Figure D-0-6. A summary of the pumping test results is given in Table 6-3.

Conceptual cross sections are given in Figure 6-1 to Figure 6-6 indicating the results from drilling and aquifer testing and zones with increased hydraulic conductivity.

Table 6-3: Pumping test results summary indicating SDT, CDT, and recovery test details and calculated aquifer transmissivities.

Site ID	Monitoring Borehole ID	Distance from pumping borehole [m]	Static Water Level	Geology	Pump Inlet Depth	Step Test			Constant Rate Test				Recovery		Transmissivity
						Duration	Yield	Maximum Drawdown	Duration	Yield	Available Drawdown	Maximum Drawdown			Cooper-Jacob (1946)
			[mbgl]		[mbgl]	[min]	[L/s]	[m]	[min]	[L/s]	[m]	[m]	[min]	[%]	[m²/day]
BH_T7_01	BH_T8_01	125	13.67	Karoo / Basement	49	60	0.2	4.6	1350	0.2	35.3	35.3	560	96	1.0E-01
	BH_T9_01	36				60	0.3	7.6							
						60	0.4	13.5							
BH_T8_01	BH_T7_01	140	17.13	Basement	59	N/A	N/A	N/A	155	0.2	41.9	41.9	720	99	4.6E-02
	BH_T9_01	125													
BH_T9_01	BH_T7_01	140	11.74	Karoo / Basement	46	60	2.0	0.4	960	8.0	34.3	5.15	190	99	8.0E+01
						60	4.0	0.7							
	BH_T8_01	36				60	7.0	1.3							
BH_T5_01	BH_T5_03	40	12.13	Karoo / Basement	59	60	1.2	2.4	2880	4.0	46.9	23.0	996	90	3.4E+00
						60	2.4	3.0							
						60	3.0	4.0							
						60	4.5	31.2							
BH_T4_01	N/A	N/A	2.2	Karoo	70	N/A	N/A	N/A	1681	0.2	67.8	67.8	245	99	8.3E-01
BH_T5_03	BH_T5_01	40	15.51	Basement	59	N/A	N/A	N/A	60	0.2	43.5	43.5	2880	99	2.9E-02

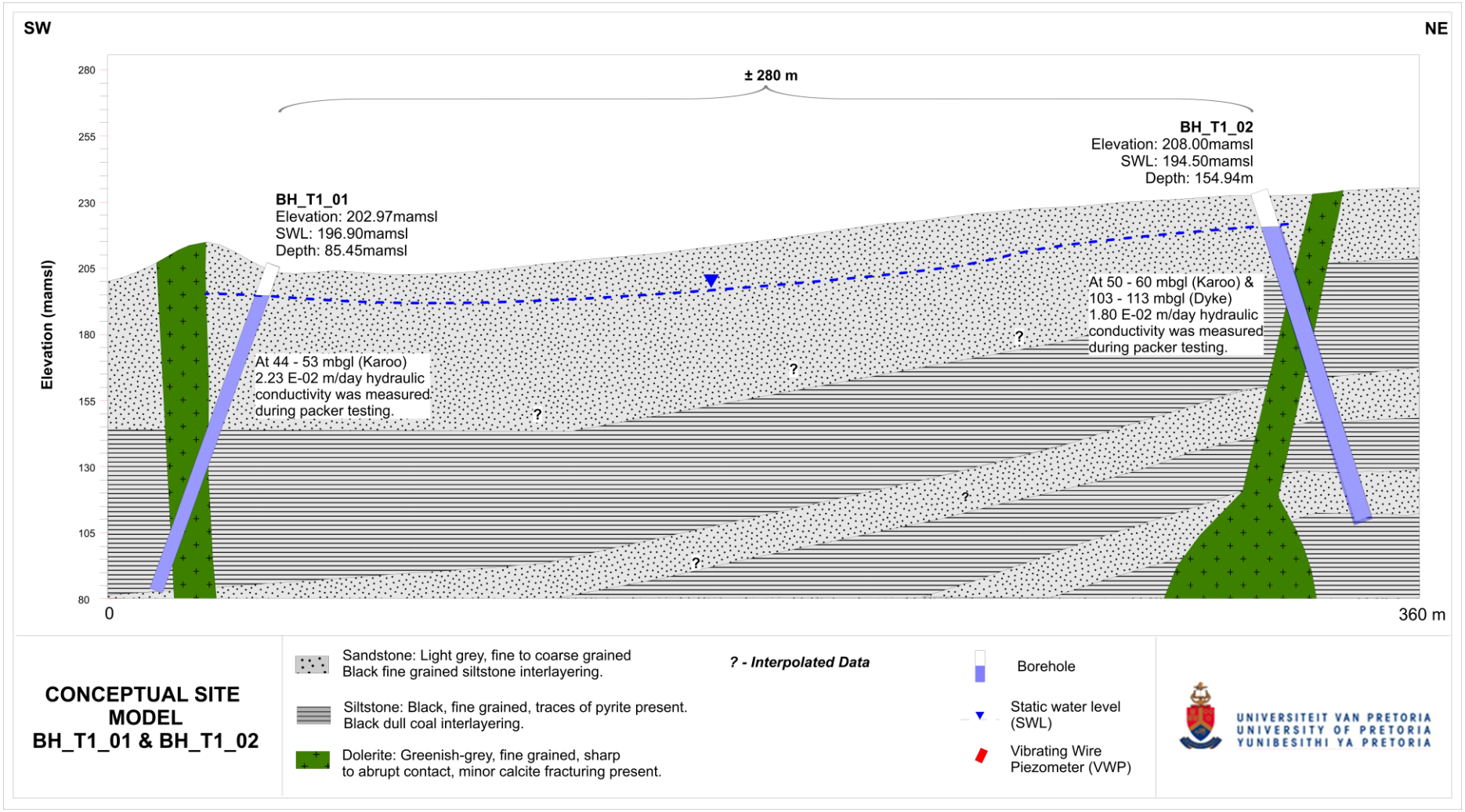

Figure 6-1: Conceptual site model for BH_T1_01 and BH_T1_02 indicating results from drilling and packer testing.

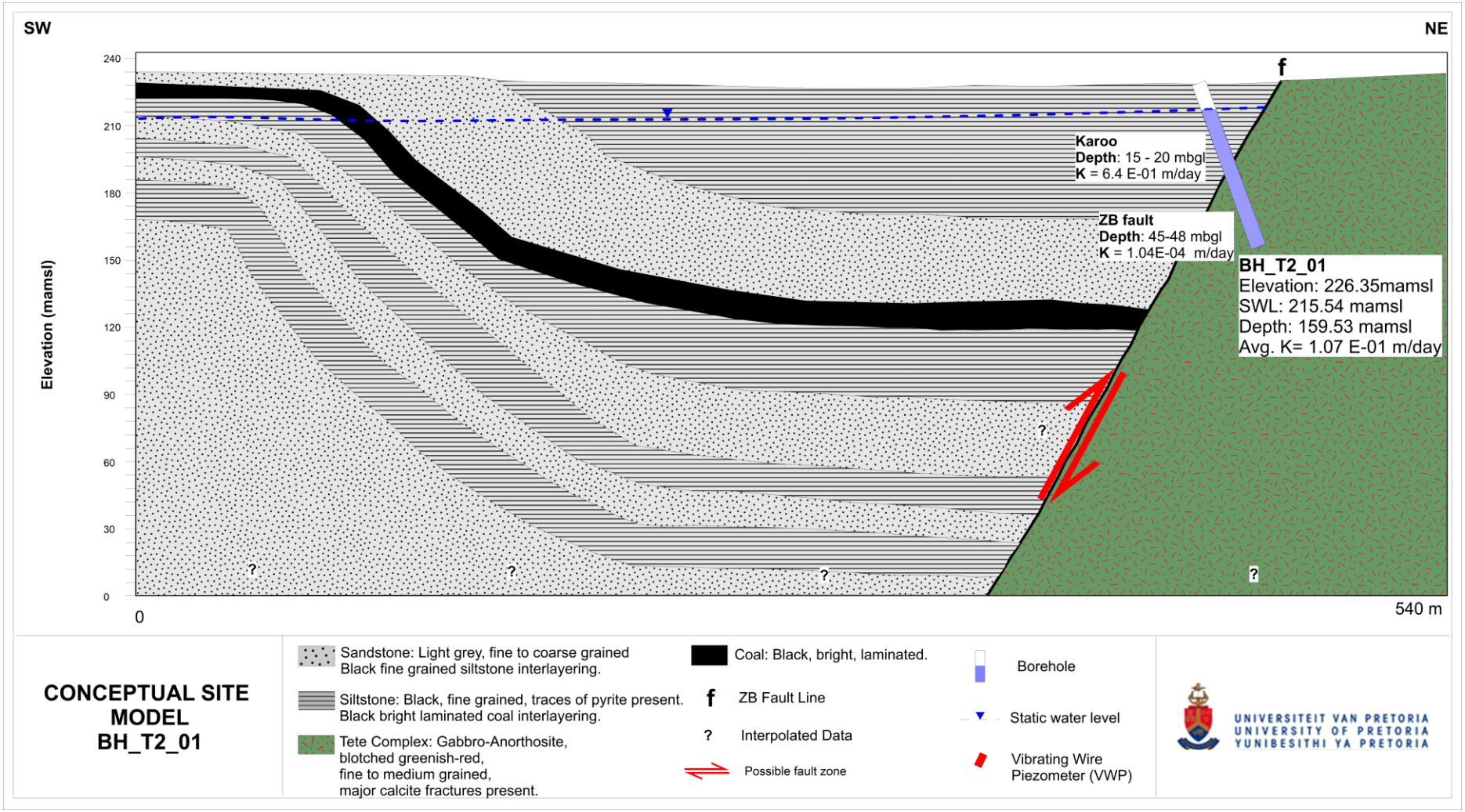

Figure 6-2: Conceptual site model for BH_T2_01 indicating results from drilling and packer testing.

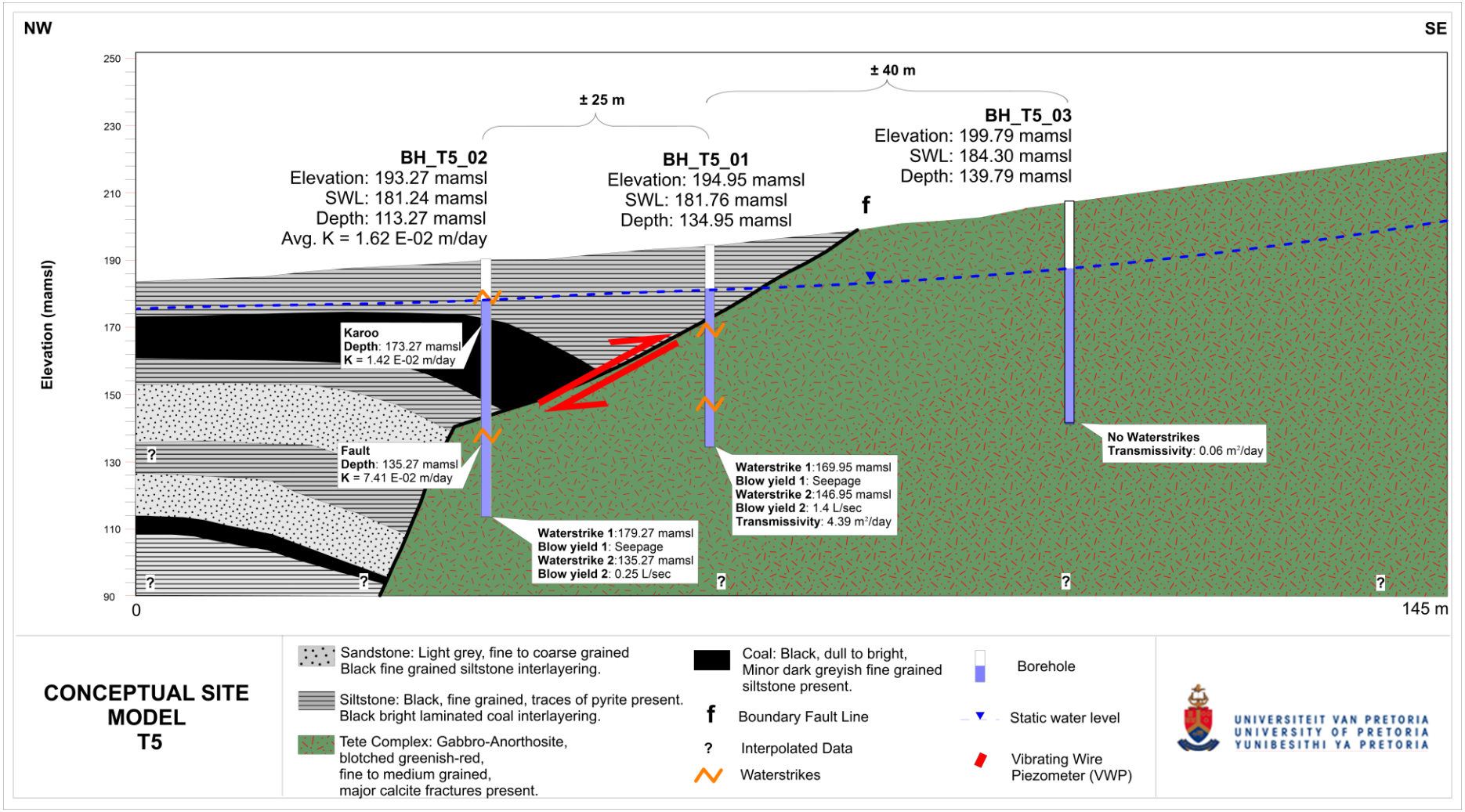

Figure 6-3: Conceptual site model for BH_T5_01, BH_T5_02 and BH_T5_03 indicating results from drilling and aquifer testing.

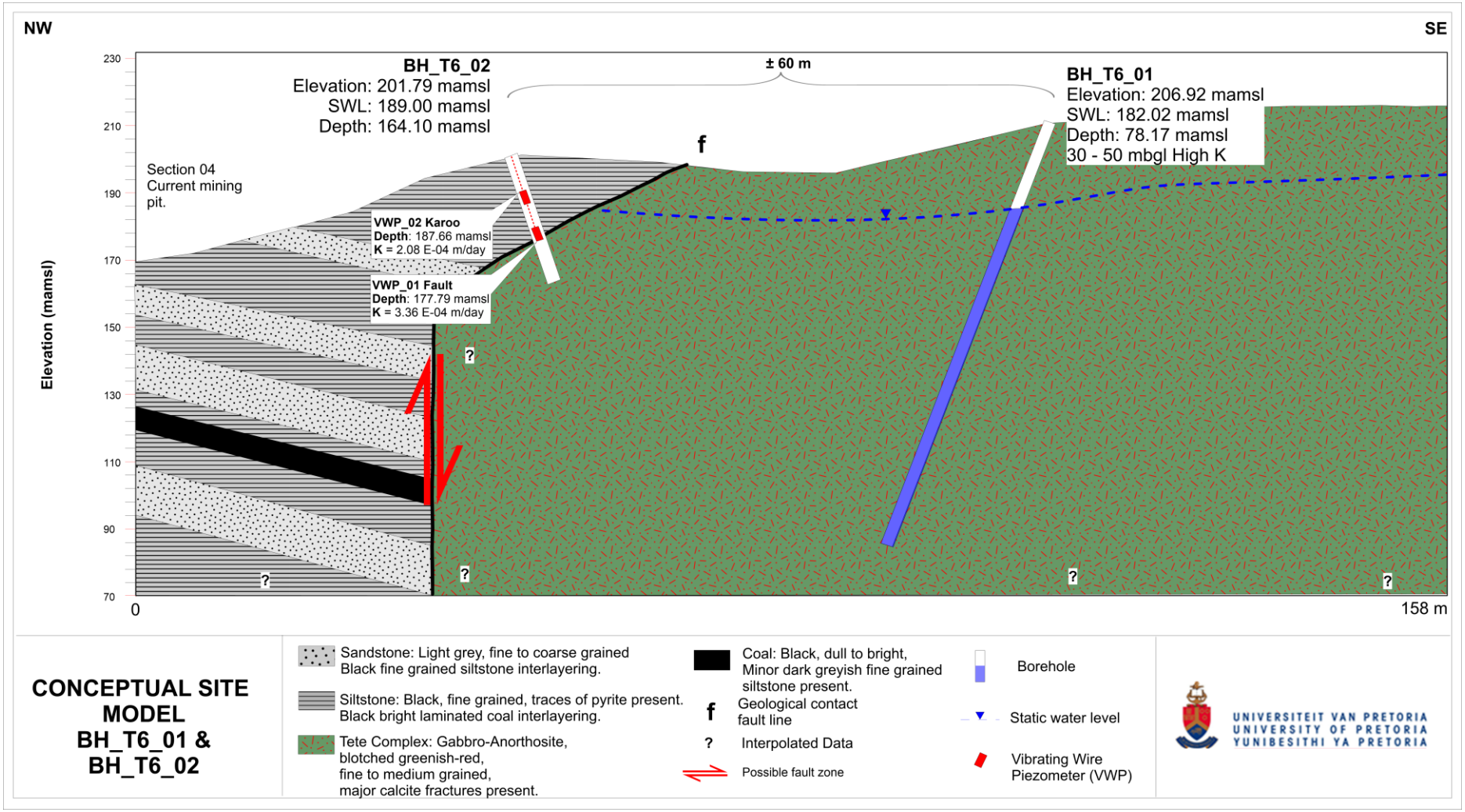

Figure 6-4: Conceptual site model for BH_T6_01 and BH_T6_02 indicating results from drilling and packer testing.

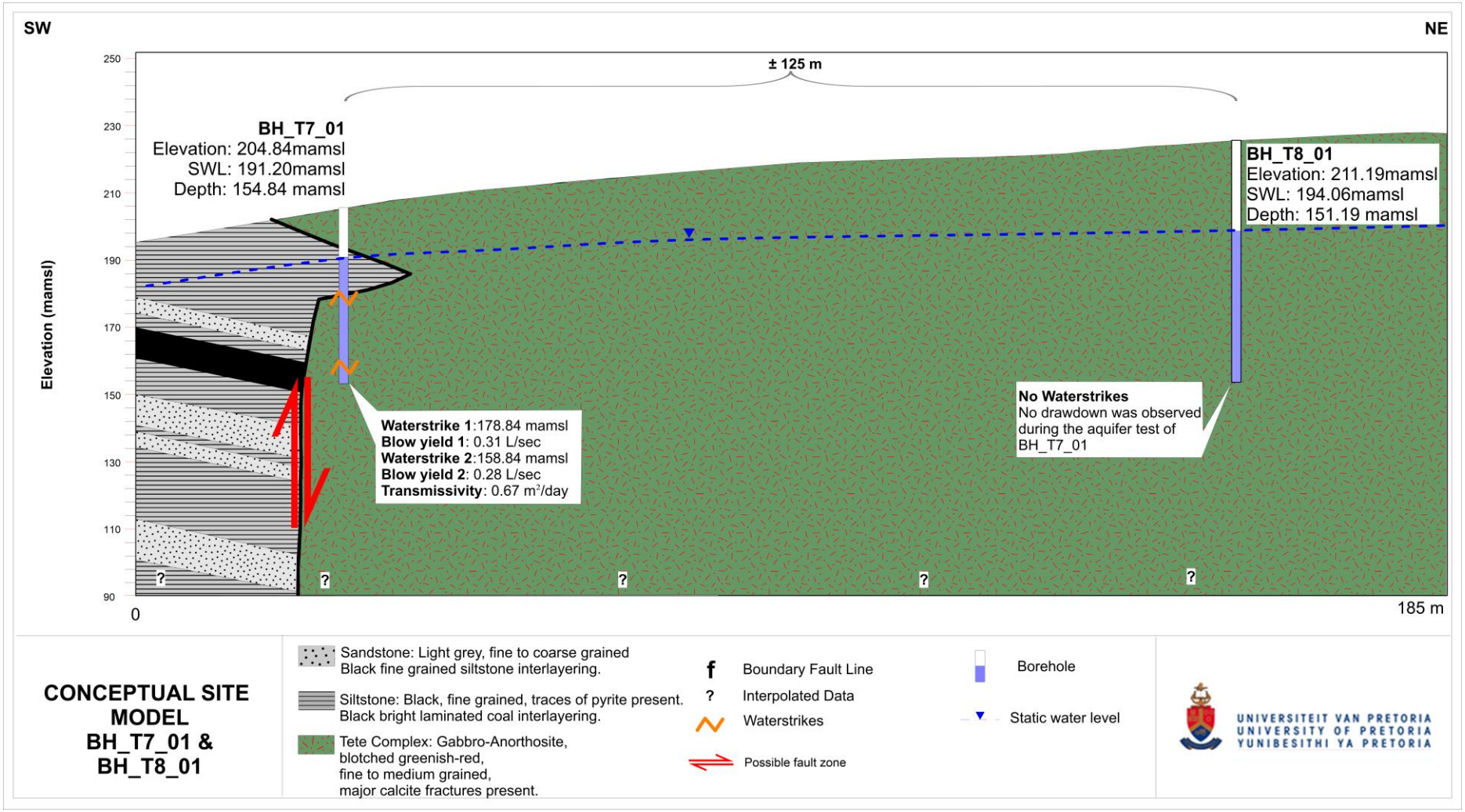

Figure 6-5: Conceptual site model for BH_T7_01 and BH_T8_01 indicating results from drilling and pumping testing.

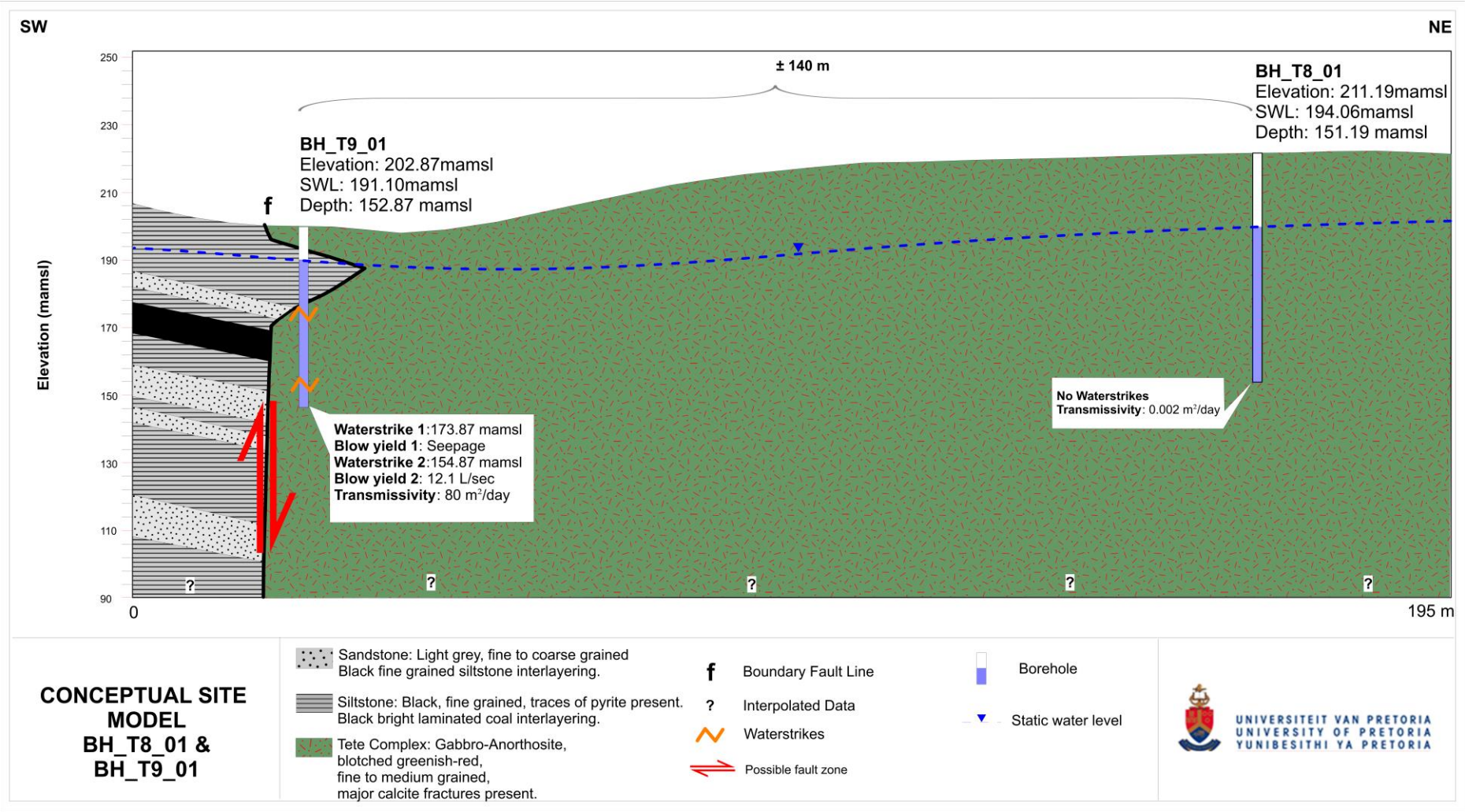

Figure 6-6: Conceptual site model for BH_T8_01 and BH_T9_01 indicating results from drilling and pumping testing.

6.4 Vibrating wire piezometers

Subsequent to the drilling and packer testing a total of 5 multilevel VWPs were installed in boreholes BH_T6_02 and BH_TX_01, within the Basement- and Karoo-formations as well as the geological contact faults. All VWP datalogger units were set to record measurements at two-hour intervals after the calibration, installation and stabilisation period.

6.4.1 BH_T6_02

BH_T6_02 intersected the Karoo- and Basement formations as well as the geological contact fault. Relatively high permeability was observed within the Karoo formation above the geological contact fault zone between 17.30 mbgl to 22.30 mbgl. Furthermore, relatively high permeability was observed in the geological contact zone between 27.30 mbgl to 32.30 mbgl. Two multilevel VWPs were installed within these relatively high permeable zones at 20.50 mbgl and 31 mbgl.

Figure 6-7 illustrates the hydrograph of the recorded BH_T6_02 VWP measurements between 10 October 2016 and 13 February 2017. The VWP recordings were plotted together with daily recorded rainfall at the site. After the grouting and stabilisation period, both VWPs showed a gradual decline in piezometric surface (mamsl). During the middle period of available monitored data, the VWPs showed no significant change in the piezometric surface. The piezometric surface of both VWPs started to increase approximately two months after the first measured rainfall event of the hydrological year. Region A of Figure 6-7 (b) shows that during the period of increasing piezometric surface, both VWPs equilibrated to approximately equal piezometric levels. Region B displayed a decrease in piezometric surface from 03-02-2017 up until 07-02-2017, which corresponded to the only external stress applied to the groundwater system, namely the CDT of BH_T5_01, conducted between 03-02-2017 and 05-02-2017. VWP 1 and VWP 2 showed a reduction in piezometric surface of 0.503 and 0.267 metres, respectively during this period. BH_T5_01 is located approximately 330 metres northeast of BH_T6_02.

No further data could be gathered after February 2017, during scheduled site visits, as borehole BH_T6_02 and all VWP instrumentation were destroyed.

6.4.2 BH_TX_01

Permeability was generally low throughout the entire borehole with moderate permeability between 60 and 70 mbgl within the Basement formation, and moderate-to-high permeability from 30 to 40 mbgl within the Karoo formation and geological contact fault.

Two multilevel VWPs were installed at these relatively high permeable zones at 65 mbgl and 32.10 mbgl. An additional vibrating wire piezometer was also installed in the geological contact fault at 25 mbgl.

Figure 6-8 illustrates the hydrograph of the recorded measurements between 10 October 2016 and 13 February 2017. The VWP recordings were plotted together with daily recorded rainfall at the site. After the grouting and stabilisation period, all three VWPs showed a gradual decline in piezometric surface (mamsl). During the middle period of available monitored data, the VWPs showed no significant change in the piezometric surface. The piezometric surface of all three VWPs increase approximately two months after the first measured rainfall event of the hydrological year. Region A of Figure 6-8 (b) shows a decrease in piezometric surface on 22-01-2017, which corresponded to the only external stress applied to the groundwater system, namely the CDT of BH_T7_01 conducted from 22-01-2017. Region B displayed a decrease in piezometric surface on 01-02-2017, which corresponded to the only external stress applied to the groundwater system at that time, namely the CDT of BH_T5_03, conducted from 01-02-2017. VWP 1 and VWP 2 showed a reduction in piezometric surface of 0.503 and 0.267 metres, respectively during this period. BH_TX_01 is located approximately 4.8 kilometres west of BH_T7_01 and 530 metres south of BH_T5_03. VWP1, VWP2 and VWP3 showed a reduction in piezometric surface of 0.201, 0.243, and 0.141 metres, respectively, during period A. During period B, VWP1, VWP2, and VWP3 showed a reduction in piezometric surface of 0.124, 0.437, and 0.307 metres, respectively.

No further data could be gathered after February 2017, during scheduled site visits, as borehole BH_TX_01 and all VWP instrumentation were destroyed.

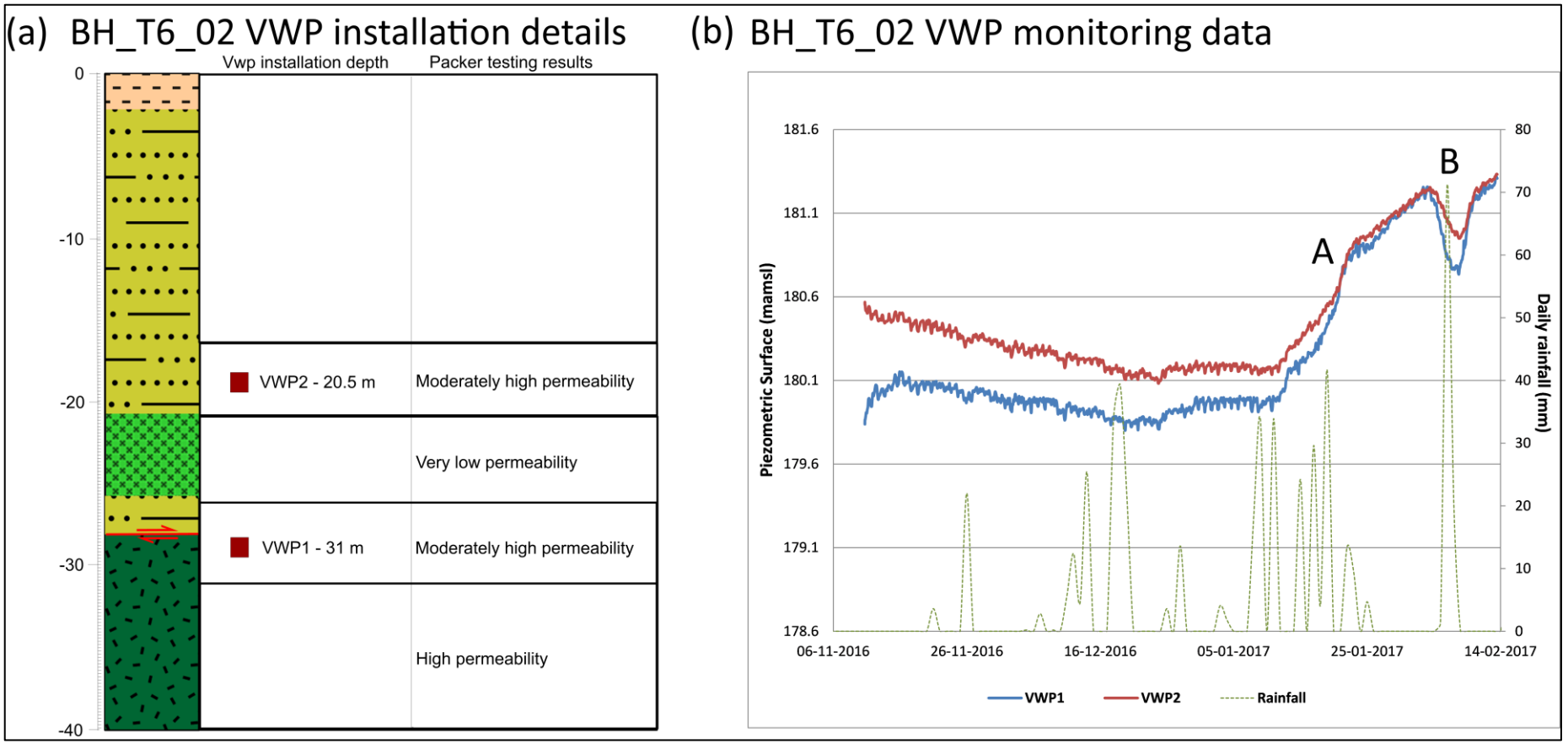

Figure 6-7: (a) Installed depths of BH_T6_02 VWPs. (b) Hydrograph of monitored piezometric surface (mamsl) data of BH_T6_02 VWPs plotted with daily recorded rainfall.

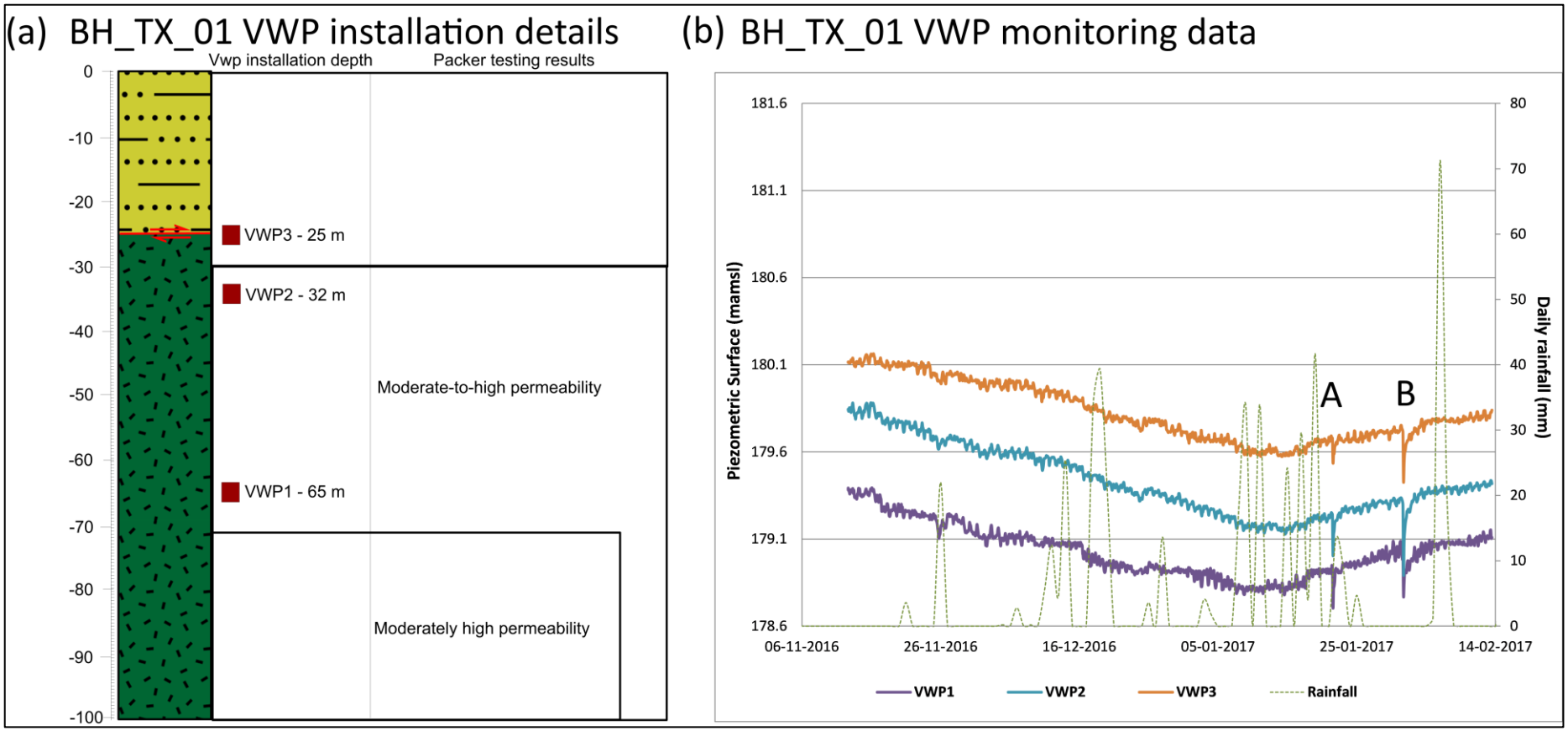

Figure 6-8: (a) Installed depths of BH_TX_01 VWPs. (b) Hydrograph of monitored piezometric surface (mamsl) data of BH_TX_01 VWPs plotted with daily recorded rainfall.

6.4.3 Summary of VWP monitoring results

A total of 5 multilevel vibrating wire piezometers (VWPs) were installed in boreholes BH_T6_02 and BH_TX_01, within the Basement- and Karoo-formations as well as the geological contact faults. The VWPs in both boreholes showed a delayed increase in piezometric surface approximately two months after the first rainfall event of the hydrological year.

Both VWPs in BH_T6_02 increased to approximately equal piezometric levels and continued to increase during the wet season. The CDT of BH_T5_01, located approximately 330 metres northeast of BH_T6_02, caused a decrease in the piezometric surface in both piezometers.

BH_TX_01 is located approximately 4.8 kilometres west of BH_T7_01, and the piezometric pressure in all three VWPs in borehole BH_TX_01 decreased during the CDT of borehole BH_T7_01. All three piezometers also showed a decrease in piezometric surface during the CDT of borehole BH_T5_03, located approximately 530 metres north of BH_TX_01.

7 DATA APPRAISAL

7.1 Geological faulting

The hydraulic properties of the boreholes that intersected the ZB fault and the geological contact fault were highly variable. Packer testing indicated a relatively large increase in permeability at the ZB fault location compared to the practically impermeable Basement formation. Packer testing results similarly indicated the geological contact fault zone had increased permeability compared to the Basement- and Karoo- formations. Pumping testing resulted in transmissivity ranging between 0.1 m^2/day and 80 m^2/day for the ZB fault and between 0.03 m^2/day and 3 m^2/day for the geological contact fault. The aquifer testing results agree with the statements made by Cook (2003), Kruseman and de Ridder (1994), Witthüser et al. (2011), and Woodford and Chevallier (2002) that in fractured rock aquifers the variability of hydraulic properties is often highly anisotropic. Furthermore, the very high transmissivity of BH_T9_01 is consistent with studies conducted by Kirchner (2009) in Basement formations and Chevallier et al. (2001) and Bredenkamp et al. (2017) in Karoo formations, stating that groundwater occurrence is increased due to the presence of fracturing, especially near faults and dolerite dykes. The low transmissivity of borehole BH_T7_01 and BH_T5_03 is consistent with results from studies conducted by Holland and Witthüser (2011) and Botha et al. (1998), concluding that although fractures are able to store and transmit water through them, the transmissivity of these secondary hydrogeological features is highly dependent on the dimension, fracture aperture, frequency and interconnectivity. The ZB- and geological contact- fault is characterised by a high degree of variability in hydraulic properties and is highly dependent on the characteristics of individual and fracture network.

The ZB- and geological contact-faults not only have a high degree of variability in hydraulic properties but also do not exhibit the characteristics of a barrier to groundwater flow. During the pumping testing of boreholes that intersected the ZB fault, drawdown was measured within the observation boreholes also located in the ZB fault but not in the single Basement formation observation borehole. The aquifer testing of a borehole intersecting the ZB fault resulted in a decrease in the piezometric surface of in all three vwps installed in a borehole located approximately 4.8 kilometres away. During the pumping testing of boreholes located in the geological contact faults, the observation boreholes also located in the geological contact faults had measurable drawdown. However, the borehole located within the Basement formation did not display any significant drawdown. Both boreholes

equipped with VWPs responded to the aquifer testing of the borehole that intersected the geological contact fault as well as the borehole that only intersected Basement formation in close proximity to the geological contact faulting. The measured drawdown observation data indicates that the ZB- and geological contact-faults cannot be barriers to groundwater flow. The observation boreholes located in Basement formation did not have any significant drawdown in excess of 0.1 metres, which may suggest the ZB- and geological contact- faults could be possible barriers to groundwater flow. However, this is most likely attributed to the very low hydraulic characteristics of the Basement aquifers as evident from the pumping test results. Holland and Witthüser (2011) found that generally all groundwater storage and movement in Basement aquifers are within secondary hydrogeological structures, since the matrix of the Basement formation has extremely low primary permeability. Aquifer testing resulted in drawdown in observation boreholes as well as a reduction in piezometric surface in the VWPs, indicating the ZB- and geological contact- faults are not barriers to groundwater flow.

7.2 Dolerite dykes

Dolerite dykes intersected within the study site had discreet zones of increased permeability. Packer testing results indicated that there were discreet zones of increased permeability present within two of the intersected dolerite dykes. The higher permeability supports the conclusion of Woodford and Chevallier (2002) stating that dolerite dykes of the Karoo Supergroup are typically associated with higher permeability. The relatively thin dyke intersected had very low permeability and was practically impermeable, which agrees with Wyk and Witthüeser (2011) stating that dolerite dykes may under certain circumstances act as semi- to impermeable- barriers to the movement of groundwater. All three dykes encountered within the study site trended NW-SE and exhibited variable hydraulic properties, as there were discreet zones of increased permeability as well as a dyke being completely impermeable, which does not completely support the statement made by Bredenkamp et al. (2017) that all NW-SE trending dolerite dykes in the Tete area are possible barriers to groundwater flow. The variable hydraulic nature of the NW-SE trending dolerite dykes within the study site agrees with the statement made by Woodford and Chevallier (2002), which stressed that the mechanism and degree of dyke fracturing ultimately determines groundwater occurrence. Not all the NW-SE trending dykes acted as

barriers to groundwater flow, as there were discreet intervals with relatively high permeability present.

8 CONCLUSIONS

One of the main characteristics of groundwater flow and occurrence in fractured rock aquifers are that they are structurally controlled (Dippenaar et al., 2009). The characteristics of fractured rock aquifers are highly dependent on several factors such as the composition of the host rock mass, neotectonics, weathering, climatic conditions (historic and prevailing), geomorphology, and intrusion of younger lithologies (Dippenaar and Van Rooy, 2014). Therefore, faults and dolerite dykes within Basement and Karoo aquifers in northern Mozambique may increase groundwater occurrence but may also be barriers to groundwater flow (Bredenkamp et al., 2017). Zones of increased groundwater occurrence are typical targets for water supply but constitutes a major operational challenge and potential hazard in certain sectors (i.e. mining).

The study site provided a unique opportunity to qualitatively determine the flow characteristics of several secondary hydrogeological features in northern Mozambique. The main objectives of the study were to:

- Determine if the regional Zambezi Boundary (ZB) Fault is a hydrogeological barrier to groundwater flow or not.
- Determine if geological contact faults between the Basement and Karoo aquifers are hydrogeological boundaries or not.
- Establish if northwest/southeast trending dolerite dyke intrusions are hydrogeological barriers or not.

Should observation boreholes drilled into these faults and dykes show a response to aquifer testing, it would be deduced that these features are not hydrogeological barriers to groundwater flow.

The study made use of a geophysical survey consisting of electrical resistivity tomography and ground magnetic to identify these secondary hydrogeological structures in the field. Drilling targets were identified primarily at inferred anomalies from the geophysical survey results. A percussion rotary drill rig was commissioned to drill the vertical test boreholes and a core drill rig was commissioned to undertake inclined core drilling. The Basement formations intersected during drilling were associated with very high resistivity zones and the Karoo formations were characterised by low to intermediately high resistivity zones. The geological contact and ZB faults were targeted where a contact zone between the very high and low resistivity areas at depth were noticed. Drilling results from six boreholes indicated

that the contact zone between the high and low resistivity zones represents the unconformable geological contact fault between the Basement and Karoo formations as well as the ZB fault located in the northeast section of the study site.

The secondary hydrogeological features intersected during drilling were subjected to aquifer testing. Five inclined rotary core and two vertical percussion boreholes underwent packer testing and six vertical percussion boreholes underwent pumping testing. After completion of the drilling and packer testing, two boreholes were selected for the installation of multi-level vibrating wire piezometers to monitor aquifer response due to pumping testing, natural piezometric surface fluctuations and rainfall events. Several observation boreholes, installed in different aquifer units, were also used to monitor the response of the aquifer units during pumping testing.

The ZB- and geological contact- fault is characterised by a high degree of variability in hydraulic properties and is highly dependent on the characteristics of individual and fracture network. Aquifer testing resulted in drawdown in observation boreholes as well as a reduction in piezometric surface in certain VWPs, indicating the ZB- and geological contact-faults are not barriers to groundwater flow. Dolerite dykes intersected within the study site had discreet zones of increased permeability. Not all the NW-SE trending dykes acted as barriers to groundwater flow, as there were discreet intervals with relatively high permeability present.

Basement- and Karoo-aquifers within the study site were characterised by the high degree of variability of hydraulic properties for both the secondary hydrogeological features and the primary rock matrix. The presence of local and regional faulting as well as dolerite dyke intrusions resulted in discreet zones of increased permeability within the Basement- and Karoo-aquifers, and these structures do not act as barriers to groundwater flow.

9 BIBLIOGRAPHY

Ajayakumar, P., Rajendran, S. and Mahadevan, T.M., 2017. Geophysical lineaments of Western Ghats and adjoining coastal areas of central Kerala, southern India and their temporal development. Geoscience Frontiers 8: 1089 – 1104.

Adams, S., 2009. Basement aquifers of southern Africa: Overview and Research Needs. *In:* Titus, R, Beekman, H, Adams, S, and Strachan, L (eds). The Basement Aquifers of Southern Africa. WRC Report No. TT 428-09. Water Research Commission, Pretoria.

Auken, E., Pellerin. L., Christensen, N.B., and Sorensen, K., 2006. A survey of current trends in near-surface electrical and electromagnetic methods. Geophysics 71: G249-G260.

Ajayakumar, P., Rajendran, S. and Mahadevan, T.M., 2017. Geophysical lineaments of Western Ghats and adjoining coastal areas of central Kerala, southern India and their temporal development. Geoscience Frontiers 8: 1089 – 1104.

Bakundukize, C., Mtoni, Y., Martens, K., Van Camp, M., and Walraevens, K., 2016. Poor understanding of the hydrogeological structure is a main cause of hand-dug wells failure in developing countries: A case study of a Precambrian basement aquifer in Bugesera region (Burundi). Journal of African Earth Sciences 121: 180-199.

Balakrishna, S., Balaji, S.M., and Narshimulu, G., 2014. Ground water in fractured aquifers of ophiolite formations, Port Blair, South Andaman Islands using electrical resistivity tomography (ERT) and vertical electrical sounding (VES). J Geol Soc India 83: 393-402.

Bear, J., 1993. Modeling Flow and Contaminant Transport in Fractured Rocks. From: Bear, J., Tsang, C. and de Marsily, G., Flow and Contaminant Transport in Fractured Rock, Academic Press, California, pp. 1 – 35.

Bicca, M.M., Philipp, R.P., Jelinek, A.R., Ketzer, J.M.M, dos Santos Scherer, C.M., Jamal, D.L. and dos Reis, A.D. 2017. Permian-Early Triassic tectonics and stratigraphy of the Karoo Supergroup in northwestern Mozambique. Journal of African Earth Sciences 130: 8-27.

Botha, J.F., Verwey, J.P., Van der Voort, I., Vivier, J.J.P., Colliston, W.P. and Loock, J.C., 1998. Karoo Aquifers. Their Geology, Geometry and Physical Behaviour. WRC Report No. 487/1/98. Water Research Commission, Pretoria.

Botha, J.F. and Cloot, A.H.J., 2004. Deformations and the Karoo aquifers of South Africa. Advances in Water Resources 27: 383-398.

Boulton, N.S. and Streltsova, T.D., 1977. Unsteady Flow to a Pumped Well in a Fissured Water-Bearing Formation. Journal of Hydrology, 35, pp. 257 – 270.

Braune, E. and Mutheiwana, S., 2009. Towards sustainable utilization of Basement aquifers in southern Africa. *In:* Titus, R, Beekman, H, Adams, S, and Strachan, L (eds). The Basement Aquifers of Southern Africa. WRC Report No. TT 428-09. Water Research Commission, Pretoria.

Bredenkamp, B., Levay, E., Marias, A. and van 't Zelfde, A. 2017. Finely discretized numerical flow model of complex multiple open pit mine for reliable inflow and pore pressure simulations – An African perspective. In: Wolkersdorfer, C., Sartz, L., Sillanpää, M. and Häkkinen, A. (eds.) Mine water and circular economy (Vol I). – p. 510 – 517. Lappeenranta, Finland (Lappeenranta University of Technology).

Bufford, K.M., Atekwana, E.A., Abdelsalam, M.G., Shemang, E., Atekwana, E.A., Mickus, K., Moidaki, M., Modisi, M.P. and Molwalefhe, L. 2012. Geometry and faults tectonic activity of the Okavango Rift Zone, Botswana: Evidence from magnetotelluric and electrical resistivity tomography imaging. Journal of African Earth Sciences 65: 61-71.

Campbell, S.A., Lenhardt, N., Dippenaar, M.A. and Götz, A.E., 2016. Geothermal energy from the Main Karoo Basin (South Africa): An outcrop analogue of Permian sandstone reservoir formations. Energy Procedia 97: 186-193.

Caputo, R., Piscitelli, S., Oliveto, A., Rizzo, E. and Lapenna, V. 2003. The use of electrical resistivity tomographies in active tectonics: examples from the Tyrnavos Basin, Greece. Journal of Geodynamics 36: 19-35.

Catuneanu, O., Wopfner, H., Eriksson, P.G., Cairncross, B., Rubidge, B.S., Smith, R.M.H. and Hancox, P.J. 2005. The Karoo basins of south-central Africa. Journal of African Earth Sciences 43: 211-253.

Chambers, J.E., Wilkinson, P.B., Weller, A., Meldrum, P.I., Kuras, O., Ogilvy, R.D., Aumonier, J., Bailey, E., Griffiths, N., Matthews, B., Penn, S. and Wardrop, D., 2011. Characterising sand and gravel deposits using electrical resistivity tomography (ERT): case histories from England and Wales. In: Hunger, E. and Walton, G. (eds.) Proceedings of the 16th extractive industry geology conference, EIG Conferences Ltd p. 166-172.

Chandra, S., Dewandel, B., Dutta, S. and Ahmed, S. 2010. Geophysical model of geological discontinuities in a granitic aquifer: analyzing small scale variability of electrical resistivity for groundwater occurences. Journal of Applied Geophysics 71: 137-148.

Chevallier, L., Goedhart, M. and Woodford, A.C., 2001. The influences of dolerite sill and ring complexes on the occurrence of groundwater in Karoo fractured aquifers: A morpho-tectonic approach. WRC Report No. 937/1/01. Water Research Commission, Pretoria.

Chirindja, F.J., Dahlin, T., Juizo, D. and Steinbruch, F. 2017. Reconstructing the formation of a coastal aquifer in Nampula province, Mozambique, from ERT and IP methods for water prospection. Environ Earth Sci 76: 36.

Colella, A., Lapenna, V. and Rizzo, E. 2004. High-resolution imaging of the High Agri Valley Basin (Southern Italy) with electrical resistivity tomography. Tectonophysics 386: 29-40.

Contreras, I.A., Grosser, A.T. and Ver Strate, R.H., 2008. The Use of the Fully-grouted Method for Piezometer Installation. Geotech News 26: 30 – 40.

Cook, N.G.W, 1982. Ground-water problems in open-pit and underground mines. Recent trends in Hydrogeology. In: Narasimhan, T.N. (Editor), Recent trends in hydrogeology. Geological Society of America, Special Paper 189. Boulder, Colorado, 69 pp.

Cook, P.G., 2003. A guide to regional groundwater flow in fractured rock aquifers. CSIRO, Australia.

Cooper, H.H. and Jacob, C.E., 1946. A generalized graphical method for evaluating formation constants and summarizing well field history. American Geophysical Union Transactions 27: 526–534.

Cushman, J. and Tartakovsky, D., 2017. The Handbook of Groundwater Engineering. Thrid ed. CRC Press, Boca Raton.

Dahlin, T. and Zhou, B. 2004. A numerical comparison of 2D resistivity imaging with 10 electrode arrays. Geophysical Prospecting 52: 379-398.

Deyassa, G., Kebede, S., Ayenew, T. and Kidane, T., 2014. Crystalline basement aquifers of Ethiopia: Their genesis, classification and aquifer properties. Journal of African Earth Sciences 100: 191-202.

Dippenaar, M.A., Witthüser, K.T., and Van Rooy, J.L. 2009. Groundwater occurrence in Basement aquifers in Limpopo Province, South Africa: model-setting-scenario approach. Environ Earth Sci 59: 459-464.

Dippenaar, M.A., van Rooy, J.L., Breedt, N., Huisamen, A., Muravha, S.E., Mahlangu, S. and Mulders, J.A., 2014. Vadose Zone Hydrology: Concepts and Techniques. WRC Report No. TT 584/13. Water Research Commission, Pretoria.

Dippenaar, M.A. and Van Rooy, J.L., 2014. Review of engineering, hydrogeological and vadose zone hydrological aspects of the Lanseria Gneiss, Goudplaats-Hout River Gneiss and Nelspruit Suite Granite (South Africa). Journal of African Earth Sciences 91: 12-31.

Dippenaar, M.A. and Van Rooy, J.L., 2016. On the cubic law and variably saturated flow through discrete open roughwalled discontinuities. International Journal of Rock Mechanics & Mining Sciences 89: 200-211.

Enslin, J.F., 1951. Geophysical methods of tracing and determining contacts of dolerite dykes in Karoo sediments in connection with the siting of boreholes for water. Trans. Geol. Soc. S Afr., V53, pp. 193 – 204.

Fernandes, P., Cogné, N., Chew, D.M., Rodrigues, B., Jorge, R.C.G.S., Marques, J., Jamal, D. and Vasconcelos, L., 2015. The thermal history of the Karoo Moatize-Minjova Basin, Tete Province, Mozambique: An integrated vitrinite reflectance and apatite fission track thermochronology study. Journal of African Earth Sciences 112: 55-72.

Freeze, R. and Cherry, J., 1979. Groundwater. Prentice Hall Inc.

Ganyaglo, S.Y., Osae, S., Akiti, T., Armah, T., Gourcy, L., Vitvar, T., Ito, M. and Otoo, I., 2017. Groundwater residence time in basement aquifers of the Ochi-Narkwa Basin in the Central Region of Ghana. Journal of African Earth Sciences 134: 590-599.

Gibson, P.J., Lyle, P. and George, D.M., 2004. Application of resistivity and magnetometry geophysical techniques for near-surface investigations in karstic terranes in Ireland. Journal of Cave and Karst Studies, v. 66, no. 2, pp. 35 – 38.

GTK, 2006. Explanatory notes of the 1:250.000 geological maps of sheets Mecumbura (1631), Chioco (1632), Tete (1633), Tambara (1634), Guro (1732,1733), Chemba (1734), Manica (1832), Catandica (1833), Gorongosa (1834), Rotanda (1932),

Chimoio (1933) and Beira (1934). Ministry of Mineral Resources, National Directorate of Geology, vol. II. GTK Consortium. Maputo, Mozambique, 499pp.

Hatton, W. and Fardell, A., 2012. New discoveries of coal in Mozambique – Development of the coal resource estimation methodology for international resource reporting standards. International Journal of Coal Geology 89: 2-12.

Holland, M. and Witthüser, K.T., 2011. Evaluation of geologic and geomorphologic influences on borehole productivity in crystalline bedrock aquifers of Limpopo Province, South Africa. Hydrogeol J 19: 1065-1083.

Jones, B.R., Van Rooy J.L. and Mouton, D.J., 2017. Verifying the ground treatment as proposed by the Secondary Permeability Index during dam foundation grouting. Bulletin of Engineering Geology and the Environment.

Kirchner, J., 2009. Basement aquifer Groundwater recharge, storage and flow. *In:* Titus, R, Beekman, H, Adams, S, and Strachan, L (eds). The Basement Aquifers of Southern Africa. WRC Report No. TT 428-09. Water Research Commission, Pretoria.

Kruseman, G.P. and De Ridder, N.A., 1994. Analysis and Evaluation of Pumping Test Data. Second ed. ILRI, The Netherlands.

Kumar, D., Mondal, S., Nandan, M.J. and Harini, P. 2016. Two-dimensional electrical resistivity tomography (ERT) and time-domain-induced polarization (TDIP) study in hard rock for groundwater investigation: a case study at Choutuppal Telangana, India. Arab J Geosci 9: 355.

Laletsang, K., Modisi, M.P., Shemang, E.M., Moffat, L. and Moagi, O.R., 2007. Shallow seismic refraction and magnetic studies at Lake Ngami, The Okavango Delta, Northwest Botswana. Journal of African Earth Sciences 48: 95 – 99.

Larsen, F., Owen, R., Dahlin, T., Pride, M., and Barmen, G., 2002. A preliminary analysis of the groundwater recharge to the Karoo formations, mid-Zambezi basin, Zimbabwe. Physics and Chemistry of the Earth 27: 765-772.

Loke, M.H. and Barker, R.D., 1996. Practical techniques for 3D resistivity surveys and data inversion. Geophysical Prospecting 44 (3): 499-523.

Loke, M.H. and Dahlin, T., 2002. A comparison of the Gauss-Newton and quasi-Newton methods in resistivity imaging inversion. Journal of Applied Geophysics 49: 149-162.

Lovell, C. J. (2009). Challenges of basement aquifers in southern Africa. In: Titus, R, Beekman, H, Adams, S, and Strachan, L (eds). The Basement Aquifers of Southern Africa. WRC Report No. TT 428-09. Water Research Commission, Pretoria.

MacDonald, A., Davies, J., Calow, R. and Chilton, J., 2005. Developing Groundwater: A guide for rural water supply. British Geological Survey, ITDG Publishing.

Macdonald, D.M.J. and Edmunds, W.M., 2014. Estimation of groundwater recharge in weathered basement aquifers, southern Zimbabwe; a geochemical approach. Applied Geochemistry 42: 86-100.

Marefat, V., Duhaime, F., Chapuis, R.P. and Le Borgne, V., 2017. Fully grouted piezometers in a soft Champlain clay deposit – Part I: Piezometer installation. Geotech News 35 (3): 35 – 38.

McClymont, A.F., Roy, J.W., Hayashi, M., Bentley, L.R., Maurer, H. and Langston, G. 2011. Investigating groundwater flow paths within proglacial moraine using multiple geophysical methods. Journal of Hydrology 399: 57-69.

Mikkelsen, P.E. and Green, G.E., 2003. Piezometers in fully grouted boreholes. International Symposium on Geomechanics. Oslo, Norway. September 2003.

Mojica, A., Pérez, T., Toral, J., Miranda, R., Franceschi, P., Calderón, C. and Vergara, F. 2017. Shallow electrical resistivity imaging of the Limón fault, Chagres River Watershed, Panama Canal. Journal of Applied Geophysics 138: 135-142.

Morton, K.L., Muresan, M.C. and Ramsden, F., 2008. Importance of Pore Pressure Monitoring in High Walls. The Southern Africa Institute of Mining and Metallurgy - Surface Mining, pp. 225 – 238.

Mussett, A.E. and Aftab Khan, M., 2000. Looking into the Earth: An introduction to geological geophysics. Cambridge University Press, United Kingdom.

Rizzo, E., Colella, A., Lapenna, V. and Piscitelli, S. 2004. High-resolution images of the fault-controlled High Agri Valley basin (Southern Italy) with deep and shallow electrical resistivity tomographies. Physics and Chemistry of the Earth 29: 321-327.

Royle, B.M., 2002. Standard operating procedures for borehole packer testing. Robertson GeoConsultants. Vancouver, BC, Canada.

SABS [South African Bureau of Standards], 1998. Code of Practice: Development, maintenance and management of ground water resources. Part 4: Test-pumping of

water boreholes. South African National Standard SANS 0299-4. SABS Standards Division. Pretoria.

Sami, K., 2009. Groundwater exploration and development in Basement aquifers in Botswana. *In:* Titus, R, Beekman, H, Adams, S, and Strachan, L (eds). The Basement Aquifers of Southern Africa. WRC Report No. TT 428-09. Water Research Commission, Pretoria.

Shuter, E. and Teasdale, W.E., 1989. Techniques of Water-Resouce Investigations of the United States Geological Survey. United States Geological Survey, Washington.

Simeoni, L., De Polo, F., Caloni, G. and Pezzetti, G., 2011. Field performance of fully grouted piezometers. *In:* Proceedings of the FMGM Congress.

Singhal, B.B.S., Gupta, R.P., 2010. Applied Hydrogeology of Fractured Rocks, second ed. Springer, New York.

SRK, 2014. Feasibility Study for the Tete Pig Iron and Ferro-Vanadium Project, Mozambique. Report No. 466974/Groundwater interim. Illovo, Johannesburg.

Suski, B., Brocard, G., Authemayou, C., Muralles, B.C., Teyssier, C. and Holliger, K. 2010. Localization and characterization of an active fault in an urbanized area in central Guatemala by means of geoelectrical imaging. Tectonophysics 480: 88-98.

Tamma Roa, G., Gurunadha, V.V.S., Padalu, G., Dhakate, R. and Subrahmanya Sarma, V. 2014. Application of electrical resistivity tomography methods for delineation of groundwater contamination and potential zones. Arab J Geosci 7: 1373-1384.

Telford, W.M, Geldart, L.P. and Sheriff, R.E. 1990. Applied geophysics. 2nd edition. Cambridge University Press, Cambrige, 770 pp.

Thiem, G., 1906. Hydologisch Methoden. J.M. Gebhardt, Leipzig, pp. 56.

Van Wyk, Y. and Witthueser, K., 2011. A forced-gradient tracer test on the Hansrivier Dyke: Beaufort West, South Africa. Water SA Vol. 37 No. 4. Water Research Commission, Pretoria.

Vasconcelos, L., Chafy, A. and Xerinda, L. 2014. Determination of the limit of oxidation in zones of sub-outcropping Chipanga Coal Seam, Moatize Coal Basin, Mozambique. Journal of African Earth Sciences 99: 554-567.

Wan, M.S.P. and Standing, J.R., 2014. Lessons learnt from installation of field instrumentation. Geotechnical Engineering 167: 491 – 506.

Weight, W.D., 2008. Hydrogeology field manual. McGraw Hill.

Woodford, A.C. and Chevallier, L., 2002. Hydrogeology of the main Karoo Basin: Current Knowledge and Future research needs. WRC Report No. 653/1/02. Water Research Commission, Pretoria.

Yihdego, Y., 2017. Hydraulic In situ Testing for Mining and Engineering Design: Packer Test Procedure, Preparation, Analysis and Interpretation. Geotech Geol Eng 35: 29 – 44.

Zhou, W., Beck, B.F. and Stephenson, J.B. 2000. Reliability of dipole-dipole electrical resistivity tomography for defining depth to bedrock in covered karst terranes. Environmental Geology 7: 39.

Zielke-Olivier, J.S.D.R., Vermeulen, P.D. 2017. Utilizing geophysics as a delineation tool for groundwater flow paths and contaminants along a graben. In: Wolkersdorfer, C., Sartz, L., Sillanpää, M. and Häkkinen, A. (eds.) Mine water and circular economy (Vol I). – p. 320 – 327. Lappeenranta, Finland (Lappeenranta University of Technology).

APPENDIX A – ERT AND MAG GEOPHYSICAL SURVEY CROSS SECTIONS

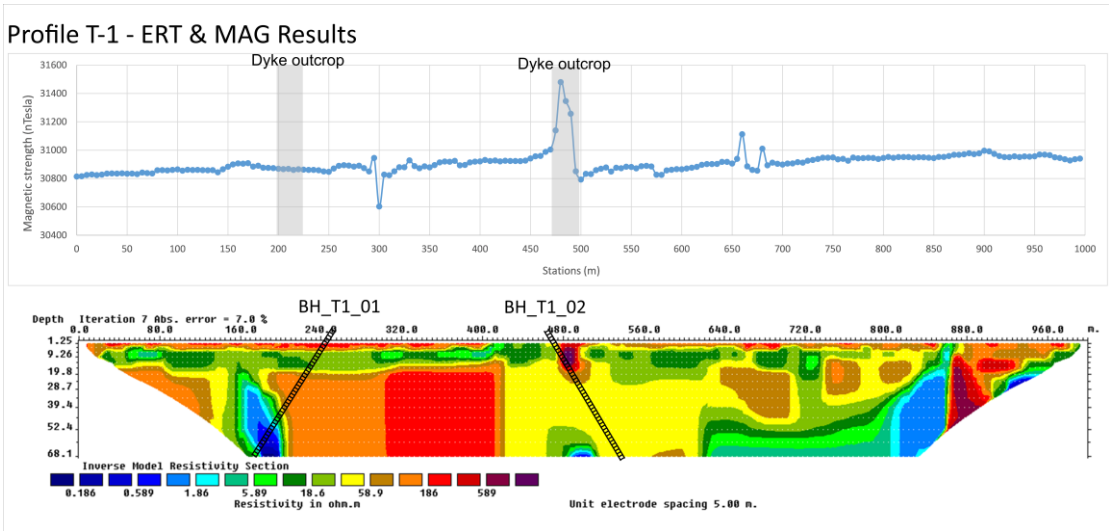

Figure A-0-1: Detailed electrical resistivity tomography (ERT) 2D pseudo-sections of traverse T-1, illustrating the location and orientation of the proposed boreholes.

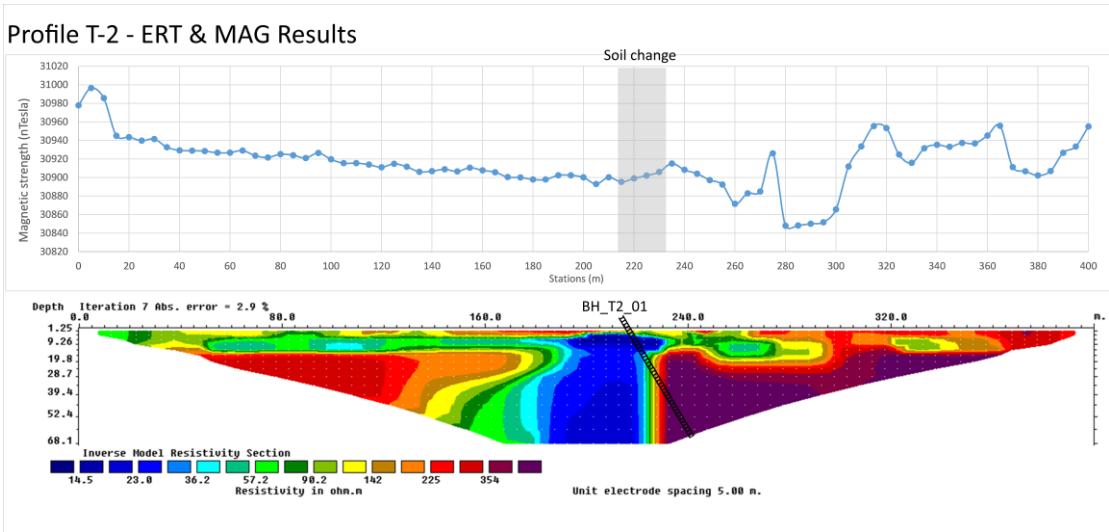

Figure A-0-2: Detailed electrical resistivity tomography (ERT) 2D pseudo-sections of traverse T-2, illustrating the location and orientation of the proposed boreholes.

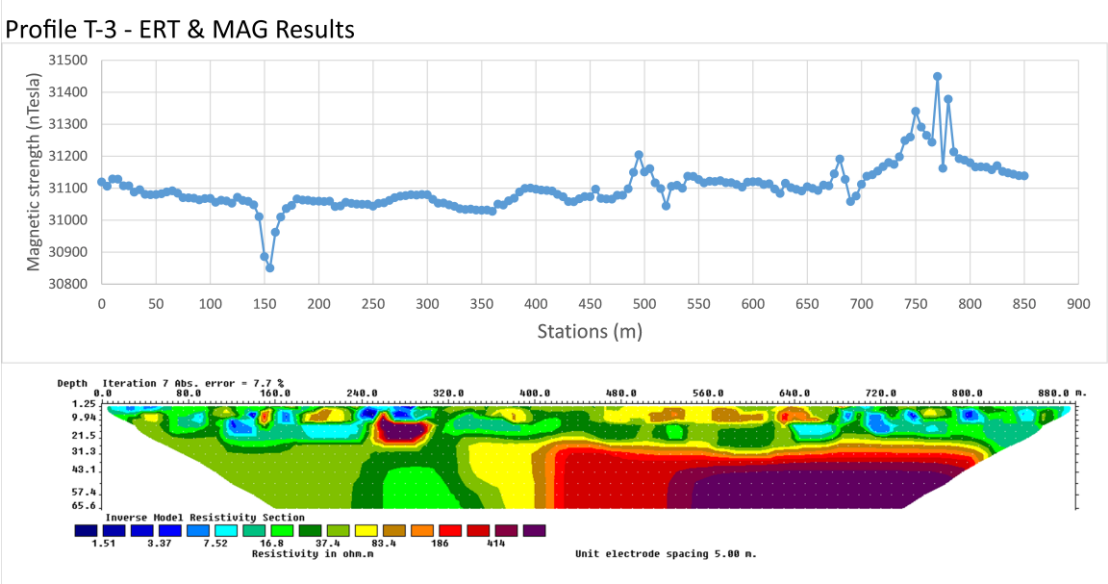

Figure A-0-3: Detailed electrical resistivity tomography (ERT) 2D pseudo-sections of traverse T-3, illustrating the location and orientation of the proposed boreholes.

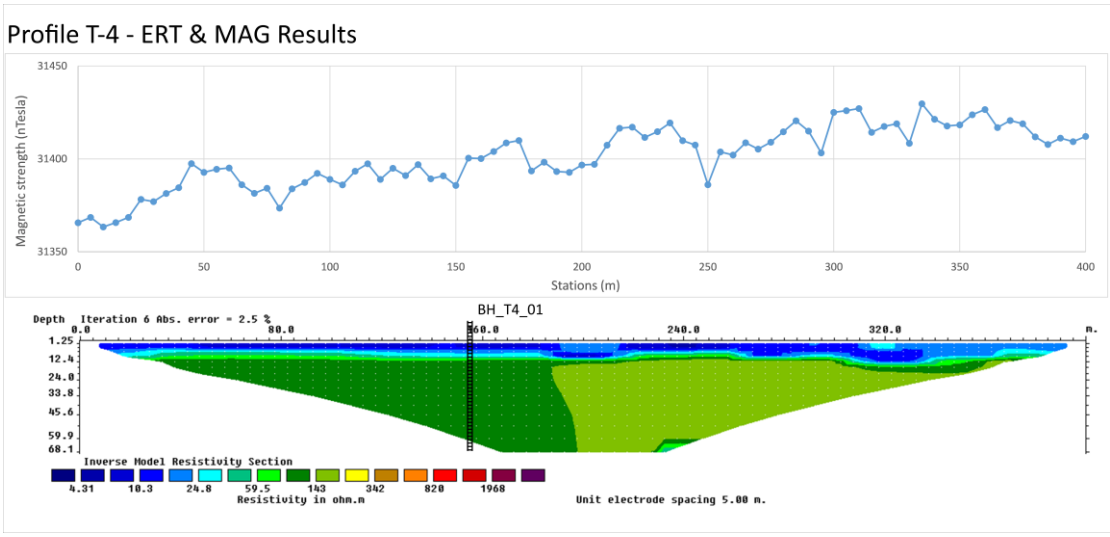

Figure A-0-4: Detailed electrical resistivity tomography (ERT) 2D pseudo-sections of traverse T-4, illustrating the location and orientation of the proposed boreholes.

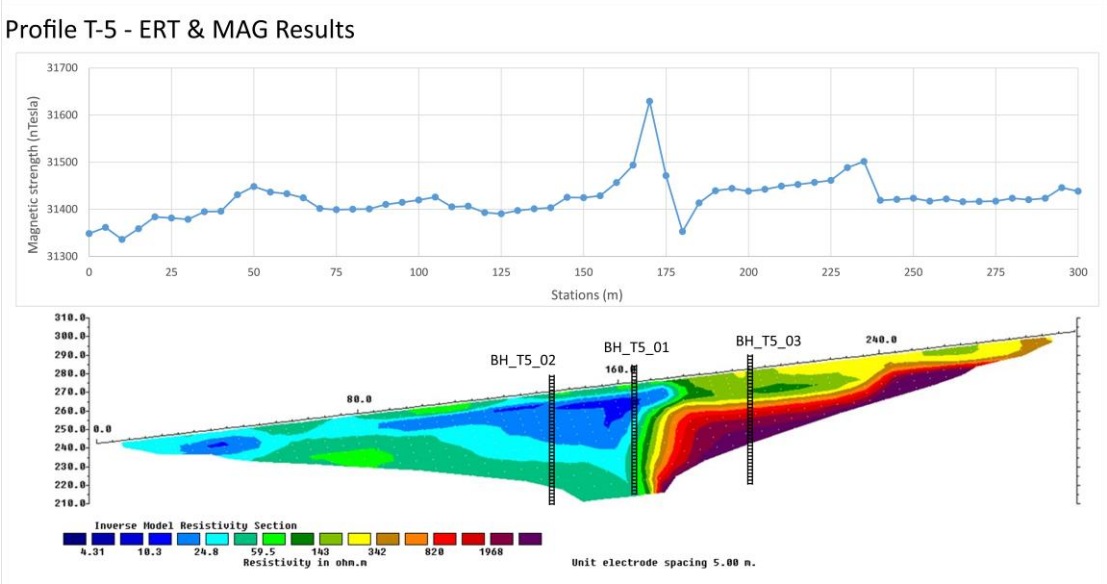

Figure A-0-5: Detailed electrical resistivity tomography (ERT) 2D pseudo-sections of traverse T-5, illustrating the location and orientation of the proposed boreholes.

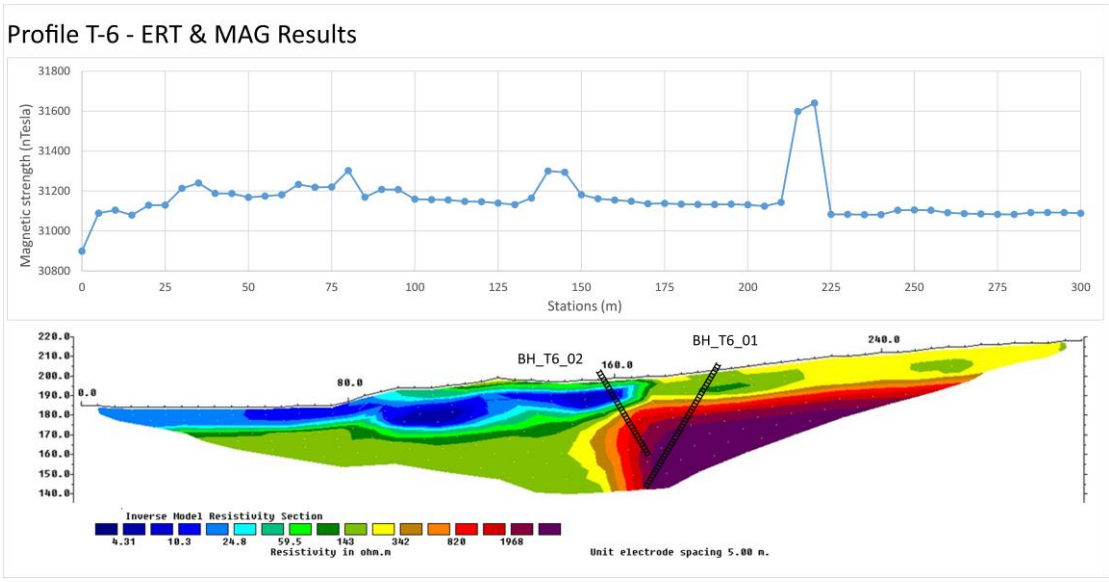

Figure A-0-6: Detailed electrical resistivity tomography (ERT) 2D pseudo-sections of traverse T-6, illustrating the location and orientation of the proposed boreholes.

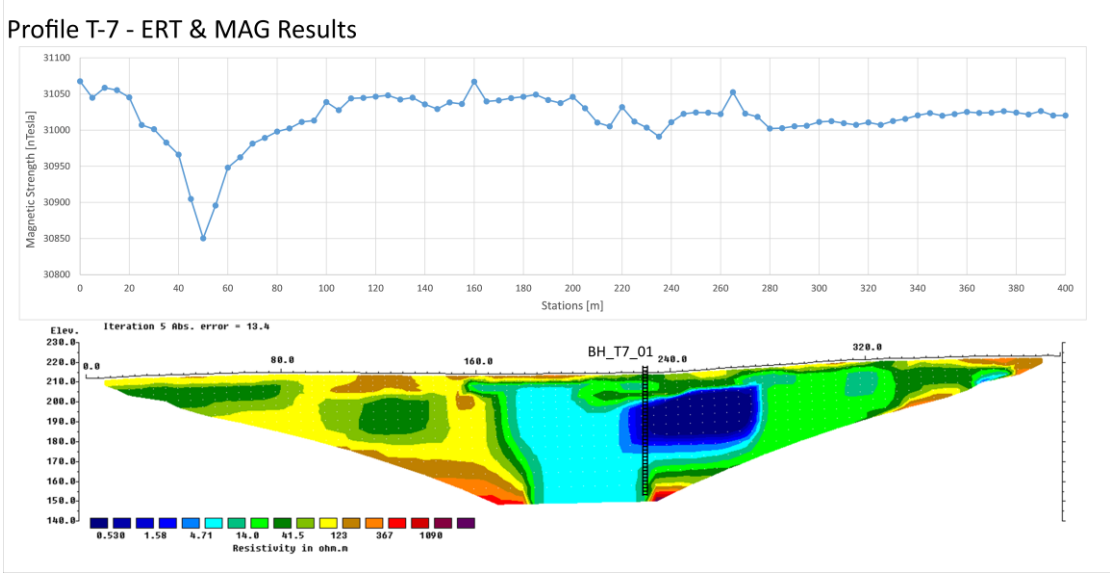

Figure A-0-7: Detailed electrical resistivity tomography (ERT) 2D pseudo-sections of traverse T-7, illustrating the location and orientation of the proposed boreholes.

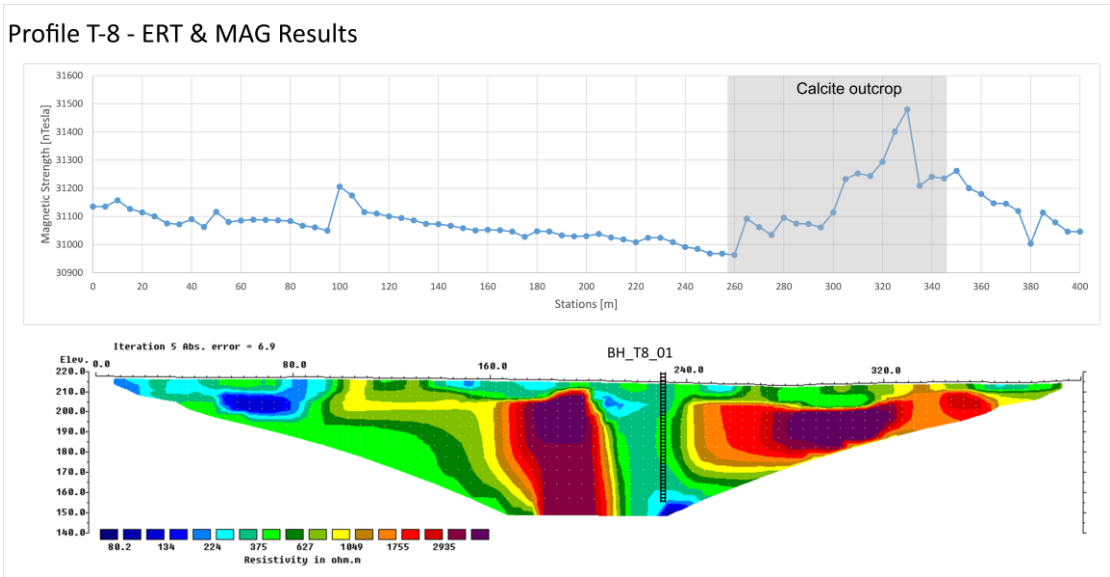

Figure A-0-8: Detailed electrical resistivity tomography (ERT) 2D pseudo-sections of traverse T-8, illustrating the location and orientation of the proposed boreholes.

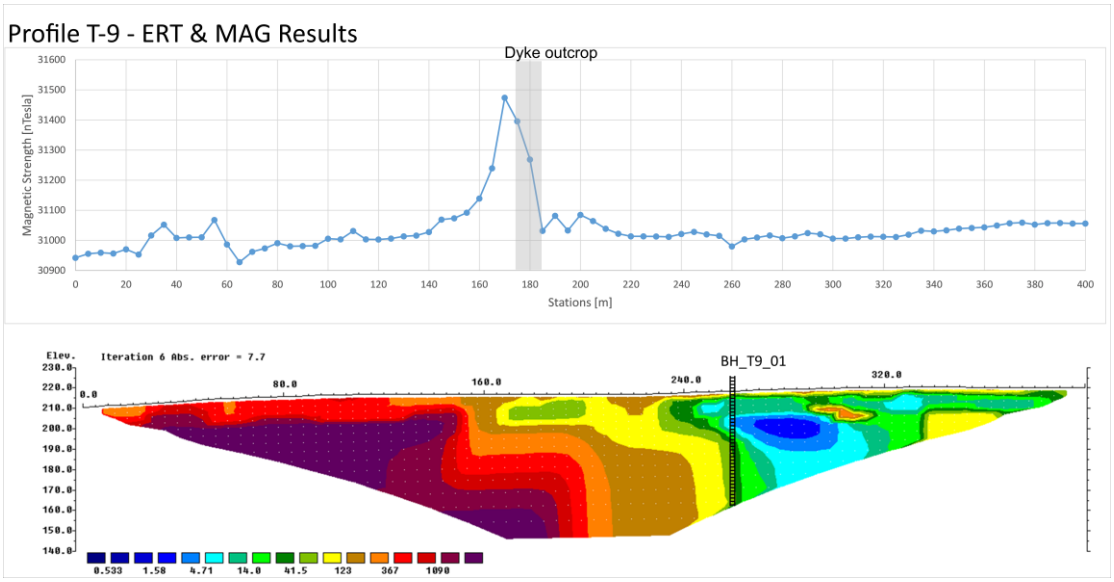

Figure A-0-9: Detailed electrical resistivity tomography (ERT) 2D pseudo-sections of traverse T-9, illustrating the location and orientation of the proposed boreholes.

APPENDIX B – GEOLOGICAL BOREHOLE LOGS

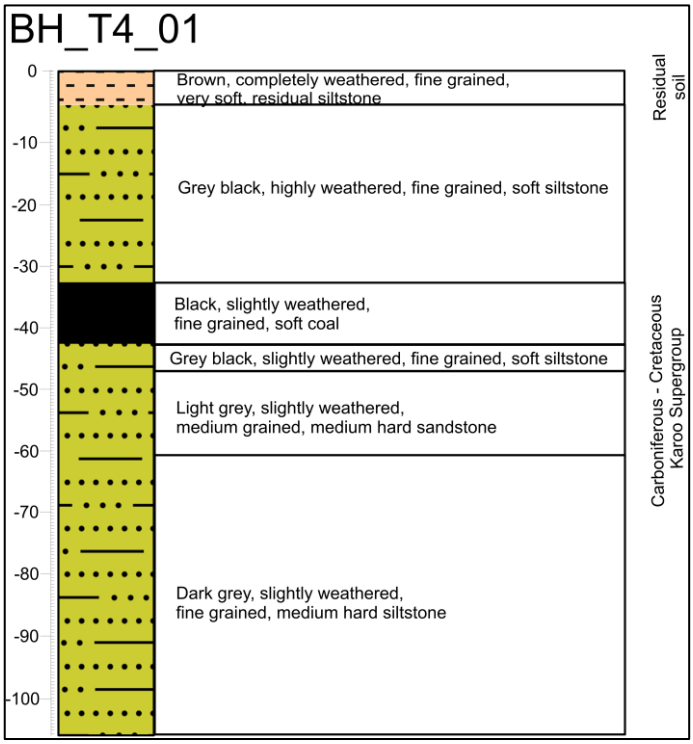

Figure B-0-1: Drilling geological log of borehole BH_T8_01, indicating colour, degree of weathering, consistency, structure and origin.

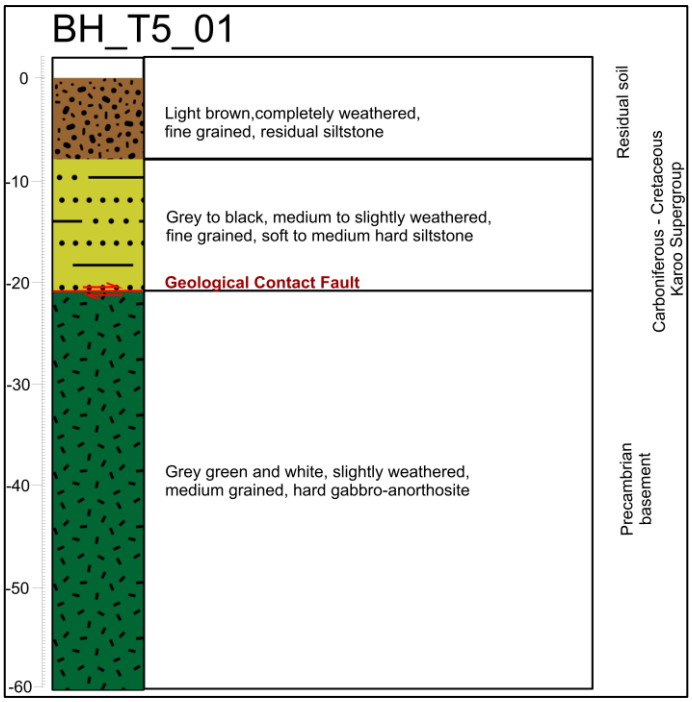

Figure B-0-2: Drilling geological log of borehole BH_T5_01, indicating colour, degree of weathering, consistency, structure and origin. Position of the geological contact fault is indicated at the contact between the Basement and Karoo Supergroup formations.

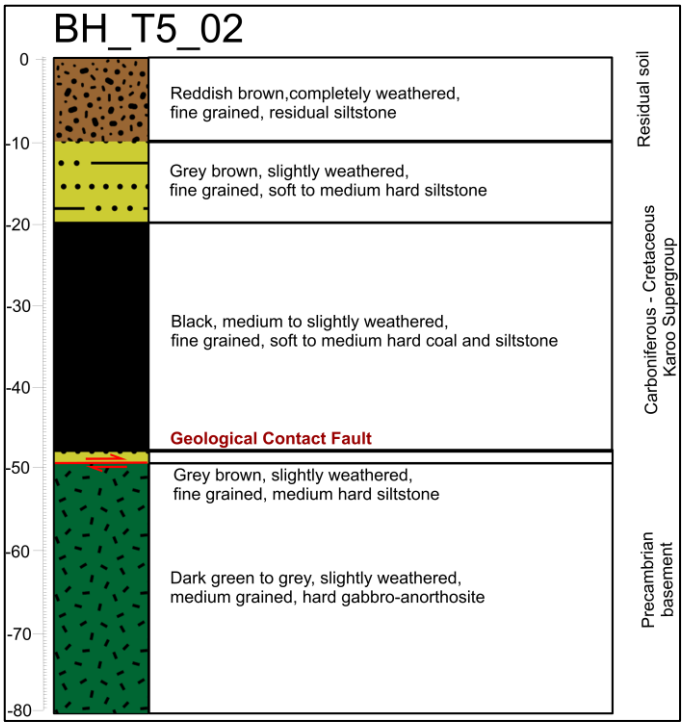

Figure B-0-3: Drilling geological log of borehole BH_T5_02, indicating colour, degree of weathering, consistency, structure and origin. Position of the geological contact fault is indicated at the contact between the Basement and Karoo Supergroup formations.

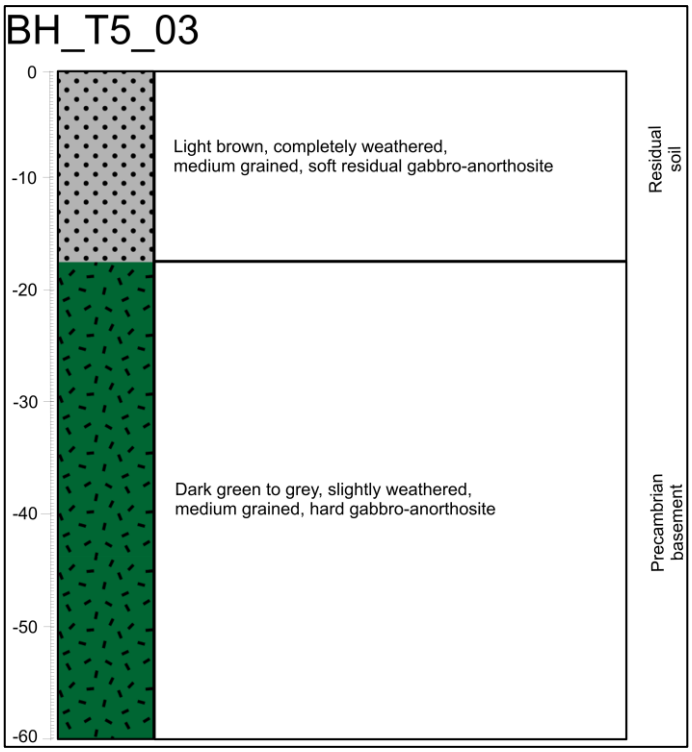

Figure B-0-4: Drilling geological log of borehole BH_T5_03, indicating colour, degree of weathering, consistency, structure and origin.

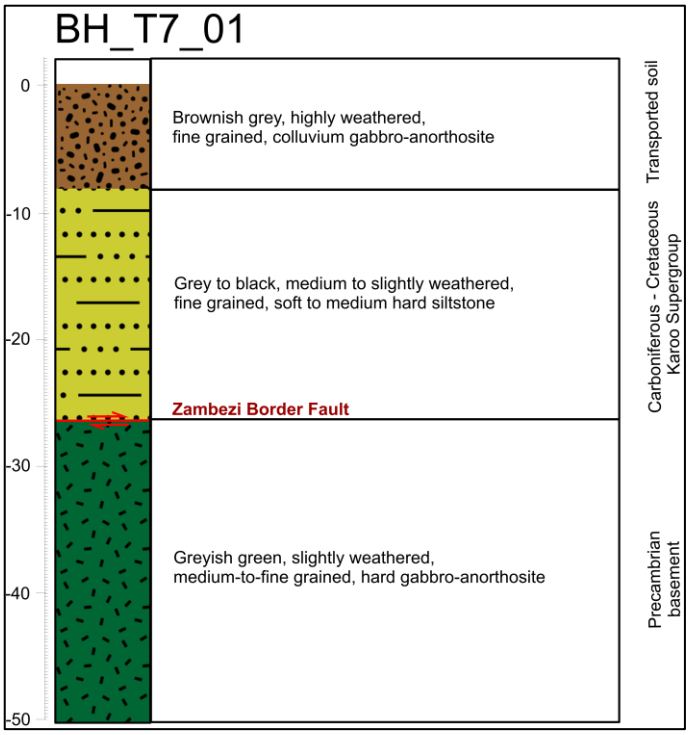

Figure B-0-5: Drilling geological log of borehole BH_T7_01, indicating colour, degree of weathering, consistency, structure and origin. Position of the Zambezi Border fault is indicated at the contact between the Basement and Karoo Supergroup formations.

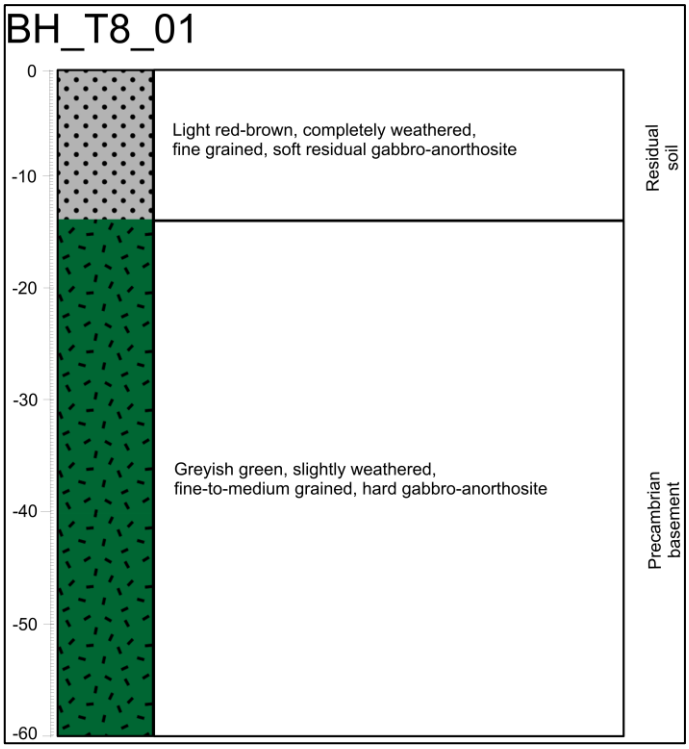

Figure B-0-6: Drilling geological log of borehole BH_T8_01, indicating colour, degree of weathering, consistency, structure and origin.

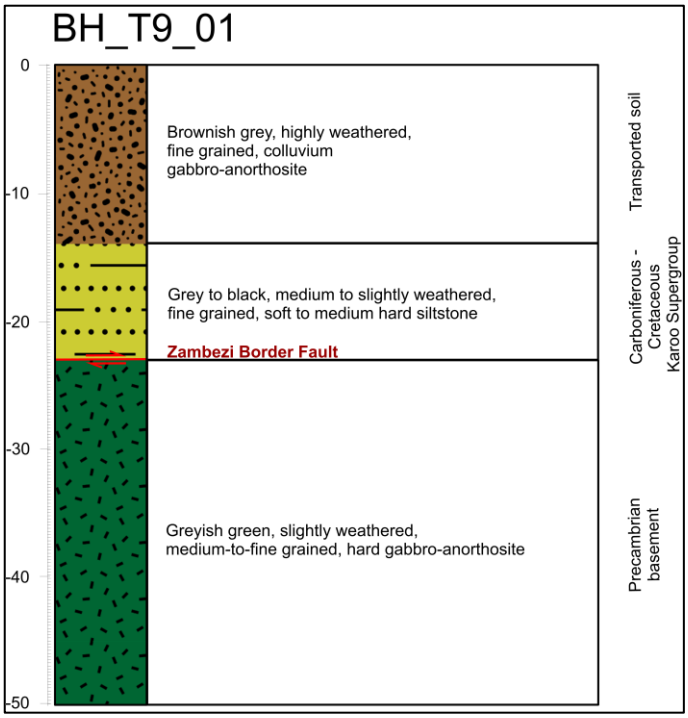

Figure B-0-7: Drilling geological log of borehole BH_T9_01, indicating colour, degree of weathering, consistency, structure and origin. Position of the Zambezi Border fault is indicated at the contact between the Basement and Karoo Supergroup formations.

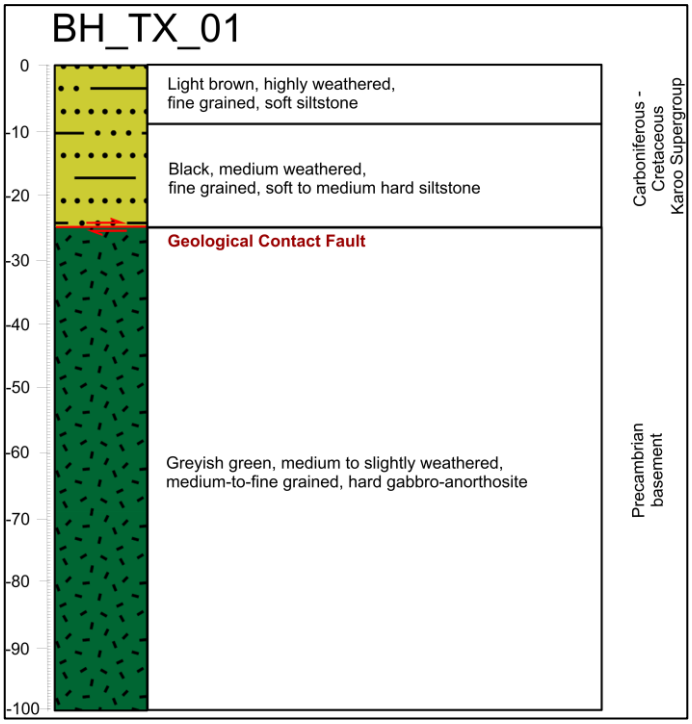

Figure B-0-8: Drilling geological log of borehole BH_TX_01, indicating colour, degree of weathering, consistency, structure and origin. Position of the geological contact fault is indicated at the contact between the Basement and Karoo Supergroup formations.

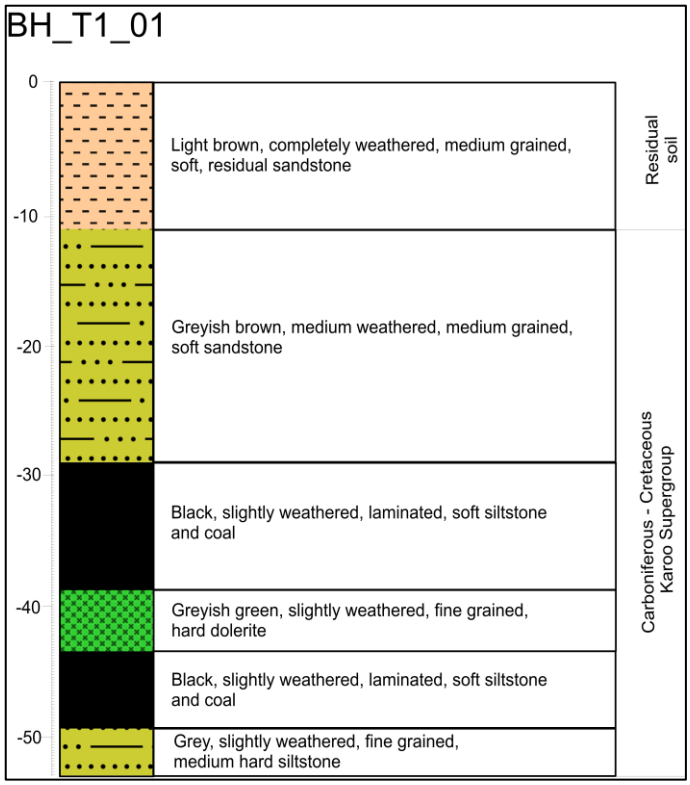

Figure B-0-9: Drilling geological log of borehole BH_T1_01, indicating colour, degree of weathering, consistency, structure and origin.

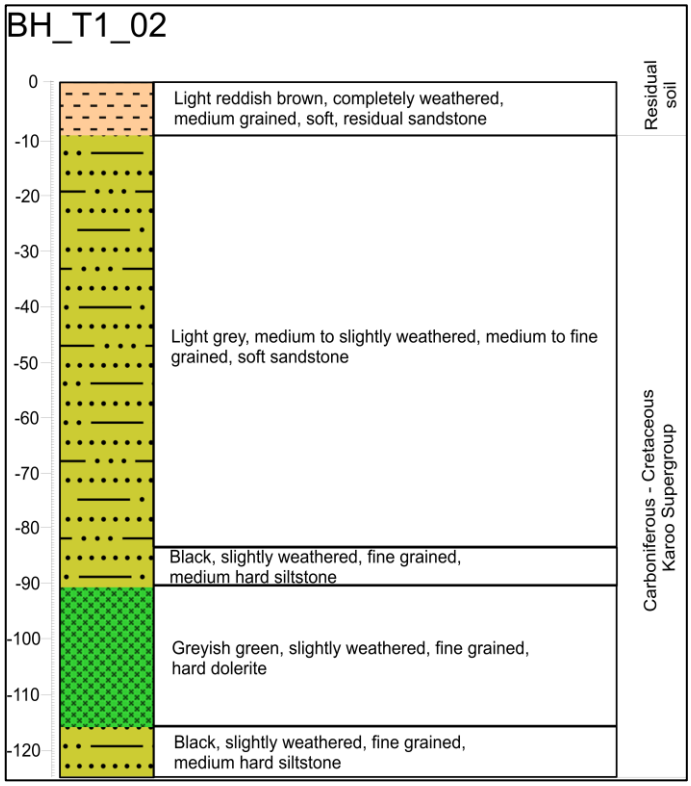

Figure B-0-10: Drilling geological log of borehole BH_T1_02, indicating colour, degree of weathering, consistency, structure and origin.

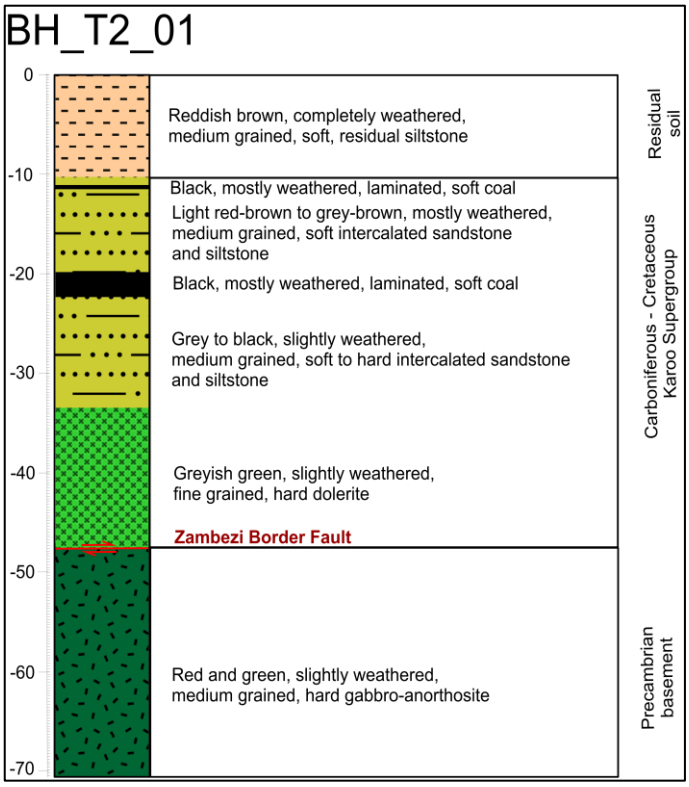

Figure B-0-11: Drilling geological log of borehole BH_T2_01, indicating colour, degree of weathering, consistency, structure and origin. Position of the Zambezi Border fault is indicated at the contact between the Basement and Karoo Supergroup formations.

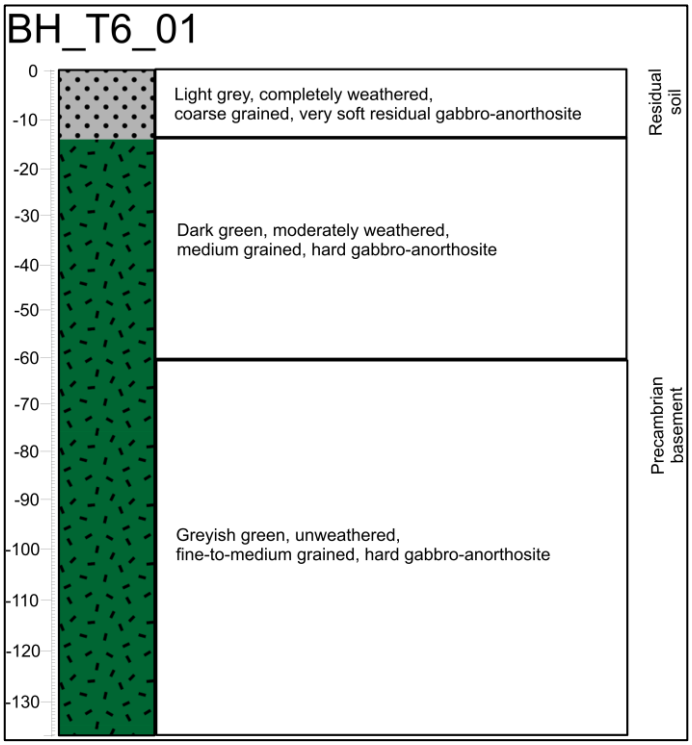

Figure B-0-12: Drilling geological log of borehole BH_T6_01, indicating colour, degree of weathering, consistency, structure and origin.

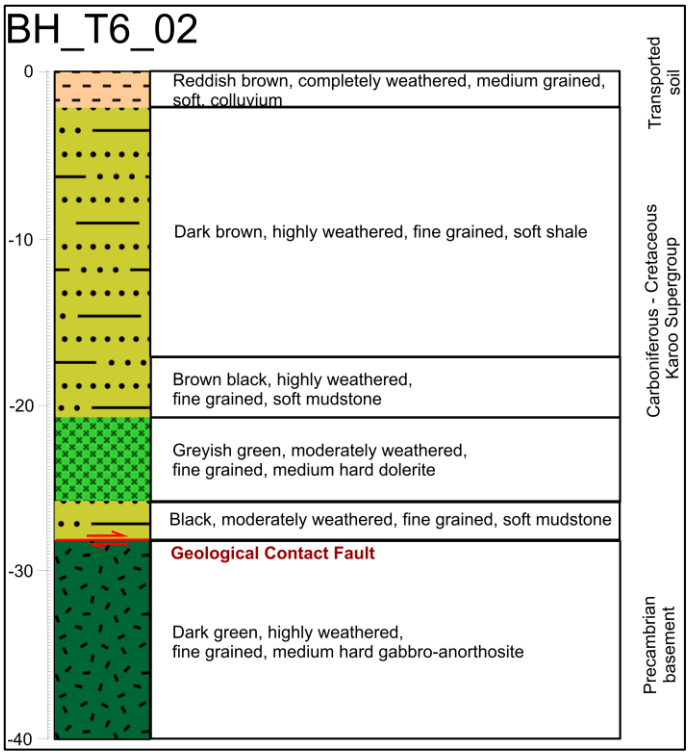

Figure B-0-13: Drilling geological log of borehole BH_T6_02, indicating colour, degree of weathering, consistency, structure and origin. Position of the geological contact fault is indicated at the contact between the Basement and Karoo Supergroup formations.

APPENDIX C – PACKER TEST RESULTS

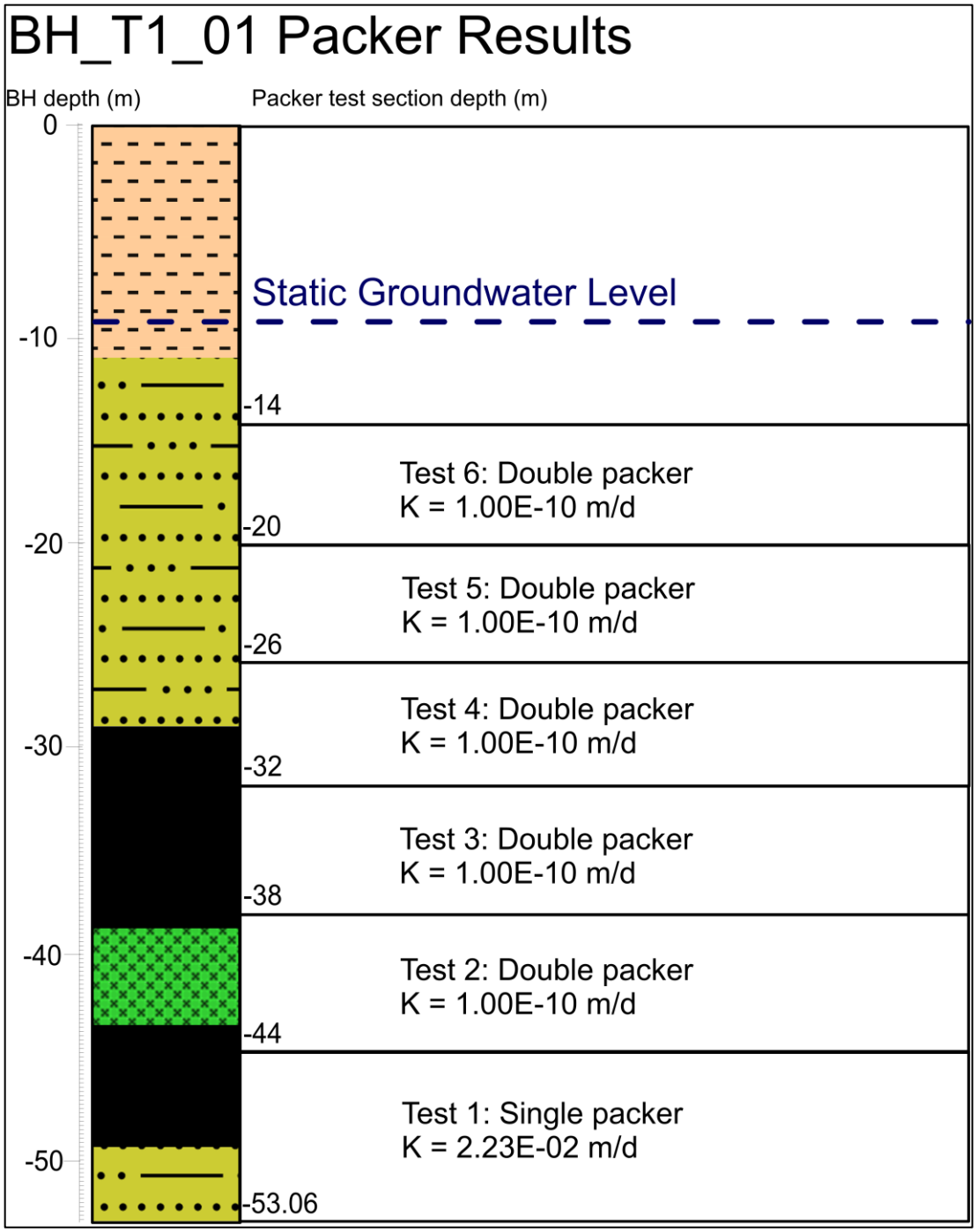

Figure C-0-1: BH_T1_01 packer test results for each test section relative to the encountered geological units described during the drilling phase results.

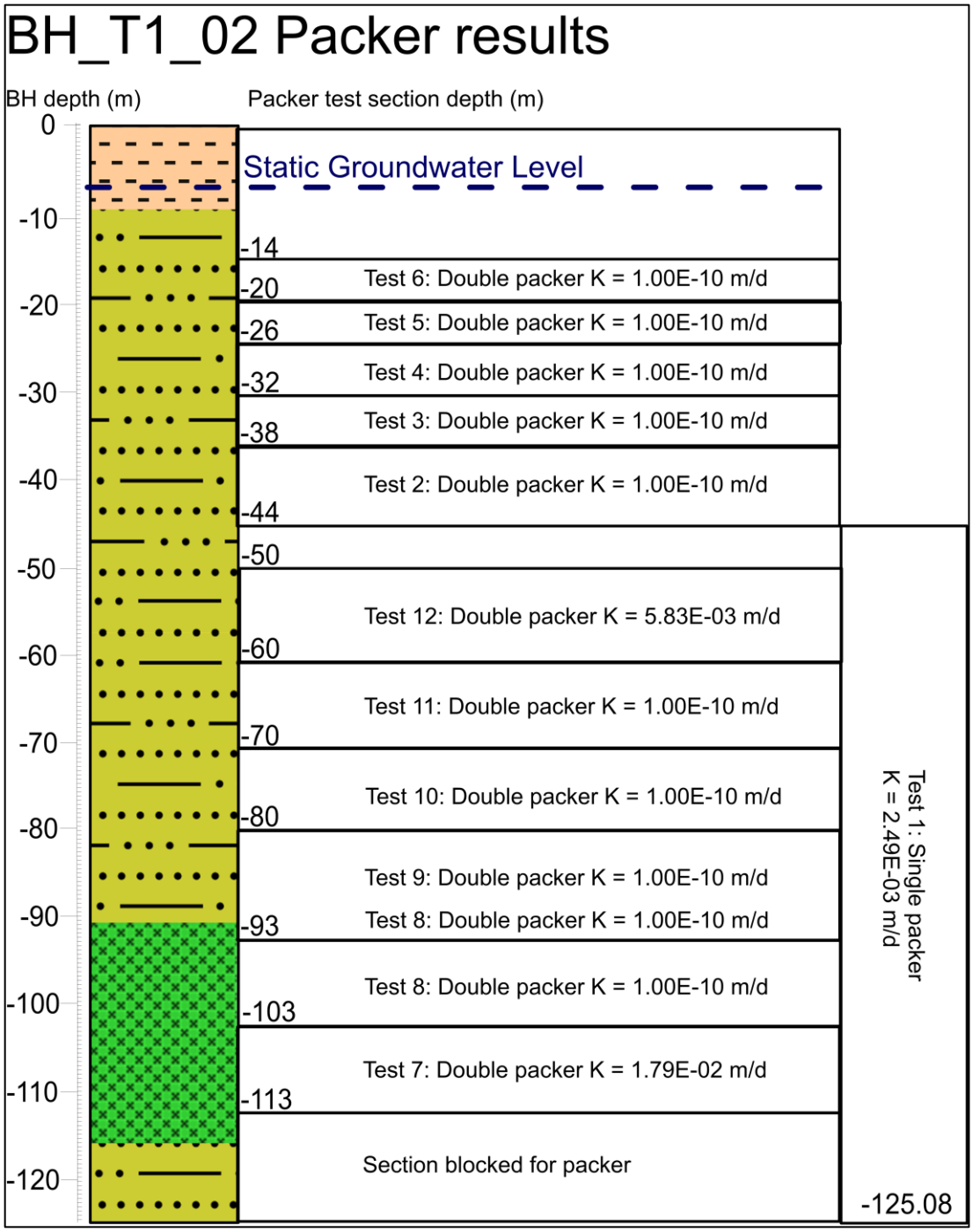

Figure C-0-2: BH_T1_02 packer test results for each test section relative to the encountered geological units described during the drilling phase results.

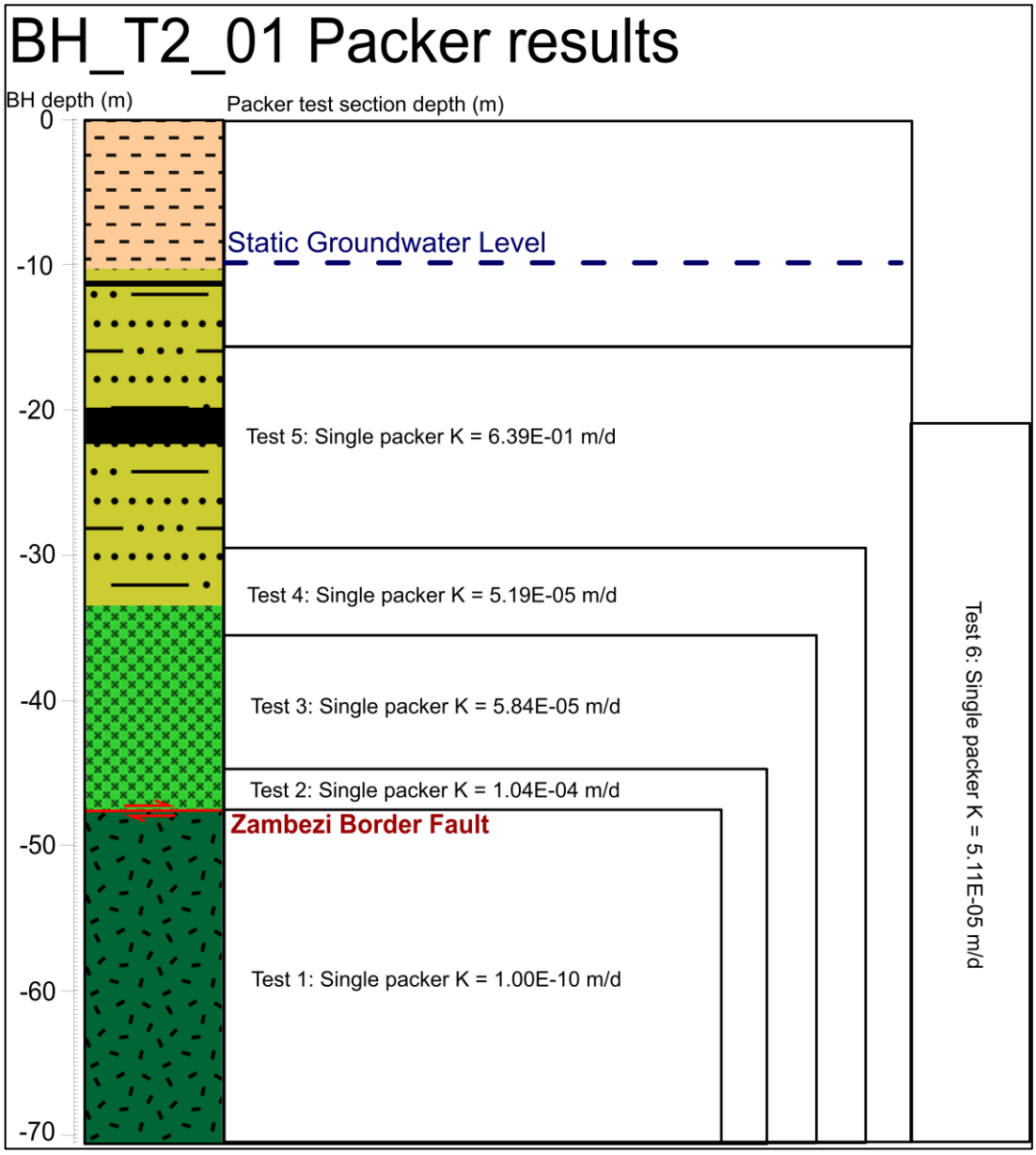

Figure C-0-3: BH_T2_01 packer test results for each test section relative to the encountered geological units described during the drilling phase results.

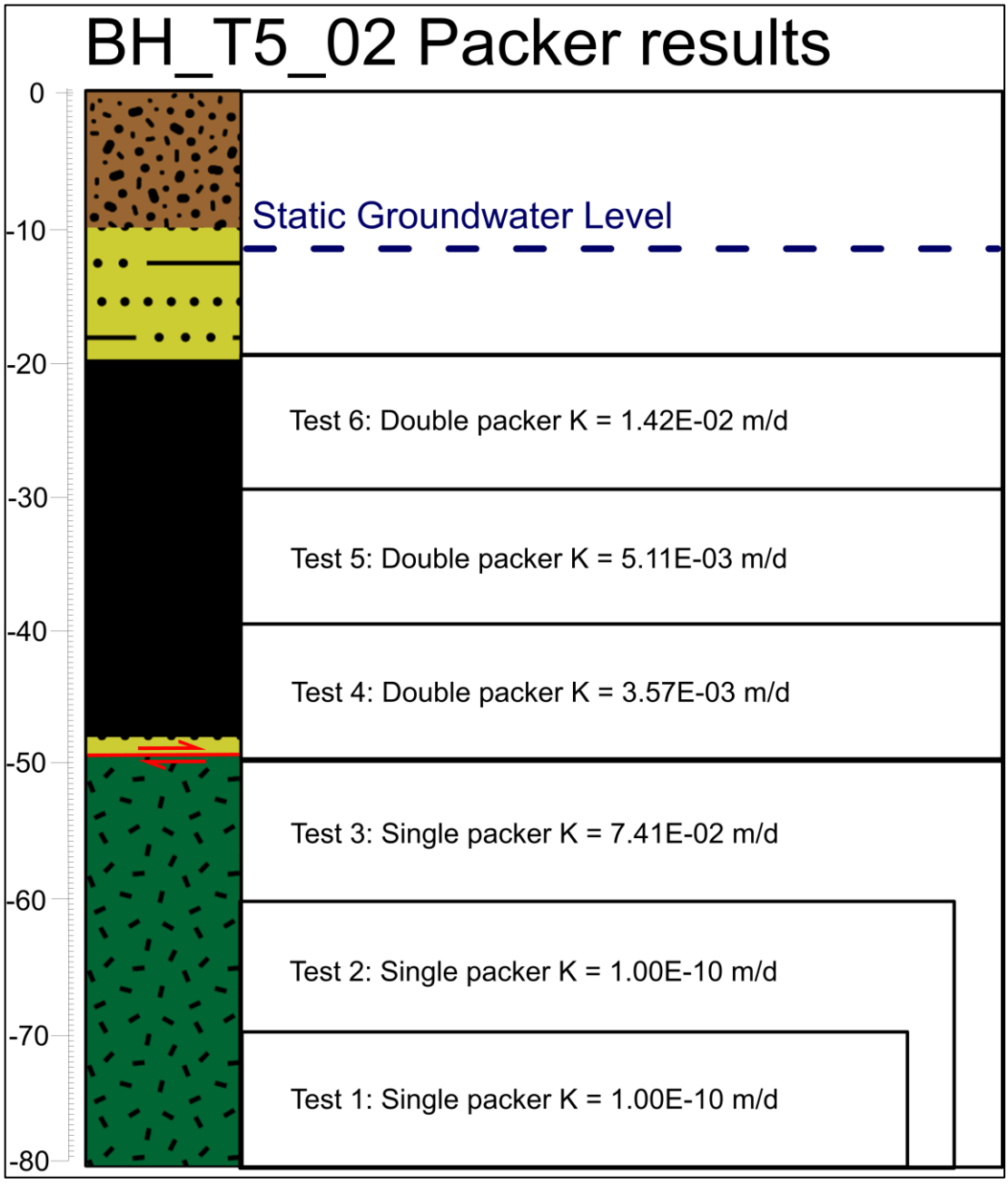

Figure C-0-4: BH_T5_02 packer test results for each test section relative to the encountered geological units described during the drilling phase results.

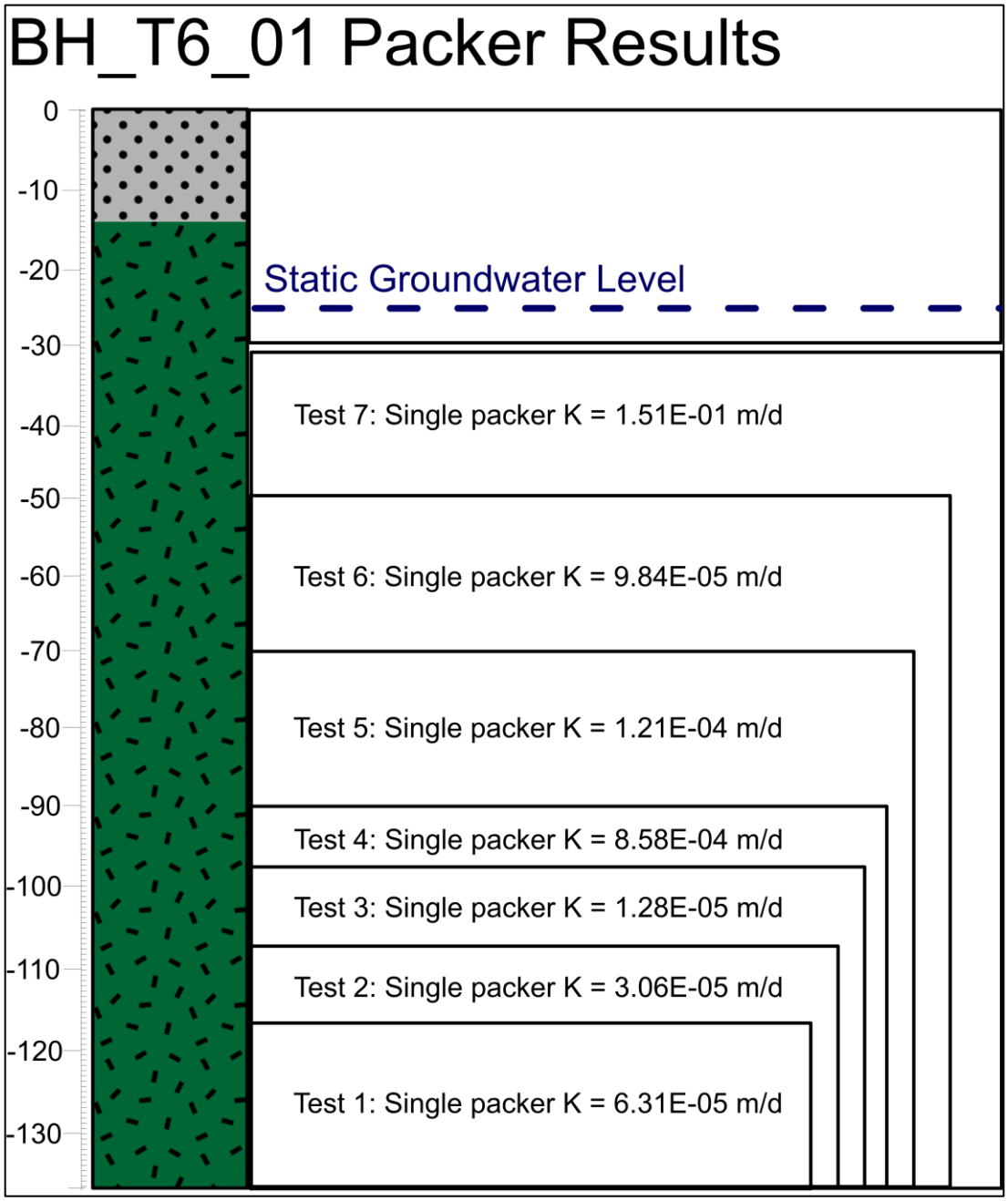

Figure C-0-5: BH_T6_01 packer test results for each test section relative to the encountered geological units described during the drilling phase results.

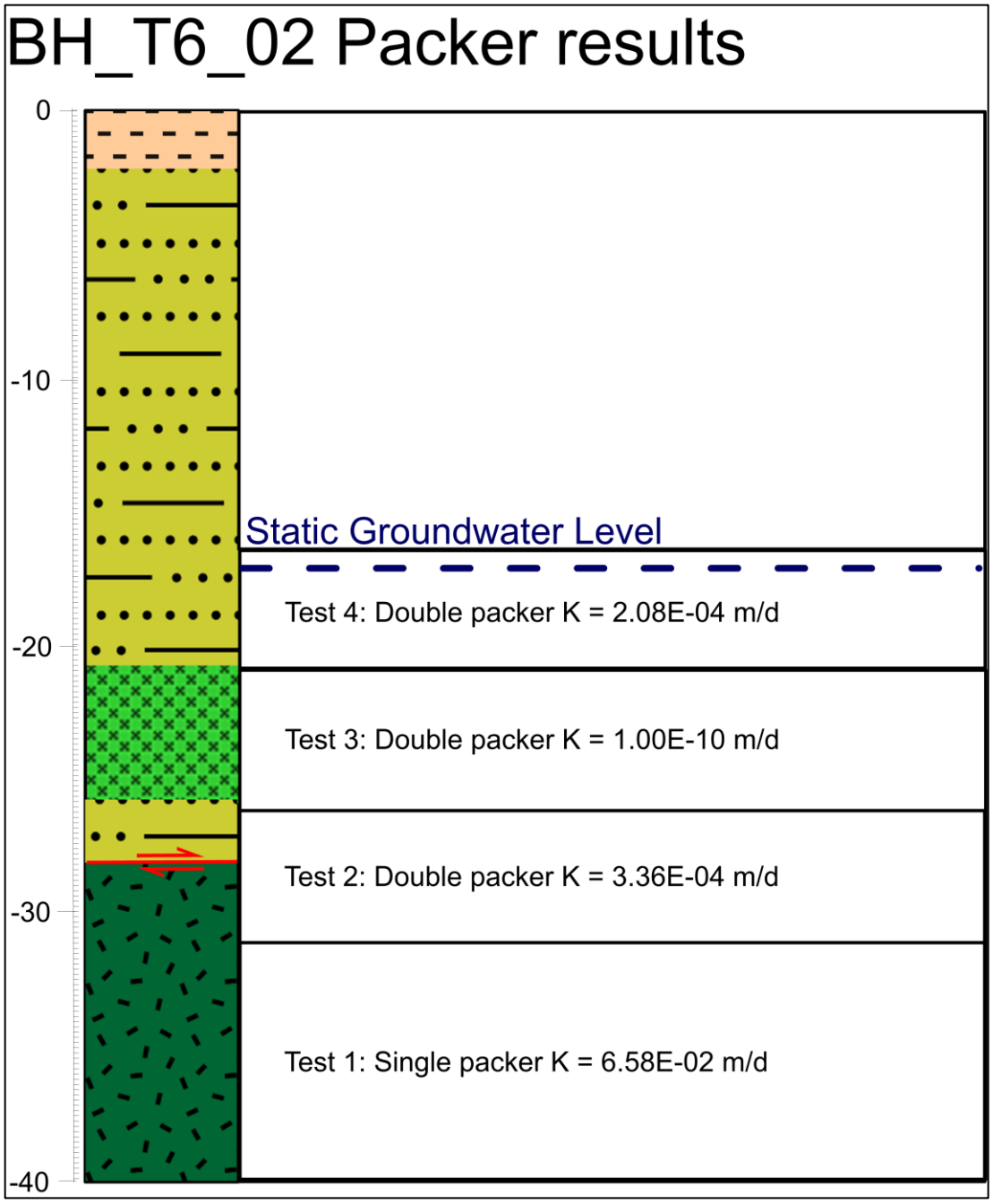

Figure C-0-6: BH_T6_02 packer test results for each test section relative to the encountered geological units described during the drilling phase results.

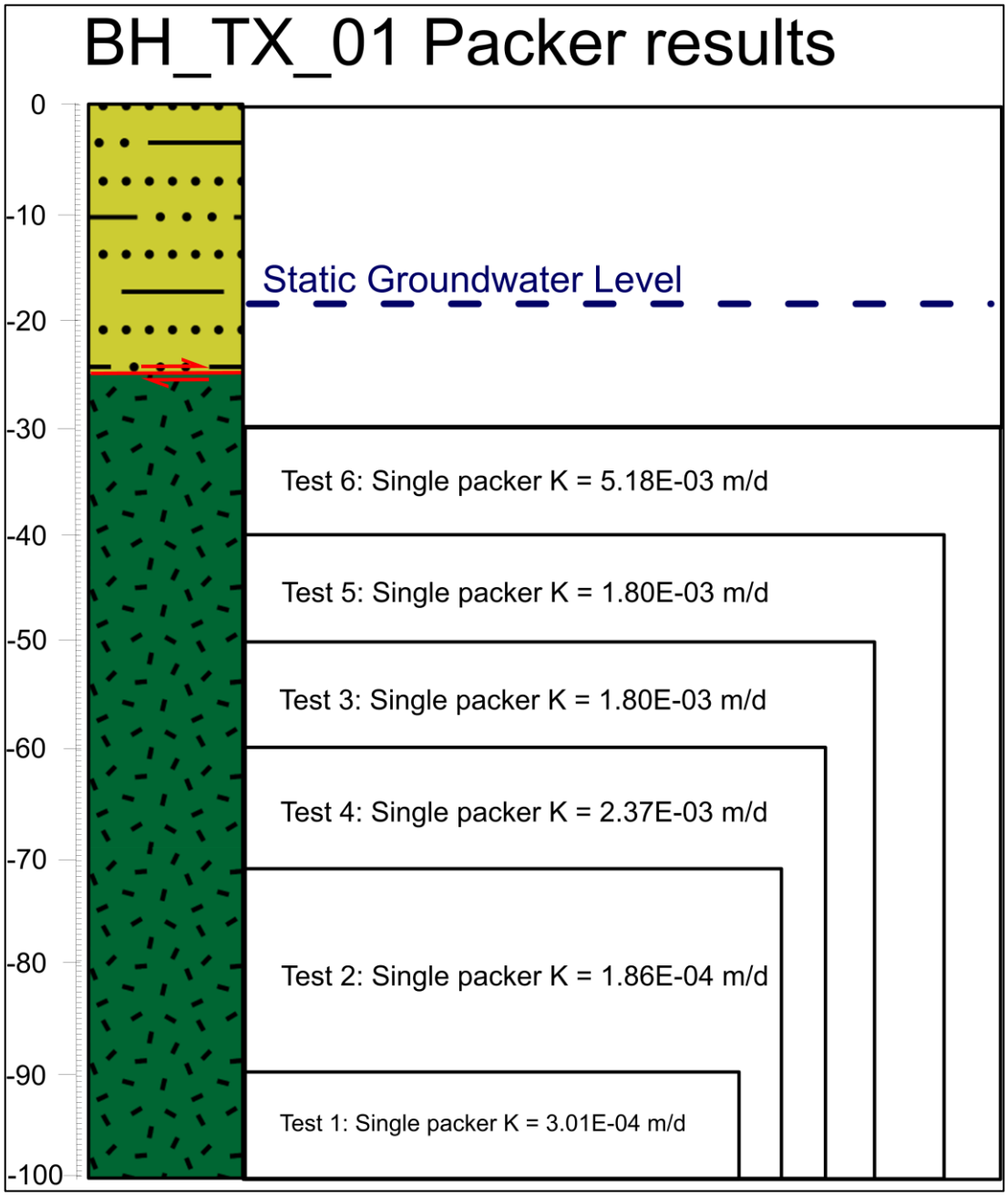

Figure C-0-7: BH_TX_01 packer test results for each test section relative to the encountered geological units described during the drilling phase results.

PACKER PERMEABILITY TEST

Borehole ID:	**BH_T1_01**	Test No:	**1**				
Packer type:	56mm Single Geopro	Date of Test:	26/10/2016				
Casing Details:	6m (PVC)	Packer inflation pressure (KPa):	1500				
Diameter of Hole (mm):	96.00	Test carried out by:	R C Minnaar				
Depth of hole (m):	53.06	Inclination of hole:	-70	degrees			
Depth of groundwater (mbgl):	10.50	Test section (m):	From:	**44.00**	to	**53.06**	
Vertical waterlevel (mbgl):	9.86	Test section length (m):	**9.06**				
Piezometer Guage Factor	**0.08381934**	Piezo zero reading (Digital):	**8371**				

Description of Test section	Average Flow Rate (l/min)	Gauge Pressure (KPa)	Piezometer Reading (Digital)	Total excess Head (mH2O)
See Geotech/geological log for details.	0			0
	0.30	100	8344	2.26
	3.25	200	8169	16.93
	8.80	300	7880	41.16
	5.20	210	8006	30.59
	2.20	100	8146	18.86

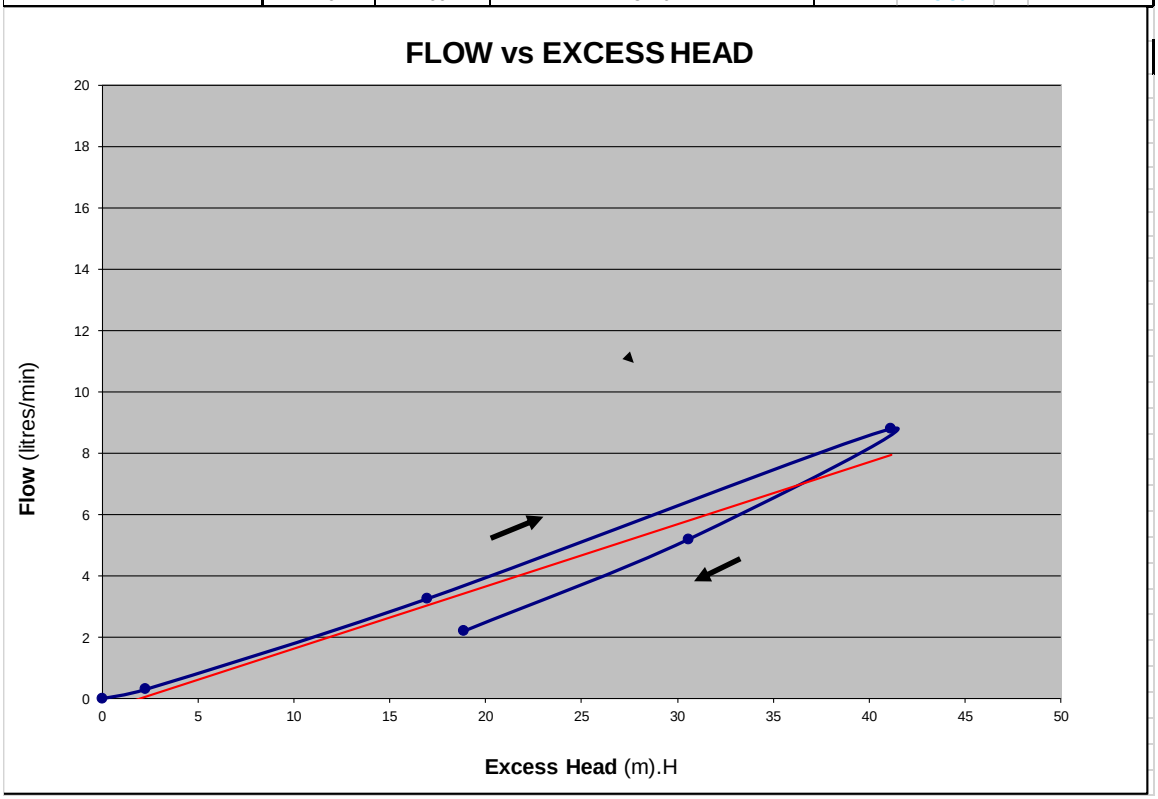

PACKER PERMEABILITY TEST

Borehole ID:	**BH_T1_01**	Test No:	**2**				
Packer type:	56mm Double Geopro	Date of Test:	27/10/2016				
Casing Details:	6m (PVC)	Packer inflation pressure (KPa):	1500				
Diameter of Hole (mm):	96.00	Test carried out by:	R C Minnaar				
Depth of hole (m):	53.06	Inclination of hole:	-70	degrees			
Depth of groundwater (mbgl):	10.50	Test section (m):	From:	**38.00**	to	**44.00**	
Vertical waterlevel (mbgl):	9.86	Test section length (m):	**6.00**				
Piezometer Guage Factor	**0.08381934**	Piezo zero reading (Digital):	**8426**				

Description of Test section	**Average Flow Rate** (l/min)	**Gauge Pressure** (KPa)	**Piezometer Reading** (Digital)	**Total excess Head** (mH2O)
	0			0
See Geotech/geological log for details. Dolerite dyke from 39m to 43.5m.	0.00	100	8292	11.23
	0.00	200	8162	22.13
	0.00	300	8034	32.86

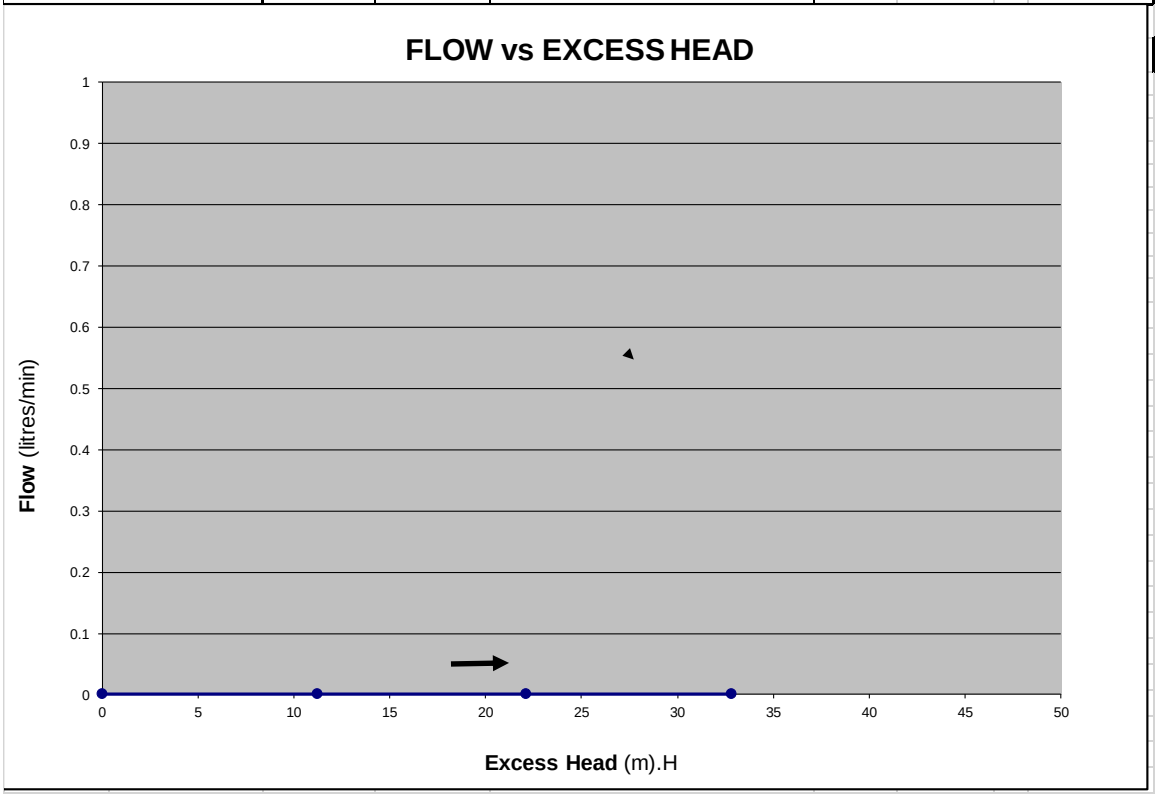

PACKER PERMEABILITY TEST

Borehole ID:	**BH_T1_01**	Test No:	**3**				
Packer type:	56mm Double Geopro	Date of Test:	27/10/2016				
Casing Details:	6m (PVC)	Packer inflation pressure (KPa):	1400				
Diameter of Hole (mm):	96.00	Test carried out by:	R C Minnaar				
Depth of hole (m):	53.06	Inclination of hole:	-70	degrees			
Depth of groundwater (mbgl):	10.50	Test section (m):	From:	**32.00**	to	**38.00**	
Vertical waterlevel (mbgl):	9.86	Test section length (m):	**6.00**				
Piezometer Guage Factor	**0.08381934**	Piezo zero reading (Digital):	**8469**				

Description of Test section	**Average Flow Rate** (l/min)	**Gauge Pressure** (KPa)	**Piezometer Reading** (Digital)	**Total excess Head** (mH2O)
	0			0
See Geotech/geological log for details.	0.00	100	8329	11.73
	0.00	200	8210	21.71
	0.00	300	8093	31.52

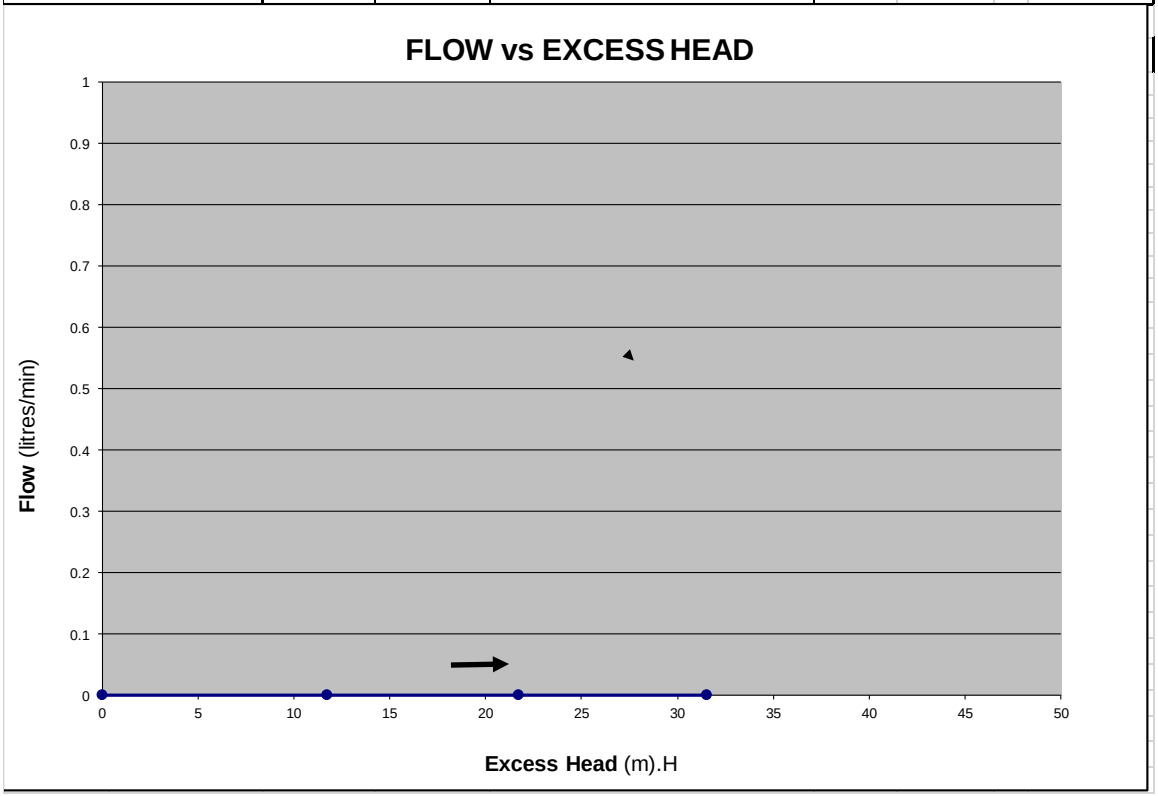

PACKER PERMEABILITY TEST

Borehole ID:	**BH_T1_01**	Test No:	**4**				
Packer type:	56mm Double Geopro	Date of Test:	27/10/2016				
Casing Details:	6m (PVC)	Packer inflation pressure (KPa):	1300				
Diameter of Hole (mm):	96.00	Test carried out by:	R C Minnaar				
Depth of hole (m):	53.06	Inclination of hole:	-70	degrees			
Depth of groundwater (mbgl):	10.50	Test section (m):	From:	**26.00**	to	**32.00**	
Vertical waterlevel (mbgl):	9.86	Test section length (m):	**6.00**				
Piezometer Guage Factor	**0.08381934**	Piezo zero reading (Digital):	**8530**				

Description of Test section	**Average Flow Rate** (l/min)	**Gauge Pressure** (KPa)	**Piezometer Reading** (Digital)	**Total excess Head** (mH2O)
	0			0
See Geotech/geological log for details.	0.00	100	8395	11.32
	0.00	200	8274	21.46
	0.00	300	8161	30.93

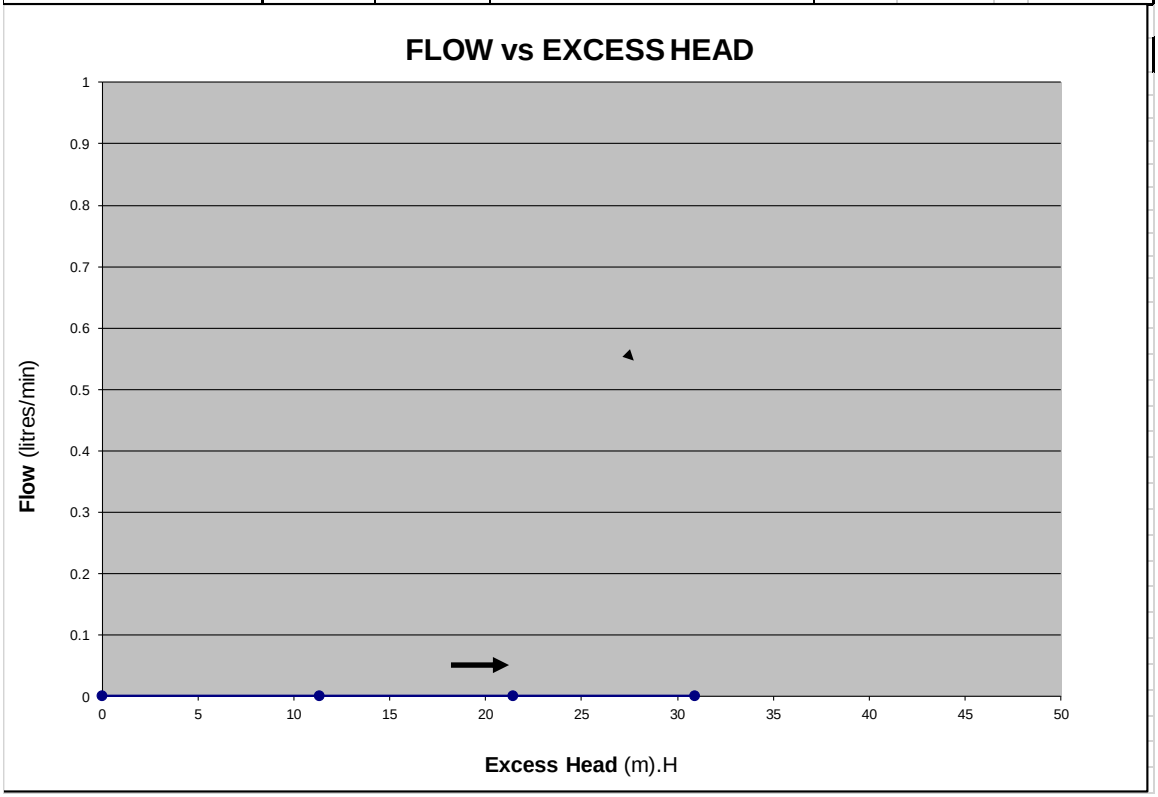

PACKER PERMEABILITY TEST

Borehole ID:	**BH_T1_01**	Test No:	**5**				
Packer type:	56mm Double Geopro	Date of Test:	27/10/2016				
Casing Details:	6m (PVC)	Packer inflation pressure (KPa):	1300				
Diameter of Hole (mm):	96.00	Test carried out by:	R C Minnaar				
Depth of hole (m):	53.06	Inclination of hole:	-70	degrees			
Depth of groundwater (mbgl):	10.50	Test section (m):	From:	**20.00**	to	**26.00**	
Vertical waterlevel (mbgl):	9.86	Test section length (m):	**6.00**				
Piezometer Guage Factor	**0.08381934**	Piezo zero reading (Digital):	**8595**				

Description of Test section	**Average Flow Rate** (l/min)	**Gauge Pressure** (KPa)	**Piezometer Reading** (Digital)	**Total excess Head** (mH2O)
	0			0
See Geotech/geological log for details.	0.00	100	8459	11.40
	0.00	200	8338	21.54
	0.00	300	8210	32.27

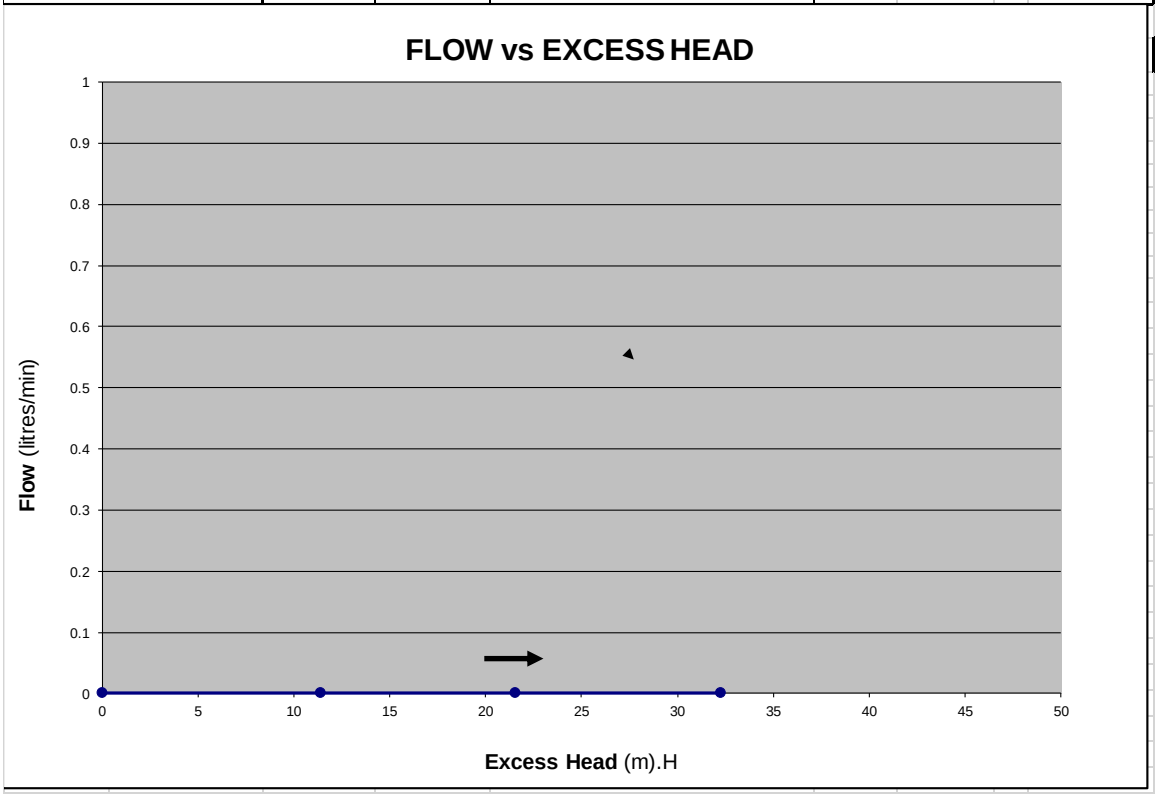

PACKER PERMEABILITY TEST

Borehole ID:	**BH_T1_01**	Test No:	**6**				
Packer type:	56mm Double Geopro	Date of Test:	27/10/2016				
Casing Details:	6m (PVC)	Packer inflation pressure (KPa):	1300				
Diameter of Hole (mm):	96.00	Test carried out by:	R C Minnaar				
Depth of hole (m):	53.06	Inclination of hole:	-70	degrees			
Depth of groundwater (mbgl):	10.50	Test section (m):	From:	**14.00**	to	**20.00**	
Vertical waterlevel (mbgl):	9.86	Test section length (m):	**6.00**				
Piezometer Guage Factor	**0.08381934**	Piezo zero reading (Digital):	**8675**				

Description of Test section	**Average Flow Rate** (l/min)	**Gauge Pressure** (KPa)	**Piezometer Reading** (Digital)	**Total excess Head** (mH2O)
	0			0
See Geotech/geological log for details.	0.00	100	8585	7.54
	0.00	200	8417	21.63
	0.00	300	8273	33.70

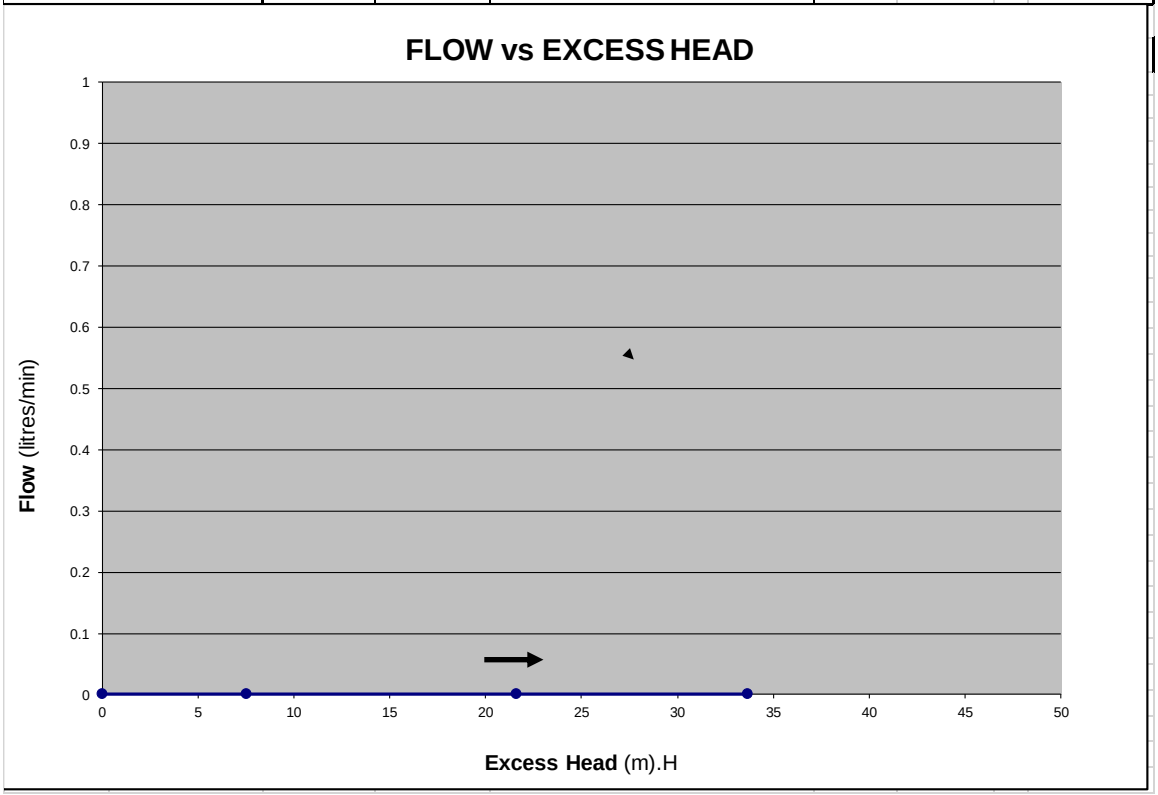

PACKER PERMEABILITY TEST

Borehole ID:	**BH_T1_02**	Test No:	**1**				
Packer type:	56mm Single Geopro	Date of Test:	26/10/2016				
Casing Details:	6m (PVC)	Packer inflation pressure (KPa):	1500				
Diameter of Hole (mm):	96.00	Test carried out by:	R C Minnaar				
Depth of hole (m):	125.08	Inclination of hole:	-70	degrees			
Depth of groundwater (mbgl):	10.50	Test section (m):	From:	**44.00**	to	**125.08**	
Vertical waterlevel (mbgl):	9.86	Test section length (m):	**81.08**				
Piezometer Guage Factor	**0.08381934**	Piezo zero reading (Digital):	**8371**				

Description of Test section	**Average Flow Rate** (l/min)	**Gauge Pressure** (KPa)	**Piezometer Reading** (Digital)	**Total excess Head** (mH2O)
	0			0
See Geotech/geological log for details.	0.30	100	8344	2.26
	3.25	200	8169	16.93
	8.80	300	7880	41.16
	5.20	210	8006	30.59
	2.20	100	8146	18.86

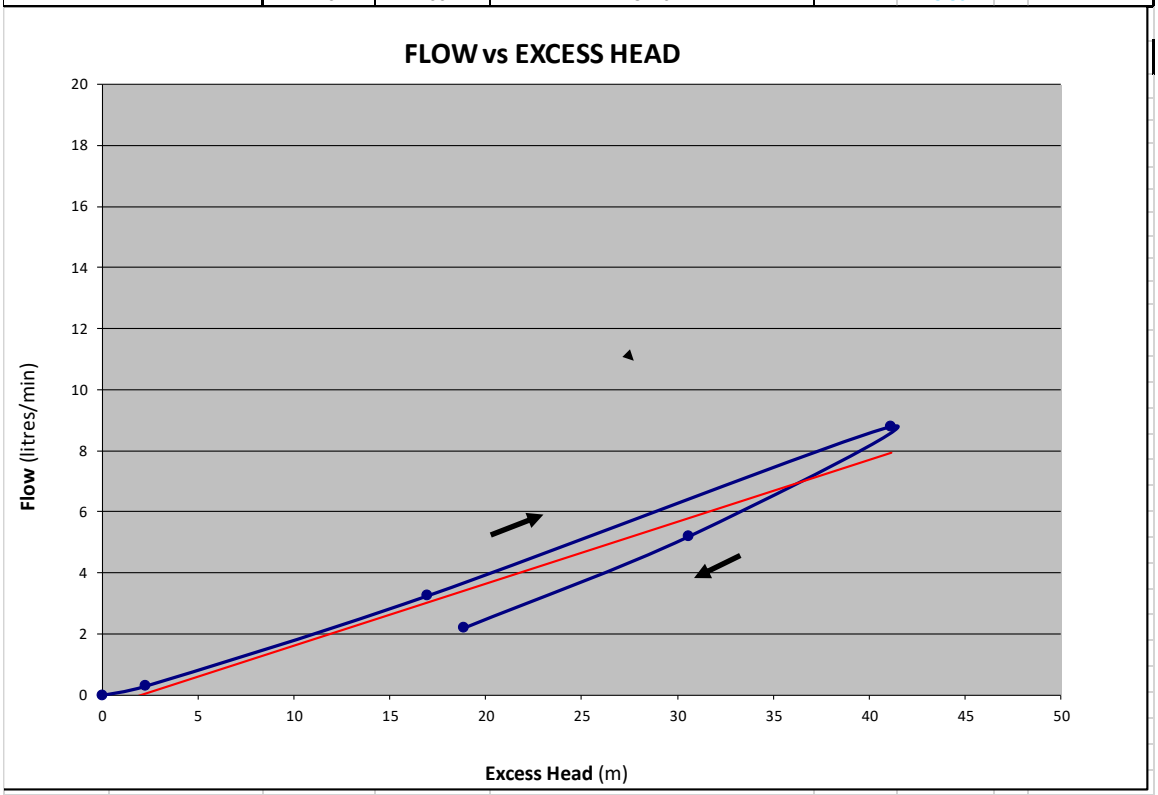

PACKER PERMEABILITY TEST

Borehole ID:	**BH_T1_02**	Test No:	**2**				
Packer type:	56mm Double Geopro	Date of Test:	27/10/2016				
Casing Details:	6m (PVC)	Packer inflation pressure (KPa):	1500				
Diameter of Hole (mm):	96.00	Test carried out by:	R C Minnaar				
Depth of hole (m):	125.08	Inclination of hole:	-70	degrees			
Depth of groundwater (mbgl):	10.50	Test section (m):	From:	**38.00**	to	**44.00**	
Vertical waterlevel (mbgl):	9.86	Test section length (m):	**6.00**				
Piezometer Guage Factor	**0.08381934**	Piezo zero reading (Digital):	**8426**				

Description of Test section	**Average Flow Rate** (l/min)	**Gauge Pressure** (KPa)	**Piezometer Reading** (Digital)	**Total excess Head** (mH2O)
See Geotech/geological log for details. Dolerite dyke from 39m to 43.5m.	0			0
	0.00	100	8292	11.23
	0.00	200	8162	22.13
	0.00	300	8034	32.86

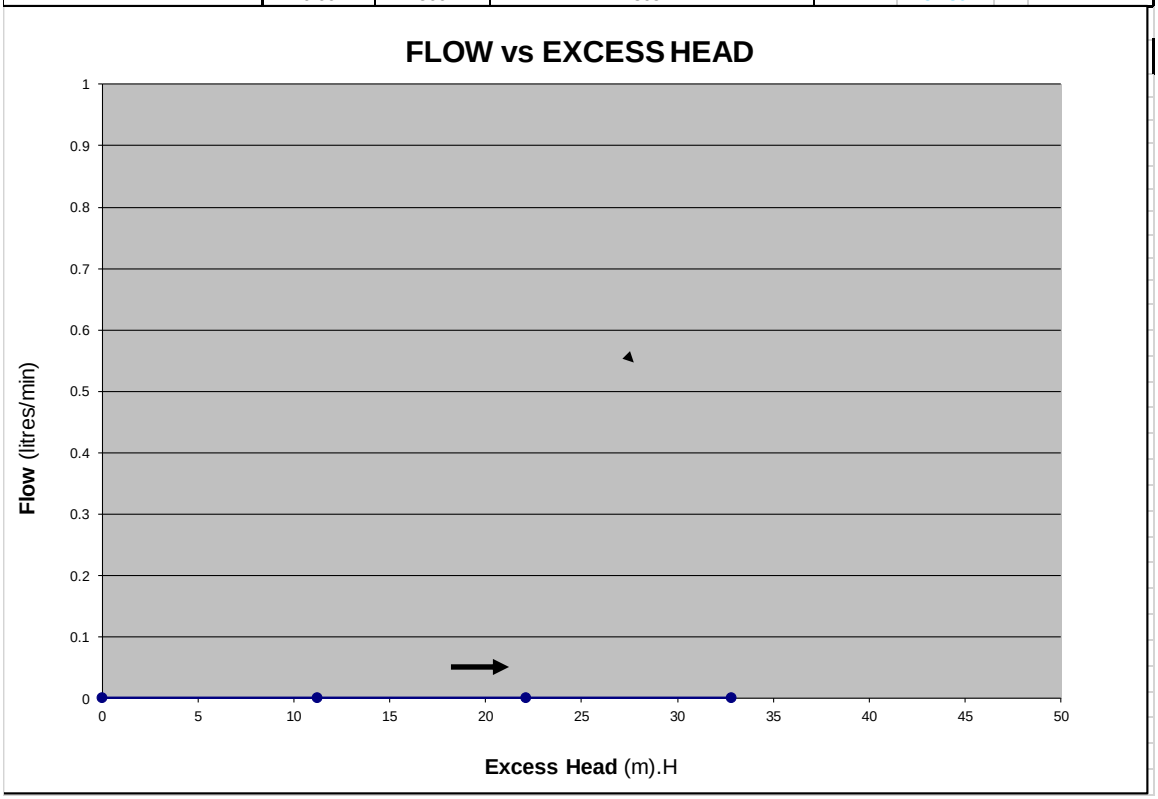

PACKER PERMEABILITY TEST

Borehole ID:	**BH_T1_02**	Test No:	**3**				
Packer type:	56mm Double Geopro	Date of Test:	27/10/2016				
Casing Details:	6m (PVC)	Packer inflation pressure (KPa):	1400				
Diameter of Hole (mm):	96.00	Test carried out by:	R C Minnaar				
Depth of hole (m):	125.08	Inclination of hole:	-70	degrees			
Depth of groundwater (mbgl):	10.50	Test section (m):	From:	**32.00**	to	**38.00**	
Vertical waterlevel (mbgl):	9.86	Test section length (m):	**6.00**				
Piezometer Guage Factor	**0.08381934**	Piezo zero reading (Digital):	**8469**				

Description of Test section	**Average Flow Rate** (l/min)	**Gauge Pressure** (KPa)	**Piezometer Reading** (Digital)	**Total excess Head** (mH2O)
	0			0
See Geotech/geological log for details.	0.00	100	8329	11.73
	0.00	200	8210	21.71
	0.00	300	8093	31.52

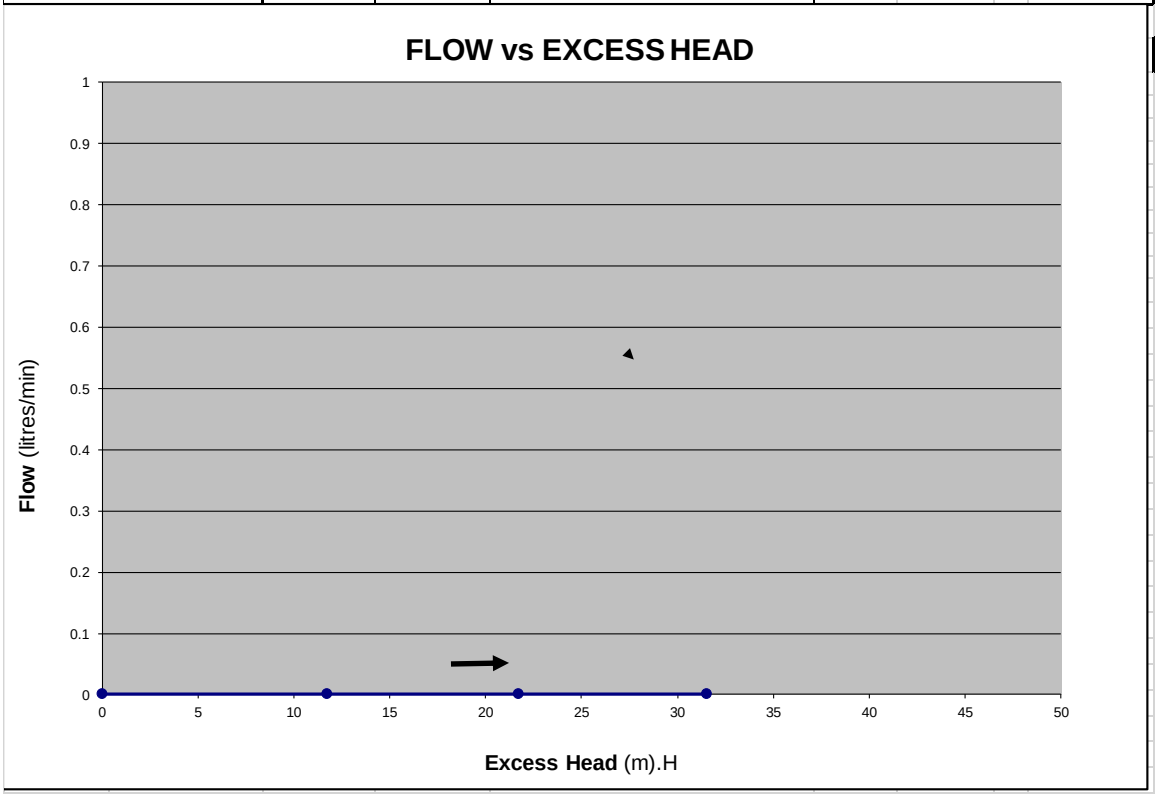

PACKER PERMEABILITY TEST

Borehole ID:	**BH_T1_02**	Test No:	**4**				
Packer type:	56mm Double Geopro	Date of Test:	27/10/2016				
Casing Details:	6m (PVC)	Packer inflation pressure (KPa):	1300				
Diameter of Hole (mm):	96.00	Test carried out by:	R C Minnaar				
Depth of hole (m):	125.08	Inclination of hole:	-70	degrees			
Depth of groundwater (mbgl):	10.50	Test section (m):	From:	**26.00**	to	**32.00**	
Vertical waterlevel (mbgl):	9.86	Test section length (m):	**6.00**				
Piezometer Guage Factor	**0.08381934**	Piezo zero reading (Digital):	**8530**				

Description of Test section	**Average Flow Rate** (l/min)	**Gauge Pressure** (KPa)	**Piezometer Reading** (Digital)	**Total excess Head** (mH2O)
See Geotech/geological log for details.	0			0
	0.00	100	8395	11.32
	0.00	200	8274	21.46
	0.00	300	8161	30.93

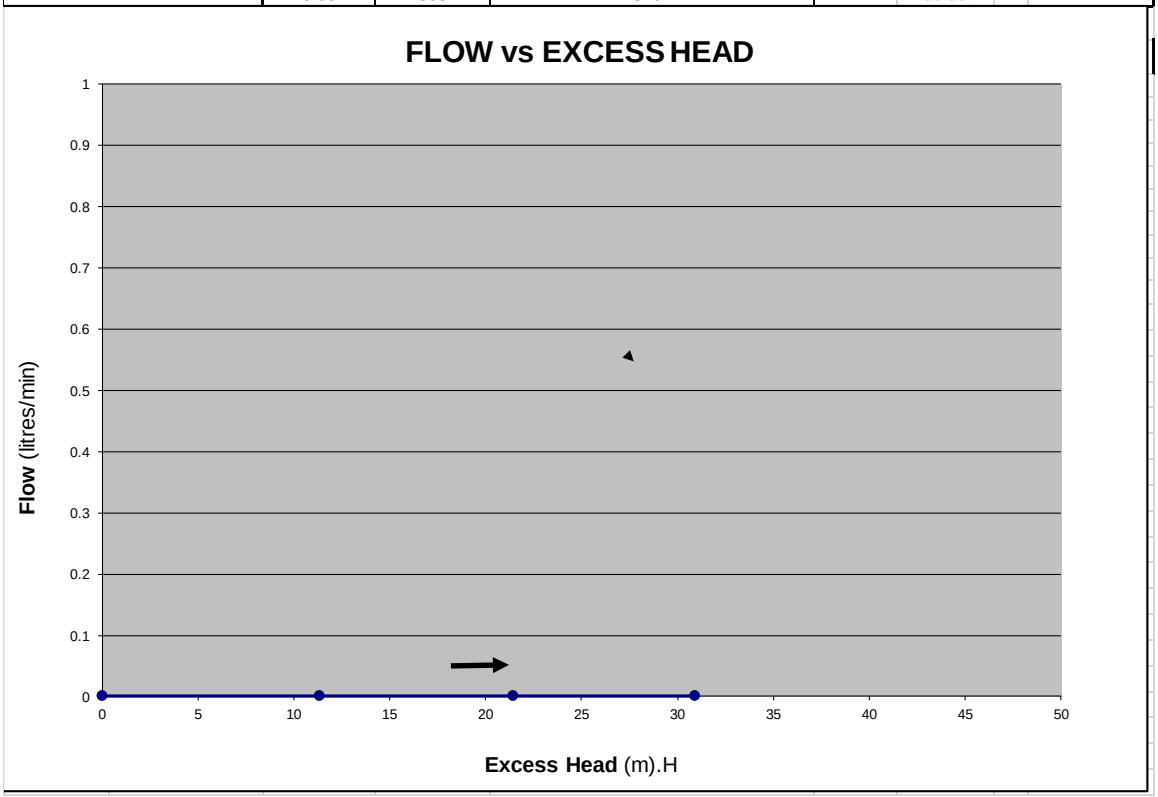

PACKER PERMEABILITY TEST

Borehole ID:	**BH_T1_02**	Test No:	**5**				
Packer type:	56mm Double Geopro	Date of Test:	27/10/2016				
Casing Details:	6m (PVC)	Packer inflation pressure (KPa):	1300				
Diameter of Hole (mm):	96.00	Test carried out by:	R C Minnaar				
Depth of hole (m):	125.08	Inclination of hole:	-70	degrees			
Depth of groundwater (mbgl):	10.50	Test section (m):	From:	**20.00**	to	**26.00**	
Vertical waterlevel (mbgl):	9.86	Test section length (m):	**6.00**				
Piezometer Guage Factor	**0.08381934**	Piezo zero reading (Digital):	**8595**				

Description of Test section	**Average Flow Rate** (l/min)	**Gauge Pressure** (KPa)	**Piezometer Reading** (Digital)	**Total excess Head** (mH2O)
See Geotech/geological log for details.	0			0
	0.00	100	8459	11.40
	0.00	200	8338	21.54
	0.00	300	8210	32.27

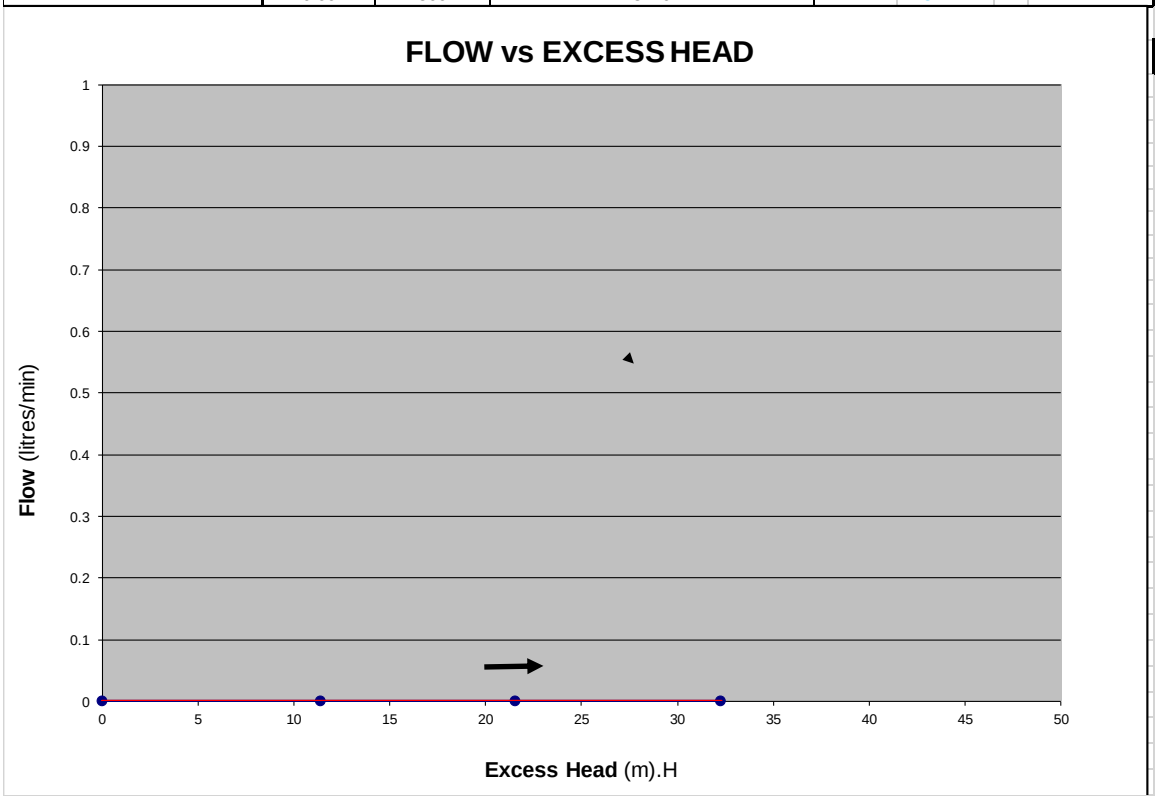

PACKER PERMEABILITY TEST

Borehole ID:	**BH_T1_02**	Test No:	**6**				
Packer type:	56mm Double Geopro	Date of Test:	27/10/2016				
Casing Details:	6m (PVC)	Packer inflation pressure (KPa):	1300				
Diameter of Hole (mm):	96.00	Test carried out by:	R C Minnaar				
Depth of hole (m):	125.08	Inclination of hole:	-70	degrees			
Depth of groundwater (mbgl):	10.50	Test section (m):	From:	**14.00**	to	**20.00**	
Vertical waterlevel (mbgl):	9.86	Test section length (m):	**6.00**				
Piezometer Guage Factor	**0.08381934**	Piezo zero reading (Digital):	**8675**				

Description of Test section	**Average Flow Rate** (l/min)	**Gauge Pressure** (KPa)	**Piezometer Reading** (Digital)	**Total excess Head** (mH2O)
	0			0
See Geotech/geological log for details.	0.00	100	8585	7.54
	0.00	200	8417	21.63
	0.00	300	8273	33.70

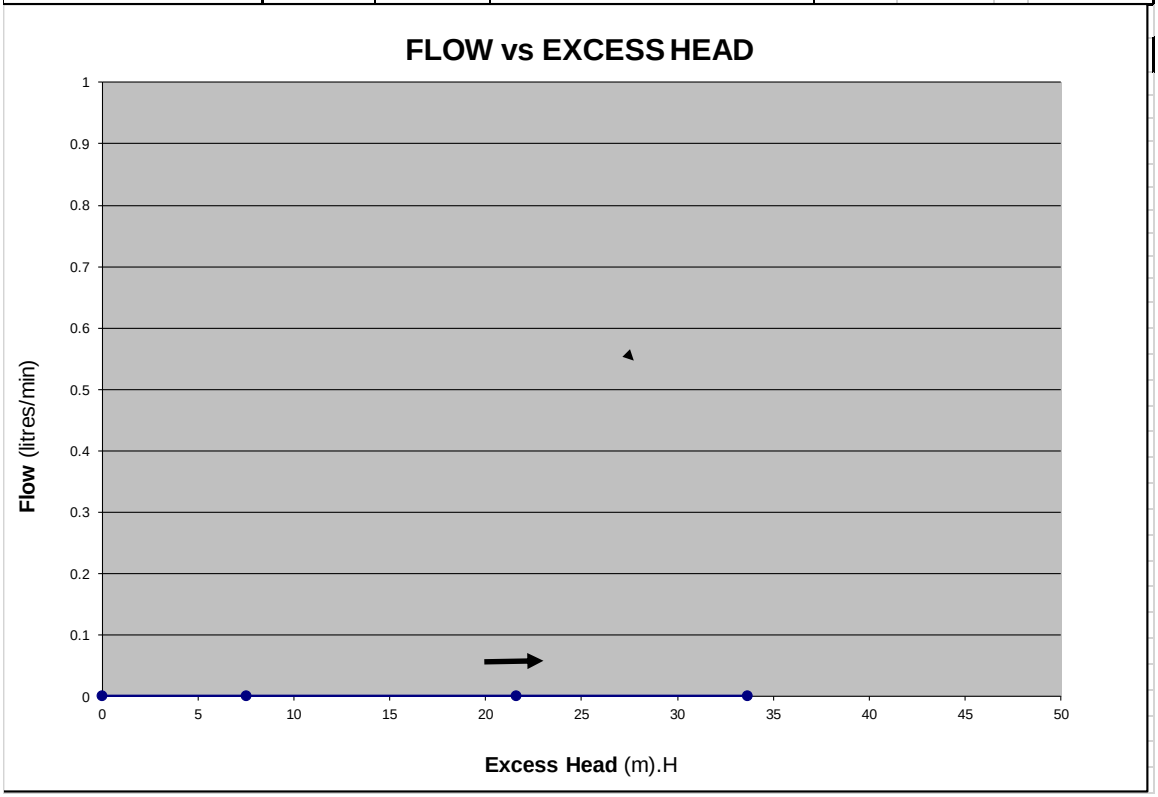

PACKER PERMEABILITY TEST

Borehole ID:	**BH_T1_02**	Test No:	**7**				
Packer type:	56mm Double Geopro	Date of Test:	05/11/2016				
Casing Details:	6m (PVC)	Packer inflation pressure (KPa):	1900				
Diameter of Hole (mm):	96.00	Test carried out by:	R C Minnaar				
Depth of hole (m):	125.08	Inclination of hole:	-70	degrees			
Depth of groundwater (mbgl):	10.50	Test section (m):	From:	**103.00**	to	**113.00**	
Vertical waterlevel (mbgl):	9.86	Test section length (m):		**10.00**			
Piezometer Guage Factor	**0.08381934**	Piezo zero reading (Digital):		**7710**			

Description of Test section	**Average Flow Rate** (l/min)	**Gauge Pressure** (KPa)	**Piezometer Reading** (Digital)	**Total excess Head** (mH2O)
See Geotech/geological log for details. Borehole blocked @ approximately 118m depth.	0			0
	1.80	100	7578	11.06
	3.35	200	7437	22.88
	4.70	300	7285	35.62
	3.35	200	7424	23.97
	1.95	100	7556	12.91

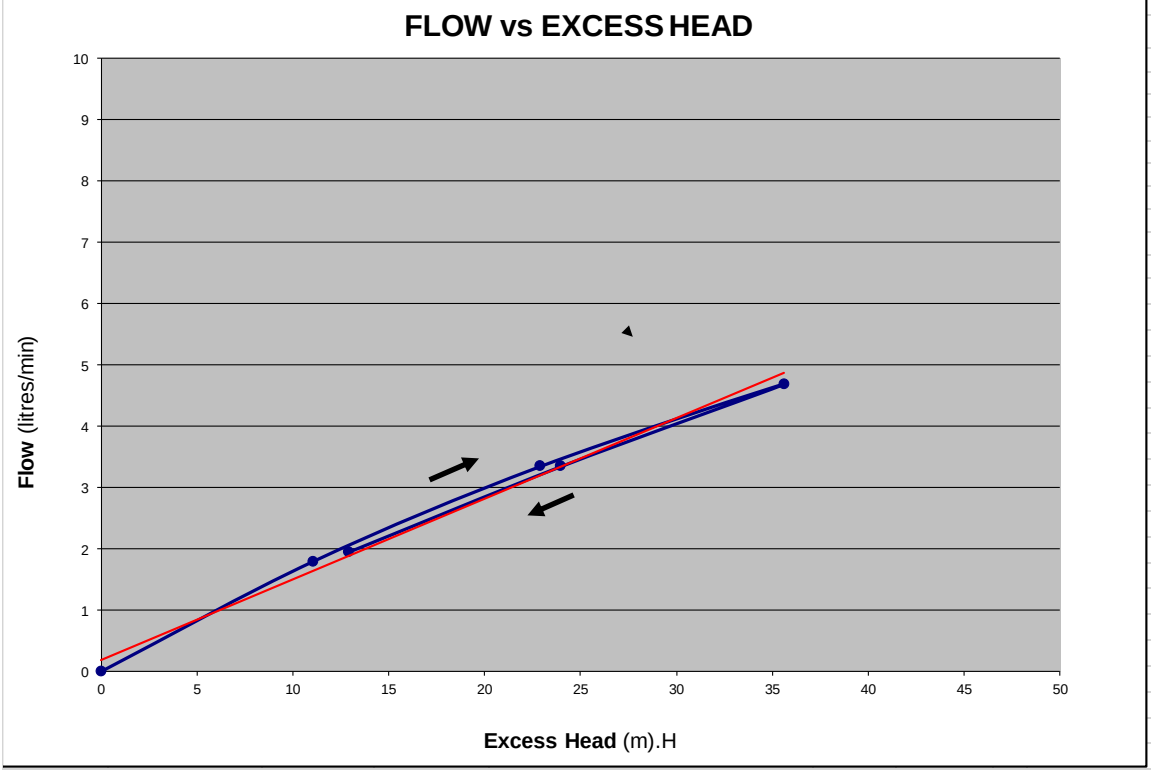

PACKER PERMEABILITY TEST

Borehole ID:	**BH_T1_02**	Test No:	**8**				
Packer type:	56mm Double Geopro	Date of Test:	05/11/2016				
Casing Details:	6m (PVC)	Packer inflation pressure (KPa):	2000				
Diameter of Hole (mm):	96.00	Test carried out by:	R C Minnaar				
Depth of hole (m):	125.08	Inclination of hole:	-70	degrees			
Depth of groundwater (mbgl):	10.50	Test section (m):	From:	**93.00**	to	**103.00**	
Vertical waterlevel (mbgl):	9.86	Test section length (m):	**10.00**				
Piezometer Guage Factor	**0.08381934**	Piezo zero reading (Digital):	**7786**				

Description of Test section	**Average Flow Rate** (l/min)	**Gauge Pressure** (KPa)	**Piezometer Reading** (Digital)	**Total excess Head** (mH2O)
	0			0
See Geotech/geological log for details.	0.00	100	7654	11.06
	0.00	200	7510	23.13
	0.00	300	7373	34.62

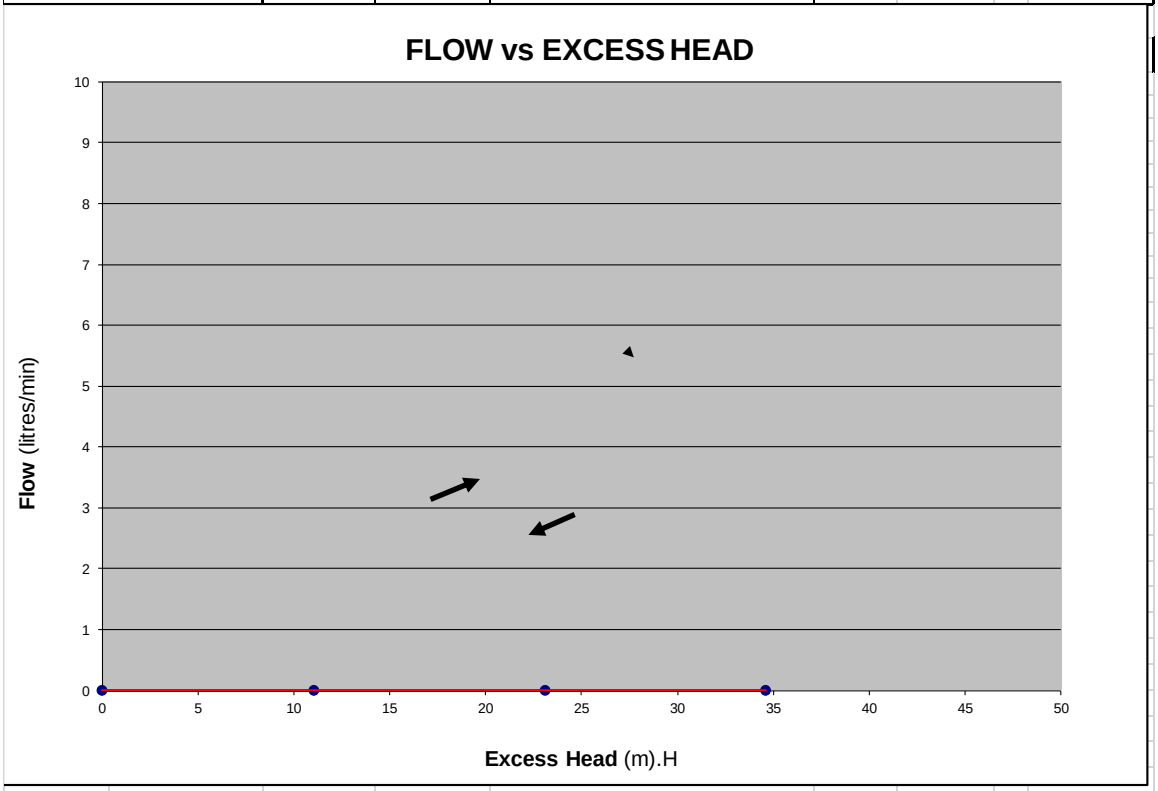

PACKER PERMEABILITY TEST

Borehole ID:	**BH_T1_02**	Test No:	**8 (re-test)**				
Packer type:	56mm Double Geopro	Date of Test:	05/11/2016				
Casing Details:	6m (PVC)	Packer inflation pressure (KPa):	2000				
Diameter of Hole (mm):	96.00	Test carried out by:	R C Minnaar				
Depth of hole (m):	125.08	Inclination of hole:	-70				degrees
Depth of groundwater (mbgl):	10.50	Test section (m):	From:	**83.00**	to	**93.00**	
Vertical waterlevel (mbgl):	9.86	Test section length (m):		**10.00**			
Piezometer Guage Factor	**0.08381934**	Piezo zero reading (Digital):		**7904**			

Description of Test section	**Average Flow Rate** (l/min)	**Gauge Pressure** (KPa)	**Piezometer Reading** (Digital)	**Total excess Head** (mH2O)
	0			0
See Geotech/geological log for details.	0.00	100	7751	12.82
	0.00	200	7615	24.22
	0.00	300	7483	35.29

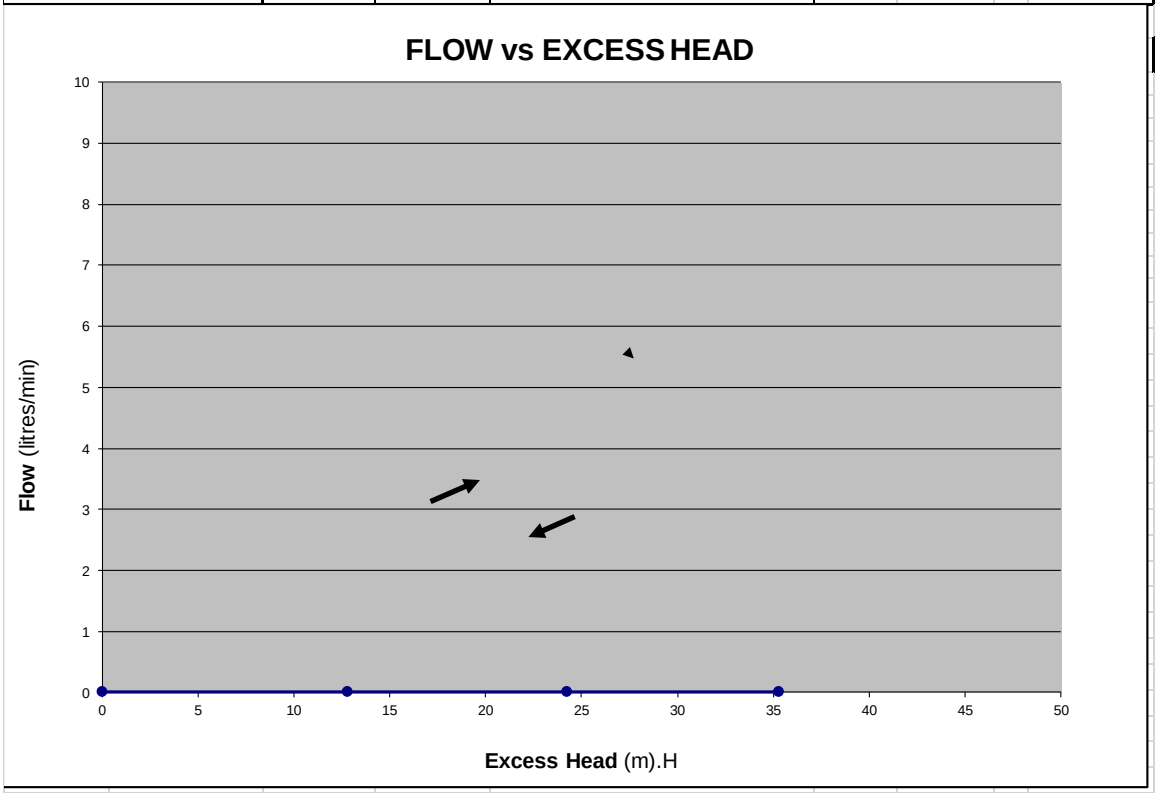

PACKER PERMEABILITY TEST

Borehole ID:	**BH_T1_02**	Test No:	**9**				
Packer type:	56mm Double Geopro	Date of Test:	05/11/2016				
Casing Details:	6m (PVC)	Packer inflation pressure (KPa):	1900				
Diameter of Hole (mm):	96.00	Test carried out by:	R C Minnaar				
Depth of hole (m):	125.08	Inclination of hole:	-70	degrees			
Depth of groundwater (mbgl):	10.50	Test section (m):	From:	**80.00**	to	**90.00**	
Vertical waterlevel (mbgl):	9.86	Test section length (m):	**10.00**				
Piezometer Guage Factor	**0.08381934**	Piezo zero reading (Digital):	**7931**				

Description of Test section	**Average Flow Rate** (l/min)	**Gauge Pressure** (KPa)	**Piezometer Reading** (Digital)	**Total excess Head** (mH2O)
	0			0
See Geotech/geological log for details.	0.00	100	7777	12.91
	0.00	200	7647	23.80
	0.00	300	7519	34.53

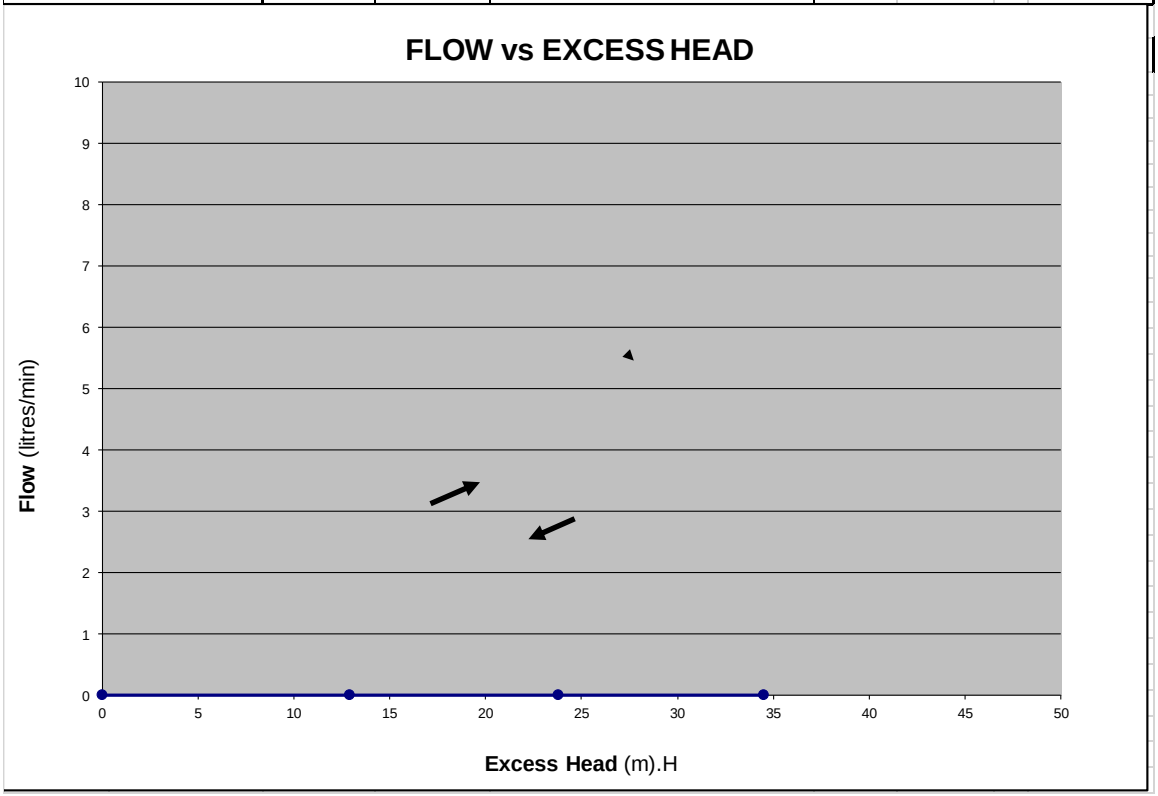

PACKER PERMEABILITY TEST

Borehole ID:	**BH_T1_02**	Test No:	**10**				
Packer type:	56mm Double Geopro	Date of Test:	05/11/2016				
Casing Details:	6m (PVC)	Packer inflation pressure (KPa):	2000				
Diameter of Hole (mm):	96.00	Test carried out by:	R C Minnaar				
Depth of hole (m):	125.08	Inclination of hole:	-70	degrees			
Depth of groundwater (mbgl):	10.50	Test section (m):	From:	**70.00**	to	**80.00**	
Vertical waterlevel (mbgl):	9.86	Test section length (m):	**10.00**				
Piezometer Guage Factor	**0.08381934**	Piezo zero reading (Digital):	**8046**				

Description of Test section	**Average Flow Rate** (l/min)	**Gauge Pressure** (KPa)	**Piezometer Reading** (Digital)	**Total excess Head** (mH2O)
	0			0
See Geotech/geological log for details.	0.00	100	7888	13.24
	0.00	200	7746	25.15
	0.00	300	7620	35.71

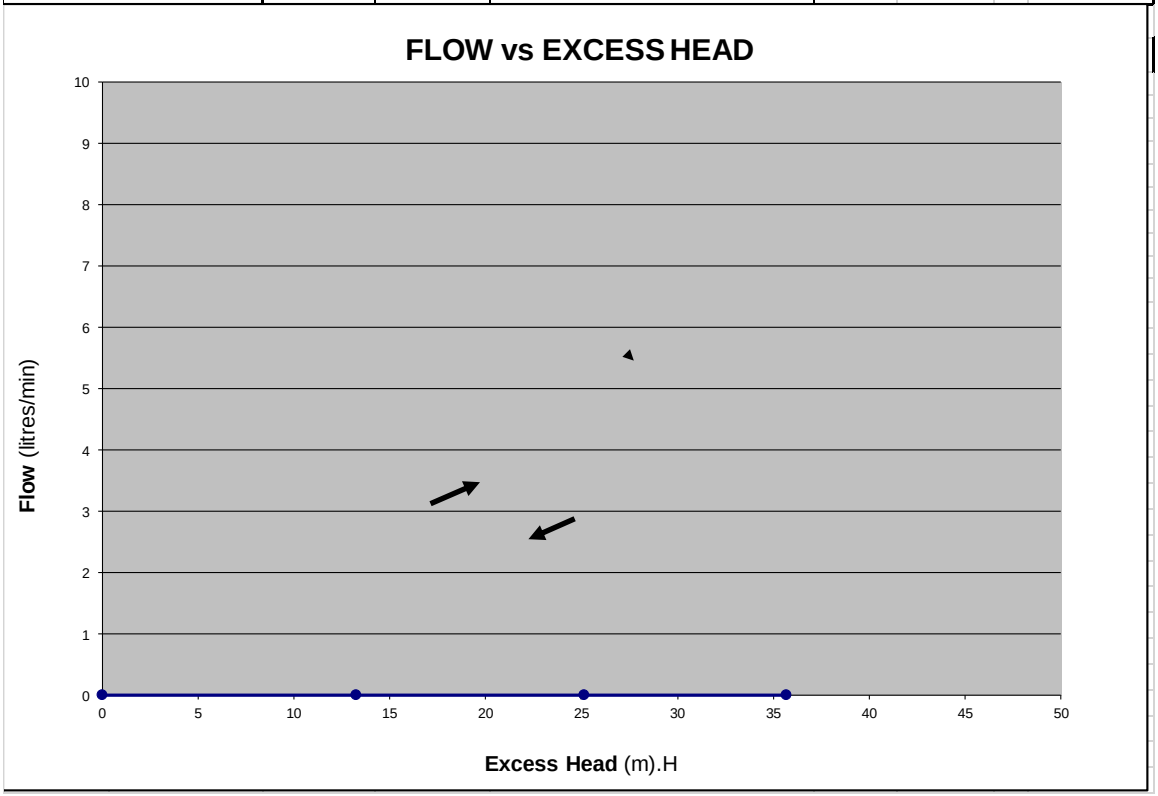

PACKER PERMEABILITY TEST

Borehole ID:	**BH_T1_02**	Test No:	**11**				
Packer type:	56mm Double Geopro	Date of Test:	05/11/2016				
Casing Details:	6m (PVC)	Packer inflation pressure (KPa):	2000				
Diameter of Hole (mm):	96.00	Test carried out by:	R C Minnaar				
Depth of hole (m):	125.08	Inclination of hole:	-70	degrees			
Depth of groundwater (mbgl):	10.50	Test section (m):	From:	**60.00**	to	**70.00**	
Vertical waterlevel (mbgl):	9.86	Test section length (m):	**10.00**				
Piezometer Guage Factor	**0.08381934**	Piezo zero reading (Digital):	**8151**				

Description of Test section	**Average Flow Rate** (l/min)	**Gauge Pressure** (KPa)	**Piezometer Reading** (Digital)	**Total excess Head** (mH2O)
See Geotech/geological log for details.	0			0
	0.00	100	7991	13.41
	0.00	200	7856	24.73
	0.00	300	7725	35.71

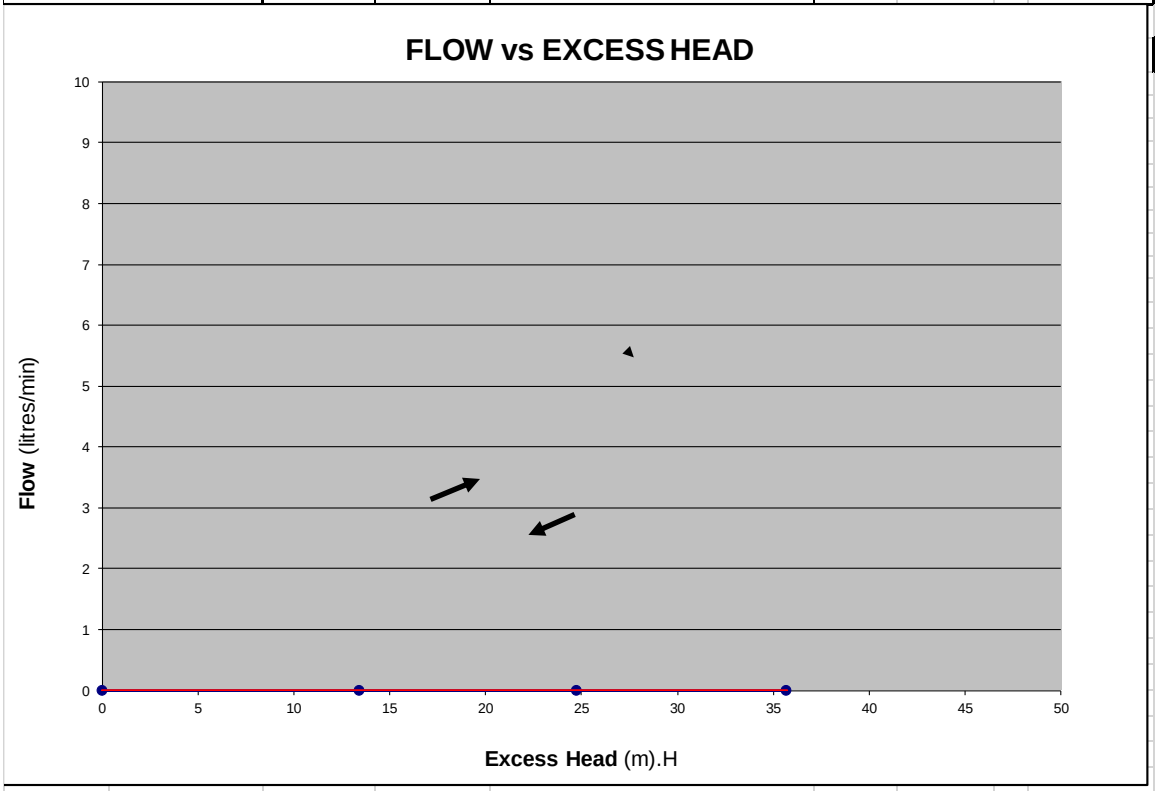

PACKER PERMEABILITY TEST

Borehole ID:	**BH_T1_02**	Test No:	**12**				
Packer type:	56mm Double Geopro	Date of Test:	05/11/2016				
Casing Details:	6m (PVC)	Packer inflation pressure (KPa):	1600				
Diameter of Hole (mm):	96.00	Test carried out by:	R C Minnaar				
Depth of hole (m):	125.08	Inclination of hole:	-70	degrees			
Depth of groundwater (mbgl):	10.50	Test section (m):	From:	**50.00**	to	**60.00**	
Vertical waterlevel (mbgl):	9.86	Test section length (m):	**10.00**				
Piezometer Guage Factor	**0.08381934**	Piezo zero reading (Digital):	**8266**				

Description of Test section	**Average Flow Rate** (l/min)	**Gauge Pressure** (KPa)	**Piezometer Reading** (Digital)	**Total excess Head** (mH2O)
	0			0
See Geotech/geological log for details.	0.72	100	8102	13.75
	1.25	200	7967	25.06
	1.80	300	7843	35.46
	0.95	200	7964	25.31
	0.43	100	8091	14.67

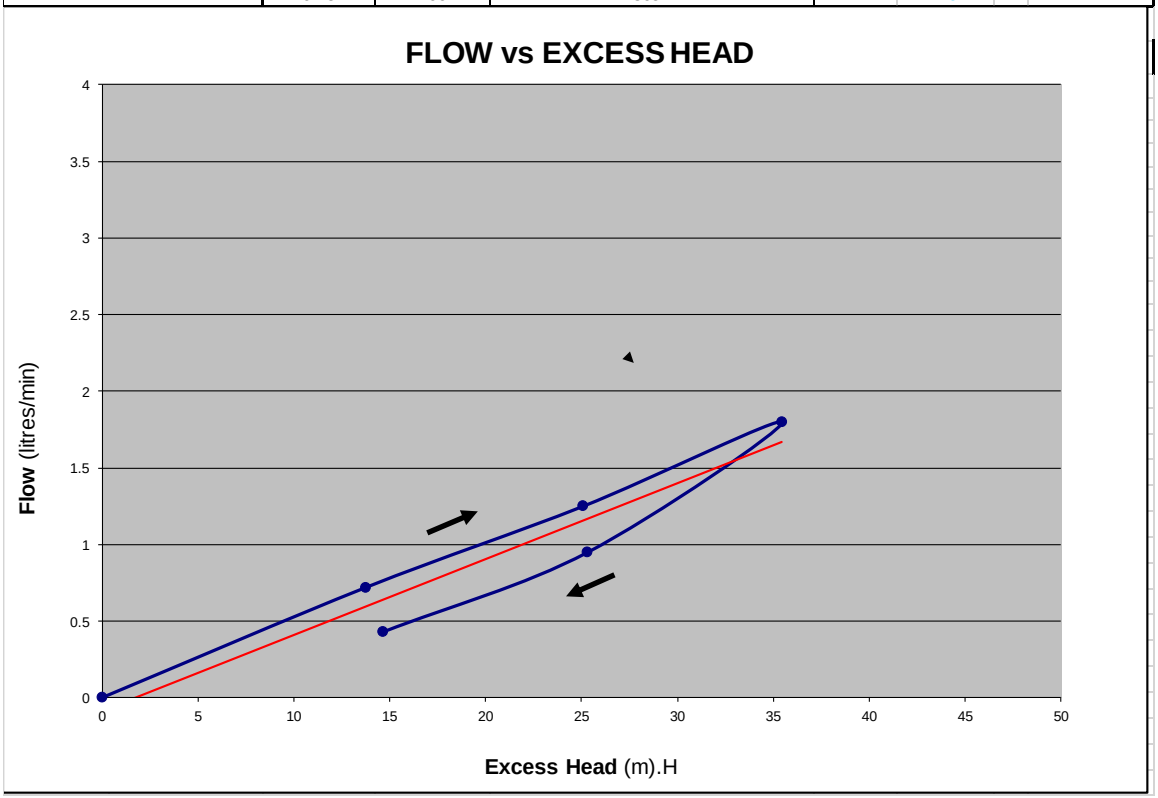

PACKER PERMEABILITY TEST

Borehole ID:	**BH_T2_01**	Test No:	**1**				
Packer type:	56mm Single Geopro	Date of Test:	03/11/2016				
Casing Details:	9m (PVC)	Packer inflation pressure (KPa):	1300				
Diameter of Hole (mm):	96.00	Test carried out by:	R C Minnaar				
Depth of hole (m):	71.12	Inclination of hole:	-70				degrees
Depth of groundwater (mbgl):	11.51	Test section (m):	From:	**48.00**	to	**71.12**	
Vertical waterlevel (mbgl):	10.81	Test section length (m):	**23.12**				
Piezometer Guage Factor	**0.08381934**	Piezo zero reading (Digital):	**8327**				

Description of Test section	**Average Flow Rate** (l/min)	**Gauge Pressure** (KPa)	**Piezometer Reading** (Digital)	**Total excess Head** (mH2O)
	0			0
See Geotech/geological log for details.	0.00	100	8189	11.57
	0.00	200	8076	21.04
	0.00	300	7938	32.61

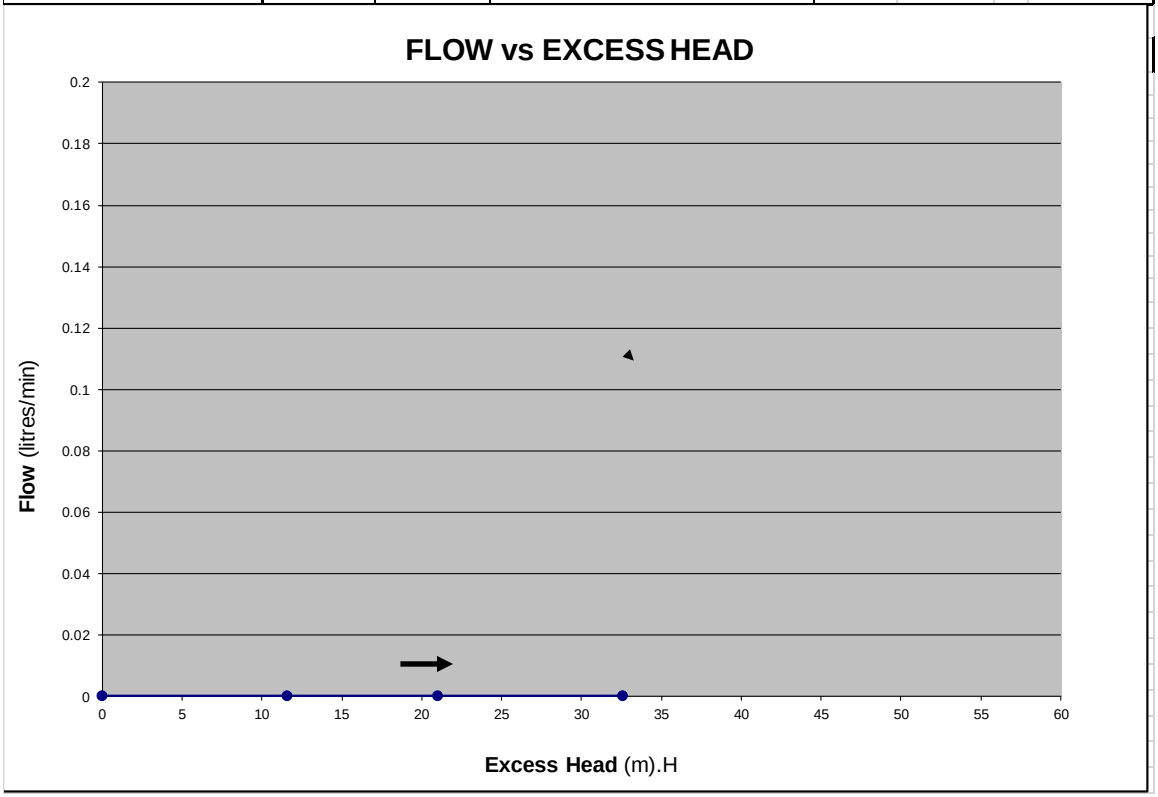

PACKER PERMEABILITY TEST

Borehole ID:	**BH_T2_01**	Test No:	**2**				
Packer type:	56mm Single Geopro	Date of Test:	03/11/2016				
Casing Details:	9m (PVC)	Packer inflation pressure (KPa):	1300				
Diameter of Hole (mm):	96.00	Test carried out by:	R C Minnaar				
Depth of hole (m):	71.12	Inclination of hole:	-70	degrees			
Depth of groundwater (mbgl):	11.51	Test section (m):	From:	**45.00**	to	**71.12**	
Vertical waterlevel (mbgl):	10.81	Test section length (m):	**26.12**				
Piezometer Guage Factor	**0.08381934**	Piezo zero reading (Digital):	**8367**				

Description of Test section	**Average Flow Rate** (l/min)	**Gauge Pressure** (KPa)	**Piezometer Reading** (Digital)	**Total excess Head** (mH2O)
See Geotech/geological log for details.	0			0
	0.03	100	8243	10.39
	0.05	200	8123	20.45
	0.07	300	7963	33.86
	0.05	200	8093	22.97
	0.02	100	8207	13.41

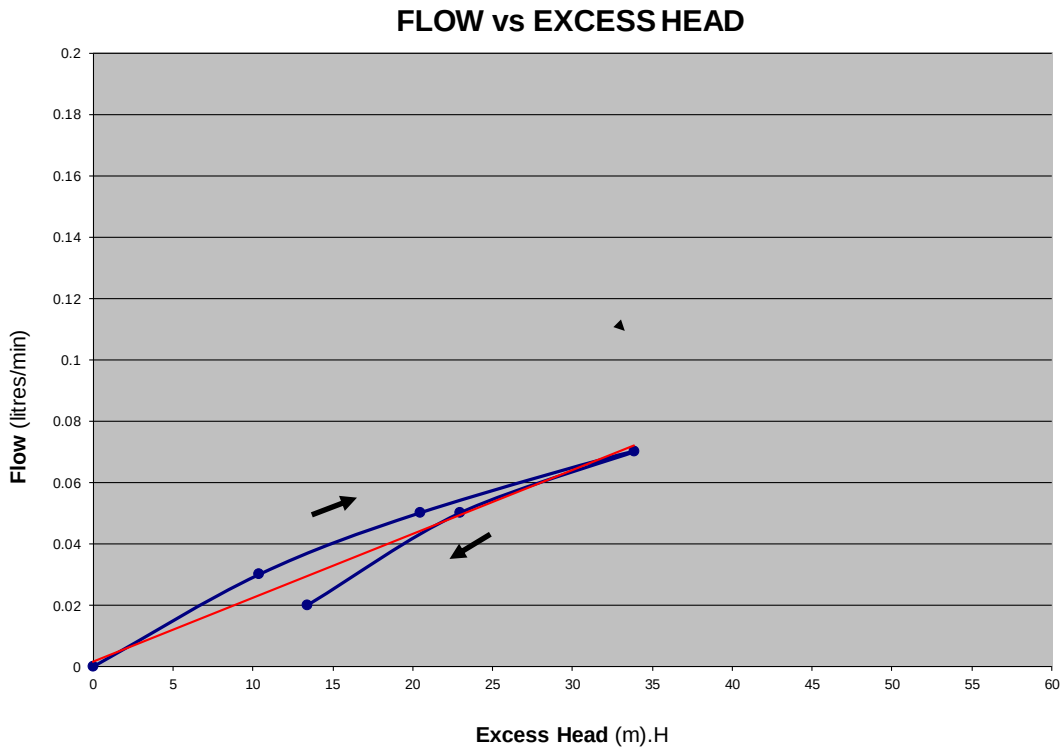

PACKER PERMEABILITY TEST

Borehole ID:	**BH_T2_01**	Test No:	**3**				
Packer type:	56mm Single Geopro	Date of Test:	03/11/2016				
Casing Details:	9m (PVC)	Packer inflation pressure (KPa):	1300				
Diameter of Hole (mm):	96.00	Test carried out by:	R C Minnaar				
Depth of hole (m):	71.12	Inclination of hole:	-70	degrees			
Depth of groundwater (mbgl):	11.51	Test section (m):	From:	**35.00**	to	**71.12**	
Vertical waterlevel (mbgl):	10.81	Test section length (m):	**36.12**				
Piezometer Guage Factor	**0.08381934**	Piezo zero reading (Digital):	**8474**				

Description of Test section	**Average Flow Rate** (l/min)	**Gauge Pressure** (KPa)	**Piezometer Reading** (Digital)	**Total excess Head** (mH2O)
See Geotech/geological log for details.	0			0
	0.02	100	8343	10.98
	0.05	200	8203	22.72
	0.07	300	8067	34.11
	0.02	200	8182	24.48

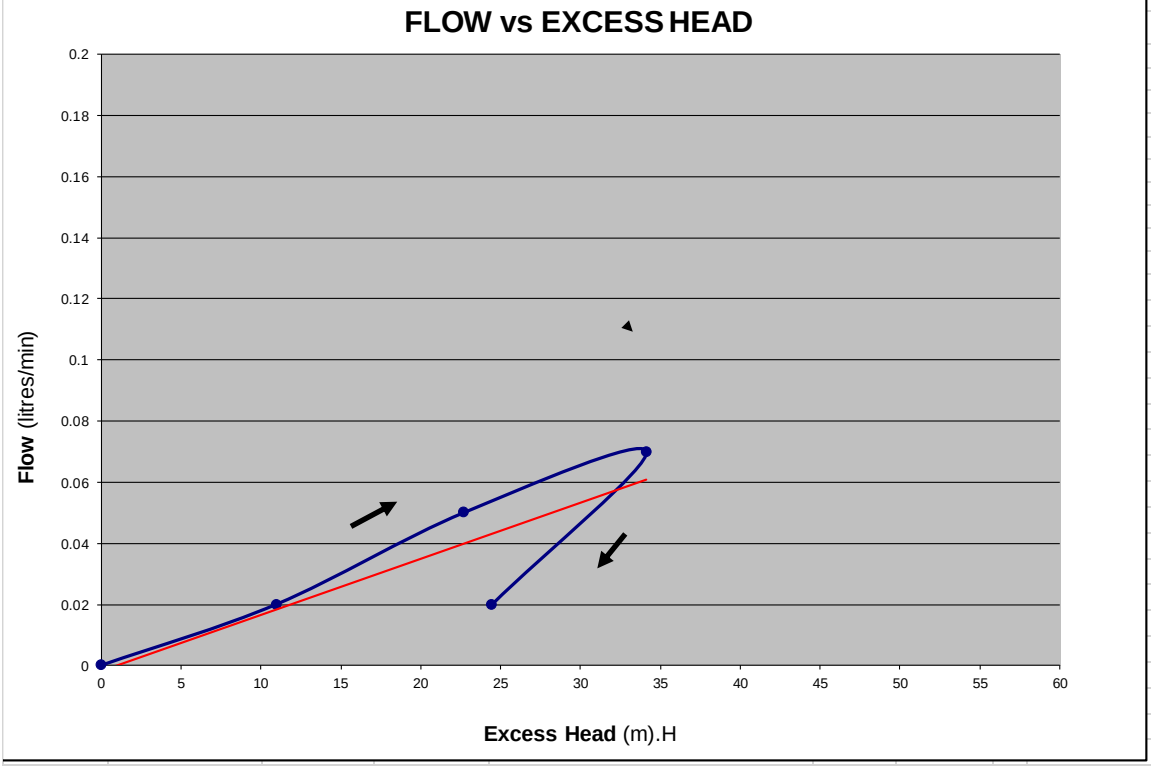

PACKER PERMEABILITY TEST

Borehole ID:	**BH_T2_01**		Test No:	**4**			
Packer type:	56mm Single Geopro		Date of Test:	03/11/2016			
Casing Details:	9m (PVC)		Packer inflation pressure (KPa):	1300			
Diameter of Hole (mm):	96.00		Test carried out by:	R C Minnaar			
Depth of hole (m):	71.12		Inclination of hole:	-70			degrees
Depth of groundwater (mbgl):	11.51		Test section (m):	From:	**30.00**	to	**71.12**
Vertical waterlevel (mbgl):	10.81		Test section length (m):		**41.12**		
Piezometer Guage Factor	**0.08381934**		Piezo zero reading (Digital):		**8529**		

Description of Test section	Average Flow Rate (l/min)	Gauge Pressure (KPa)	Piezometer Reading (Digital)	Total excess Head (mH2O)
See Geotech/geological log for details.	0			0
	0.01	100	8403	10.56
	0.05	200	8266	22.04
	0.07	300	8116	34.62

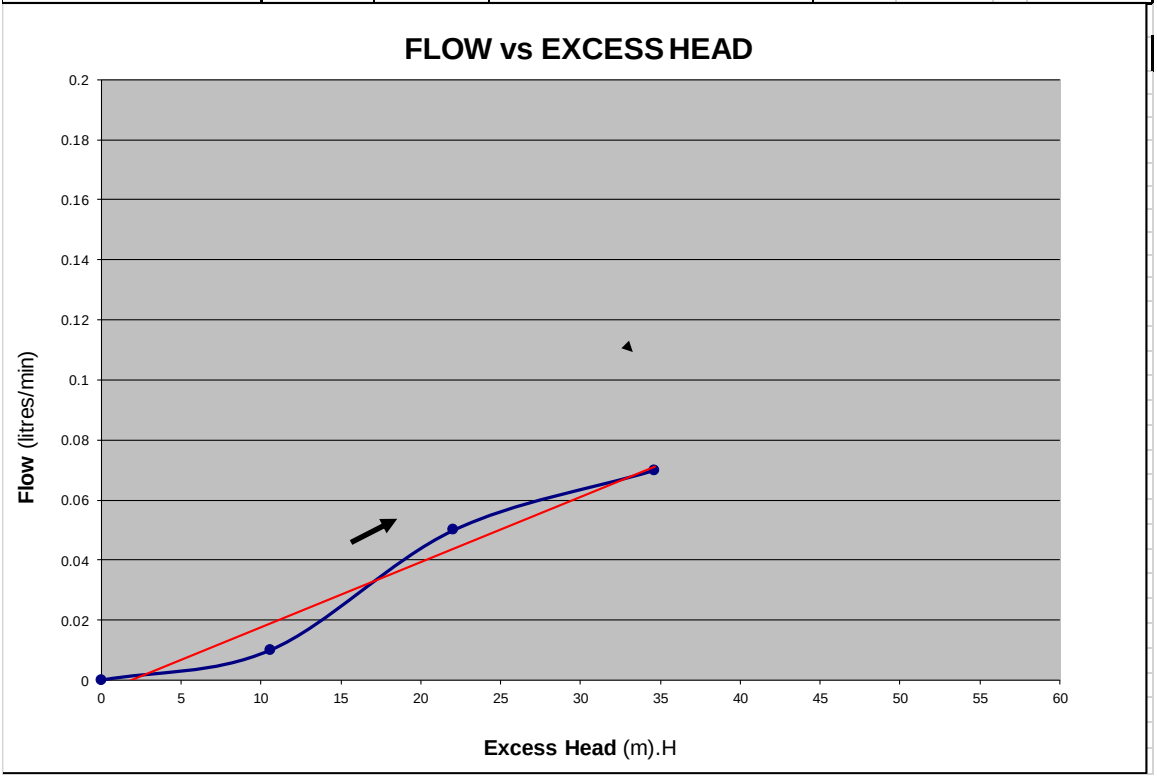

PACKER PERMEABILITY TEST

Borehole ID:	**BH_T2_01**	Test No:	**5**				
Packer type:	56mm Single Geopro	Date of Test:	03/11/2016				
Casing Details:	9m (PVC)	Packer inflation pressure (KPa):	1300				
Diameter of Hole (mm):	96.00	Test carried out by:	R C Minnaar				
Depth of hole (m):	71.12	Inclination of hole:	-70			degrees	
Depth of groundwater (mbgl):	11.51	Test section (m):	From:	**15.00**	to	**20.00**	
Vertical waterlevel (mbgl):	10.81	Test section length (m):		**5.00**			
Piezometer Guage Factor	**0.08381934**	Piezo zero reading (Digital):		**8695**			

Description of Test section	**Average Flow Rate** (l/min)	**Gauge Pressure** (KPa)	**Piezometer Reading** (Digital)	**Total excess Head** (mH2O)
	0			0
See Geotech/geological log for details.	28.00	100	8544	12.66
	42.00	190	8504	16.01
	47.00	250	8469	18.94
	38.00	150	8529	13.91
	28.00	50	8584	9.30

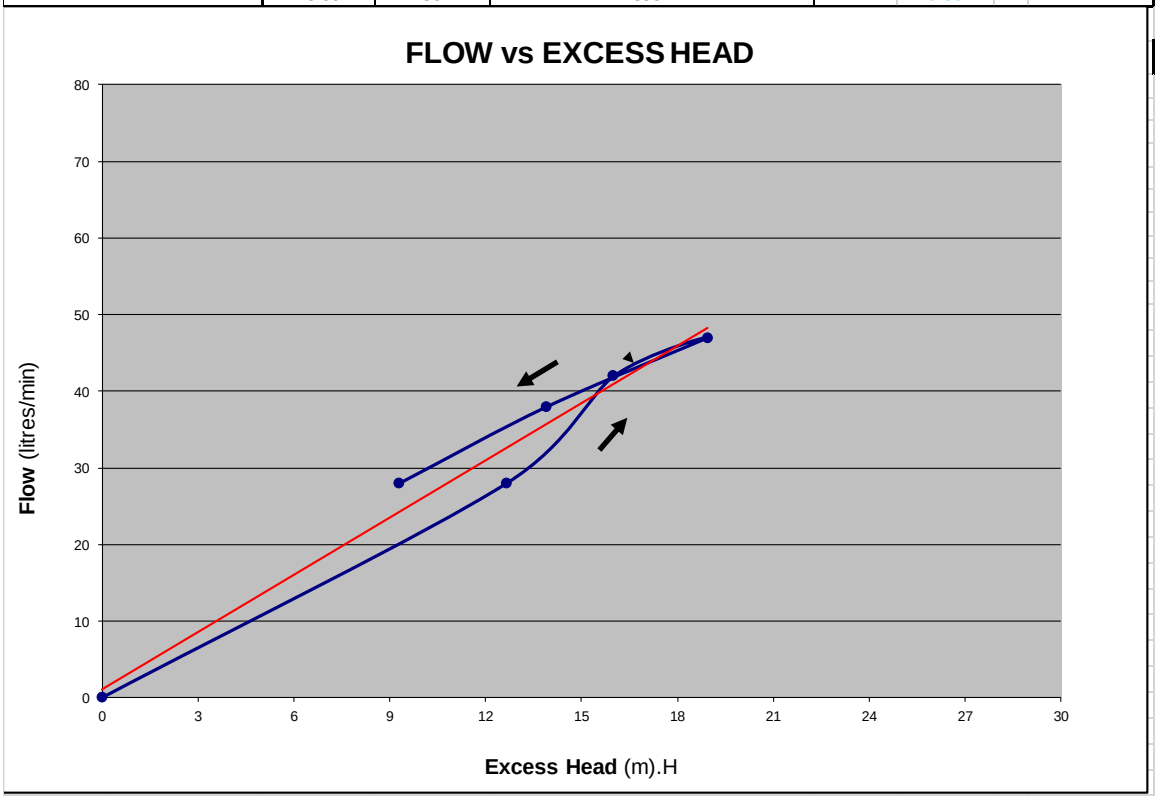

PACKER PERMEABILITY TEST

Borehole ID:	**BH_T2_01**	Test No:	**6**				
Packer type:	56mm Single Geopro	Date of Test:	03/11/2016				
Casing Details:	9m (PVC)	Packer inflation pressure (KPa):	1300				
Diameter of Hole (mm):	96.00	Test carried out by:	R C Minnaar				
Depth of hole (m):	71.12	Inclination of hole:	-70	degrees			
Depth of groundwater (mbgl):	11.51	Test section (m):	From:	**20.00**	to	**71.12**	
Vertical waterlevel (mbgl):	10.81	Test section length (m):	**51.12**				
Piezometer Guage Factor	**0.08381934**	Piezo zero reading (Digital):	**8605**				

Description of Test section	**Average Flow Rate** (l/min)	**Gauge Pressure** (KPa)	**Piezometer Reading** (Digital)	**Total excess Head** (mH2O)
See Geotech/geological log for details. Test to confirm high permeability in previous test is between 15m & 20m depth.	0			0
	0.03	100	8435	14.25
	0.06	200	8286	26.74
	0.08	300	8141	38.89

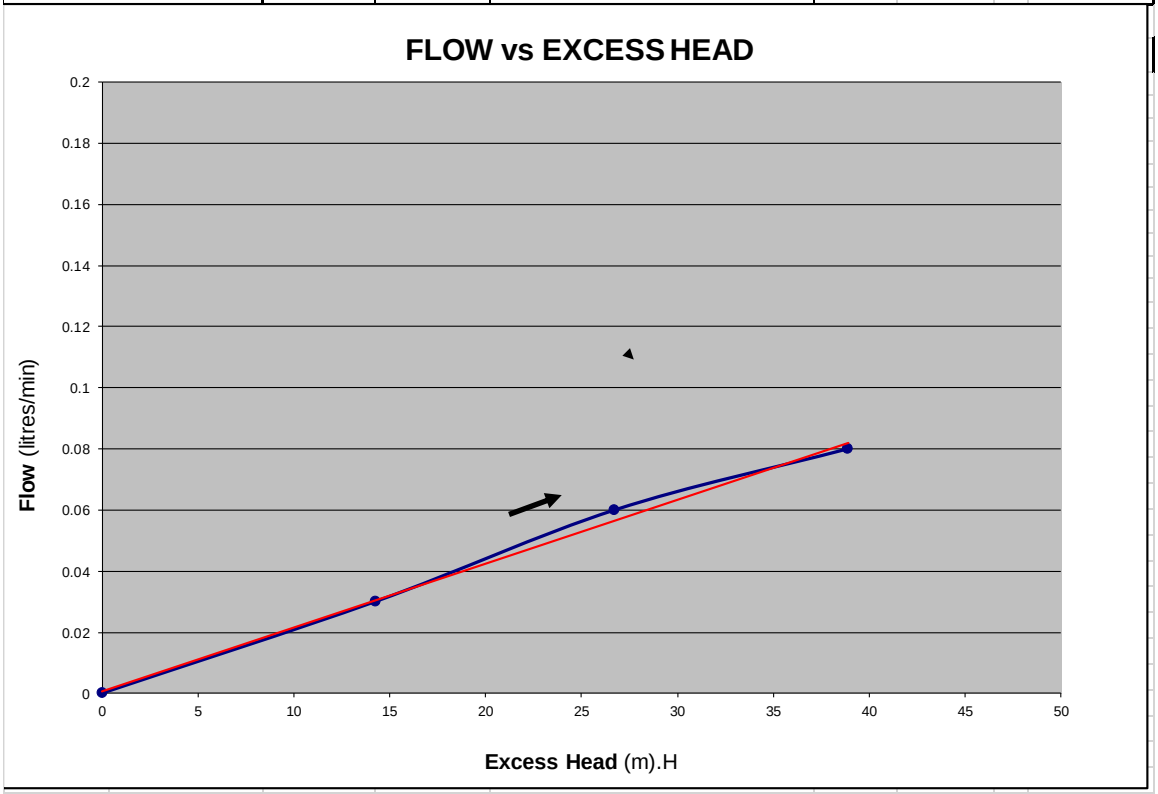

PACKER PERMEABILITY TEST

Borehole ID:	**BH_T5_02**	Test No:	**1**				
Packer type:	85mm Single Geopro	Date of Test:	29/10/2016				
Casing Details:	15m (Steel)	Packer inflation pressure (KPa):	1500				
Diameter of Hole (mm):	165.00	Test carried out by:	R C Minnaar				
Depth of hole (m):	80.00	Inclination of hole:	-90	degrees			
Depth of groundwater (mbgl):	11.60	Test section (m):	From:	**70.00**	to	**80.00**	
Vertical waterlevel (mbgl):	11.60	Test section length (m):	**10.00**				
Piezometer Guage Factor	**0.08381934**	Piezo zero reading (Digital):	**8070**				

Description of Test section	**Average Flow Rate** (l/min)	**Gauge Pressure** (KPa)	**Piezometer Reading** (Digital)	**Total excess Head** (mH2O)
	0			0
See Geotech/geological log for details.	0.00	100	7924	12.24
	0.00	200	7780	24.31
	0.00	300	7632	36.71

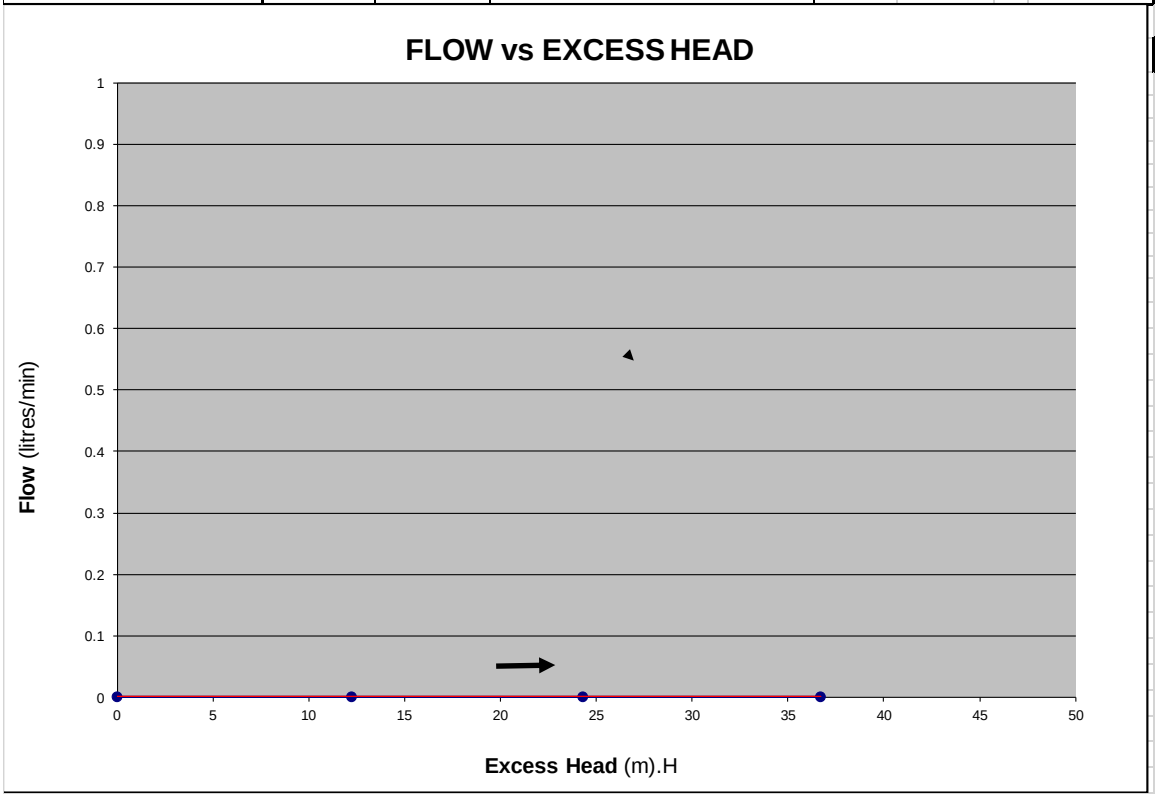

PACKER PERMEABILITY TEST

Borehole ID:	**BH_T5_02**	Test No:	**2**				
Packer type:	85mm Single Geopro	Date of Test:	29/10/2016				
Casing Details:	15m (Steel)	Packer inflation pressure (KPa):	1500				
Diameter of Hole (mm):	165.00	Test carried out by:	R C Minnaar				
Depth of hole (m):	80.00	Inclination of hole:	-90	degrees			
Depth of groundwater (mbgl):	11.60	Test section (m):	From:	**60.00**	to	**80.00**	
Vertical waterlevel (mbgl):	11.60	Test section length (m):	**20.00**				
Piezometer Guage Factor	**0.08381934**	Piezo zero reading (Digital):	**8175**				

Description of Test section	**Average Flow Rate** (l/min)	**Gauge Pressure** (KPa)	**Piezometer Reading** (Digital)	**Total excess Head** (mH2O)
	0			0
See Geotech/geological log for details.	0.00	100	8002	14.50
	0.00	200	7851	27.16
	0.00	300	7710	38.98

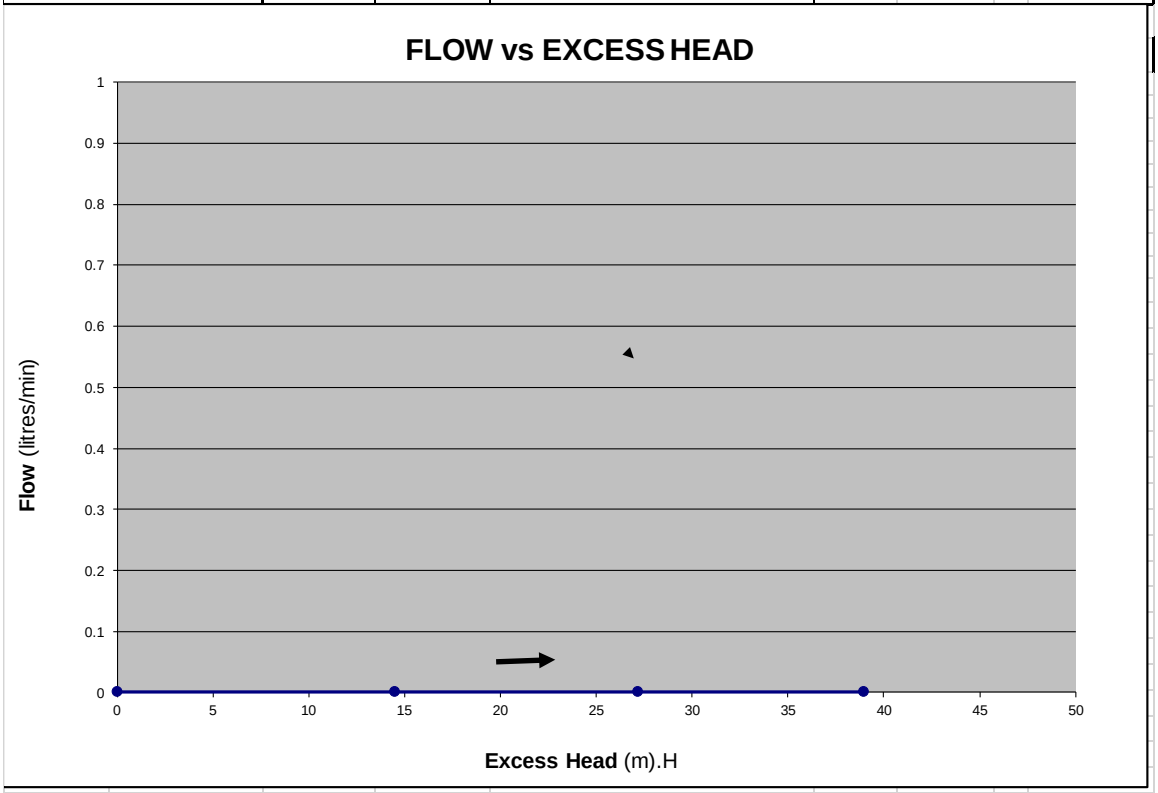

PACKER PERMEABILITY TEST

Borehole ID:	**BH_T5_02**	Test No:	**3**				
Packer type:	85mm Single Geopro	Date of Test:	29/10/2016				
Casing Details:	15m (Steel)	Packer inflation pressure (KPa):	1500				
Diameter of Hole (mm):	165.00	Test carried out by:	R C Minnaar				
Depth of hole (m):	80.00	Inclination of hole:	-90	degrees			
Depth of groundwater (mbgl):	11.60	Test section (m):	From:	**50.00**	to	**60.00**	
Vertical waterlevel (mbgl):	11.60	Test section length (m):	**10.00**				
Piezometer Guage Factor	**0.08381934**	Piezo zero reading (Digital):	**8304**				

Description of Test section	**Average Flow Rate** (l/min)	**Gauge Pressure** (KPa)	**Piezometer Reading** (Digital)	**Total excess Head** (mH2O)
See Geotech/geological log for details. Note that this test was actually conducted from 50m to 80m, but Test 1 & 2 from 60m to 80m proved completely impermeable so it can be assumed that all the permeability in this test was betwwen 50m & 60m.	0			0
	18.00	100	8031	22.88
	23.00	200	7914	32.69
	26.00	300	7798	42.41
	20.00	200	7914	32.69
	15.00	100	8030	22.97

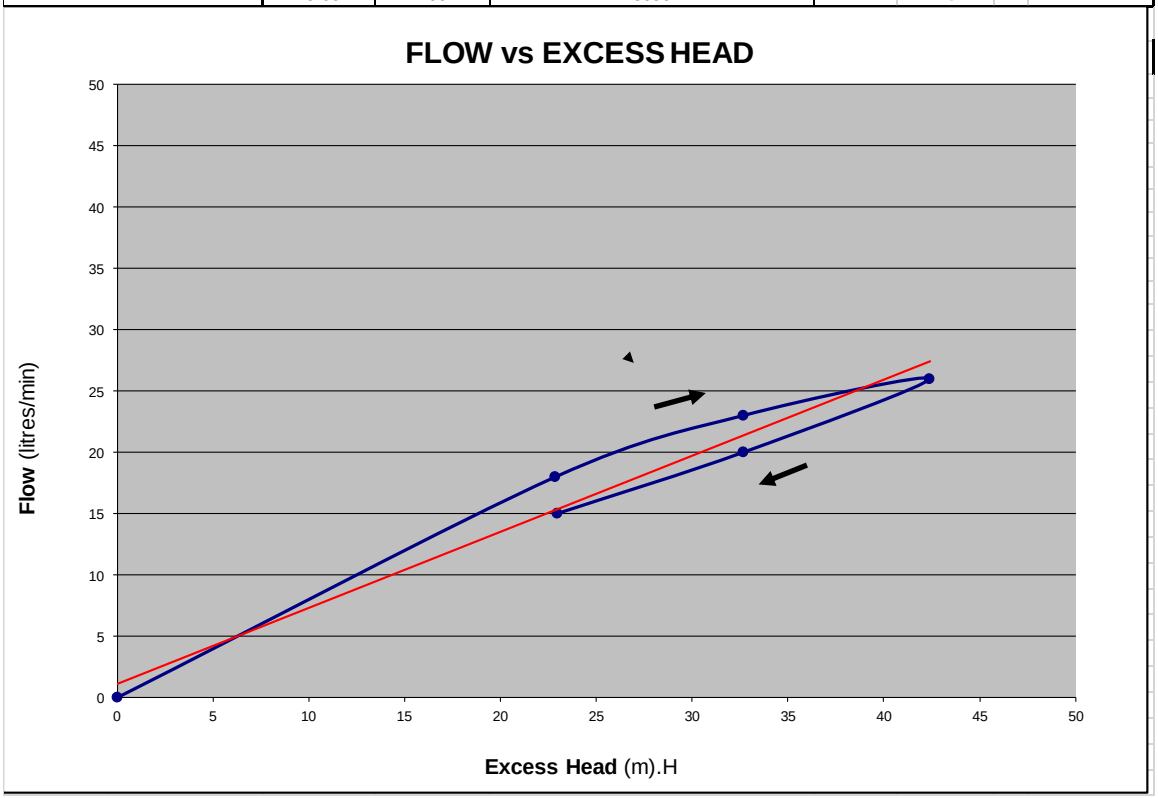

PACKER PERMEABILITY TEST

Borehole ID:	**BH_T5_02**	Test No:	**4**				
Packer type:	85mm Double Geopro	Date of Test:	29/10/2016				
Casing Details:	15m (Steel)	Packer inflation pressure (KPa):	1500				
Diameter of Hole (mm):	165.00	Test carried out by:	R C Minnaar				
Depth of hole (m):	80.00	Inclination of hole:	-90	degrees			
Depth of groundwater (mbgl):	11.60	Test section (m):	From:	**40.00**	to	**50.00**	
Vertical waterlevel (mbgl):	11.60	Test section length (m):	**10.00**				
Piezometer Guage Factor	**0.08381934**	Piezo zero reading (Digital):	**8410**				

Description of Test section	**Average Flow Rate** (l/min)	**Gauge Pressure** (KPa)	**Piezometer Reading** (Digital)	**Total excess Head** (mH2O)
	0			0
See Geotech/geological log for details.	0.22	100	8335	6.29
	0.77	200	8168	20.28
	1.15	300	8004	34.03
	0.59	200	8159	21.04
	0.30	100	8281	10.81

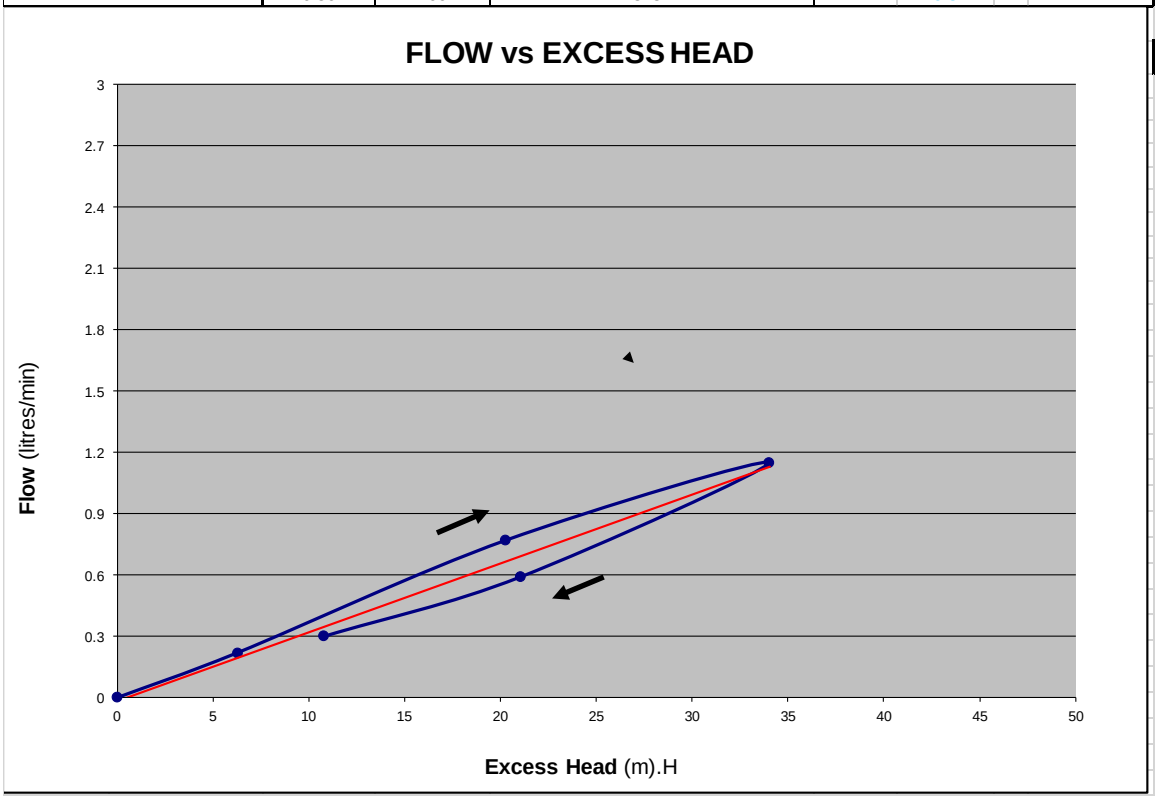

PACKER PERMEABILITY TEST

Borehole ID:	**BH_T5_02**	Test No:	**5**				
Packer type:	85mm Double Geopro	Date of Test:	29/10/2016				
Casing Details:	15m (Steel)	Packer inflation pressure (KPa):	1500				
Diameter of Hole (mm):	165.00	Test carried out by:	R C Minnaar				
Depth of hole (m):	80.00	Inclination of hole:	-90	degrees			
Depth of groundwater (mbgl):	11.60	Test section (m):	From:	**30.00**	to	**40.00**	
Vertical waterlevel (mbgl):	11.60	Test section length (m):	**10.00**				
Piezometer Guage Factor	**0.08381934**	Piezo zero reading (Digital):	**8534**				

Description of Test section	Average Flow Rate (l/min)	Gauge Pressure (KPa)	Piezometer Reading (Digital)	Total excess Head (mH2O)
	0			0
See Geotech/geological log for details.	0.00	100	8444	7.54
	1.10	200	8268	22.30
	1.70	300	8112	35.37
	1.30	200	8262	22.80
	0.60	100	8442	7.71

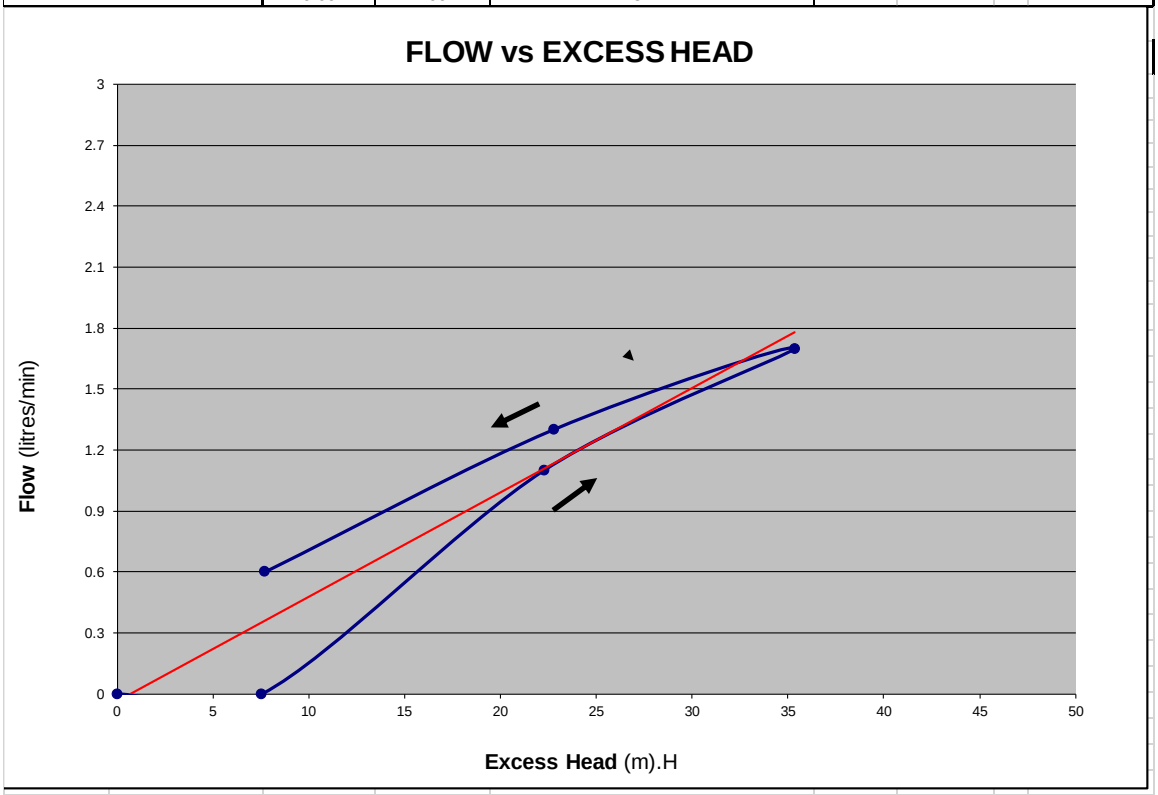

PACKER PERMEABILITY TEST

Borehole ID:	**BH_T5_02**	Test No:	**6**				
Packer type:	85mm Double Geopro	Date of Test:	29/10/2016				
Casing Details:	15m (Steel)	Packer inflation pressure (KPa):	1500				
Diameter of Hole (mm):	165.00	Test carried out by:	R C Minnaar				
Depth of hole (m):	80.00	Inclination of hole:	-90	degrees			
Depth of groundwater (mbgl):	11.60	Test section (m):	From:	**20.00**	to	**30.00**	
Vertical waterlevel (mbgl):	11.60	Test section length (m):	**10.00**				
Piezometer Guage Factor	**0.08381934**	Piezo zero reading (Digital):	**8688**				

Description of Test section	**Average Flow Rate** (l/min)	**Gauge Pressure** (KPa)	**Piezometer Reading** (Digital)	**Total excess Head** (mH2O)
	0			0
See Geotech/geological log for details.	1.70	100	8546	11.90
	3.50	200	8386	25.31
	4.90	300	8231	38.31
	3.20	200	8372	26.49
	1.65	100	8516	14.42

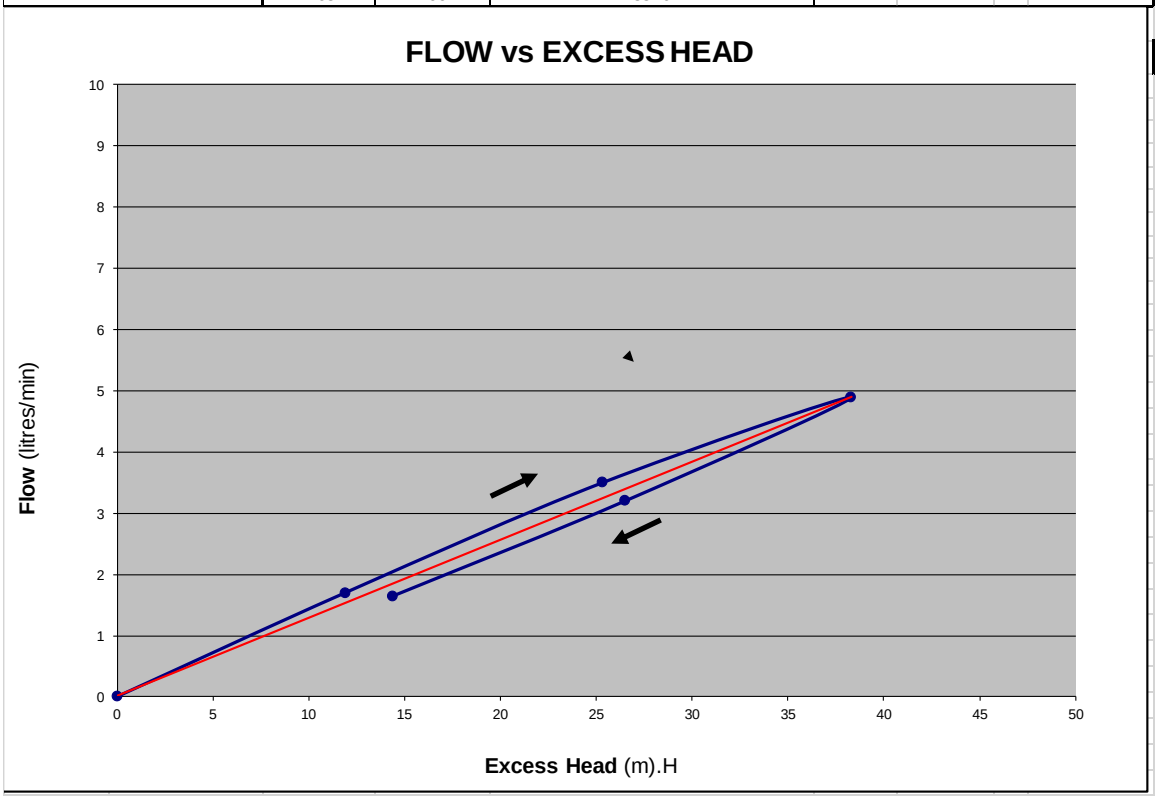

PACKER PERMEABILITY TEST

Borehole ID:	**BH_T6_01**	Test No:	**1**				
Packer type:	56mm Single Geopro	Date of Test:	24/10/2016				
Casing Details:	9m (PVC)	Packer inflation pressure (KPa):	2200				
Diameter of Hole (mm):	96.00	Test carried out by:	R C Minnaar				
Depth of hole (m):	137.05	Inclination of hole:	-70	degrees			
Depth of groundwater (mbgl):	26.50	Test section (m):	From:	**118.00**	to	**137.05**	
Vertical waterlevel (mbgl):	24.90	Test section length (m):	**19.05**				
Piezometer Guage Factor	**0.08381934**	Piezo zero reading (Digital):	**7734**				

Description of Test section	**Average Flow Rate** (l/min)	**Gauge Pressure** (KPa)	**Piezometer Reading** (Digital)	**Total excess Head** (mH2O)
	0			0
See Geotech/geological log for details.	0.01	100	7582	12.74
	0.04	200	7413	26.91
	0.07	300	7231	42.16
	0.00	200	7356	31.68

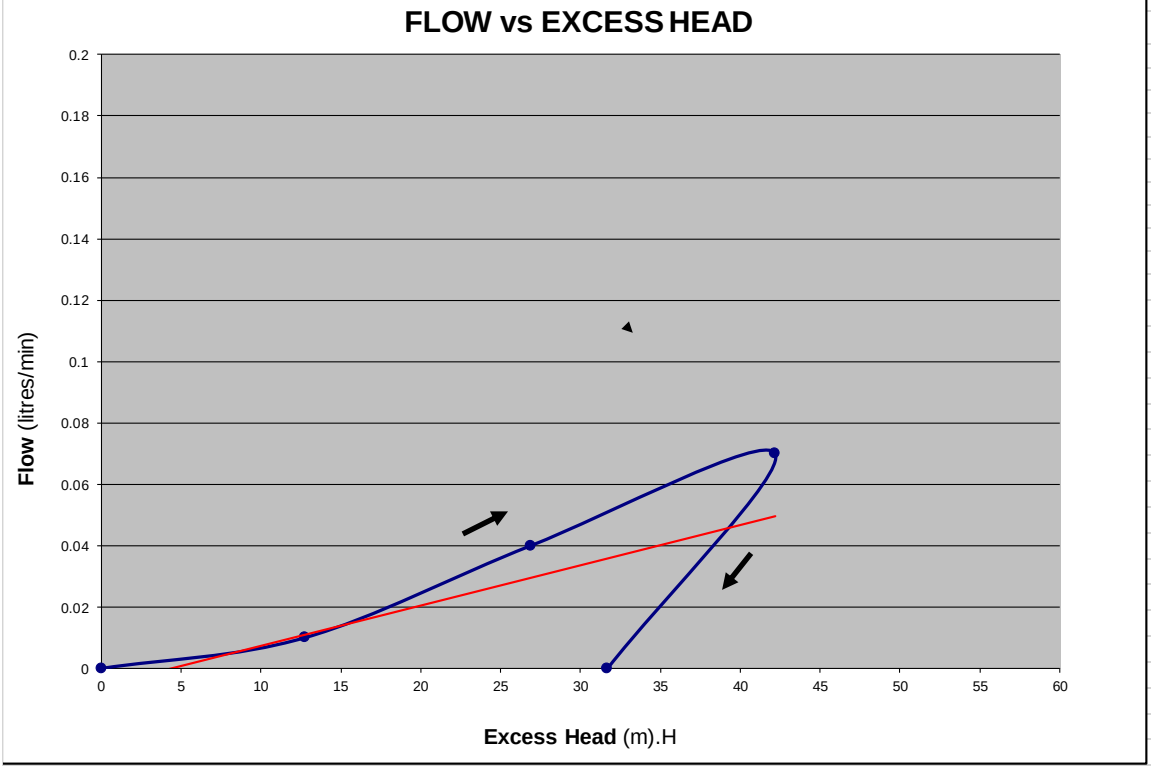

PACKER PERMEABILITY TEST

Borehole ID:	**BH_T6_01**	Test No:	**2**				
Packer type:	56mm Single Geopro	Date of Test:	24/10/2016				
Casing Details:	9m (PVC)	Packer inflation pressure (KPa):	2200				
Diameter of Hole (mm):	96.00	Test carried out by:	R C Minnaar				
Depth of hole (m):	137.05	Inclination of hole:	-70	degrees			
Depth of groundwater (mbgl):	26.50	Test section (m):	From:	**108.00**	to	**137.05**	
Vertical waterlevel (mbgl):	24.90	Test section length (m):	**29.05**				
Piezometer Guage Factor	**0.08381934**	Piezo zero reading (Digital):	**7848**				

Description of Test section	**Average Flow Rate** (l/min)	**Gauge Pressure** (KPa)	**Piezometer Reading** (Digital)	**Total excess Head** (mH2O)
See Geotech/geological log for details.	0			0
	0.01	100	7680	14.08
	0.03	200	7503	28.92
	0.05	300	7332	43.25
	0.00	200	7441	34.11

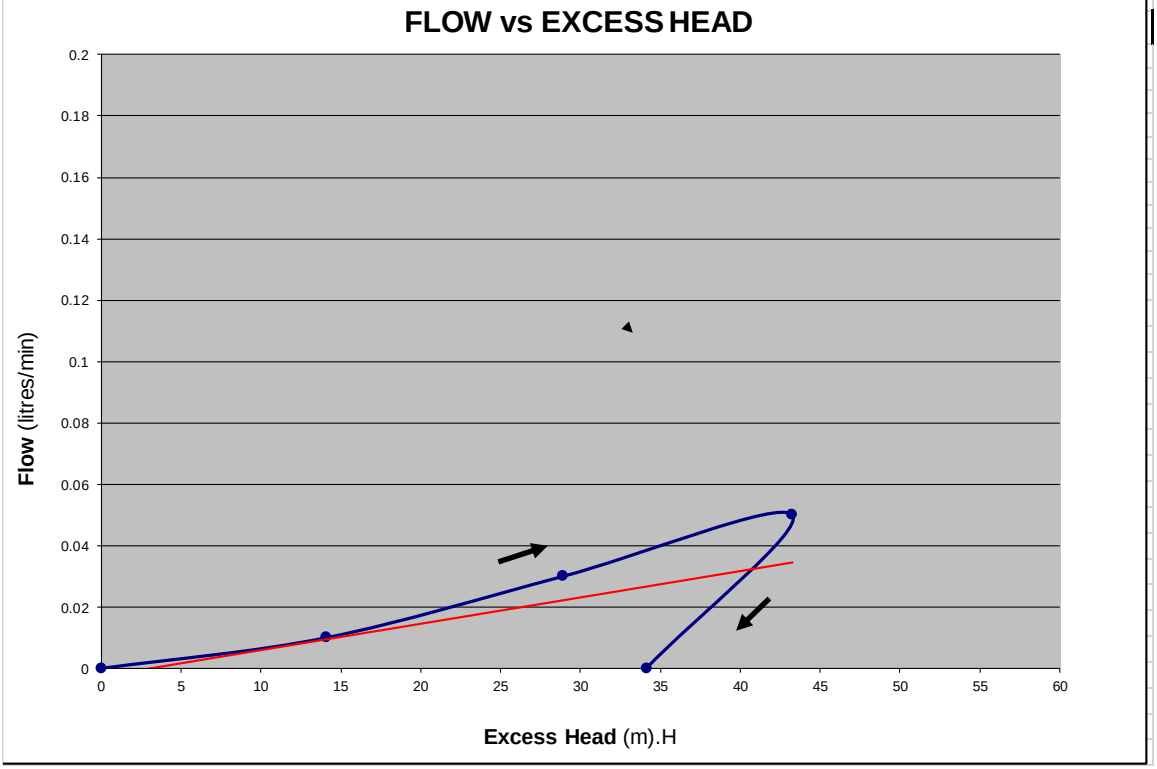

PACKER PERMEABILITY TEST

Borehole ID:	**BH_T6_01**	Test No:	**3**				
Packer type:	56mm Single Geopro	Date of Test:	24/10/2016				
Casing Details:	9m (PVC)	Packer inflation pressure (KPa):	2400				
Diameter of Hole (mm):	96.00	Test carried out by:	R C Minnaar				
Depth of hole (m):	137.05	Inclination of hole:	-70	degrees			
Depth of groundwater (mbgl):	26.50	Test section (m):	From:	**98.00**	to	**137.05**	
Vertical waterlevel (mbgl):	24.90	Test section length (m):	**39.05**				
Piezometer Guage Factor	**0.08381934**	Piezo zero reading (Digital):	**7951**				

Description of Test section	**Average Flow Rate** (l/min)	**Gauge Pressure** (KPa)	**Piezometer Reading** (Digital)	**Total excess Head** (mH2O)
	0			0
See Geotech/geological log for details.	0.00	100	7801	12.57
	0.02	200	7610	28.58
	0.04	300	7441	42.75
	0.00	200	7544	34.11

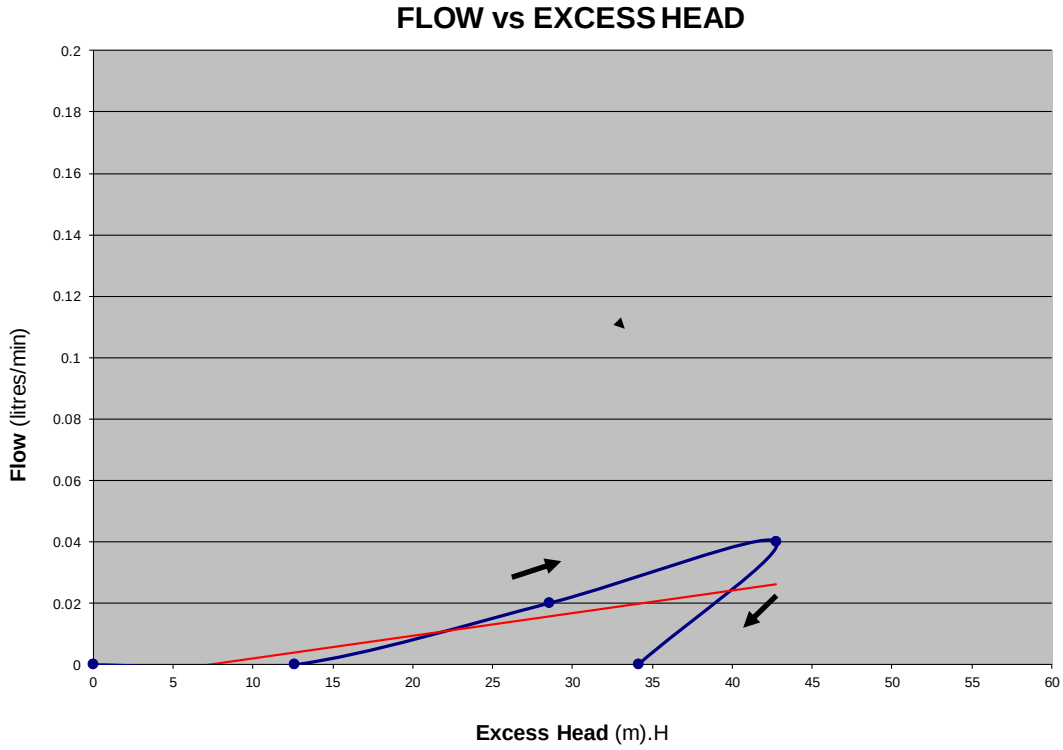

PACKER PERMEABILITY TEST

Borehole ID:	**BH_T6_01**	Test No:	**4**				
Packer type:	56mm Single Geopro	Date of Test:	24/10/2016				
Casing Details:	9m (PVC)	Packer inflation pressure (KPa):	2200				
Diameter of Hole (mm):	96.00	Test carried out by:	R C Minnaar				
Depth of hole (m):	137.05	Inclination of hole:	-70	degrees			
Depth of groundwater (mbgl):	26.50	Test section (m):	From:	**90.00**	to	**137.05**	
Vertical waterlevel (mbgl):	24.90	Test section length (m):	**47.05**				
Piezometer Guage Factor	**0.08381934**	Piezo zero reading (Digital):	**8041**				

Description of Test section	Average Flow Rate (l/min)	Gauge Pressure (KPa)	Piezometer Reading (Digital)	Total excess Head (mH2O)
See Geotech/geological log for details.	0			0
	0.24	100	7907	11.23
	0.71	200	7701	28.50
	1.30	300	7526	43.17
	1.23	200	7681	30.17
	0.65	100	7879	13.58

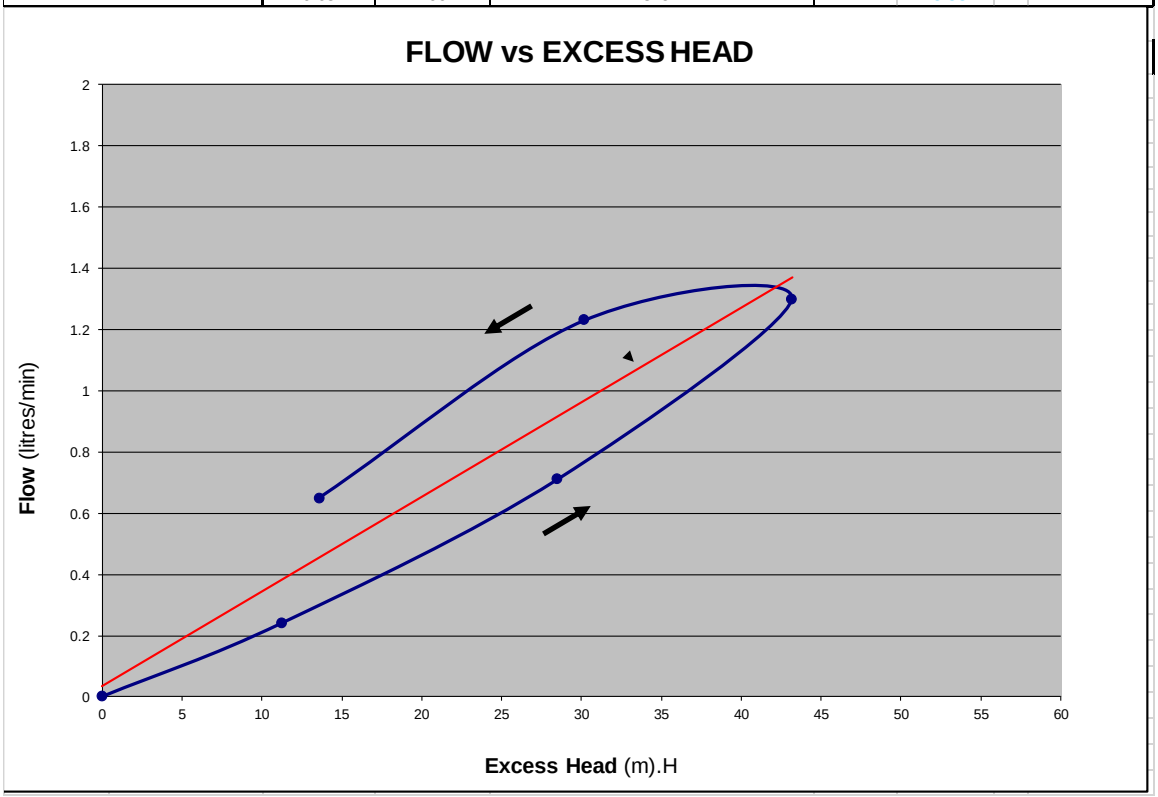

PACKER PERMEABILITY TEST

Borehole ID:	**BH_T6_01**	Test No:	**5**				
Packer type:	56mm Single Geopro	Date of Test:	24/10/2016				
Casing Details:	9m (PVC)	Packer inflation pressure (KPa):	2200				
Diameter of Hole (mm):	96.00	Test carried out by:	R C Minnaar				
Depth of hole (m):	137.05	Inclination of hole:	-70	degrees			
Depth of groundwater (mbgl):	26.50	Test section (m):	From:	**70.00**	to	**137.05**	
Vertical waterlevel (mbgl):	24.90	Test section length (m):	**67.05**				
Piezometer Guage Factor	**0.08381934**	Piezo zero reading (Digital):	**8243**				

Description of Test section	**Average Flow Rate** (l/min)	**Gauge Pressure** (KPa)	**Piezometer Reading** (Digital)	**Total excess Head** (mH2O)
	0			0
See Geotech/geological log for details. Reverse flow when reducing pressure (back-pressure).	0.20	100	8063	15.09
	0.30	200	7881	30.34
	0.37	300	7719	43.92
	0.06	200	7826	34.95
	0.00	100	7907	28.16

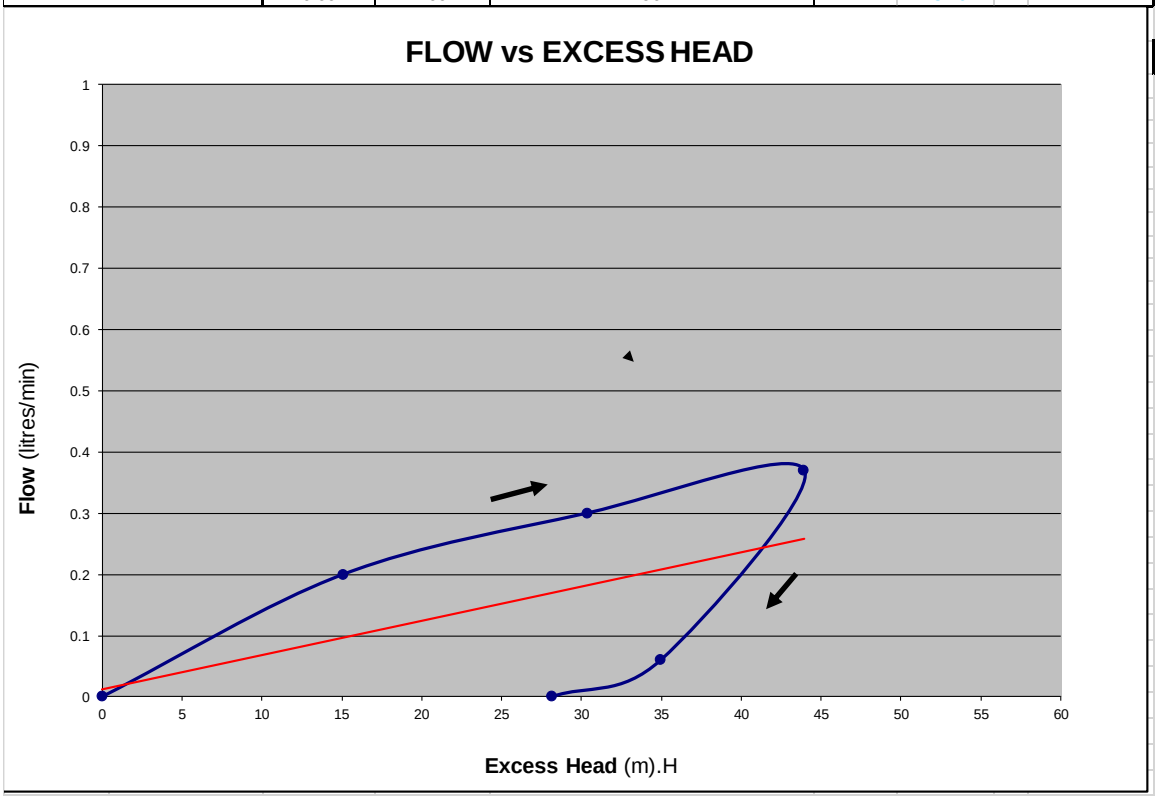

PACKER PERMEABILITY TEST

Borehole ID:	**BH_T6_01**	Test No:	**6**				
Packer type:	56mm Single Geopro	Date of Test:	24/10/2016				
Casing Details:	9m (PVC)	Packer inflation pressure (KPa):	2000				
Diameter of Hole (mm):	96.00	Test carried out by:	R C Minnaar				
Depth of hole (m):	137.05	Inclination of hole:	-70	degrees			
Depth of groundwater (mbgl):	26.50	Test section (m):	From:	**50.00**	to	**137.05**	
Vertical waterlevel (mbgl):	24.90	Test section length (m):	**87.05**				
Piezometer Guage Factor	**0.08381934**	Piezo zero reading (Digital):	**8455**				

Description of Test section	Average Flow Rate (l/min)	Gauge Pressure (KPa)	Piezometer Reading (Digital)	Total excess Head (mH2O)
See Geotech/geological log for details. Reverse flow when reducing pressure (back-pressure).	0			0
	0.17	100	8273	15.26
	0.35	200	8085	31.01
	0.41	300	7934	43.67
	0.06	200	8038	34.95
	0.04	100	8127	27.49

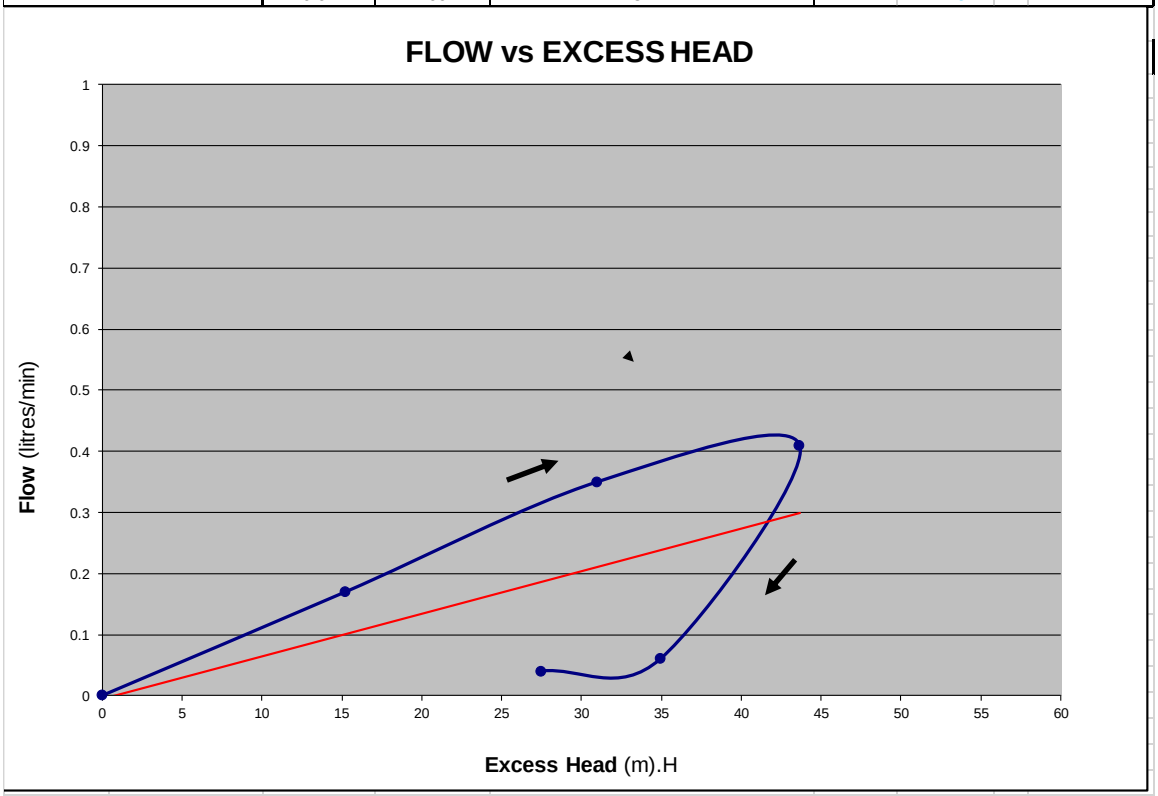

PACKER PERMEABILITY TEST

Borehole ID:	**BH_T6_01**	Test No:	**7**				
Packer type:	56mm Single Geopro	Date of Test:	24/10/2016				
Casing Details:	9m (PVC)	Packer inflation pressure (KPa):	2200				
Diameter of Hole (mm):	96.00	Test carried out by:	R C Minnaar				
Depth of hole (m):	137.05	Inclination of hole:	-70				degrees
Depth of groundwater (mbgl):	26.50	Test section (m):	From:	**30.00**	to	**50.00**	
Vertical waterlevel (mbgl):	24.90	Test section length (m):		**20.00**			
Piezometer Guage Factor	**0.08381934**	Piezo zero reading (Digital):		**8683**			

Description of Test section	Average Flow Rate (l/min)	Gauge Pressure (KPa)	Piezometer Reading (Digital)	Total excess Head (mH2O)
	0			0
See Geotech/geological log for details.	34.50	100	8517	13.91
	40.00	200	8453	19.28
	45.00	280	8444	20.03
	38.50	150	8503	15.09
	33.00	50	8550	11.15

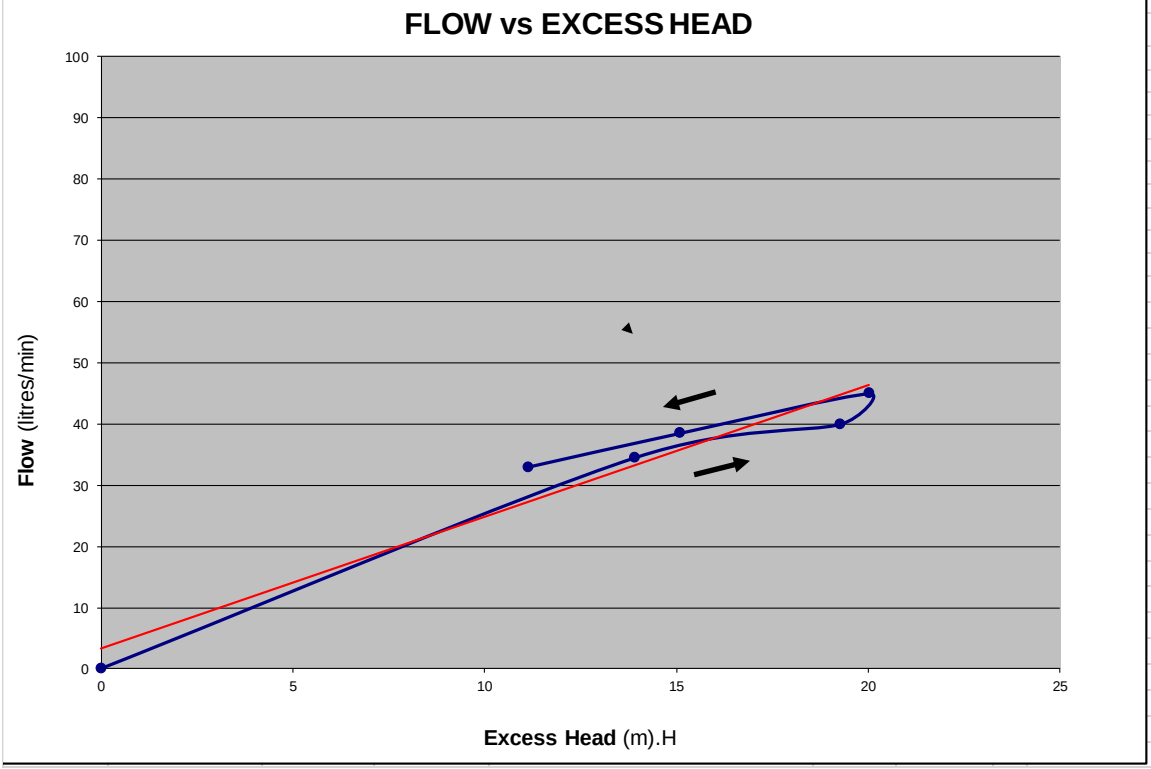

PACKER PERMEABILITY TEST

Borehole ID:	**BH_T6_02**	Test No:	**1**				
Packer type:	56mm Single Geopro	Date of Test:	21/10/2016				
Casing Details:	9m (PVC)	Packer inflation pressure (KPa):	1300				
Diameter of Hole (mm):	96.00	Test carried out by:	R C Minnaar				
Depth of hole (m):	40.12	Inclination of hole:	-70	degrees			
Depth of groundwater (mbgl):	18.00	Test section (m):	From:	**32.30**	to	**40.12**	
Vertical waterlevel (mbgl):	16.91	Test section length (m):	**7.82**				
Piezometer Guage Factor	**0.08381934**	Piezo zero reading (Digital):	**8570**				

Description of Test section	Average Flow Rate (l/min)	Gauge Pressure (KPa)	Piezometer Reading (Digital)	Total excess Head (mH2O)
See Geotech/geological log for details.	0			0
	0.15	90	8485	7.12
	5.50	200	8279	24.39
	21.10	250	8116	38.05
	17.80	150	8228	28.67
	13.80	50	8328	20.28

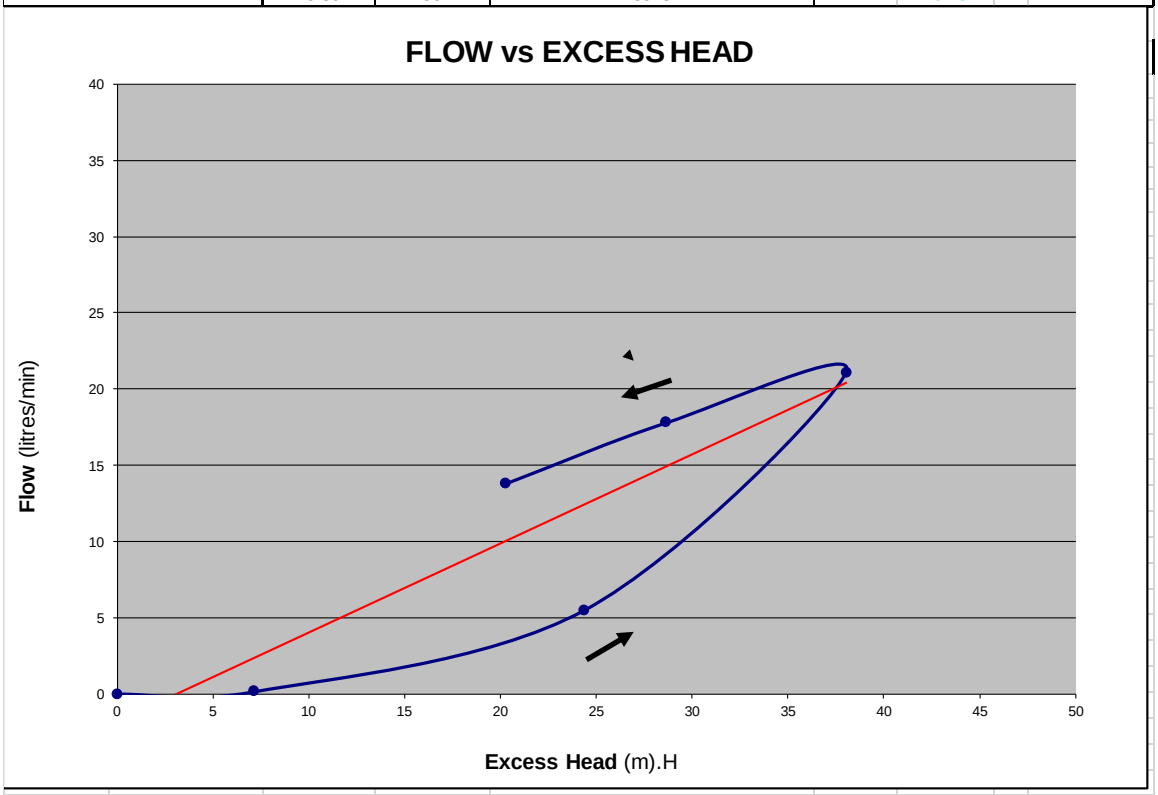

PACKER PERMEABILITY TEST

Borehole ID:	**BH_T6_02**	Test No:	**2**				
Packer type:	56mm Double Geopro	Date of Test:	22/10/2016				
Casing Details:	9m (PVC)	Packer inflation pressure (KPa):	1250				
Diameter of Hole (mm):	96.00	Test carried out by:	R C Minnaar				
Depth of hole (m):	40.12	Inclination of hole:	-70	degrees			
Depth of groundwater (mbgl):	18.00	Test section (m):	From:	**27.30**	to	**32.30**	
Vertical waterlevel (mbgl):	16.91	Test section length (m):	**5.00**				
Piezometer Guage Factor	**0.08381934**	Piezo zero reading (Digital):	**8612**				

Description of Test section	Average Flow Rate (l/min)	Gauge Pressure (KPa)	Piezometer Reading (Digital)	Total excess Head (mH2O)
See Geotech/geological log for details.	0			0
	0.00	100	8458	12.91
	0.03	200	8360	21.12
	0.09	300	8193	35.12
	0.07	200	8322	24.31
	0.00	100	8431	15.17

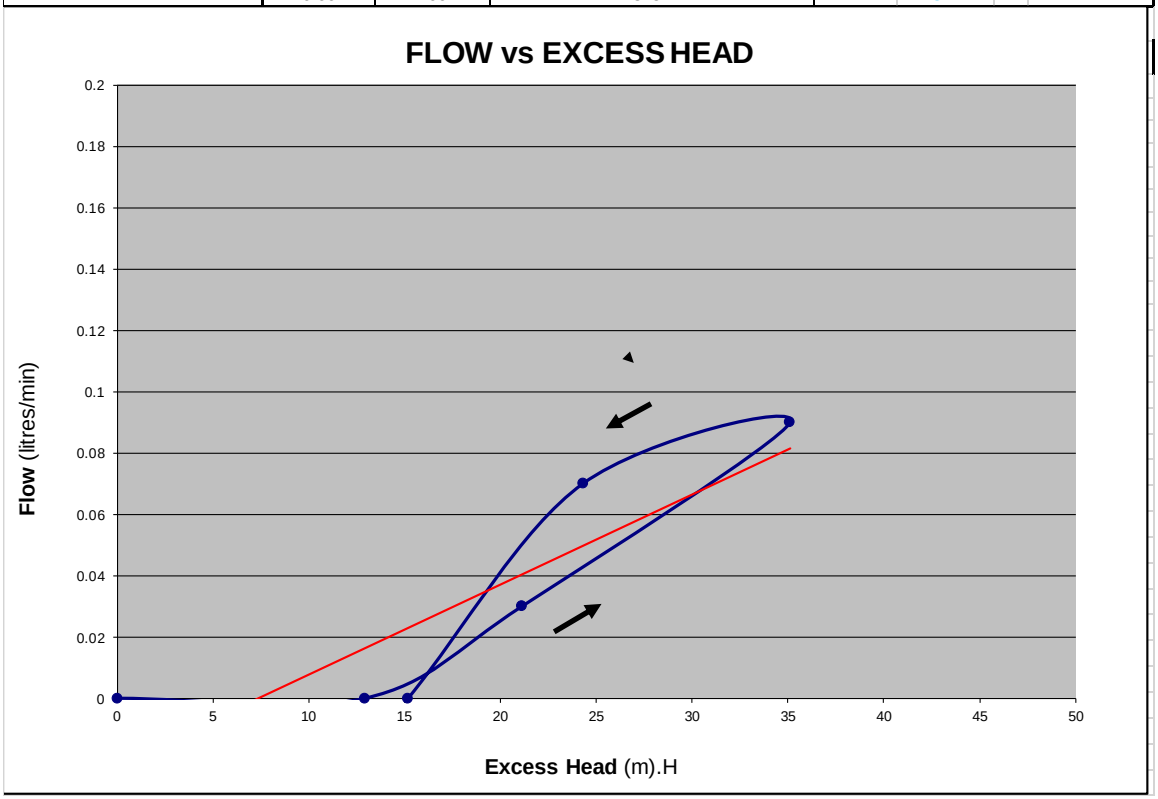

PACKER PERMEABILITY TEST

Borehole ID:	**BH_T6_02**	Test No:	**3**				
Packer type:	56mm Double Geopro	Date of Test:	22/10/2016				
Casing Details:	9m (PVC)	Packer inflation pressure (KPa):	1250				
Diameter of Hole (mm):	96.00	Test carried out by:	R C Minnaar				
Depth of hole (m):	40.12	Inclination of hole:	-70	degrees			
Depth of groundwater (mbgl):	18.00	Test section (m):	From:	**22.30**	to	**27.30**	
Vertical waterlevel (mbgl):	16.91	Test section length (m):	**5.00**				
Piezometer Guage Factor	**0.08381934**	Piezo zero reading (Digital):	**8645**				

Description of Test section	**Average Flow Rate** (l/min)	**Gauge Pressure** (KPa)	**Piezometer Reading** (Digital)	**Total excess Head** (mH2O)
	0			0
See Geotech/geological log for details. Test stopped early due to no water-take.	0.00	100	8581	5.36
	0.00	200	8406	20.03
	0.00	300	8144	41.99

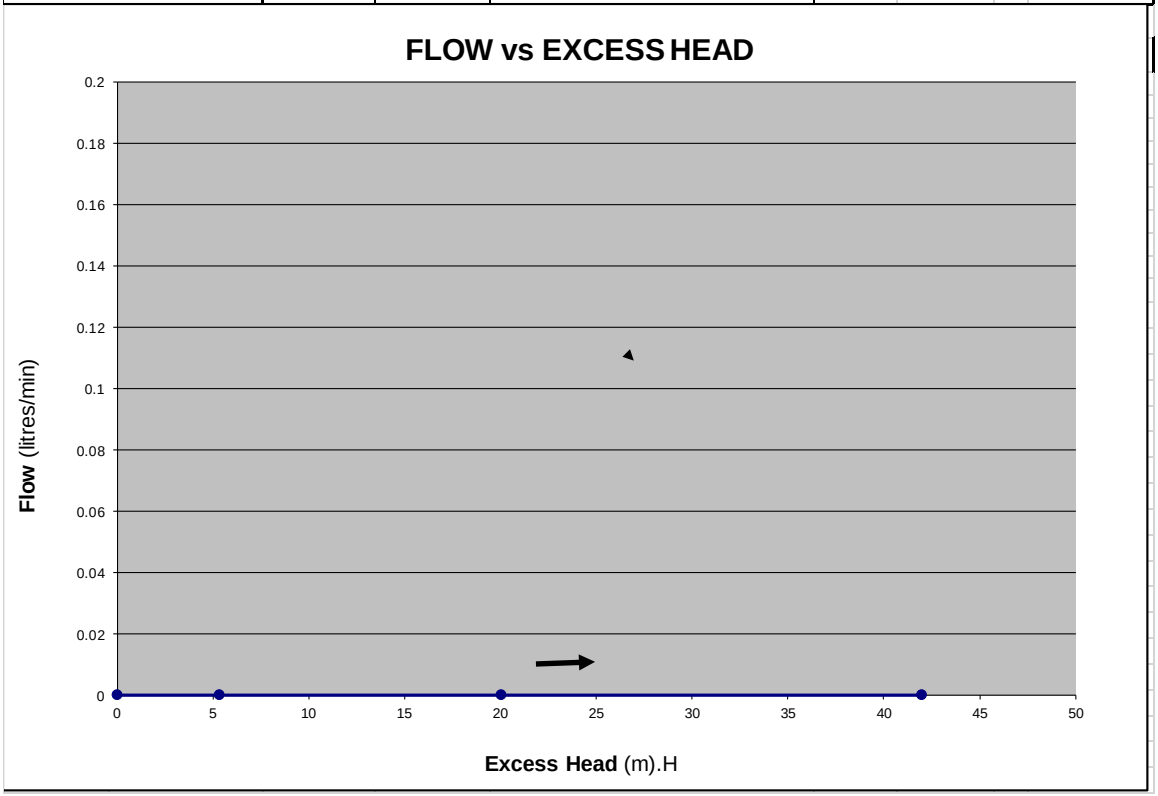

PACKER PERMEABILITY TEST

Borehole ID:	**BH_T6_02**	Test No:	**4**				
Packer type:	56mm Double Geopro	Date of Test:	22/10/2016				
Casing Details:	9m (PVC)	Packer inflation pressure (KPa):	1250				
Diameter of Hole (mm):	96.00	Test carried out by:	R C Minnaar				
Depth of hole (m):	40.12	Inclination of hole:	-70	degrees			
Depth of groundwater (mbgl):	18.00	Test section (m):	From:	**17.30**	to	**22.30**	
Vertical waterlevel (mbgl):	16.91	Test section length (m):	**5.00**				
Piezometer Guage Factor	**0.08381934**	Piezo zero reading (Digital):	**8720**				

Description of Test section	**Average Flow Rate** (l/min)	**Gauge Pressure** (KPa)	**Piezometer Reading** (Digital)	**Total excess Head** (mH2O)
See Geotech/geological log for details.	0			0
	0.02	100	8508	17.77
	0.04	200	8354	30.68
	0.05	300	8219	41.99
	0.02	200	8342	31.68
	0.00	100	8452	22.46

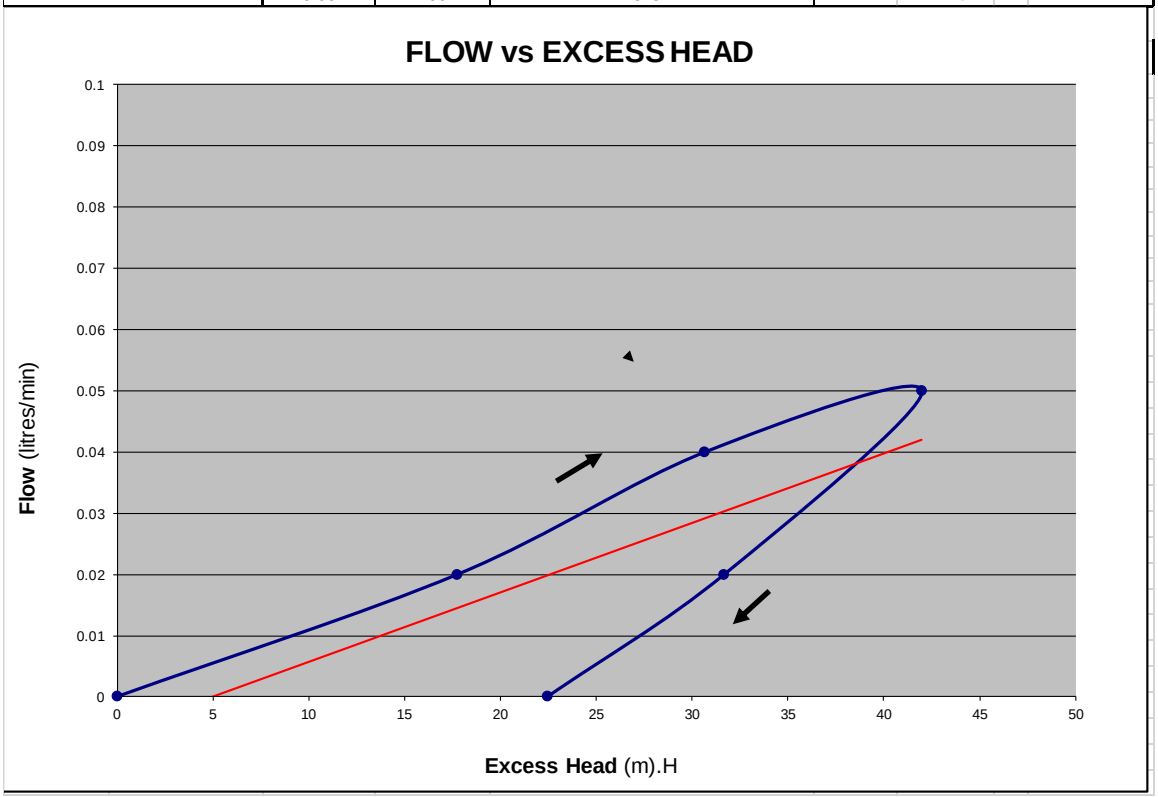

PACKER PERMEABILITY TEST

Borehole ID:	**BH_TX_01**	Test No:	**1**				
Packer type:	85mm Single Geopro	Date of Test:	25/10/2016				
Casing Details:	9m (Steel)	Packer inflation pressure (KPa):	1700				
Diameter of Hole (mm):	165.00	Test carried out by:	R C Minnaar				
Depth of hole (m):	100.00	Inclination of hole:	-90	degrees			
Depth of groundwater (mbgl):	19.60	Test section (m):	From:	**90.00**	to	**100.00**	
Vertical waterlevel (mbgl):	19.60	Test section length (m):	**10.00**				
Piezometer Guage Factor	**0.08381934**	Piezo zero reading (Digital):	**7920**				

Description of Test section	**Average Flow Rate** (l/min)	**Gauge Pressure** (KPa)	**Piezometer Reading** (Digital)	**Total excess Head** (mH2O)
	0			0
See Geotech/geological log for details.	0.00	100	7707	17.85
	0.14	200	7545	31.43
	0.21	310	7375	45.68
	0.11	200	7518	33.70
	0.04	100	7652	22.46

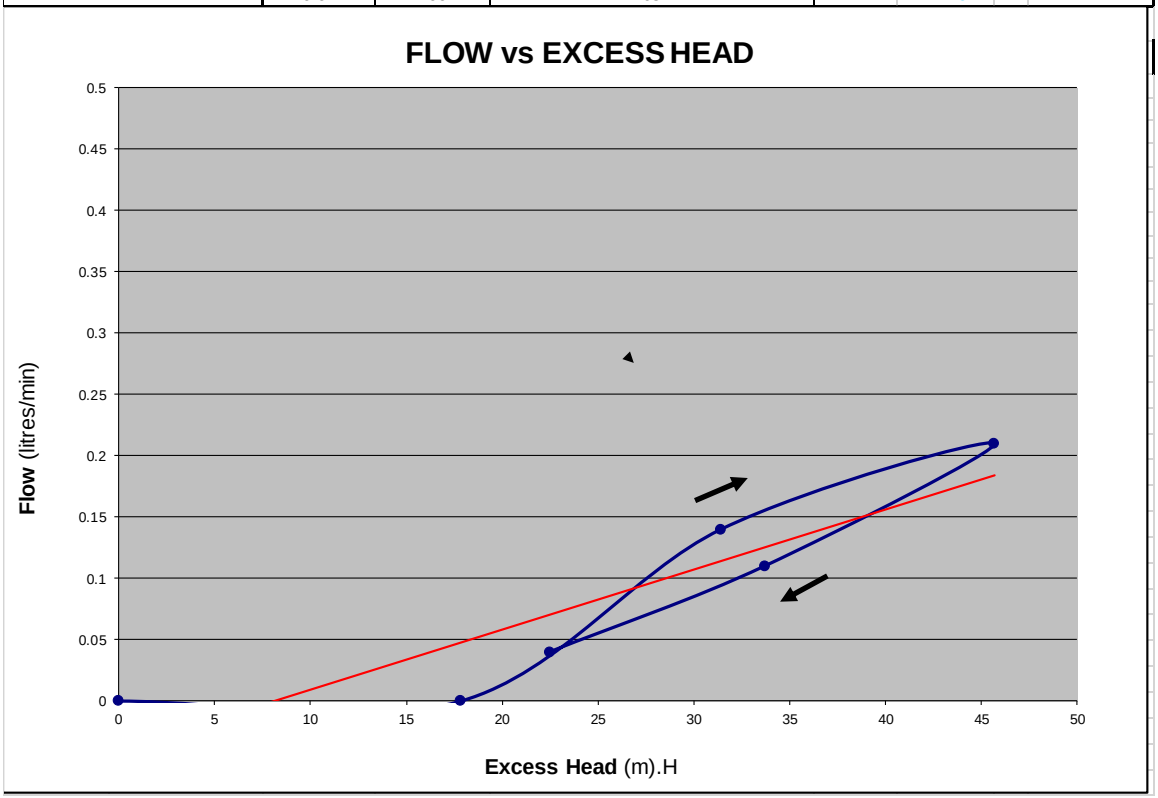

PACKER PERMEABILITY TEST

Borehole ID:	**BH_TX_01**	Test No:	**2**				
Packer type:	85mm Single Geopro	Date of Test:	25/10/2016				
Casing Details:	9m (Steel)	Packer inflation pressure (KPa):	1700				
Diameter of Hole (mm):	165.00	Test carried out by:	R C Minnaar				
Depth of hole (m):	100.00	Inclination of hole:	-90	degrees			
Depth of groundwater (mbgl):	19.60	Test section (m):	From:	**70.00**	to	**100.00**	
Vertical waterlevel (mbgl):	19.60	Test section length (m):	**30.00**				
Piezometer Guage Factor	**0.08381934**	Piezo zero reading (Digital):	**8154**				

Description of Test section	**Average Flow Rate** (l/min)	**Gauge Pressure** (KPa)	**Piezometer Reading** (Digital)	**Total excess Head** (mH2O)
	0			0
See Geotech/geological log for details.	0.14	100	7879	23.05
	0.21	200	7728	35.71
	0.26	300	7591	47.19
	0.15	200	7718	36.55
	0.10	100	7839	26.40

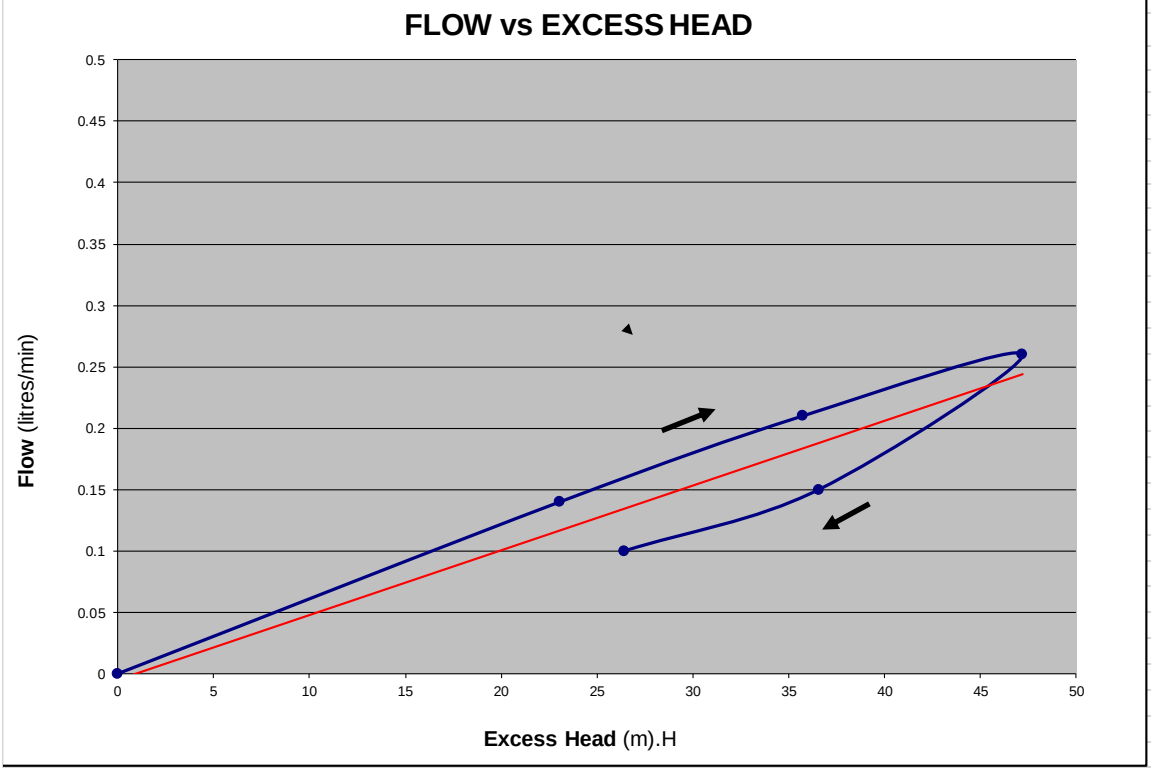

PACKER PERMEABILITY TEST

Borehole ID:	**BH_TX_01**	Test No:	**3**				
Packer type:	85mm Single Geopro	Date of Test:	25/10/2016				
Casing Details:	9m (Steel)	Packer inflation pressure (KPa):	1500				
Diameter of Hole (mm):	165.00	Test carried out by:	R C Minnaar				
Depth of hole (m):	100.00	Inclination of hole:	-90	degrees			
Depth of groundwater (mbgl):	19.60	Test section (m):	From:	**50.00**	to	**100.00**	
Vertical waterlevel (mbgl):	19.60	Test section length (m):	**50.00**				
Piezometer Guage Factor	**0.08381934**	Piezo zero reading (Digital):	**8394**				

Description of Test section	Average Flow Rate (l/min)	Gauge Pressure (KPa)	Piezometer Reading (Digital)	Total excess Head (mH2O)
See Geotech/geological log for details.	0			0
	2.10	100	8139	21.37
	2.90	200	7977	34.95
	3.70	300	7828	47.44
	2.70	200	7966	35.87
	1.75	100	8118	23.13

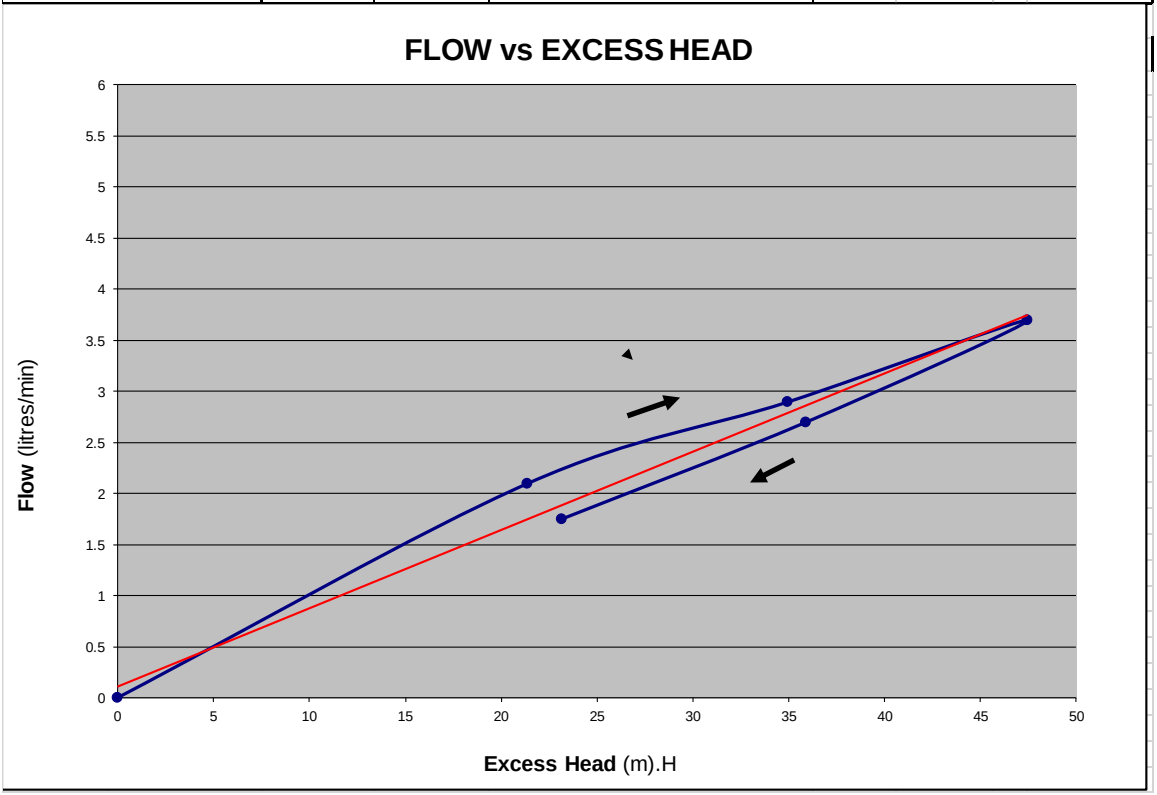

PACKER PERMEABILITY TEST

Borehole ID:	**BH_TX_01**	Test No:	**4**				
Packer type:	85mm Single Geopro	Date of Test:	25/10/2016				
Casing Details:	9m (Steel)	Packer inflation pressure (KPa):	1500				
Diameter of Hole (mm):	165.00	Test carried out by:	R C Minnaar				
Depth of hole (m):	100.00	Inclination of hole:	-90	degrees			
Depth of groundwater (mbgl):	19.60	Test section (m):	From:	**60.00**	to	**100.00**	
Vertical waterlevel (mbgl):	19.60	Test section length (m):	**40.00**				
Piezometer Guage Factor	**0.08381934**	Piezo zero reading (Digital):	**8248**				

Description of Test section	**Average Flow Rate** (l/min)	**Gauge Pressure** (KPa)	**Piezometer Reading** (Digital)	**Total excess Head** (mH2O)
	0			0
See Geotech/geological log for details. Permeability confirmation test.	2.20	100	8011	19.87
	2.90	200	7856	32.86
	3.60	300	7703	45.68
	2.60	200	7845	33.78
	1.70	100	7984	22.13

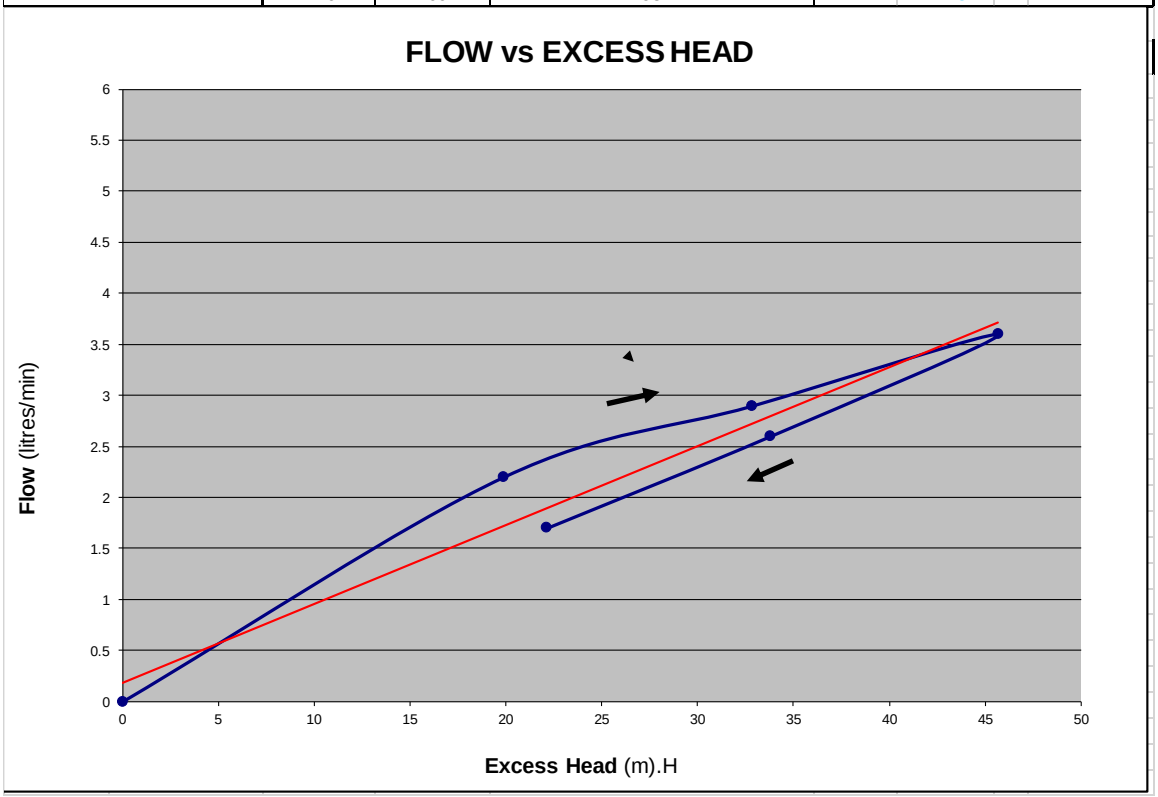

PACKER PERMEABILITY TEST

Borehole ID:	**BH_TX_01**	Test No:	**5**				
Packer type:	85mm Single Geopro	Date of Test:	25/10/2016				
Casing Details:	9m (Steel)	Packer inflation pressure (KPa):	1400				
Diameter of Hole (mm):	165.00	Test carried out by:	R C Minnaar				
Depth of hole (m):	100.00	Inclination of hole:	-90	degrees			
Depth of groundwater (mbgl):	19.60	Test section (m):	From:	**40.00**	to	**100.00**	
Vertical waterlevel (mbgl):	19.60	Test section length (m):	**60.00**				
Piezometer Guage Factor	**0.08381934**	Piezo zero reading (Digital):	**8497**				

Description of Test section	**Average Flow Rate** (l/min)	**Gauge Pressure** (KPa)	**Piezometer Reading** (Digital)	**Total excess Head** (mH2O)
See Geotech/geological log for details. Permeability confirmation test.	0			0
	2.70	100	8244	21.21
	3.50	200	8095	33.70
	4.10	300	7948	46.02
	3.05	200	8083	34.70
	1.85	100	8235	21.96

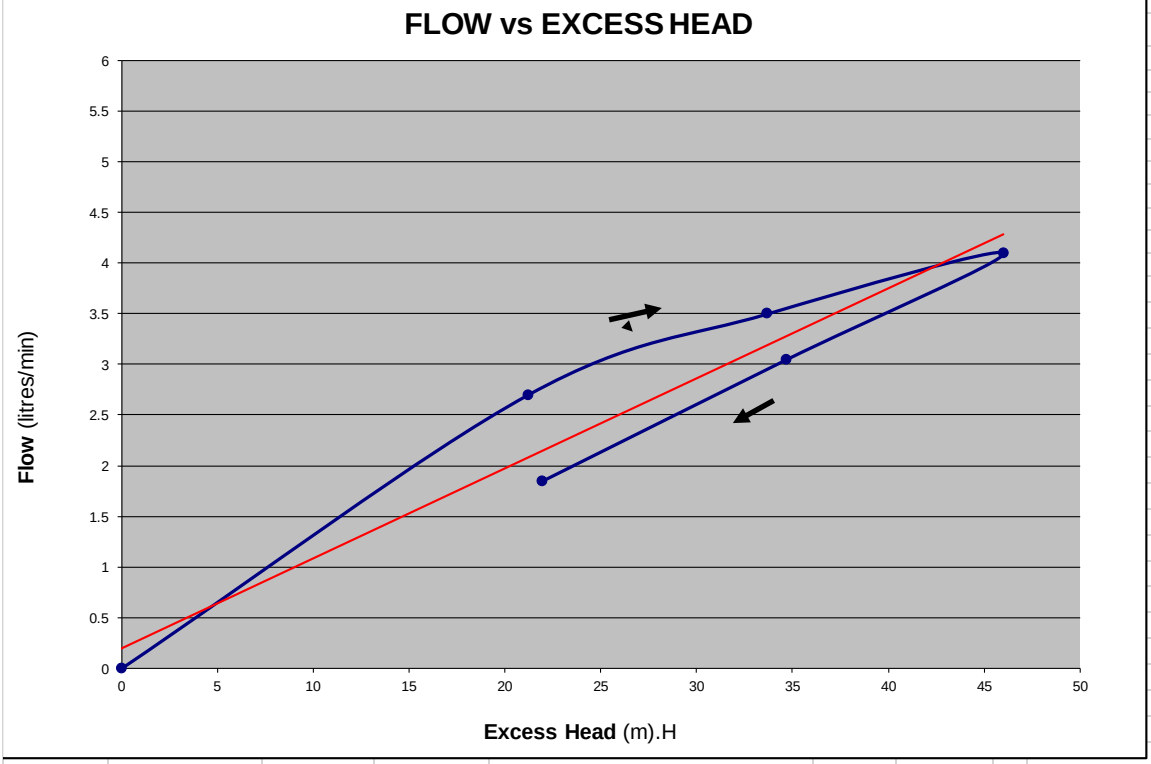

PACKER PERMEABILITY TEST

Borehole ID:	**BH_TX_01**	Test No:	**6**				
Packer type:	85mm Single Geopro	Date of Test:	25/10/2016				
Casing Details:	9m (Steel)	Packer inflation pressure (KPa):	1100				
Diameter of Hole (mm):	165.00	Test carried out by:	R C Minnaar				
Depth of hole (m):	100.00	Inclination of hole:	-90	degrees			
Depth of groundwater (mbgl):	19.60	Test section (m):	From:	**30.00**	to	**100.00**	
Vertical waterlevel (mbgl):	19.60	Test section length (m):	**70.00**				
Piezometer Guage Factor	**0.08381934**	Piezo zero reading (Digital):	**8616**				

Description of Test section	Average Flow Rate (l/min)	Gauge Pressure (KPa)	Piezometer Reading (Digital)	Total excess Head (mH2O)
See Geotech/geological log for details. Permeability confirmation test.	0			0
	11.50	100	8258	30.01
	13.50	200	8135	40.32
	16.10	300	8009	50.88
	12.30	200	8139	39.98
	9.40	100	8252	30.51

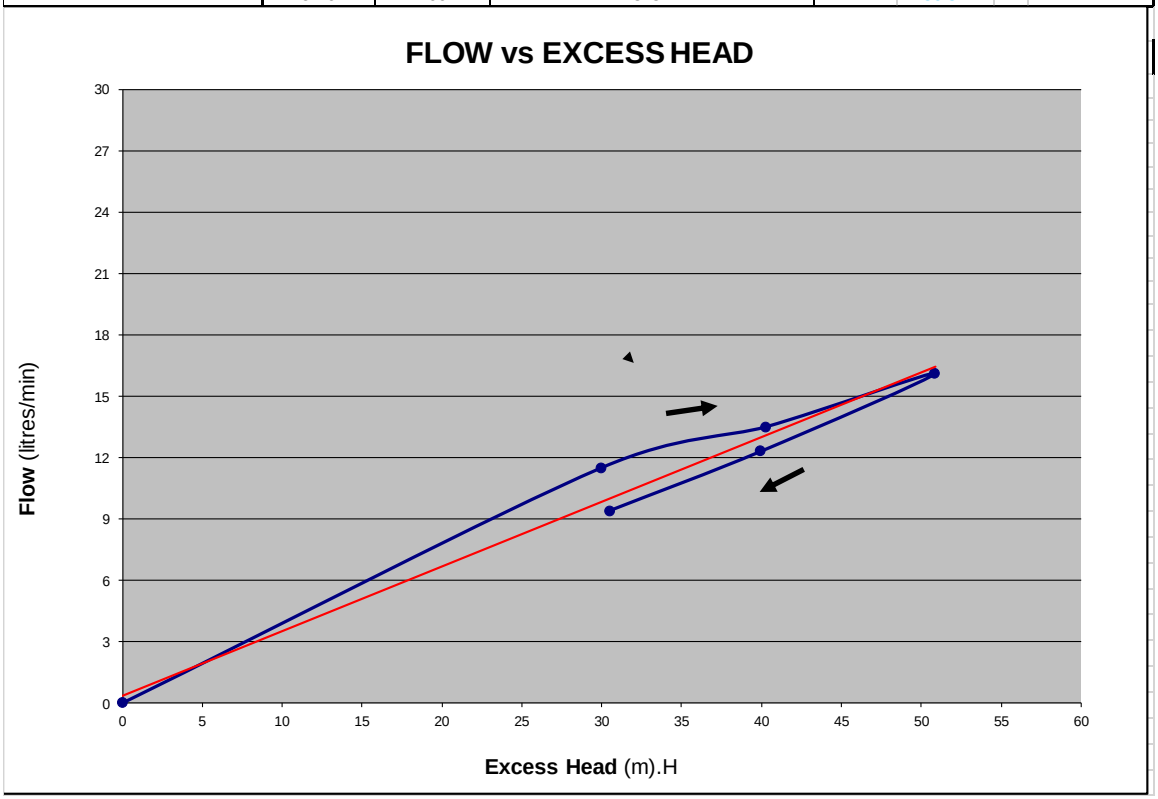

APPENDIX D – PUMPING TEST RESULTS

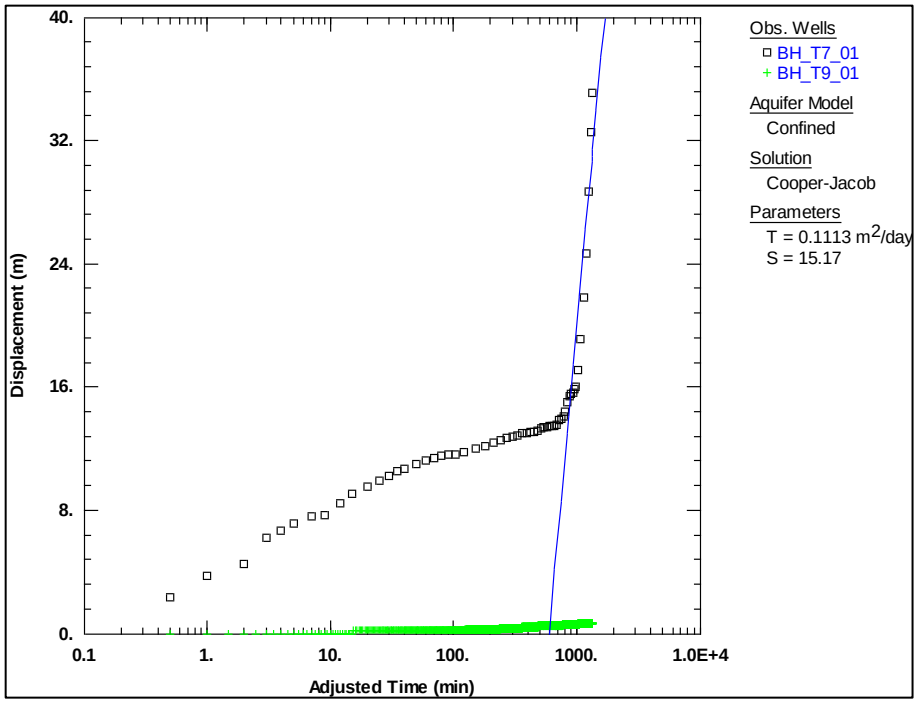

Figure D-0-1: Processed pumping test data for borehole BH_T7_01 and observation data from monitored borehole BH_T9_01.

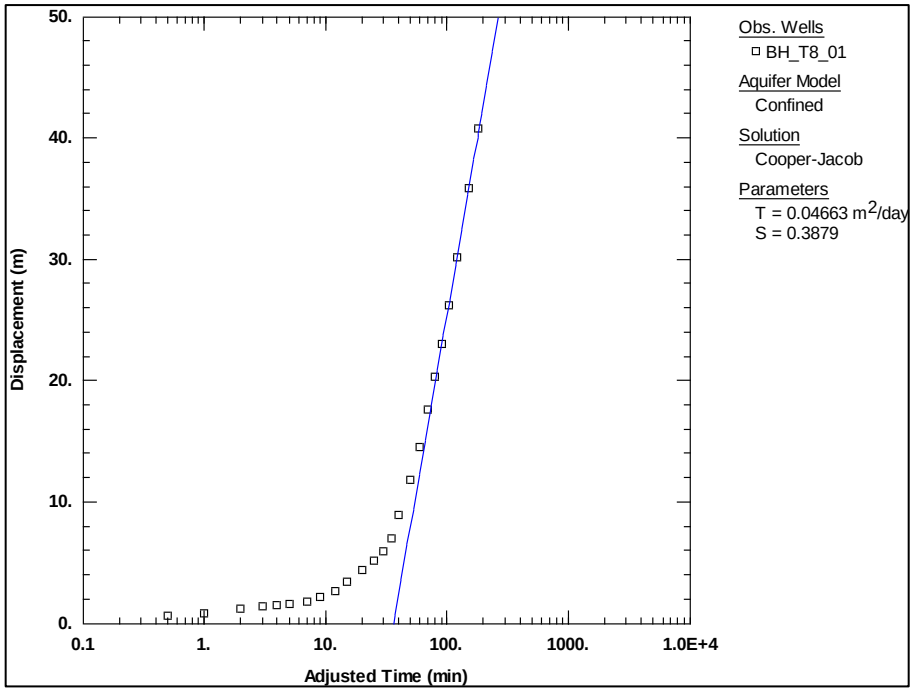

Figure D-0-2: Processed pumping test data for borehole BH_T8_01.

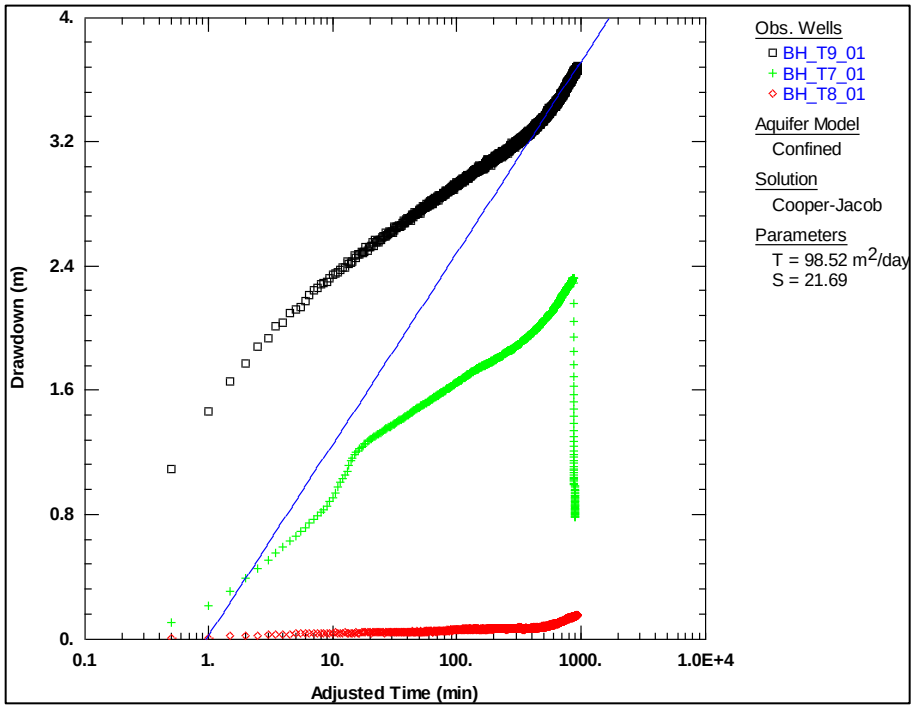

Figure D-0-3: Processed pumping test data for borehole BH_T9_01 and observation data from monitored boreholes BH_T7_01 and BH_T8_01.

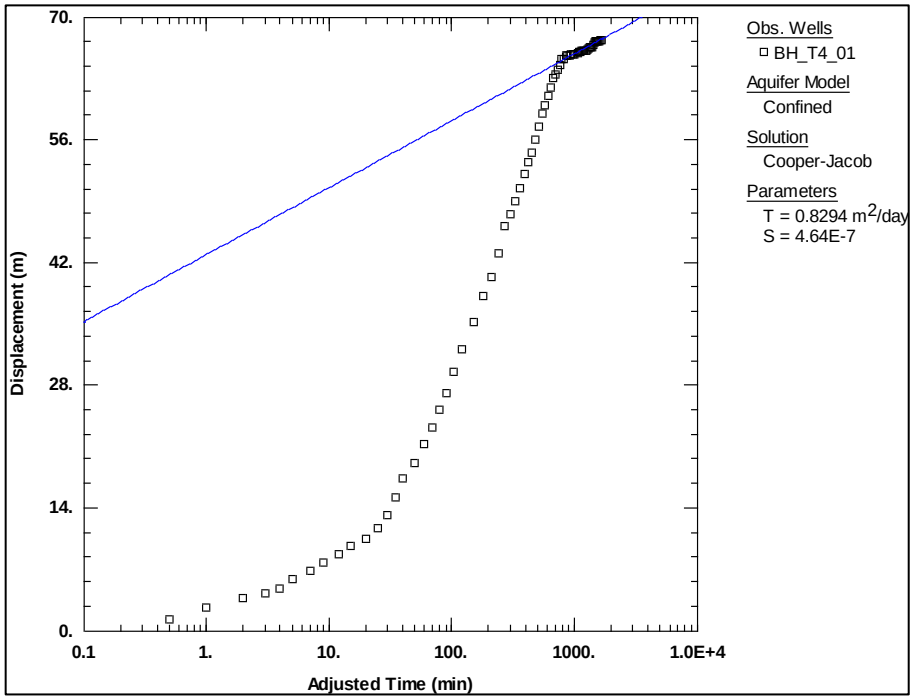

Figure D-0-4: Processed pumping test data for borehole BH_T4_01.

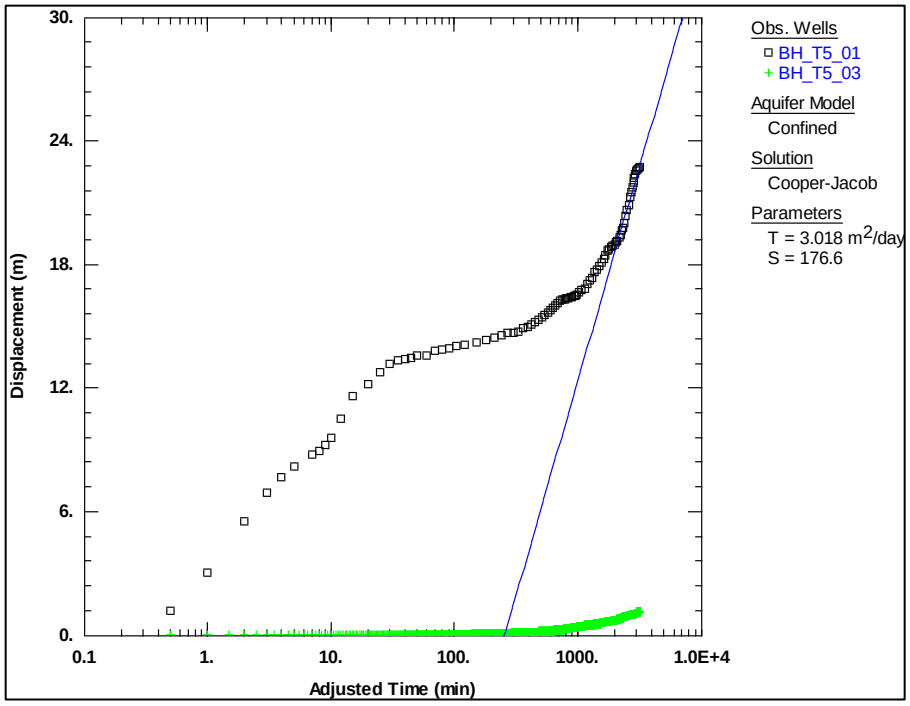

Figure D-0-5: Processed pumping test data for borehole BH_T5_01 and observation data from monitored borehole BH_T5_03.

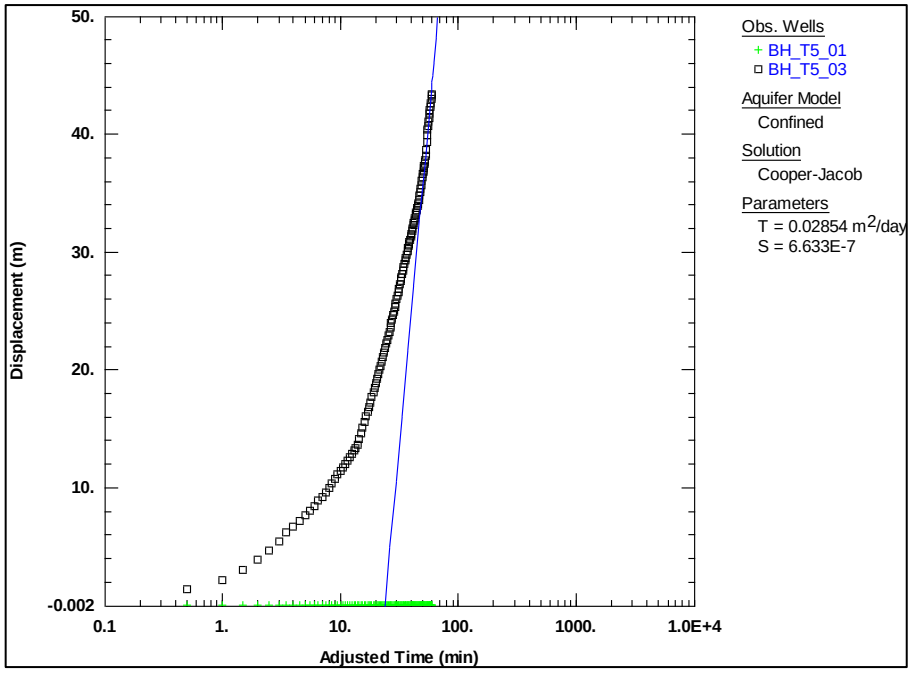

Figure D-0-6: Processed pumping test data for borehole BH_T5_03 and observation data from monitored borehole BH_T5_01.